BMR JOURNAL of Australian Geology & Geophysics

VOLUME 3, NUMBER 2, JUNE 1978

BMR Journal of Australian Geology & Geophysics Volume 3, (2)

Department of National Development, Australia

Minister: The Hon. K. E. Newman, M.P.
Secretary: A. J. Woods

Bureau of Mineral Resources, Geology and Geophysics

Director: L. C. Noakes, O.B.E.
Editor, BMR Journal: J. F. Truswell

The BMR Journal of Australian Geology and Geophysics is a quarterly journal of research and related activities. Contributions are from officers of the BMR, from BMR officers working in collaboration with others, or requested work sponsored by the BMR. In addition to articles the Journal may include shorter notes and discussion of papers published in it. Discussion of papers is invited from anyone.

Annual subscription to the Journal is at the rate of $10 (Australian). Individual numbers, if available, cost $3. Subscriptions, etc., made payable to the Receiver of Public Moneys in Australian dollars, should be sent to the Director, Bureau of Mineral Resources, Geology & Geophysics, P.O. Box 378, Canberra, A.C.T. 2601, Australia. The Journal can also be obtained from the offices of the Department of National Development in Sydney and Melbourne.

Other matters concerning the Journal should be sent to the Director, marked for the attention of the Editor, BMR Journal.

BMR JOURNAL of Australian Geology & Geophysics

Volume 3, Number 2
June 1978

AUSTRALIAN GOVERNMENT PUBLISHING SERVICE
CANBERRA 1978

Front cover:

Manganese nodule, displaying a complex growth history.

Radial upward growth led to coalescing into a continuous crust. This was coated with horizontal layers. After fracturing, and infilling of cracks with calcareous sediment, further layers encased the nodule.

Dredged from 2050 m on the Scott Plateau northwest of Australia during 1977 cruise of RV *Valdivia*. Results from the cruise will be published in a forthcoming issue of the Journal.

Photograph (x3/4): U. Von Stackelberg, Bundesanstalt für Geowissenschaften und Rohstoffe, Hannover, West Germany.

ISSN 0312-9608

Printed by Graphic Services Pty Ltd, 516-518 Grand Junction Road, Northfield, S.A. 5085

BMR Journal of Australian Geology & Geophysics, 3, 1978, 85-92

Skeletal carbonate variation on the continental shelf of eastern Australia

John F. Marshall and Peter J. Davies

Sediments on the continental shelf of eastern Australia increase in carbonate content away from the present shoreline. However, the high values of the outer shelf sands show little latitudinal variation, both tropical and temperate continental shelves being mantled with sediments which are relatively pure carbonates. Thus a high calcimass productivity is not restricted to tropical regions. However, the types of carbonate-scereting organisms do show marked latitudinal variations. North of latitude 24°S the outer continental shelf is dominated by the Great Barrier Reef, and inter-reef and outer shelf sediments contain the remains of hermatypic corals and calcareous green algae, mainly *Halimeda*, together with varying amounts of foraminifera, Mollusca, Bryozoa, and calcareous red algae. Corals and *Halimeda* are not present in the sediments south of 24°S, which consists of foraminifera, mollusca, bryozoa and calcareous red algae. The bryozoan content of the sediments increases to the south, and between 38° and 44°S bryozoans become the dominant component of the outer shelf sands.

Present-day sea-surface temperature and salinity data have been analysed to predict the distribution of carbonate particle associations. The observed distribution agrees with the predicted one, but the presence of relict carbonate sediments must be taken into account.

Introduction

Most studies of modern marine carbonates relate to tropical latitudes, and the presence of carbonate sediments on temperate continental shelves has often been construed as inconsequential because of their supposedly low abundance and relative unimportance. However, in recent years it has become apparent that certain temperate continental shelves throughout the world contain a high proportion of carbonate sediments (Chave, 1967; Conolly & von der Borch, 1967; Milliman, 1974).

It has been maintained that the distribution of skeletal carbonates is not haphazard, but varies systematically with changes in physical, chemical, and biological conditions (Ginsburg & others, 1963). Factors such as currents, water depths, availability of nutrients, temperature, salinity, and turbidity determine the type of carbonate-secreting organism present on the sea floor. Lees & Buller (1972) recognised that there are two major associations of skeletal carbonate sediments related to latitude: one is a tropical assemblage (*chlorozoan*) in which hermatypic coral and calcareous green algae are diagnostic types. The other is a temperate-water assemblage (*foramol*) in which the predominant constituents are foraminifera, Mollusca, Bryozoa, calcareous red algae, and barnacles. Lees (1975) considered the distribution of these two associations to be related primarily to water temperature and salinity.

The continental shelf of eastern Australia extends from Torres Strait (10°S) to the southern tip of Tasmania (44°S), a distance of some 4000 km. In the north the outer shelf is dominated by the Great Barrier Reef, which extends as an almost continuous barrier between 10° and 24°S. From 24° to 44°S the shelf is of the open type.

Surface sediment samples south of 22°S have been collected by BMR on a 10 nautical-mile grid (Jongsma & Marshall, 1971; Davies & Marshall, 1972; 1973). Sampling interval was reduced to 5 nm on the narrower parts of the shelf. Samples have been collected on a closer but less systematic pattern on the central and northern Queensland shelf (Maxwell, 1968). Data on all these samples include grainsize, carbonate content, and distribution of skeletal components. Fairly detailed salinity and temperature data collected by the CSIRO Division of Fisheries and Oceanography exist for the eastern Australian continental shelf. It has been possible, therefore, to plot the skeletal carbonate variation along a single, continuous continental shelf, and to use these data to test Lees' (1975) hypothesis of both temperature and salinity dependence for this variation.

Textural and carbonate distribution

The textural distribution of the superficial sediments on the continental shelf of eastern Australia is shown in Figure 1. Sandy muds (>40 percent mud) and muddy sands (10-40 percent mud) are dominant on the northern Queensland shelf. Between Cairns and Rockhampton a wide, continuous zone of carbonate sands extends along the outer shelf, co-incident with the line of maximum reef development. In the same area there is a predominance of muddy sands and sandy muds nearshore; these are gradually displaced eastwards to the south until they occupy the mid-shelf region, and sands take their place on the inner shelf. South of 24°S sands of mixed origin are predominant over the entire shelf, with only relatively minor amounts of muddy sediment.

The sediments on the continental shelf of eastern Australia increase in carbonate content from the shoreline to the edge of the shelf, except in Bass Strait where carbonate values are higher on the shallower parts of the shelf than at its edge (Fig. 2). However, carbonate values greater than 60 percent are present along almost the entire length of the outer shelf and very high values (>80%) are present on the southern temperate shelf as well as on the northern tropical shelf (Fig. 2). Therefore, there is no latitudinal decrease in carbonate values as one moves from tropical to temperate waters such as exists on the Atlantic shelf of North America (Milliman, 1972), and the outer shelf in both zones can be considered a carbonate province.

On the southern part of the shelf there appears to be a correlation between areas of low carbonate and the position of river mouths, suggesting that river discharge onto the shelf, presumably during periods of low sea level, has had an adverse effect on carbonate production.

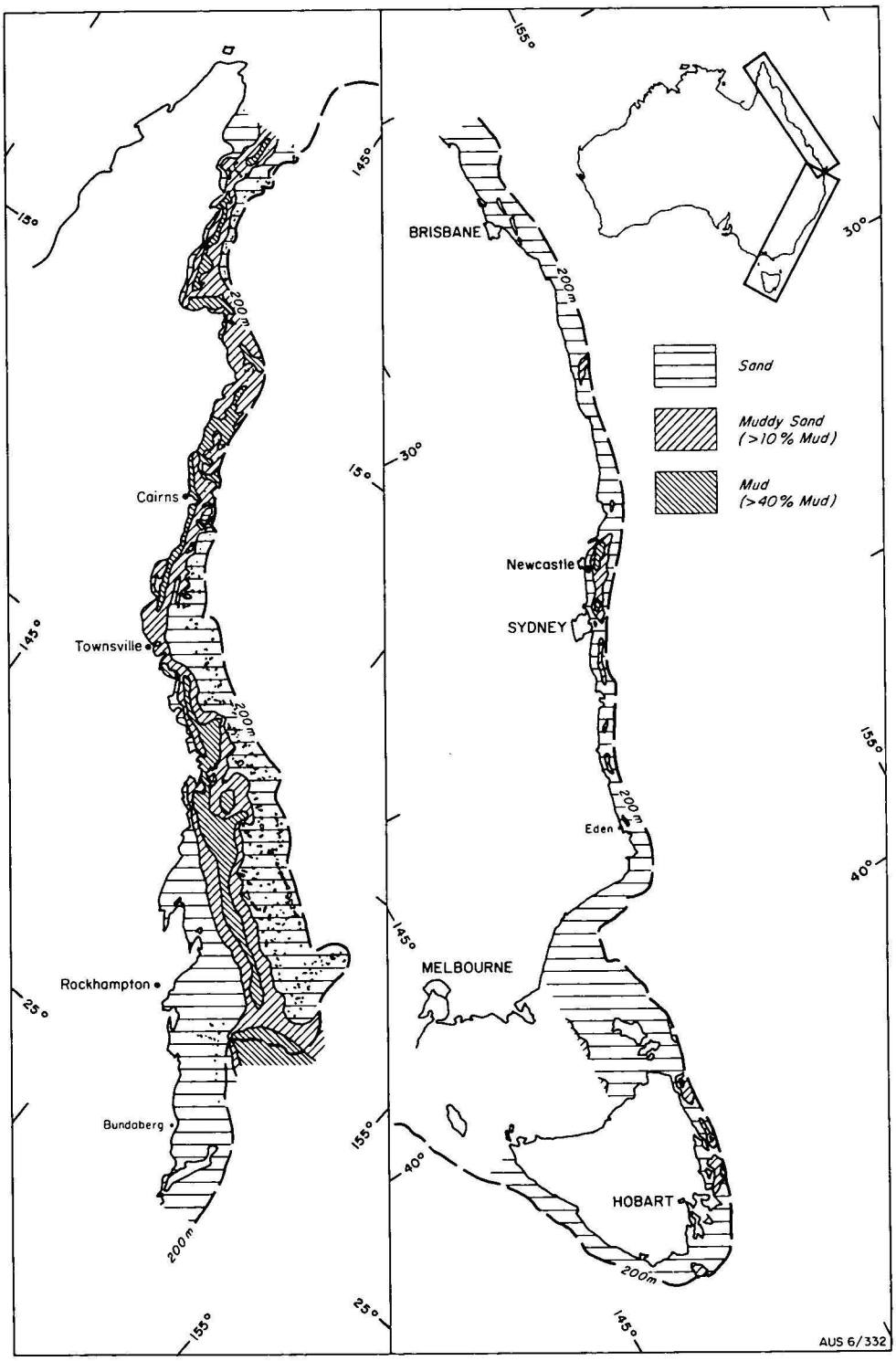

Figure 1. Textural distribution of the superficial sediments on the continental shelf of eastern Australia.

Skeletal carbonate distribution

Although high carbonate values are present along almost the entire length of the outer shelf there are marked latitudinal variations in the types of carbonate-secreting organisms that form these sediments. The east Australian shelf contains two broad skeletal associations, a northern chlorozoan assemblage and a southern foramol assemblage (terminology of Lees & Buller, 1972). The chlorozoan assemblage may contain any of the foramol constituents, but the presence of hermatypic corals and calcareous green algae is diagnostic. On the east Australian shelf the boundary between the two associations occurs at 24°S. The boundary is well defined, and this is attributed to the termination of surface reefs on the outer shelf at this latitude.

The distribution of the various skeletal components on the outer shelf is shown in Figure 3. The main features outlined by this diagram are:

(1) the absence of corals and *Halimeda* south of the Great Barrier Reef

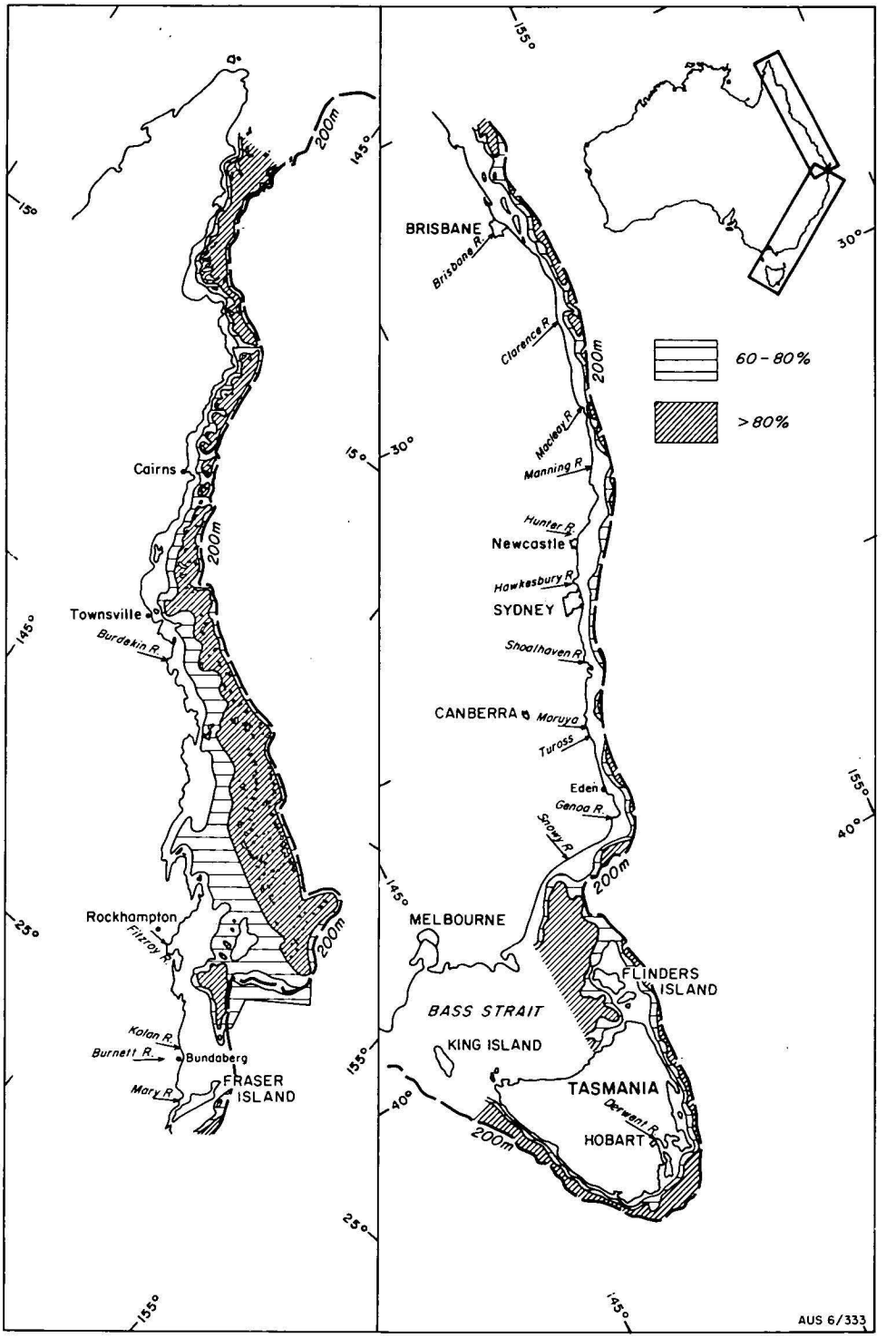

Figure 2. Distribution of carbonate-rich sediments on the continental shelf of eastern Australia.

(2) the marked increase in the proportion of Bryozoa in southern latitudes
(3) the ubiquity of the molluscan and foraminiferal components along the entire shelf.

The distribution and abundance of the various components is discussed below.

Corals

The coral component of the shelf sediments is obviously related to areas of reef development, but this component commonly only makes up a small proportion of the sediment around the reefs, usually less than 10 percent. One explanation for this, by T. F. Goreau (in Bathurst, 1975) is that the corals have a tendency to break down directly into the aragonite needles of the sclerodermites, and so are not readily identified in the sand fraction. Another explanation, by Ginsburg and others (1963), is that large hemispherical corals are resistant to breakdown because of their size and the cellular nature of their micro-structure. Whatever the reason, given the great areal distribution of the reefs, some 12 000 km^2 (Maxwell, 1973), it is obvious

that corals are greatly under-represented compared with other organisms. Highest coral values in the sediments tend to be in the southern Barrier Reef, where there is a great density of reefal masses when compared to the northern Barrier Reef.

There is no coral in the sediment south of 24°S, although isolated fringing reefs are present as far south as Coffs Harbour (30°15'S) (Veron, 1974).

Halimeda

Like the corals, *Halimeda* is closely related to reef development, but it generally has a slightly higher concentration in the sediments than the corals. In favourable localities *Halimeda* may be as high as 60 percent (Maxwell, 1973), but usually near reefs it is of the order of 10-30 percent. *Halimeda* is absent from the shelf sediments south of the Barrier Reef.

Bryozoa

Bryozoans show a marked change in abundance with latitude, and in the south it forms the dominant component of the sediment (Fig. 3). Bryozoa are sporadically present in the reef province, and they do tend to be reasonably well developed on the mid-shelf at the southern end of the Barrier Reef where values of the order of 30 percent may be found (Maxwell, 1968, 1973). Between Brisbane and Sydney there is a variable distribution of this component, but south of Sydney there are relatively high concentrations of bryozoan detritus on the outer shelf. Between 36° and 44°S this component makes up 30-70 percent of the outer shelf sediments, and south of 38°S it commonly exceeds 60 percent. These figures are similar to those for the southern shelf of Australia where Bryozoa make up 20-50 percent of the sediment (Conolly & von der Borch, 1967). The abundance of Bryozoa on the outer shelf in southern latitudes is possibly related to the upwelling of nutrient-rich, intermediate Antarctic water along the southern shelf (Wass & others, 1970).

Calcareous red algae

On the northern part of the shelf calcareous red algae are essentially reef-controlled, but there are large parts of the reef province where this component is rare in the sediments. However, Maxwell (1973) has found that values may be as high as 40 percent on reef edges, and that its apparent sparseness in the sediments is a consequence of its resistance to erosion, largely because of its encrusting nature.

The highest concentration of this component occurs south of the reefs, on the outer shelf between Fraser Island and Brisbane (Fig. 3). Hardgrounds and banks are a common feature of this part of the shelf, and because of the absence of corals and *Halimeda* at these latitudes, these banks have been preferentially colonised by calcareous red algae. Significant abundances of calcareous red algae extend as far south as 30°S, and minor amounts are present as far south as Tasmania.

Mollusca

Relatively high concentrations of molluscs (>20 percent) are present along the entire shelf, except in some parts of the Barrier Reef where molluscs are diluted by coral and *Halimeda* fragments, and on parts of the Tasmanian shelf where there are high concentrations of bryozoans. Molluscs are generally distributed over the entire shelf, unlike other components which are mostly restricted to the outer shelf.

Foraminifera

Like the molluscs, foraminifera are widespread and are commonly the dominant component. Values often exceed 25 percent on parts of the shelf. The northern rimmed shelf has a higher proportion of benthonic forms, while on the southern open shelf there tends to be an increase in the number of pelagic forms.

Therefore, the criterion for discriminating the warm water (chlorozoan) assemblage from the colder water (foramol) assemblage in the sediments on the eastern shelf of Australia is the presence or absence of coral and *Halimeda*. This is in agreement with Lees & Buller's (1972) and Lees' (1975) assessment of carbonate shelf sediments throughout the world. However, on the east Australian shelf the chlorozoan assemblage extends to only 24°S, whereas this assemblage is commonly present in latitudes as high as 30° on other continental shelves. The abundance of the bryozoan component south of 36°S is a characteristic feature of the foramol assemblage on the east Australian shelf. The relatively low abundance of the bryozoan component between 24° and 36°S is possibly a result of less nutrient-rich waters affecting this area, but it may partly be a result of the distribution of relict sediments on the outer continental shelf.

Modern and relict carbonates

The high carbonate sediments on the outer continental shelf of eastern Australia can be divided into three facies (modern, relict, and mixed), based on the presence or absence of relict sediments (Fig. 4).

The northern region is dominated by the Great Barrier Reef, and the depths of the shelf break in this area are relatively shallow. Evidence from boreholes on the fringing reef of Hayman Island (Marshall, 1975) indicates that recolonisation of the reefs during the Holocene transgression began at about 8 500 yr B.P. Since that time there was vertical growth of reefs until sea level stabilised at about 6000 yr B.P. (Thom & Chappell, 1975), after which the reefs began to grow laterally. Probably most of the superficial carbonate sediments present on the outer shelf in this area have been deposited since this time, and therefore they represent an essentially modern facies. C^{14} ages of foraminifera in the southern part of the Barrier Reef (Maxwell, 1969) confirm this assumption. Areas of relict sediments are present at the southern end of the Barrier Reef, and these are related to times of lower sea level on the deeper parts of the shelf (Maxwell, 1968; Veeh & Veevers, 1970; Marshall, 1977).

South of Fraser Island to 36°S the outer shelf is dominated by relict sediments. On the outer shelf between Fraser Island and Brisbane there is a discontinuous line of algal banks, predominantly of encrusting red algae, generally in water depths of 60-100 m (Fig. 4). Some of the larger banks are terraced, and the depth and iron-staining of the algal material is suggestive of a relict facies. Farther south the outer shelf carbonate sands are strongly iron-stained. Offshore from Sydney and extending to 36°S there is an appreciable amount of quartz sand in the outer shelf sediments, as well as iron-staining of the carbonate material. These relict carbonate sands are present on the outer shelf between 130-200 m. The presence of a relict facies on this part of the shelf is confirmed by C^{14} ages on beachrock at a depth of 128 m (Phipps, 1970) which give pre-Holocene ages (Fig. 4).

The outer shelf in the eastern part of Bass Strait and around Tasmania is covered by a mixed facies containing both modern and relict skeletal carbonate, mainly Bryozoa. Forests of living Bryozoa are present

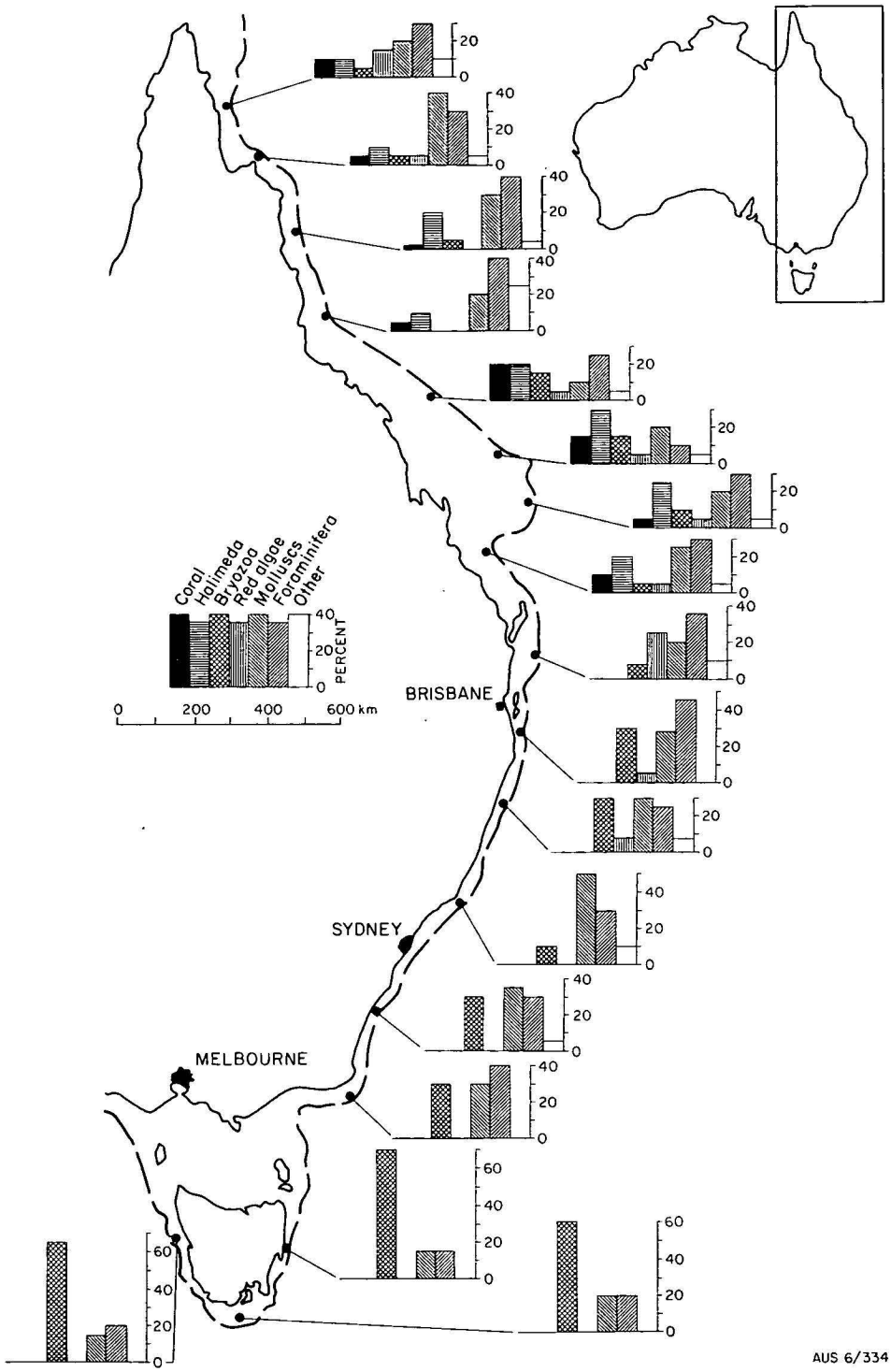

Figure 3. Histograms showing the type of skeletal carbonate variation on the outer continental shelf, eastern Australia.

on the outer shelf, and material from this source is continually being added to the surrounding relict sediments.

Effects of temperature and salinity on the skeletal carbonate variation of the east Australian shelf

Lees (1975) postulated that the distribution of shelf carbonate grain associations could be predicted on the basis of maximum and minimum values of surface sea temperature and salinity. By constructing Salinity Temperature Annual Range (STAR) diagrams, in which maximum temperature is plotted against minimum salinity, and minimum temperature against maximum salinity, Lees was able to draw boundaries between the various associations (Fig. 5). One of the rules he put forward was that if a point falls into the foramol field (lower class) on one graph, but into the chlorozoan field (higher class) on the other graph, then the lower one (i.e., foramol) is correct. Other associations delineated by the STAR diagrams, but not used here are

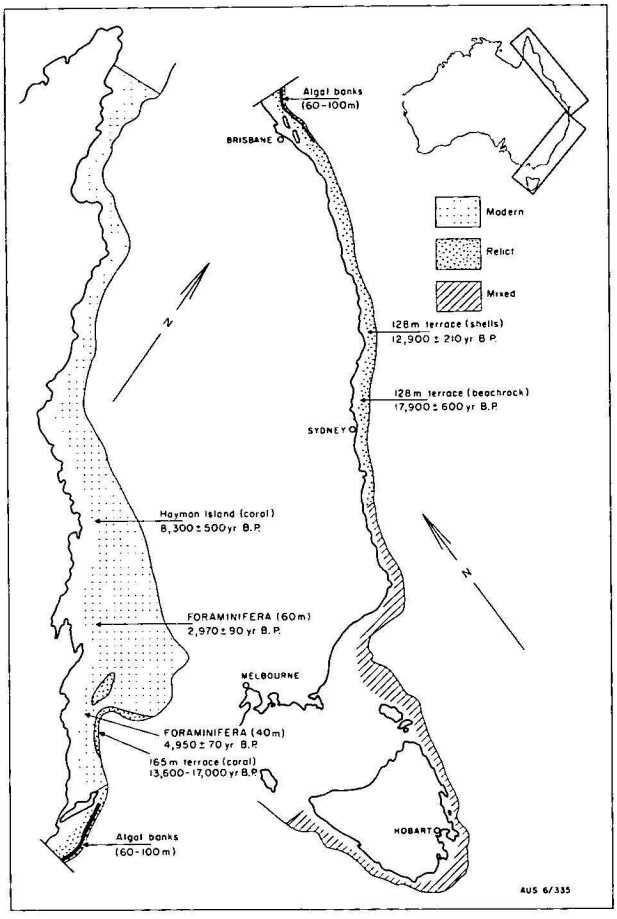

Figure 4. Distribution of modern, relict, and mixed sediments on the outer continental shelf.

chloralgal, which includes sediments containing calcareous green algae but no corals, and an overlapping *extended chlorozoan* which includes corals, in areas of high salinity such as the Persian Gulf and the Red Sea. Both these associations generally have a restricted geographical distribution; most shelf carbonates fall into the chlorozoan or foramol fields.

Sea surface temperatures on the east Australian continental shelf vary from 31.5°C to 10.5°C. The waters of the Great Barrier Reef range in temperature from 31.5°C to 19.8°C (annual range). The optimum temperature for coral growth is within the range 25°-29°C, but hermatypic corals can survive a minimum temperature of 16°-17°C (Wells, 1957). The average annual temperature for Barrier Reef water is approximately 25.4°C.

South of the Barrier Reef there is a gradual cooling of the surface water with increasing latitude. Between Brisbane and Hobart there is a decrease in temperature of some 10°C. Coldest water is present on the shelf around Tasmania and in Bass Strait, where surface temperatures during winter are in the range 10.9° to 12.6°C.

The salinity over the northern part of the shelf (north of 20°S) varies seasonally. This is largely a result of the high rainfall during the summer monsoon season. During spring and early summer salinity is greatest on the inner shelf and decreases seawards to the shelf edge reefs. At the end of the monsoon the trend is reversed and lower salinity water is present nearshore (Brandon, 1973). On this part of the shelf salinities range from 31.3 to 36.0‰.

From 20°S to as far south as Tasmania the waters of the continental shelf have only a small salinity variation. The variation in mean annual salinity between 22° and 44°S is 35.01-35.62‰.

Figure 5 shows the values of salinity/temperature maxima and minima for the east Australian shelf, and the type of assemblage present for each degree of latitude. In Figure 5a six of the foramol points plot within the chlorozoan field, and one chlorozoan point plots within the foramol field. The six foramol points are from latitudes 25° to 30°S, and the one chlorozoan point is from 17°S. In Figure 5b only three of the foramol points plot within the chlorozoan field; these represent latitudes 25°-27°S. Using Lees' criteria the predicted boundary between the chlorozoan and foramol assemblages is at 27°S, whereas the actual boundary from the known skeletal distribution is at 24°S.

This discrepancy between the predicted and the actual assemblages can be explained by the presence of relict sediments on the outer continental shelf south of 25°S (Fig. 4). From the available C^{14} dates on the outer shelf it would appear that carbonate sediments deeper than 130 m were deposited during the last glaciation. Reconstruction of sea-surface temperatures at 18 000 yr B.P. by CLIMAP project members (1976) suggests that the surface water temperature was about 2°C colder at about 25°S than it is now. So the foramol assemblage for latitudes 25°-27°S within the chlorozoan field in Figure 5b would shift into the foramol field.

The chlorozoan assemblage at 17°S, which plots in the foramol field in Figure 5a, can be explained by the very low salinities present on this part of the shelf during the monsoon season. Reef development at this latitude is not as profuse as to the north and south, presumably a direct cause of the low salinity. However, for two-thirds of the year salinities on this part of the shelf are greater than 32‰ and the skeletal assemblage is rightly chlorozoan.

Therefore, taking into account the relict nature of the outer shelf sediments between 25°-27°S, and the specialised conditions that occur on certain parts of the shelf, the observed distribution of the foramol and chlorozoan assemblage agree with Lees' predicted distribution. However, while salinity variations are obvious in Figure 5a it is apparent that for maximum salinities, as shown in Figure 5b, there is little variation along the entire length of the shelf. In this case it is only temperature that appears to be a controlling factor. This suggests that salinity only becomes an important factor influencing the type of skeletal carbonate produced at extreme values, rather than at the normal sea water salinity values that exist on most continental shelves.

Acknowledgements

We would like to thank D. Rochford and R. Edwards of CSIRO Division of Fisheries and Oceanography for providing us with temperature and salinity data for the east Australian shelf. Drs. H. A. Jones and G. C. Wilford, and Associate Professor C. V. G. Phipps, reviewed the manuscript and offered critical suggestions.

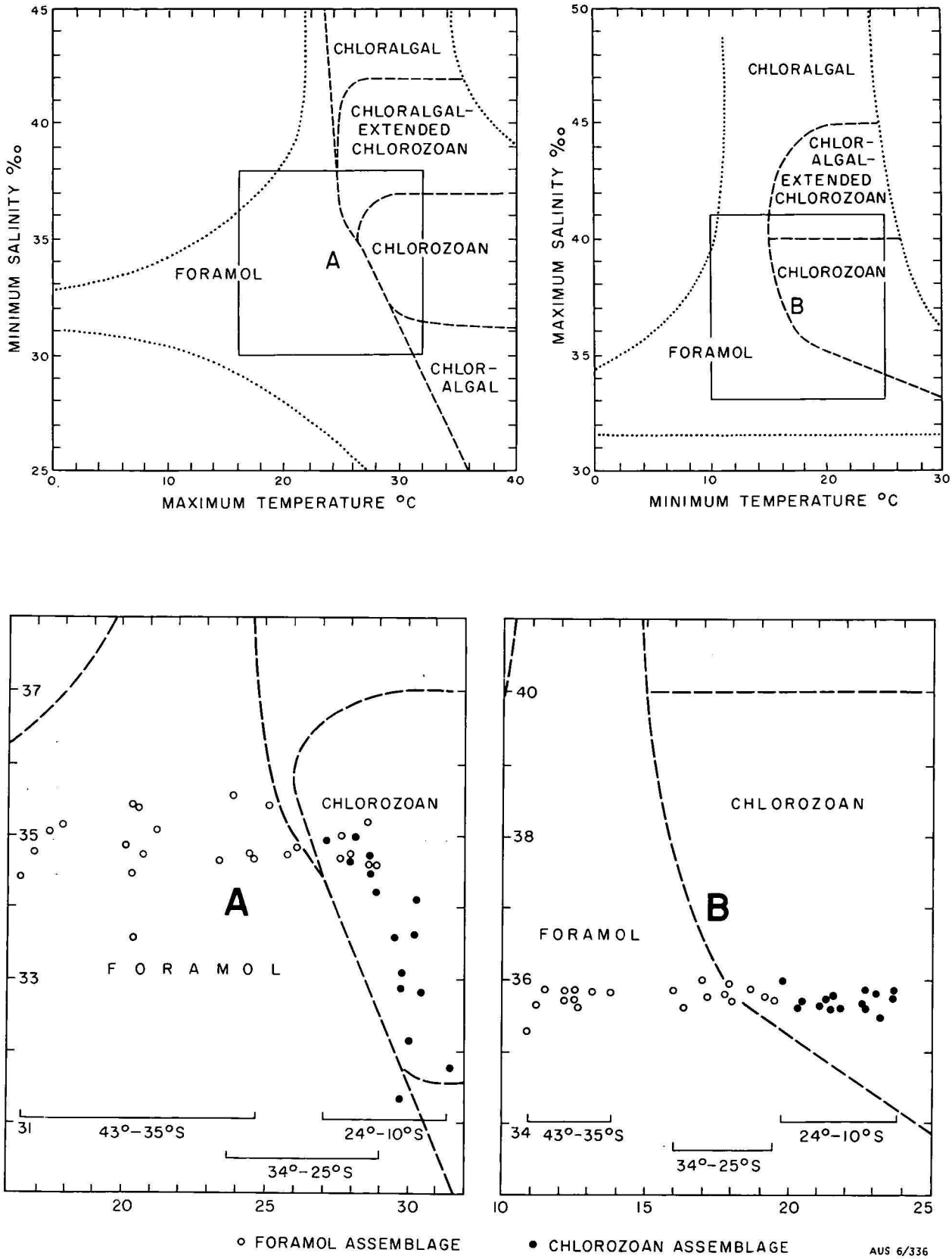

Figure 5. STAR diagrams (after Lees, 1975) showing fields A and B where the type of assemblage for the east Australian Shelf has been plotted for each degree of latitude.

In the top diagram the dotted lines indicate the approximate limits of the grain associations found in present-day shelf seas while the dashed lines define the salinity/temperature fields occupied by the various associations.

References

BATHURST, R. G. C., 1975—CARBONATE SEDIMENTS AND THEIR DIAGENESIS (2nd Edition). *Elsevier, Amsterdam.*

BRANDON, D. E., 1973—Waters of the Great Barrier Reef Province. *In* JONES, O. A., & ENDEAN, R. (Editors), BIOLOGY AND GEOLOGY OF CORAL REEFS, **1**, Geology. *Academic Press, New York,* 187-232.

CHAVE, K. E., 1967—Recent carbonate sediments—an unconventional view. *Journal of Geological Education,* **15**, 200-4.

CLIMAP PROJECT MEMBERS, 1976—The surface of the Ice-Age Earth. *Science,* **191**, 1131-7.

CONOLLY, J. R., & VON DER BORCH, C. C., 1967—Sedimentation and physiography of the sea floor south of Australia. *Sedimentary Geology,* **1**, 181-220.

DAVIES, P. J., & MARSHALL, J. F., 1972—BMR marine geology cruise in the Tasman Sea and Bass Strait, 12.2.72 to 8.5.72. *Bureau of Mineral Resources, Australia, Record* **1972/93** (unpubl.).

DAVIES, P. J., & MARSHALL, J. F., 1973—BMR marine geology cruise in Bass Strait and Tasmanian waters—February to May, 1973. *Bureau of Mineral Resources, Australia, Record* **1973/134** (unpubl.).

GINSBURG, R. N., LLOYD, R. M., STOCKMAN, K. W., & MCCALLUM, J. S., 1963—Shallow water carbonate sediments. *In* HILL, M. N. (Editor), THE SEA. **3**. *Interscience, New York,* 554-82.

JONES, H. A., DAVIES, P. J., & MARSHALL, J. F., 1975—Origin of the shelf break off southeast Australia. *Journal of the Geological Society of Australia,* **22**, 71-8.

JONGSMA, D., & MARSHALL, J. F., 1971—BMR marine geology cruise in the southern Barrier Reef and northern Tasman Sea, 12.9.1970 to 14.12.1970. *Bureau of Mineral Resources, Australia, Record* **1971/17** (unpubl.).

LEES, A., 1975—Possible influence of salinity and temperature on modern shelf carbonate sedimentation. *Marine Geology,* **19**, 159-98.

LEES, A., & BULLER, A. T., 1972—Modern temperate-water and warm-water shelf carbonate sediments contrasted. *Marine Geology,* **13**, M67-73.

MARSHALL, J. F., 1975—Uranium-series dating of corals from the Southwest Pacific. *M.Sc. thesis, Australian National University, Canberra.*

MARSHALL, J. F., 1977—Marine geology of the Capricorn Channel area. *Bureau of Mineral Resources, Australia, Bulletin* **163**.

MAXWELL, W. G. H., 1968—ATLAS OF THE GREAT BARRIER REEF. *Elsevier, Amsterdam.*

MAXWELL, W. G. H., 1969—Radiocarbon ages of sediment: Great Barrier Reef. *Sedimentary Geology,* **3**, 331-3.

MAXWELL, W. G. H., 1973—Sediments of the Great Barrier Reef Province. *In* JONES, O. A., & ENDEAN, R. (Editors), BIOLOGY AND GEOLOGY OF CORAL REEFS, **1**. Geology. *Academic Press, New York,* 299-345.

MILLIMAN, J. D., 1972—Atlantic continental shelf and slope of the United States—petrology of the sand fraction of sediments, northern New Jersey to southern Florida. *United States Geological Survey Professional Paper,* **529-J**.

MILLIMAN, J. D., 1974—MARINE CARBONATES. *Springer-Verlag, Berlin.*

PHIPPS, C. V. G., 1970—Dating of eustatic events from cores taken in the Gulf of Carpentaria, and samples from the New South Wales continental shelf. *Australian Journal of Science,* **32**, 329-30.

THOM, B. G., & CHAPPELL, J., 1975—Holocene sea levels relative to Australia. *Search,* **6**, 90-3.

VEEH, H. H., & VEEVERS, J. J., 1970—Sea level at −175 m off the Great Barrier Reef 13 600 to 17 000 years ago. *Nature,* **226**, 536-7.

VERON, J., 1974—Southern geographic limits to the distribution of the Great Barrier Reef hermatypic corals. *Proceedings of the Second International Symposium Coral Reefs,* **1**, 465-73.

WASS, R. E., CONOLLY, J. R., & MACINTYRE, R. J., 1970—Bryozoan carbonate sand continuous along southern Australia. *Marine Geology,* **9**, 63-73.

WELLS, J. W., 1957—Corals. *In* HEDGPETH, J. (Editor), Treatise on Marine Ecology and Palaeoecology. **1**. Ecology. *Geological Society of America Memoir,* **67**, 1087-104.

Mathematical modelling of experimental systems simulating metal chelating in reducing sedimentary environments

J. R. Mooney[1], B. Bubela[2], James Ferguson, and R. O. Hallberg[3]

This paper discusses the mathematical modelling of laboratory controlled sedimentary systems that physically simulate organo-metal complex and metal sulphide formation in a reducing environment. The paper provides the general theoretical framework for modelling systems of this type. Further papers will describe specific models of specific laboratory-controlled sedimentary systems.

Techniques of modelling the following processes are described: sedimentation; supply of metal species (Cu(II) and Zn(II)); generation of H_2S and chelating agents in an organic-rich zone by bacterial action; diffusion of chemical species through the sediment; formation of metal sulphides and metal complexes, and the competition between these two processes. The diffusion and chemical interactions are represented by a set of linked partial differential equations and algebraic relationships.

Introduction

Stratabound orebodies are principal sources of copper, lead, and zinc. The main objectives of our research are to investigate the biological and abiological processes leading to such deposits, and to be able to recognise the environments of their deposition. We have approached the problem by using laboratory controlled sedimentary systems to clarify some of the processes involved (Bubela & McDonald, 1969; Lambert & Bubela, 1970; Bubela and others, 1975; Hallberg and others, in prep.). These experimental systems are intended to be physical simulations of natural sedimentary systems.

The purpose of this paper is to provide the theoretical framework and discuss the general principles of developing mathematical models of the experimental sedimentary system. The aim is to discuss the type of model that should be developed for such systems and the modelling techniques that should be used; and to clarify the concepts involved in modelling such systems and to elucidate the problems likely to be encountered. The development of mathematical models of experimental sedimentary systems is expected to increase our understanding of the important processes operating at the laboratory level and thus in turn to further our understanding of the basic processes leading to formation of orebodies in natural sediments.

As the program of experimental sedimentary systems at the Bass Becking Geobiological Laboratory proceeds specific mathematic models of these systems are being developed. The rate of progress is governed by the availability of suitable data for model validation. These specific models will be described in further papers. However, to motivate the theoretical discussion attention is focussed on the physical processes that operate in one particular laboratory system. This system is described in detail in a paper by Hallberg and others (1978) (Fig. 1). In simple terms it consists of a sedimentary column into which Cu(II) and Zn(II) are introduced from an overlying aqueous phase. The metals are at least partly complexed by organic matter present in the sediments, and are eventually deposited as metal sulphides by biologically produced H_2S. This system will be referred to as the basic system throughout the remainder of the paper. The data obtained from this experiment were not of a sufficiently detailed nature to warrant producing a specific mathematical model of this system: nothing further would have been elucidated beyond the qualitative conclusions presented in the paper (Hallberg and others, in prep.). In the further experimental work under way more detailed data will be obtained, especially data through time of time dependant processes, which will provide a secure basis for validation of the mathematical models being developed.

The principal processes that operate in the basic sedimentary system are first outlined in this paper. These processes provide a focus for the ensuing discussion, which considers techniques of modelling these processes in a general theoretical framework. Thereafter the modelling of more complex sedimentary systems is considered, extending beyond the basic system. This section also contains a discussion of certain mathematical problems that can arise in modelling these systems, and possible remedies.

Principal processes in the basic system

The basic sedimentary system is made up of (i) a supernatant brine, with sedimentary matter in suspension, (ii) a zone of sediment accumulating at a controlled rate, and (iii) an underlying fixed zone of organic-rich material (decaying algae) (see Fig. 1). The experiment is thermostatically controlled at 22°C (Hallberg and others, 1978). The system has a fixed circular cross-section, and is of uniform composition within every horizontal layer. The sedimentary material is introduced into the supernatant at a controlled rate and is of known density, chemical composition, and particle size, and forms an aqueous sediment of known void ratio ϕ (= true volume liquid/total volume).

The sedimentary material includes a proportion of dead bacteria which, together with the organic-rich algal zone, is considered to serve as a source of unknown organic species, which can form complexes with metal species. The organic-rich zone also serves as a source of H_2S produced by the sulphate-reducing bacteria. The H_2S generated diffuses upwards through the sedimentary column. The supernatant may be aerated, if required, and when aerated is essentially a homogeneous aerobic liquid phase. The H_2S is removed at the supernatant-sediment interface by aerial oxida-

1. Division of Computing Research, CSIRO, Canberra, Australia.
2. Baas Becking Geobiological Laboratory, P.O. Box 378, CSIRO, Canberra, Australia.
3. University of Stockholm, Stockholm, Sweden.

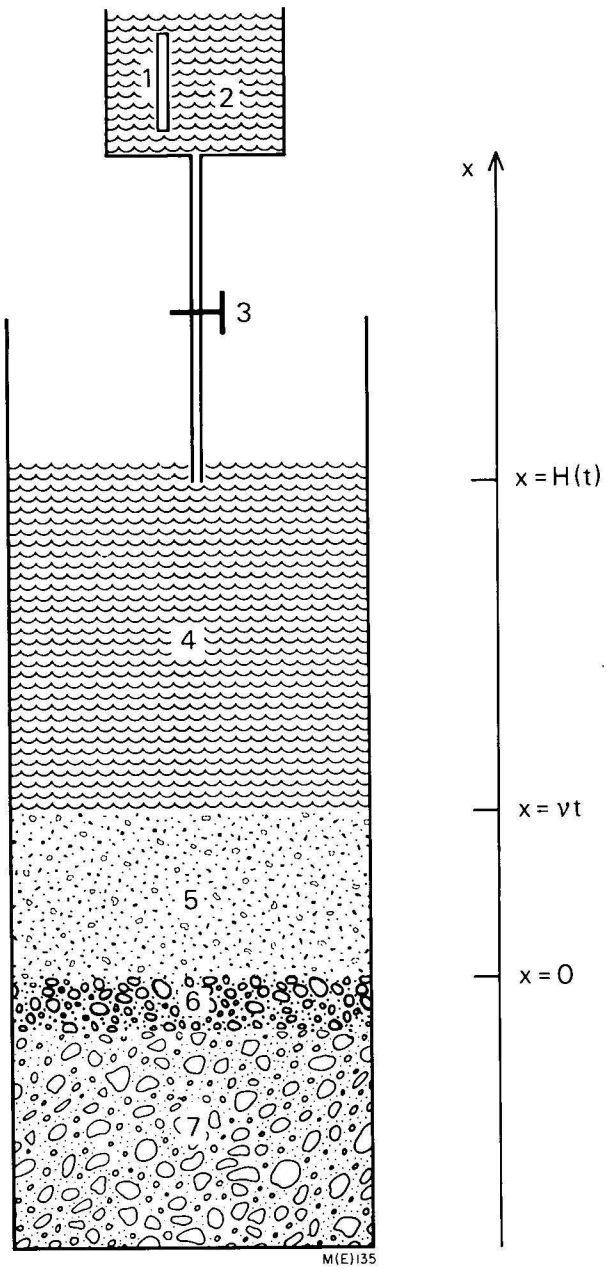

Figure 1. Schematic representation of basic sedimentary system considered in this paper. 1. source of metals; 2. liquid reservoir; 3. valve; 4. aqueous supernatant; 5. sediments; 6. decaying organic material; 7. sediments. Arrowline represents the spatial axis.

tion back to sulphate. When the supernatant is not aerated it becomes anaerobic owing to diffusion of H_2S from the sediment below.

Cu(II) and Zn(II) salts are introduced into the supernatant by diffusion from a dialysis bag. Experiments suggest (Hallberg and others, 1978) that in the absence of dissolved organic complexing agents the metals are virtually completely adsorbed on the suspended sediment particles in the supernatant, either as free metal ions or inorganic complexes. As the sediment particles settle out they carry with them the adsorbed metal species.

There is experimental evidence (Hallberg, 1972, 1974a, b; Hallberg and others, 1978) that Cu(II) forms stable species in solution in the sedimentary system. In the presence of H_2S these species are resistant to adsorption on the sediment particles or precipitation as CuS (in the sense that the total dissolved Cu(II) concentration greatly exceeds $[Cu^{+2}]$ as predicted from the solubility product of CuS). Zn(II) probably also forms such species but they appear to be less stable. These stable soluble species appear to be complexes formed with organic decay products in the system arising from the organic-rich zone and the dead bacteria in the sediment.

At the start of sedimentation the decay of the organic matter is well advanced, and a supply of organic complexing agents is assured. These diffuse upwards into the sedimentary column and, eventually, into the supernatant as well. The bacteria incorporated in the sedimentary material decompose partly in suspension in the supernatant, and partly after incorporation in the growing sediment. This provides an additional source of organic complexing agents.

Experimental conditions are such that the whole sedimentary core is anaerobic with excess H_2S, the redoxcline being maintained at (or above) the sediment-supernatant interface. There is a large excess of H_2S and organic complexing agents over total Zn(II) and Cu(II) concentrations. There is competition throughout the sedimentary column between formation of the insoluble metal sulphides CuS and ZnS by reaction with H_2S, and formation of organo-metal complexes by reaction with organic complexing agents. The organo-metal complexes are soluble and so can undergo transport by diffusion. The different stabilities of the organo-metal complexes relative to the metal sulphides, together with diffusion regimes of the complexes, allow significantly different stratification patterns of Cu and Zn to occur.

Mathematical modelling of the basic sedimentary system

Geometry of the basic sedimentary system

The basic system is essentially cylindrical. For the purposes of mathematic modelling it can be treated as a system of one spatial dimension: all significant quantities (state variables) are thus essentially functions of two variables, the vertical distance, x, through the sedimentary core (measured upwards with $x = 0$ at the interface between the sedimentary column and the organic-rich zone) and time, t. $t = 0$ at the commencement of sedimentation. The sediment-supernatant is a moving boundary $X = \nu t$, where ν is the velocity of sedimentation, a constant. (At $t = 0$, $X = 0$.)

The supernatant is best regarded as a separate compartment of the same cross-section, A, and with total volume a known function of time, V(t). (In the usual experimental set-up the volume increases at a constant rate owing to controlled input of sedimentary slurry, but minus the rate of volume increase of the compacting sediment.) The volume of the supernatant is important in that it dictates changes in concentration of a species due to addition or subtraction of mass. The initial chemical composition of the supernatant is also important; it prescribes the initial concentrations of various species, and also dictates the chemical composition of the interstitial water of the sediment as it forms.

One of the major processes to be modelled mathematically is the diffusion of various soluble chemical species through the interstitial water of the sedimentary core. Let w be the concentration of chemical species

"W" in some consistent units. If W undergoes diffusion through the sediment, then w(x, t) obeys the diffusion equation:

$$\frac{\partial w}{\partial t} = D_{sed} \frac{\partial^2 w}{\partial x^2} \quad \text{..... (1)}$$

where D_{sed} is the apparent diffusion coefficient, regarding the diffusion as taking place through a uniform sediment-water phase. In equation (1) it is assumed that D_{sed} does not vary with depth—this is valid for the experimental sedimentary system because the maximum depth of sediment is not large ($\lesssim 100$ cm). D_{sed} is dependent on the temperature of the system. D_{sed} can be related to the true diffusion coefficient D through water as follows (Saxena and others, 1974):

$$D_{sed} = \frac{\phi f}{\tau} D \quad \text{..... (2)}$$

where ϕ is the void ratio, f is a friction factor ($0 < f \leq 1$), and τ is the tortuosity factor ($\tau \geq 1$). ϕ is known. τ allows for the longer path lengths of the diffusing molecules that bypass the sediment particles. For uniform close-packed spheres τ is 2: τ is less than 2 for less than close-packed spheres. A reasonable estimate of τ for the given sediment can probably be made. The friction factor f is dependent on the nature of the sediment particles and the liquid pore size. However, experiments suggest (Saxena and others, 1974) that the frictional effect (apparently caused by viscous drag against the surfaces of the sediment particles) is negligible when the pore sizes are > 8 μm. The sediment particle sizes in the sedimentary systems of interest are > 50 μm, and so for the model f can be taken as unity.

Generation of H_2S

Free H_2S is present in the sedimentary system in the three forms H_2S, HS^-, and S^{-2}. The proportion of each is governed by the pH. The pH of the experimental sedimentary systems is usually in the range 8 to 9, and HS^- is the dominant form. For the purposes of modelling it is convenient to treat the free sulphide species as a single composite entity 'S_T' with a single diffusion coefficient and equivalent solubility products K_q^1, K_q^2 for CuS, ZnS respectively. Defining $[S_T] = [H_2S] + [HS^-]$ (for $pH < 11$ $[S^{-2}]$ is negligible) it can readily be shown that

$$[Cu^{+2}][S_T] = K_q^1 \quad \text{..... (3)}$$

where

$$K_q^1 = \frac{h(h + Ka_1)}{Ka_1 \, Ka_2} K^1_{sp} \quad \text{..... (4)}$$

where $h = [H^+]$, Ka_1, Ka_2 are the first and second acidity constants of H_2S respectively, and K^1_{sp} is the solubility product of CuS as normally defined. Thus equation (4) defines K^1_q in terms of K^1_{sp}. K^1_q is pH dependent, and is dependent on temperature because Ka_1, Ka_2 and K^1_{sp} are themselves temperature dependent. K^2_q is similarly related to K^2_{sp}, and the same remarks apply.

For H_2S there are three processes to model: generation of S_T in the organic-rich zone, diffusion of S_T through the sediment, and removal of S_T at the sediment-supernatant interface by dispersion and aeration (aerated supernatant). The diffusion equation for S_T must be solved:

$$\frac{\partial [S_T]}{\partial t} = D_{sed} \frac{\partial^2 [S_T]}{\partial x^2}, \quad 0 \leq x \leq X = vt \quad \text{..... (5)}$$

where $[S_T]$ is measured in any consistent units (e.g. mole per litre of interstitial water) and D_{sed} is the apparent diffusion coefficient. The rate of generation of H_2S in the organic-rich zone dictates the boundary condition for equation (5) at $x = o$. The simplest treatment is to assume that the generation process maintains a steady concentration of S_T: this implies the simple boundary condition:

$$[S_T] = [S_T]_o \text{ at } x = 0 \quad \text{..... (6)}$$

A more realistic treatment is to model the bacterial sulphate reduction process along the lines of Ramm & Bella (1974). They used a modified Michaelis-Menten equation to describe the rate of production of H_2S as a function of soluble carbon concentration and sulphate concentration. The rate of sulphate reduction is of course also dependent on temperature. A model of this type could be readily adapted. However, in our basic system there is a high concentration of SO_4^{-2} in the interstitial brine ($\gtrsim 1.4\%$ w/v—see Ferguson and others, 1975), and so the rate of production of H_2S is limited by the metabolic activity of bacteria and not by the supply of SO_4^{-2}. SO_4^{-2} becomes non-limiting for $[SO_4^{-2}] \gtrsim 3000$ ppm (Ramm & Bella, 1974). Thus supply and diffusion of SO_4^{-2} is not relevant to the mathematical model. A boundary condition of the following type would be imposed:

$$\text{upward flux } S_T = -D_{sed}\left(\frac{\partial [S_T]}{\partial x}\right)_{x=0} = \text{given function} \quad \text{..... (7)}$$

When the supernatant is aerated the concentration of S_T therein is very small, and can be taken as zero. This provides the upper boundary condition. The diffusion equation with these upper and lower boundary conditions can be solved by standard numerical procedures. The upper boundary condition is to be imposed at a moving boundary ($X = vt$), which makes the problem more complicated than normal.

In the case where the supernatant is not aerated, the solution of the diffusion equation must be carried through into the supernatant as well, where of course the true diffusion coefficient applies. At $x = X$ (supernatant-sediment interface) there is a jump discontinuity in the diffusion coefficient. The proper boundary condition to impose is that of continuity of mass flux (Carslaw & Jaeger, 1959), and this can be shown by virtue of relationship (2) to require that

$$\left(\frac{\partial [S_T]}{\partial x}\right)_{x = X+} = \frac{\phi^2 f}{\tau} \left(\frac{\partial [S_T]}{\partial x}\right)_{x = X-} \quad \text{..... (8)}$$

Thus at the (moving) interface there is a jump discontinuity in the gradient of $[S_T]$ (here $[S_T]$ on both sides of the interface is in terms of mass per unit volume of liquid). The concentration $[S_T]$ is itself continuous across the interface. If $x = H(t)$ is the top of the supernatant, the appropriate boundary condition is the zero flux condition:

$$\left(\frac{\partial [S_T]}{\partial x}\right)_{x = H} = 0 \quad \text{..... (9)}$$

Solution of the diffusion equation over the range $0 \leq x \leq H(t)$ should present no difficulties.

The most significant aspect of the diffusion of S_T is the sweep of its diffusion wave upwards through the sedimentary column, i.e. the passage of the broad front over which $[S_T]$ increases sharply. As this front passes up the sediment adsorbed Cu(II) and Zn(II) are converted to solid CuS and ZnS. This is a solid-to-solid transformation which does not involve mass transport of the metals. On the other hand some Cu(II) and Zn(II) may be present in solution in the interstitial water as complexes resulting from the prior

passage of organic complexing agents. The H_2S will substantially reprecipitate most of the Cu(II) and Zn(II). However, in either case the total concentration of the metals are likely to be much less than the concentration of S_T (say $\leq$ 70 ppm as compared to 3000 ppm). Thus the formation of the metal sulphides will hardly deplete the free sulphide concentration. Thus effectively the diffusion equation for S_T can be solved independently of the metal concentration, and then the profiles of CuS, ZnS deduced as a second step. This simplifies the model mathematically. If $[S_T]$ were not so dominant over the metal concentrations the depletion of $[S_T]$ itself would have to be incorporated in the diffusion equation (5) by means of a 'sink' term on the right-hand side. The general problem of the mathematical representation of mutually interacting and diffusing species is discussed later.

Experimentally the diffusion profile of S_T can be monitored to some extent by measuring the redox potential (E_h) at various points in the system. For the half-cell reaction at a platinum electrode:

$$SO_4^{-2} + 9H^+ + 8e \rightleftharpoons HS^- + 4H_2O \quad \text{.....(10)}$$

$$E_h = E^\circ - 9pH - \frac{RT}{8F} \ln \frac{[HS^-]}{[SO_4^{-2}]} \quad \text{.....(11)}$$

where the usual thermodynamic symbols are used. Thus at any point where E_h is measured, the ratio of $[HS^-]$ to $[SO_4^{-2}]$ can be calculated. The E° value at the temperature of the system must be known: this is readily available in the literature. In practice equation (9) will only be approximately true, because the presence of organic material on or near the electrode may establish other redox reactions and so influence the potential.

Generation of the organic complexing agents

For the purposes of modelling the basic sedimentary system the hypothetical organic complexing agents are to be represented by a single unknown complexing species 'L'. The complexes 'CuL' and 'ZnL' are characterised by two (unknown) temperature-dependent stability constants, K^1_p, K^2_p respectively.

L is thought to arise from the decomposition of dead bacteria, primarily in the organic-rich zone. Experimentally the concentration of L can probably be correlated with observed concentrations of dissolved organic carbon. This may permit a simple but reasonable model for the rate of production of L to be developed. The diffusion of L upwards through the sedimentary column could then be modelled in a manner similar to that of H_2S with a lower boundary condition of the type (7). The upper boundary condition to be applied depends on whether the supernatant is aerated or not. If aerated the concentration in the supernatant is a function of time only. Mass balance requires the following boundary condition to be imposed at the supernatant-sediment interface (x = X):

$$\frac{d}{dt}\left(V(t)[L]_{x=X}\right) = \text{rate of generation of L in supernatant} - AD_{L\phi}\left(\frac{\partial[L]}{\partial x}\right)_{x=X^-} \quad \text{.....(12)}$$

(Here [L] is in mole per litre interstitial water.) The boundary condition allows for secondary generation of L in the supernatant from decomposition of the bacteria incorporated in the sedimentary material. A simple model for this can also probably be developed by correlating observed values of dissolved organic carbon in the supernatant against the known input of sedimentary material containing the bacteria. The secondary term on the right represents the flux of L across the interface (up or down). D_L is the (unknown) apparent diffusion coefficient of L, and is a parameter of the model to be determined (temperature dependent).

If the supernatant is not aerated the diffusion equation must be solved right through the supernatant and sediment. Boundary conditions of the type (8), (9) for H_2S must be used.

It may be that a significant amount of the dead bacteria incorporated in the sedimentary material does not decompose completely until after deposition in the sediment. In this case the diffusion equation for [L] in the sedimentary column must be modified to include a source term representing the rate of generation of L per unit time per unit length of core (discussed later).

Just as for H_2S, L is in considerable excess over the prevailing concentrations of Cu(II) and Zn(II). Thus again the diffusion equation for L (or diffusion-source equation) can be solved independently, and the interaction with the metal species worked out as a second step.

Solutions of the diffusion equation with the approximate boundary conditions are to be matched against experimental measures of the diffusion behaviour of L, monitored perhaps by concentrations of total soluble organic carbon. This should enable a determination of the diffusion coefficient of L. This may well throw light on the molecular weight M_L of L (probably really an 'average' molecular weight of different species). Knowledge of M_L is significant in the determination of the stability constants of CuL and ZnL, as discussed in the following section. For example, consider the following formula for the diffusion coefficient of spherical molecules (Daniels & Alberty, 1963):

$$D = \frac{RT}{N_0 6\pi\zeta} \cdot \left(\frac{4\pi N_0 \rho}{3M_L}\right)^{1/3} \quad \text{.....(13)}$$

Here R, T, N_0 have the usual thermodynamic meaning; D is the diffusion coefficient, ζ is the viscosity of the liquid medium, M_L is the molecular weight of the molecule, and ρ is the density of the condensed molecules (mass per unit volume). Thus given D, ζ, and ρ a value for M_L can be calculated. ζ is readily available, and ρ is not dependent on molecular weight and is likely to be roughly constant over series of macromolecules of similar type, e.g. proteins. Thus a fair estimate of M_L can probably be made. For non-spherical molecules formula (11) provides a maximum possible value of M_L. It may also be possible to derive other experimental indications of M_L.

Competition between metal sulphide and metal complex formation

The principal phenomenon to model is the equilibrium between CuS, ZnS, CuL, ZnL, L, and H_2S throughout the sediment. When the supernatant is not aerated it may become rich in H_2S, and the same equilibria will operate there as in the sediment.

Experimental evidence (Hallberg and others, 1978) suggests that only a small percentage (< 1%) of the Cu(II) and Zn(II) dissolves in the presence of excess H_2S. Thus the solid profiles of CuS and ZnS are hardly affected. However, there is evidence that L is also present in large excess. Clearly the quantities of CuL and ZnL that dissolve depend on the thermodynamic stabilities of the complexes relative to the

sulphides. Again experimental evidence shows that significantly more Cu(II) dissolves than Zn(II) (e.g. 0.31 ppm as compared to 0.01 ppm). Thus ZnL appears to be less stable relative to ZnS than CuL is to CuS. These ideas can be expressed quantitatively. K^1_p, K^2_p are the stability constants of CuL, ZnL, and the following equilibrium laws apply:

$$K^1_p = \frac{[CuL]}{[Cu^{+2}]\,[L]}\ ,\ K^2_p = \frac{[ZnL]}{[Zn^{+2}]\,[L]} \quad \text{..... (14)}$$

Here all concentrations are in mole per litre of interstitial water. Equations (14) are the mathematical expression of the fundamental hypothesis that a complexing species L exists and forms the two complexes CuL, ZnL. The free metal ion concentrations are governed by $[S_T]$ and the apparent solubility products K^1_q, K^2_q of CuS, ZnS. Thus

$$K^1_q = [Cu^{+2}]\,[S_T]\ ,\ K^2_q = [Zn^{+2}]\,[S_T] \quad \text{..... (15)}$$

and

$$K^1_p = \frac{[S_T]\,[CuL]}{[L]}\,(K^1_q)^{-1},\ K^2_p = \frac{[S_T]\,[ZnL]}{[L]}\,(K^2_q)^{-1} \quad \text{..... (16)}$$

Equations (16) relate the stability of the L complex as measured by K_p to the stability of the sulphide as measured by $(K_q)^{-1}$. All the equilibrium constants are dependent on temperature.

For the evaluation of K^1_p, K^1_p from equations (16), [CuL] and [ZnL] can be measured directly. A fair estimate of $[S_T]$ can probably be made from E_h measurements. Similarly, a fair estimate of [L] can probably be made from measurements of total soluble organic carbon concentration—but this will be a figure in gram per litre, not mole per litre. This must be divided by the molecular weight M_L to obtain [L] in mole per litre. Thus in this sense K^1_p, K^2_p are strongly dependent on M_L. If M_L can be estimated independently, e.g. from knowledge of the diffusion coefficient of L, then fair estimates of K^1_p, K^2_p can probably be made. Otherwise the best that can be done is to evaluate equivalent stability constants defined by equations (16), but with [L] explicitly in g/l.

The equilibria described in equations (16) are established throughout the sedimentary column. In general [CuL] and [ZnL] are expected to vary down the column. Concentration gradients are thus established, and diffusion of the complexes will occur. However, because both H_2S and L are present in excess, their time-dependent profiles will dictate the time dependent profiles of CuL and ZnL via the equilibria relations (16). Thus the diffusion of CuL and ZnL through the sulphide-rich sediment does not have to be modelled directly, and the diffusion coefficients of these species are not significant parameters. Net transport of CuL and ZnL may result—but it is the indirect result of the profiles of L and H_2S and the equilibria set up.

There are two circumstances where the diffusion of CuL and ZnL may have to be modelled directly, and hence the diffusion coefficients would be significant parameters. (If the molecular weight of L is large one would expect the diffusion coefficients of CuL and ZnL to be close to that of L itself; a first approximation would be to regard them as equal.) Firstly, if significant amounts of L accumulate in the supernatant under aerobic conditions the metal species will dissolve, and direct diffusion of CuL and ZnL to the H_2S diffusion front will take place—where they will be largely re-precipitated as CuS and ZnS. This diffusion must be modelled directly. Secondly, it is possible that in the early stages of the sediment significant quantities of L may diffuse faster through the sediment than H_2S. Thus significant quantities of CuL and ZnL may be produced by dissolution of the adsorbed metal species, and undergo diffusion. They will later on be re-precipitated as sulphides when the H_2S diffusion front reaches them. The overall result is an in-sediment net transport of Cu(II) and Zn(II) which would have to be directly modelled. This second circumstance is perhaps not very likely to occur, as H_2S can be expected to diffuse faster than L, but of course the other factor is the rates of production of L and H_2S in the organic-rich zone.

In future work with systems similar to the basic system, observed differences in the ratios of dissolved Cu to Zn and solid-state Cu to Zn are to be attributed to the different stabilities of CuL and ZnL relative to CuS and ZnS. The different distributions of Cu and Zn must be explained by choosing appropriate values for K^1_p, K^2_p. If this is possible the primary hypothesis of a model of this type—expressed mathematically by equations (14)—is valid. If observed values are inconsistent with any reasonable values for K^1_p, K^2_p, such a model must be essentially incomplete. At that stage consideration would have to be given to modelling the formation of several different types of complexes, with appropriate additional stability constants.

The different stratification patterns of different metals that can arise in sedimentary systems is a key phenomenon: a major goal of our work of developing mathematical models of these systems is to understand the mechanisms responsible for this phenomenon.

More generalised sedimentary systems and models

This section contains a discussion of more general sedimentary systems than the type discussed so far. The implications of these extensions of the basic system for mathematical modelling are considered. This is followed by a discussion of the generalised diffusion-source equation, and special cases of it that can arise in practice: this equation encompasses most of the possible extensions of the basic system.

New components and properties that are possible in a sedimentary system include the following:

(i) additional metal ions Ca^{+2}, Mg^{+2}, Pb^{+2}, etc.;
(ii) additional significant inorganic components, e.g. CO_3^{-2};
(iii) variable temperature, e.g. diurnal variation; and/or variation of temperature with depth;
(iv) more complex geometry;
(v) horizontal and/or vertical water flow.

The implications for the mathematical model are as follows: (i) and (ii): new concentration terms must be incorporated as well as additional known constants, such as solubility products, and additional unknown quantities (parameters of the model), such as stability constants of, say, CaL, PbL. It might become necessary to model two or more unknown complexing agents L, L′. This will introduce new concentration terms and new model parameters.

(iii): Changes of temperature affect stability constants, electrode potentials, rates of chemical reactions and diffusion coefficients. Thus many of the 'constants' of the model become, indirectly, (known) functions of time if, for example, temperature follows a prescribed diurnal variation; or, indirectly, functions of

depth if the temperature varies with depth. Unknown parameters of the model may just have to be regarded as averages over the appropriate temperature range.

(iv): If the geometry of the system becomes more complex the model may become very complicated indeed. In the general case all significant variables are three-dimensional functions of space and also of time, possibly with complicated boundaries. The functional complexity of the system must be judiciously minimised for successful practical modelling.

(v): Superimposed flows of water through the system in horizontal and/or vertical directions may significantly complicate the model. If there is vertical water flow the diffusion-source equation for every concentration term must be enhanced by inclusion of an advection term to allow for transport of material owing to flow of the medium itself. In one spatial dimension (vertical) this does not complicate the equations very much, especially if the water flow is prescribed, i.e. not itself an unknown function. Horizontal water flow is harder to deal with in that now all concentrations in general will become functions of at least two spatial dimensions.

Most of the above extensions or complications to the basic sedimentary system can be encompassed by the following general mathematical model. The principal quantities to be determined as functions of position and time are the concentrations of the various chemical species: these are the state variables. The state variables all obey the standard diffusion-source equation:

$$\frac{\partial w}{\partial t} = \frac{\partial}{\partial x}\left(D_w \frac{\partial w}{\partial x}\right) + Q_w \qquad \text{(17)}$$

(here for species 'W'). $\frac{\partial w}{\partial t}$ represents the rate of increase of concentration of W at any point in the system. The first term on the right-hand side is the contribution to this arising from diffusion, D_w being the diffusion coefficient. The Q_w term represents the contribution from generation or disappearance caused by chemical reaction. The equation as written considers diffusion only along one direction—the x direction, i.e. vertical—and advection is ignored. The equation can readily be extended to include three dimensional diffusion and advection. However, this does not greatly alter the spirit of the remarks to follow. The equation as written allows for variation of D_w with depth.

There is an equation of type (17) for every concentration-state variable in the system. The set of such equations comprises the mathematical representation of the system, i.e. the model. The solution of the system equations through space and time, i.e. running the model, reveals the fate of the system as a consequence of the assumptions built into the model. If the model has adjustable parameters—as is usual—they must be set so the solutions of the system equations agree with experimental results. This validates the model. If no reasonable values of the parameters produce realistic results then the model must be inadequate and some of the mechanisms must be changed.

Solid-state quantities such as CuS do not undergo diffusion—such quantities obey an equation of type (17) with the diffusion term omitted. The Q term represents the rate of precipitation minus the rate of dissolution. To fully describe the system the set of system equations must be supplemented with the appropriate initial and boundary conditions. This conveniently also includes conditions of the type (12) for concentrations in the homogeneous (aerated) supernatant. Other auxiliary equations may have to be included: for example, prescribed temperature variation.

One of the fundamental steps in setting up the model is the correct prescription of the source terms (Q_w) for each species. Account must be taken of reversible and irreversible reactions. For the 'irreversible' reaction

$$CuL + H_2S \rightarrow CuS + L \qquad \text{(18)}$$

the rate could be modelled by the term

$$k_1\,[CuL]\,[S_T] \qquad \text{(19)}$$

This term would then appear in the Q terms for CuS and L, and would appear with a negative sign in the Q terms for CuL and S_T. The Q term for any species is the composite of rate expressions with correct signs for all reactions in which that species is involved. For the reversible reaction

$$Cu^{+2} + L \rightleftharpoons CuL \qquad \text{(20)}$$

the rates of the forward and reverse paths might be modelled as follows:

$$\text{forward:}\quad \text{rate} = R_+ = k_{2+}\,[Cu^{+2}]\,[L]$$

$$\text{reverse:}\quad \text{rate} = R_- = k_{2-}\,[CuL] \qquad \text{(21)}$$

The differential rate ($R_+ - R_-$) then appears in the Q term for CuL, and appears with opposite sign in the Q terms for $[Cu^{+2}]$ and L. If the reversible reactions are left to run by themselves with no other interfering reactions or diffusion processes an equilibrium will be established in which forward and reverse reactions rates are equal. This should lead to an equilibrium expression consistent with the equilibrium law: for example in (21) this requires that

$$K^1_p = \frac{[CuL]}{[Cu^{+2}]\,[L]} \quad \frac{k_{2+}}{k_{2-}} \qquad \text{(22)}$$

Thus in principle if all the rate expressions for all significant reaction pathways are known the system set of equations can be fully prescribed, and their solution carried out by standard numerical techniques.

Certain difficulties can arise in practice with the above generalised kinetic treatment of the chemical phenomena. Firstly, some of the reaction pathways may have unknown rate expressions. Then it is necessary to model each unknown reaction rate by some simple but plausible expression. Validation of this expression is then part of the validation of the whole model. It may be that the reaction rate of a particular pathway has little effect on the behaviour of the system as a whole—i.e., the reaction pathway is not a critical process. Reactions in solution are probably not difficult to model plausibly, but heterogeneous reactions can be expected to be harder to model. In these cases the rates of reaction may depend on such things as surface area of crystals precipitated.

A second difficulty that can arise is more subtle in nature. The problem arises with very fast irreversible reactions. If the rate expression is known as well as the corresponding rate constant (large), while the system equations are well-defined mathematically the equations may be difficult to solve with standard numerical techniques. Mathematically the system contains very fast 'responses' superimposed on much slower responses: e.g., a very rapid reaction taking place together with relatively slow diffusion. A set of equations with extreme ratios of response times is said to be 'stiff', and for such a set of equations the standard numerical techniques are liable to exhibit numerical instability. Some techniques are available that can

adequately solve stiff systems of equations—at some extra cost. Alternatively, it may be adequate to model the very fast reactions with dummy kinetic expressions that merely make the rate of reaction moderately fast compared to other processes in the system, such as diffusion (thus if D = 1 in suitable units and a rate constant is 10^{10}, the latter can be replaced by 10^3). It is physically plausible that such a procedure will give solutions of sufficient accuracy, because it is the slow processes that are dictating the system behaviour: the very fast reactions take place but it is not really important just how fast. The set of system equations with modified rate expressions should be straightforward to solve with standard numerical methods.

Some well known reactions have unknown rate laws simply because they are too fast to measure experimentally: for example, the reaction between Cu^{+2} ions and H_2S to precipitate CuS. Then, just as discussed above it is valid to model the rate of this reaction by some simple formula such as k $[Cu^{+2}]$ $[S_T]$, and choose k so that the reaction is merely moderately fast compared to other processes.

The problem of very fast reaction rates can occur with reversible reactions as well. If the equilibrium constant is large or small so that the equilibrium lies very largely to the right or left (say by more than 99%), then for the purposes of the model the reaction may as well be regarded as irreversible (to right or left) and dealt with as above, assuming a fast rate of reaction. Where necessary the concentrations of components present in very small amounts can be calculated from the appropriate equilibrium laws if the concentrations of the dominant species are known, as for example in the calculation of free $[Cu^{+2}]$ from $[H_2S]$ in the presence of solid CuS from equation (15). The overall behaviour of the system is dictated by the components present in dominating amounts, whether arising from inherent large differences in total masses in the system or as the result of chemical equilibria.

The case of a reversible reaction that at equilibrium contains significant proportions of components on both sides of the equation is different. Here both forward and reverse reactions are fast (if one is fast). In this situation the appropriate equilibrium law of mass action is always satisfied—the system adjusts very rapidly to transfers of mass arising from diffusion, or from slow chemical reactions; it is probably better to model the equilibrium directly as an algebraic relation that is always satisfied. In some circumstances it may be possible to regard the components participating in the equilibrium as a single composite entity [for example S_T for H_2S, HS^-, S^{-2}].

A third problem that can arise is that of the spatial distribution of solid precipitates. The problem is illustrated by the following example. Consider a sedimentary column with H_2S diffusing upwards from below, and Cu^{+2} downwards from above. In the case where H_2S is in large excess—as considered earlier—the precipitation of CuS is governed by the diffusion front of H_2S. The location of the diffusion front establishes the transient location of the precipitation zone. There is no real problem involved in modelling the spatial distribution of CuS and the time of its formation; similarly for a symmetrically equivalent system with Cu^{+2} in large excess. However, the intermediate case of comparable concentrations of Cu^{+2} and H_2S is more difficult. Clearly H_2S will diffuse upwards into the sediment, and Cu^{+2} downwards into the sediment. They will meet in the middle and CuS will precipitate out. A steady state will arise, in which CuS will steadily precipitate out, and H_2S and Cu^{+2} will continue to diffuse into the precipitation zone. However, the precise nature of the CuS profile is unclear. It is of course overall growing with time, but it may be sharply concentrated in the middle or fairly spread out. If certain simple—but unlikely—assumptions are made about the rate of precipitation of CuS the profile can be shown to the uniform, or nearly so. Experimentally the phenomenon of liesegang banding would be expected to occur. Such a phenomenon strongly suggests the formation of randomly distributed nucleation sites, each surrounded by local micro-diffusion regimes of Cu^{+2} and H_2S to supply the growth of CuS crystals (Berner, 1969; Bubela & McDonald, 1969). The formation and location of nucleation sites is perhaps very sensitive with respect to slight changes in such parameters as diffusion coefficients and chemical nature of the sediment particles (Bubela & McDonald, 1969). Such phenomena are very difficult to model mathematically. In developing a mathematical model of a sedimentary system such profiles of solid precipitates may simply have to be treated as uniform.

Acknowledgements

The Baas Becking Laboratory is supported by the Bureau of Mineral Resources, the Commonwealth Scientific and Industrial Research Organization, and the Australian Mineral Industries Research Association Limited. We thank Drs L. Warren and P. R. Benyon for their constructive criticism of the manuscript.

References

BERNER, R. A., 1969—Migration of iron and sulphur within anaerobic sediments during early diagenesis. *American Soil Science* **267**, 19-42.

BUBELA, B., & MCDONALD, J., 1969—Formation of banded sulphides: metal ion separation and precipitation by inorganic and microbial sulphide sources. *Nature*, **221**, 465-6.

BUBELA, B., FERGUSON, J., & DAVIES, P. J., 1975—Biological and abiological processes in simulated sedimentary systems. *Journal of the Geological Society of Australia*, **22**, 135-44.

CARSLAW, H. S., & JAEGER, J. C., 1959—CONDUCTION OF HEAT IN SOLIDS. *Oxford, Clarendon Press.*

DANIELS, F., & ALBERTY, R. A., 1963—PHYSICAL CHEMISTRY. 2nd edition. *J. Wiley & Sons, New York.*

FERGUSON, J., BUBELA, B., & DAVIES, P. J., 1975—Simulation of sedimentary ore-forming processes: concentrations of Pb and Zn from brines into organic and Fe-bearing carbonate sediments. *Geologische Rundschau*, **64**, 767-82.

HALLBERG, R. O., 1972—Sedimentary sulphide mineral formation—An energy circuit system approach. *Mineralium Deposita*, **7**, 189-201.

HALLBERG, R. O., 1974a—Metal distribution along a profile of an intertidal area. *Estuarine and Coastal Marine Sciences*, **2**, 153-70.

HALLBERG, R. O., 1974b—Paleoredox conditions in eastern Gotland basin during the recent centuries. *Mexentutkimuslait*, Julk **238**, 3-16.

HALLBERG, R. O., BUBELA, B., & FERGUSON, JAMES, in prep. —Simulation of metal chelating in two reducing sedimentary systems.

LAMBERT, I. B., & BUBELA, B., 1970—Banded sulphide ores. The experimental production of monomineralic sulphide bands in sediments. *Mineralium Deposita,* **5**, 97-102.

RAMM, A. E., & BELLA, D. A., 1974—Sulphide production in anaerobic microcosms. *Limnology and Oceanography,* **19**, 110-18.

SAXENA, S. K., BOERSMA, L., LINDSTROM, F. T., & YOUNG, S. L., 1974—Effect of pore size on diffusion coefficients in porous media. *Soil Science,* **117**, 80-6.

The late Cainozoic evolution of the Carpentaria Plains, North Queensland

K. G. Grimes[1] and H. F. Doutch[2]

The Pliocene to Holocene fluvial sediments of the Carpentaria Plains southeast of the Gulf of Carpentaria, Queensland have formed sandy and silty plains in fan settings to the east, and clayey and silty flood plains to the south. This paper proposes a geological and geomorphological history of development of the flood plains and fans of past and present river systems of the Gulf Country. The formation of the depositional plains began in Pliocene times with upwarping of the marginal parts of the Karumba Basin to create an erosional source area. The deposition was in five stages, separated by periods of stability or incision. These stages were affected by continuing movements in the southeast, Pleistocene eustacy, and by climatic changes —in particular by one or more periods of aridity. The younger fans are still accumulating locally. In the southern flood plains there is at present a balance between erosion and deposition. The lithofacies distribution within the southern flood plains was controlled by differences between the source areas and by the prior topography of the depositional area, which guided streams from the different source areas and prevented mixing of the different types of sediment.

Introduction

The Carpentaria Plains include the major area of alluvial plains bordering the Gulf of Carpentaria (Fig. 1); they formed during the last of three cycles in the development of the Cainozoic Karumba Basin (Doutch, 1976).

In this paper we discuss the nature and evolution of the depositional part of the Carpentaria Plains. A brief description of the physiography of the region appears below, followed by a summary of the first two cycles in the Cainozoic evolution of the Karumba Basin. The final Claraville Cycle, during which the depositional plains achieved their present form, is then discussed in detail. The nature and development of the fans to the east of the gulf is discussed separately from that of the southern plains, but in both areas a fivefold sequence of deposition can be recognised.

This paper is based mainly on the results of a geological mapping program carried out by a combined Bureau of Mineral Resources (BMR) and Geological Survey of Queensland (GSQ) party from 1969 to 1973. This work is the subject of unpublished progress reports by Doutch and others (1970, 1972, 1973) and Grimes (1974). The present paper brings together information from these reports, and new interpretations of some of the evidence. It provides a detailed background to the reviews of Doutch (1976), and Grimes (in prep. b). Earlier reports by the Land Research and Regional Survey Division of CSIRO (Perry and others, 1964; Twidale, 1966; Galloway and others, 1970), terrain analysis (Grant, 1968), and soil surveys (Isbell and others, 1968) have also provided a basis for this study. Waterbores and stratigraphic holes are a further source of information for the area, although some of the waterbore drillers logs are of poor quality. Smart and others (1975) provided an index of drill data for the area.

Regional physiography

The term Carpentaria Plains was first used by Twidale (1956), who applied it to most of the gulf country. He subdivided the Carpentaria Plains into eight physiographic units, some depositional, some erosional. Doutch and others (1970, 1972) revised some of the subdivisions, and extended the terminology to the north. Their units are used and further revised here (Fig. 1). This paper is concerned mainly with the Pliocene to Holocene *Depositional Plains* within Twidale's Carpentaria Plains, which consist of the Gilbert and Mitchell Fans and the Claraville, Millungera, Wondoola and Armraynald Plains (Fig. 1).

The physiographic units shown in Figure 1 are described in the relevant explanatory notes to the 1:250 000 geological sheets, and by Smart and others (in prep.). The Gilbert and Mitchell Fans are the most widespread of the fans. They were formed by floodout deposits of the Gilbert and Mitchell Rivers, where the streams flowed out of the uplands and spread out across the plains. Smaller fans occur between these, and to the north and south. These have also been named after the rivers from which they were derived (Fig. 1). The fans are composed of clayey, silty and sandy soils supporting an open to fairly dense low woodland. They slope gently (1 in 1800 on average) towards the coast.

The depositional plains to the south of the gulf fall into two distinctive groups. The open, almost treeless black soil Wondoola and Armraynald Plains have gentle northerly slopes of 1 in 2500. The Wondoola Plain forms a marked contrast with the densely timbered Claraville and Millungera Plains which lie to the east (Fig. 1). The latter are similar in many respects to the fan units, but with the exception of the Clara Fan they lack the fan-shaped depositional patterns. They have an average slope to the west and northwest of about 1 in 800. The Millungera Plain has a slope of 1 in 1300, which is intermediate between that of the Claraville and Wondoola Plains. It is distinguished from the Claraville Plain by the presence of many elongated black soil depressions and valleys within the otherwise sandy plain. These black soil areas, up to 2 km wide and 10 km long, appear to be windows in the sand sheet exposing the underlying clayey Wondoola Beds (Grimes, 1973).

Narrow lateritic plains occur as marginal strips between the depositional plains and the erosional areas from which the deposits were derived. These include the Holroyd, Croydon and Strathpark Plains in the east, and parts of the Cloncurry Plain to the southwest (Fig. 1). They are the little disturbed remnants of old land

1. Geological Survey of Queensland, Brisbane, Queensland.
2. Present address—ESCAP Secretariat, UN Building, Ragdamnerm Ave., Bangkok 2, Thailand.

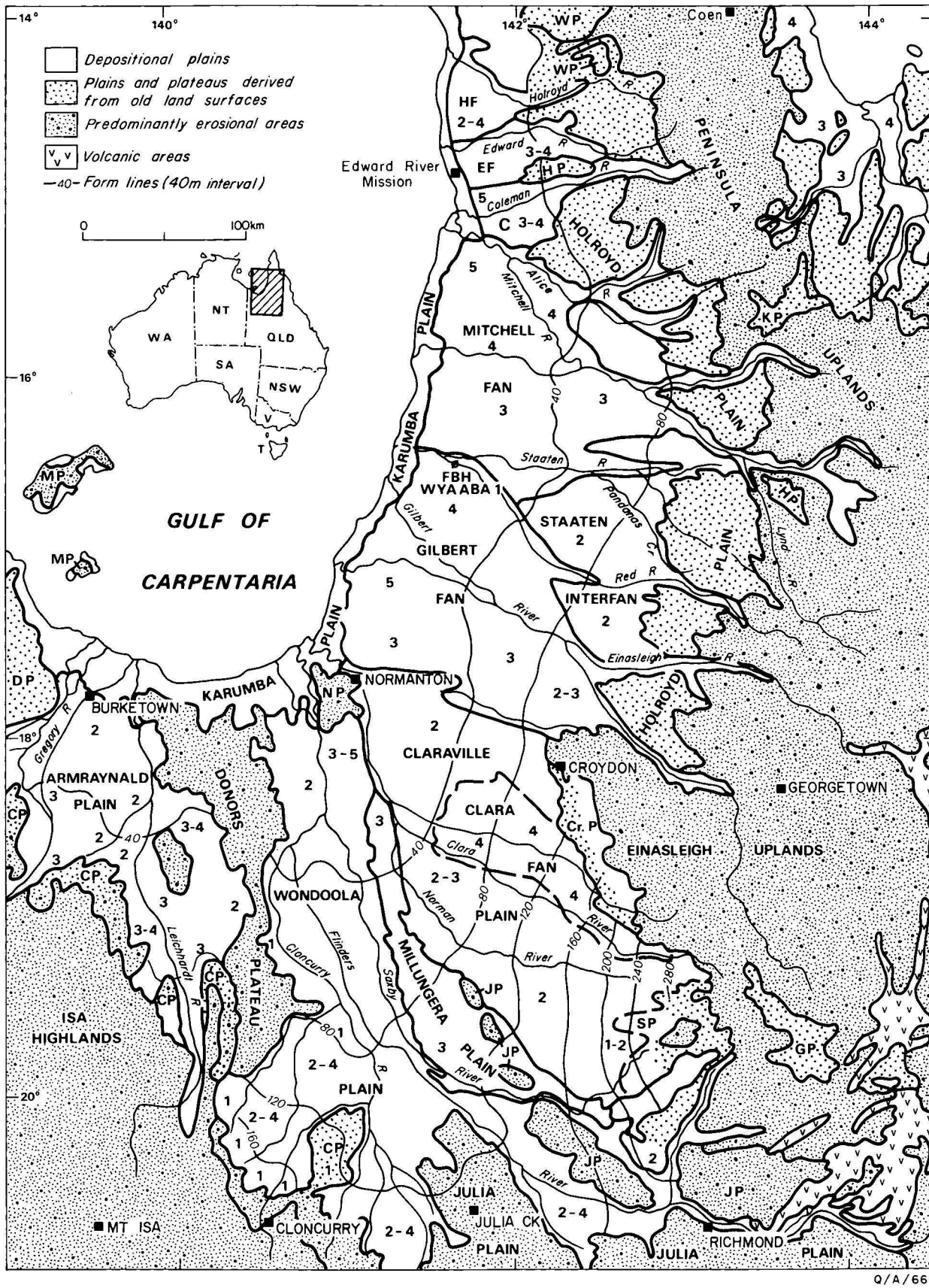

Figure 1. Locality map and physiographic units. Numerals indicate the depositional stages in any area, from oldest (1) to youngest (5).

CP, Cloncurry Plain; Cr P, Croydon Plain; DP, Doomadgee Plain; EF, Edward Fan; GP, Gilberton Plateau; HF, Holroyd Fan; HP, Holroyd Plain; JP, Julia Plain; KP, Kimba Plateau; MP, Mornington Plateau; NP, Normanton Plateau SP, Strathpark Plain; WP, Weipa Plateau.

surfaces; in particular, the early Pliocene Kendall Surface (Grimes, in prep. a).

The Peninsula and Einasleigh Uplands are active erosional areas. They range from gently undulating, through hilly, to in places strongly dissected terrain, developed on a wide range of rock types. The Isa Highlands are similar, but have a drier vegetation. The Donors and Normanton Plateaus are moderately dissected, duricrust-covered plateaus, but generally have a milder relief than the highlands. The Julia Plain in the south of the region is a gently undulating black soil peneplain developed on Mesozoic mudstones.

The Karumba Plain is a flat-lying coastal plain crossed at intervals by sandy beach ridges.

The predecessors of the plains: the Bulimba and Wyaaba Cycles

The depositional plains formed during the last of three Cainozoic cycles. Each cycle comprised an initial phase of active erosion and deposition followed by planation and stability (Grimes, in prep. a, b; Fig. 2). The deposits of the first, early Tertiary, Bulimba Cycle included the arkosic continental Bulimba Formation. Towards the end of that cycle a stable planation surface, the Aurukun Surface, developed and was deeply weathered (Doutch, 1976; Grimes, in prep. b). The second, Wyaaba Cycle commenced with warping in mid-Tertiary times. In the area to the northeast of Normanton the margins of the Karumba Basin were uplifted and the Gilbert-Mitchell Trough downwarped.

Deposition of the *Wyaaba Beds* began onshore in the Gilbert-Mitchell Trough in the Miocene (Doutch, 1976; Grimes, in prep. b). Both the Wyaaba Beds and the Bulimba Formation are commonly mottled and weathered throughout, suggesting that a warm climate prevailed, with alternating wet and dry seasons similar to that experienced in the region at present.

The source areas in Wyaaba times were similar to those of the present cycle. Sediments were derived from the Isa and Einasleigh Uplands of the time, and from the Mesozoic outcrops in the southern part of the basin. Drainage patterns were also similar. For instance, ancient channels in the Gilberton Plateau, which were eventually choked by sediment as the cycle drew to a close, followed a similar course to the present Gilbert River; the present valley of the upper Mitchell River was probably first hollowed out in these times.

Deposition of the Wyaaba Beds ended with the attainment of a stable planation state in early Pliocene times. Doutch considers the process to have been basically that of pediplanation. When the stable state was achieved, both the erosional and depositional plains were deeply weathered to form the Kendall Surface. This surface forms much of the Holroyd, Croydon, and Strathpark Plains (Fig. 1). The development of the Kendall Surface was terminated by renewed uplift of the Einasleigh and Peninsula Uplands in the mid-Pliocene.

Development of the plains: the Claraville Cycle

The present phase of erosion and deposition, the Claraville Cycle, began in the late Pliocene after upwarping of the margins of the Karumba Basin. The main source of sediments was apparently the uplifted Einasleigh Uplands, but the Isa Highlands may also have suffered some upwarping, and the more subdued terrain of the Donors & Normanton Plateau (at that time a continuous unit) together with the area now occupied by the Julia Plain, would also have provided sediment.

The main earth movements were in the Einasleigh Uplands. The southeastern headwaters of the Gilbert River had been destroyed by the block faulting and tilting that shaped the Gilberton Plateau (cf. Doutch and others, 1970). This was apparently associated with basaltic volcanism immediately to the east.

Since then, sporadic tectonism has continued in the upland areas. This activity is indicated by further bouts of basaltic volcanism, the youngest basalts being about 50 000 years old (Wyatt & Webb, 1970; Griffin & McDougall, 1975). Depositional stages during the Claraville Cycle may have been in part a response to this mild tectonism, which probably reflected the Pliocene-Holocene orogeny in New Guinea (Doutch, 1976). However, the fans themselves display no obvious signs of dislocation, although some lineaments on ERTS 1 imagery, which cut across drainage lines in the fans, appear to reflect basement structure (Simpson, 1973; Doutch, 1977). A number of eustatic fluctuations in sea level, and of related climatic changes, occurred during the Pleistocene (Bloom and others, 1974; Webster & Streten, 1972) and these would also have influenced the development of this cycle.

The evolution of the Gilbert and Mitchell Fans

Surface details of the Gilbert and Mitchell Fans are shown in Figure 3, together with smaller fan-like plains to the north discussed by Grimes (1977). The 1:1 000 000 geological map (Smart and others, 1977, in prep.) shows these features in greater detail than does Figure 3.

The BMR-GSQ 1:250 000 maps suggest that the fans are predominantly sandy. Drilling (Warner, 1968) showed that silty clay was the main lithology into which the bores spudded, though sand was common if not predominant in the top 30 m. Reconnaissance soil mapping by Isbell and others (1968) indicates that the fans are mainly loams and clays containing local linear sand bodies derived from the old stream channels and levees.

The sequence of deposition of the elements of the fans has been established mainly from photomosaics, ERTS 1 imagery, and geological and soil maps, and noting on them crosscutting relationships of the old channel deposits and related alluvia, the relative degrees of preservation of such features, and the relationships between the fans, beach ridges, and stream rejuvenations (Grimes, 1977; Grimes & Whitaker, 1977; Needham & Doutch, 1973a & b; Simpson, 1973; and Smart & Bain, 1977).

Lithology has not been used as a criterion because the differences in gross lithology between the fan elements is much less than the variations within any one unit.

The history of evolution of the fans is illustrated in Figures 4, 6. The individual fan elements are designated in the figures and text by letter symbols based on the initial letters of their parent rivers, followed by numerical subscripts which indicate the stage of development postulated, e.g. M_2 is a part of the Mitchell Fan deposited during Stage 2.

Stage 1. Stage 1 erosion of the uplands and the Kendall Surface resulted in fan deposition to the west. These Stage 1 deposits eventually built back up the erosional valleys (Fig. 4A); they are now best seen as terraces in the major valleys of the Holroyd Plain, and as the uppermost parts of the Etheridge and Red River Fans (Fig. 3, E, R). Elsewhere they have been either removed by erosion or buried by the younger fans.

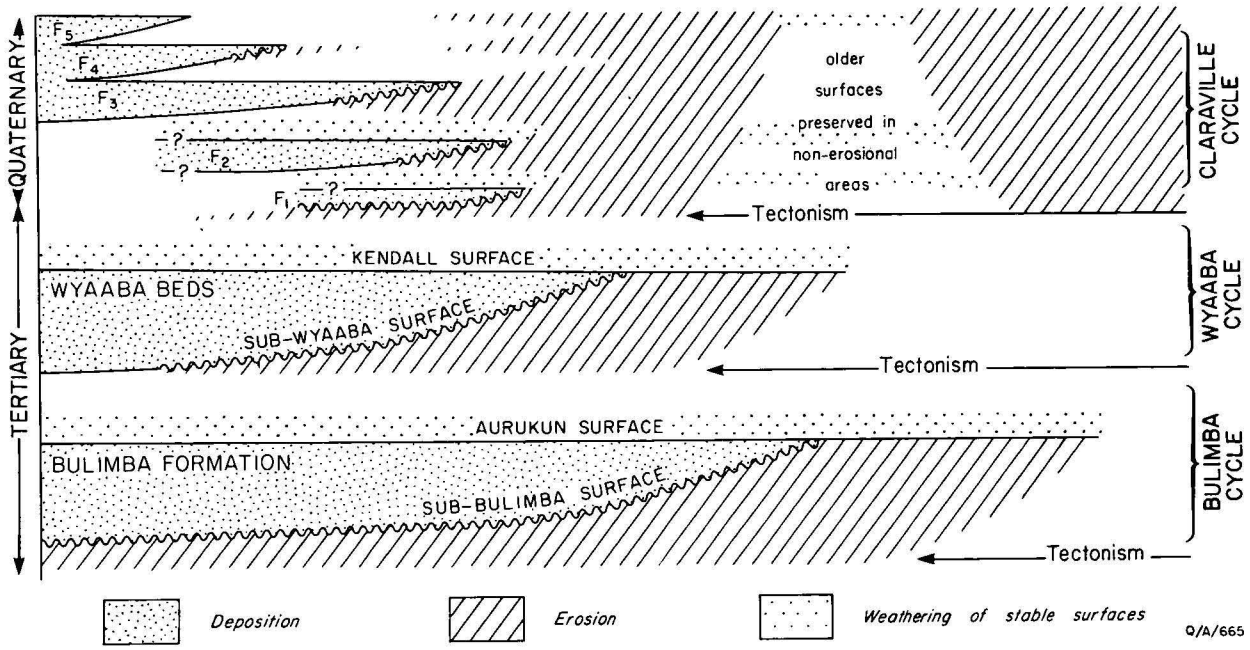

Figure 2. The relationships in time and space, of erosion, deposition, weathering, old landsurfaces, and the three cycles of development in the Karumba Basin (stages of fan deposition are indicated by F_1, F_2, . . .).

A belt of probable Stage 1 deposits can be traced along the Red River and thence up its southern tributary, Police Creek, and across the present drainage divide into the Einasleigh Valley. These deposits suggest that the upper part of the Einasleigh River was a tributary of the Red River at the time. The Lynd and Tate Rivers may also have joined the Red River during Stage 1 (Figs. 3 and 4A).

Stage 2. Stage 2 stream incision is indicated by Stage 1 terraces in the upper parts of the fans. During Stage 2 a tributary of the Gilbert-Etheridge system captured the Einasleigh tributary of the Red River; and capture of the Lynd and Tate Rivers by a tributary of the Mitchell River may have occurred at much the same time. Basalt from a small undated vent flowed into the Stage 2 valley of the Einasleigh River.

Stage 2 fan deposition buried the lower parts of Stage 1 fans, and partly filled the valleys cut into their upper parts. The R_2 element of the Red River Fan exhibits features which appear to be old dunes, now stabilised, with a photo pattern similar to the wanderrie banks of semi-arid Western Australia (Mabbutt, 1963). With the exception of a small inlier, these have been overridden to the north by deposits of the M_{3a} element of the Mitchell Fan (Fig. 3), and may thus indicate a semi-arid period separating Stage 2 from Stage 3. Both Stage 1 and 2 fans have been ferruginised and silicified.

The causes of Stages 1 and 2 of the fan sequence are not certain: tectonism, eustacy and climatic changes may all have contributed. During the late Pliocene and the Pleistocene there have been more than enough fluctuations in climate and sea levels to explain the observed stages, and indeed it is quite feasible that the two stages could contain a number of unrecognised substages; there could also be earlier stages which have been completely obliterated. Thus the time occupied by these two stages (up to two million years?), when compared with the following three stages (less than 200 000 years) probably does not reflect lack of activity so much as the ease of recognition and subdivision of the younger units.

Stage 3. The fan elements of Stage 3 can be recognised, for the most part, by their crosscutting relationships with older elements (Fig. 4B). The migrations of the Mitchell Fan (M_3) produced fan-in-fan forms, which appear to be local effects only, and do not have time equivalents elsewhere.

The G_3 element of the Gilbert Fan combined with the M_3 elements of the Mitchell Fan to bury the lower parts of the older fans. Stage 3 deposits are bounded to the west by a line of old beach ridges. These ridges occupy a similar position on the coastal plain to that of the inner barrier of the eastern coast of Australia, and are thought to be of Pleistocene age, related to the last interglacial about 110-140 000 years ago (Smart, 1976). Stage 3 deposition onshore would probably have occurred at this high stand and during the preceding rise in sea level, though it could be as young as the rise in sea level which occurred 40 000 years ago (Smart, 1977).

All surfaces of Stage 2 or older, including inner barrier beach ridges, are characterised by the presence of shallow swampy depressions which are absent from the younger surfaces. Although some of these depressions may be related to old stream courses, many are on interfluves. Two separate interpretations can be placed on these features: Doutch (1976) considers that the depressions are produced by aeolian deflation, and are a result of a period of dessication throughout the region between Stages 3 and 4, with which he associates choked valleys, sand sheets, and sand dunes. He has named the landscapes so produced the *Holroyd Surface.* On the other hand Grimes (1974) has described similar depressions on the Doomadgee Plain, to the west of the region, which he thinks formed as the result of subsurface solution and consequent subsidence related to a period of lateritisation. Stage 3 fans are ferruginised.

Whatever their origin, the depressions assist in the recognition of the break between the older deposits and the younger Stage 4 deposits. This break is also emphasised by subsequent valley incision in the higher areas, so that the older deposits stand as terraces above the heads of Stage 4 fans.

Nix & Kalma (1972), and Webster & Streten (1972), postulate that in northern Queensland drier climates would have coincided with glacial low sea levels, when the Gulf was dry land, and ocean temperatures were cooler; while warmer, humid climates, which could favour deep weathering, occurred during the interstadials. This postulate has been substantiated by the vegetation studies of Kershaw (1975). As there were several interstadials within the last glaciation, several periods of both humid and dry climates could have occurred between fan Stages 3 and 4 (Fig. 6). Doutch (1976) correlates the arid Holroyd Surface features with the last, and most pronounced, period of low sea level, about 20 000 years ago. Calcretes have been discovered beneath the present Gulf (Smart, 1977) and may also relate to one of these drier glacial stages.

Stage 4. The Stage 4 fans could have formed during the post-glacial transgression, and the related return to humidity (cf. Kershaw, 1975) but would have predated the maximum Holocene high sea level, about 7 000 years B.P. (Doutch, 1976). However, these deposits and the Holroyd Surface could both be related to earlier events within the glacial period (Fig. 6). The Stage 4 fan deposits were not sufficiently thick to bury the inner barrier beach ridges.

Stage 5. The Stage 5 fans formed during and after the highest stand of the Holocene sea, and are contemporaneous with the latest progradation of the coast, which is indicated by the multiple lines of Holocene outer barrier beach ridges. The oldest C^{14} date obtained from these ridges so far is 6440 years B.P. (Rhodes, pers. comm., *in* Smart, 1976). These fans have breached the inner barrier beach-ridge line (Fig. 4D).

It is difficult to differentiate the five fan stages in the subsurface. In places it is even difficult to pick the boundary with the underlying Wyaaba Beds. The upper 28 m of pebbly sand in FBH Wyaaba 1 (Fig. 1) probably represent several stages of fan deposits (Powell and others, 1976). Stages 3 and 4 probably dominate, but earlier stages may occur beneath these. The fans may be up to 40 m thick further to the north, where partly consolidated, mottled outcrops in incised stream beds reported by Doutch and others (1972) may be Stage 1 or 2 deposits. Alternatively, these may represent stream-channel induration of younger units. Such localised induration has also been described as 'water-table rock' in the Townsville Coastal plain by Hopley & Murtha (1975).

The evolution of the Claraville, Millungera and Wondoola Plains

The Claraville, Millungera and Wondoola Plains are examined together because of their parallel evolution. The contemporary Armraynald Plain of the Leichhardt River System (Fig. 1) has been discussed by Grant (1968), Ingram (1972, 1973) and Grimes (1974). It is not discussed further, but would appear to have a history similar to the Wondoola Plain of the Cloncurry-Flinders system. The open grasslands of the clayey Wondoola Plain abut the more sandy, timbered Claraville Plain along the Norman River just south of Normanton. Further south they are separated by the sandy Millungera Plain (Fig. 1). The nature of the basal unconformity (the Sub-Claraville Surface) will be discussed first, then the lithofacies within the deposits; finally the history of development of the plains is related to the five stages in the fans area.

The Sub-Claraville Surface. In the southern plains, sediments of the Claraville Cycle lie unconformably on Mesozoic strata. The form of this unconformity is shown by contours in Figure 5A. It is an erosional surface, the Sub-Claraville Surface of Grimes (in prep., a), which formed at the start of the Claraville Cycle and was buried as the deposits of the cycle built up. The old landsurface contained three major valleys: from east to west the Claraville, Millungera, and Wondoola Valleys, which were separated by the Savannah Downs and Mount Brown Ridges (Fig. 5).

These valleys and the ridges between them were the product of differential erosion of Mesozoic bedrock controlled by bedding strike and other structures. The Savannah Downs Ridge is developed along the strike of the relatively resistant Toolebuc Formation, and the presence of the Mount Brown Ridge is due partly to an anticlinal area of Toolebuc Formation, and partly to resistant Precambrian rocks of the Fort Bowen Ridge which crop out in the core of the anticline (Grimes, 1973).

In the northern part of the system, the main valleys originally joined, and drained to the east of the Normanton Plateau (Fig. 5). The sandstones forming this plateau (Normanton Formation) appear to have been more resistant than the mudstones of the units underlying the valleys, perhaps partly because duricrust developed on the sandstones to a greater degree (Ingram, 1972, 1973). The Normanton Plateau at that time would have been continuous with the Donors Plateau (Fig. 5) to the southwest. As deposition by the ancestral rivers built up their floodplains, the rivers would have migrated up against the plateau from time to time. The net erosive effect would probably have been to scoop out the plateau sides, in the same way as the Cloncurry River has cut a broad scoop into the Donors Plateau in recent times (Doutch and others, 1970). Similar side-cutting, enhanced by diversions caused by Pleistocene upwarping between Croydon and Normanton (see later), appears to be responsible for the isolation of the Normanton Plateau and for the present course of the Flinders River to the west of it.

Lithofacies of the Wondoola and Claraville Beds. Because of difficulty in identifying Wyaaba Beds beneath the fans deposits, Powell and others (1976) placed all the Cainozoic sediments below the Claraville Plain (Fig. 1) in a single unit named the Claraville Beds. These include both the sediments of the Claraville cycle, as well as any correlate of the Wyaaba Beds they may overlie. The corresponding sediments below the Millungera and Wondoola Plains have been named the Wondoola Beds (Smart and others, 1972). The two units interfinger, the Claraville Beds being more sandy than the Wondoola Beds.

The lithofacies distributions (Fig. 5B) can be explained in terms of two main controlling factors: the lithologies of the erosional source areas of the ancient streams; and the morphology of the sub-Claraville Surface, particularly the localising effects of the Mount Brown and Savannah Downs Ridges.

For the old Claraville Valley (Fig. 5)—containing Claraville Beds—the main sources of sediment would have been the Einasleigh Uplands. This is reflected in the deposits of the valley. There is an area of relatively pure sand and gravel in the southern part derived from the Mesozoic sandstone in and about the Gilberton Plateau, and a fringe of muds and sandy muds adjacent to the granitic and volcanic sources further north (Fig.

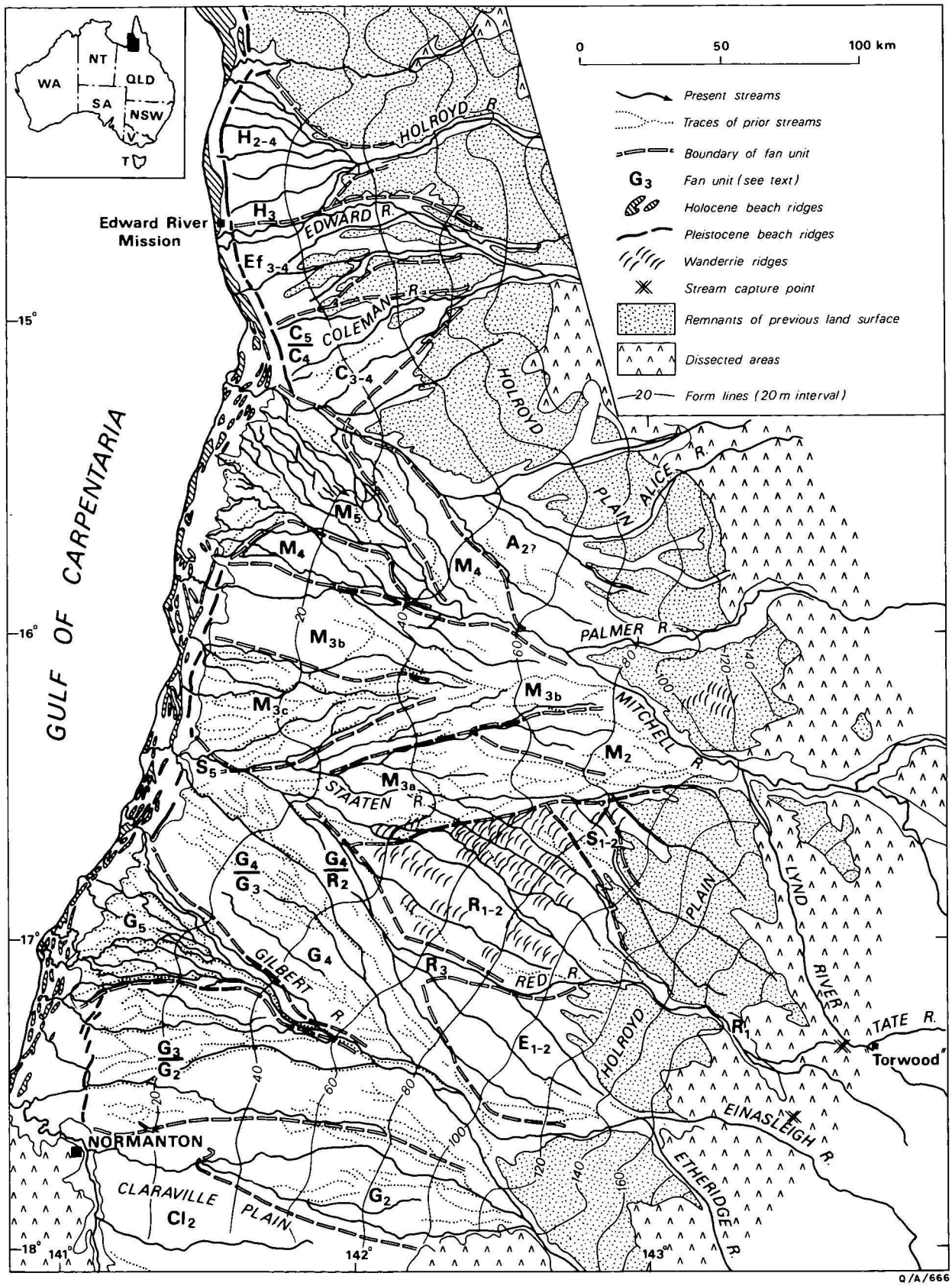

Figure 3. Patterns of present and prior streams and the location of fan units.

From north to south the fans are: H, Holroyd Fan; Ef, Edward Fan; C, Coleman Fan; A, Alice Plain; M, Mitchell Fan; S, Staaten Fan; R, Red Fan; G, Gilbert Fan; E, Einasleigh Fan; Cl, Claraville Plain. Within each fan the stages of development are indicated by the subscriptions 1 to 5 from oldest to youngest.

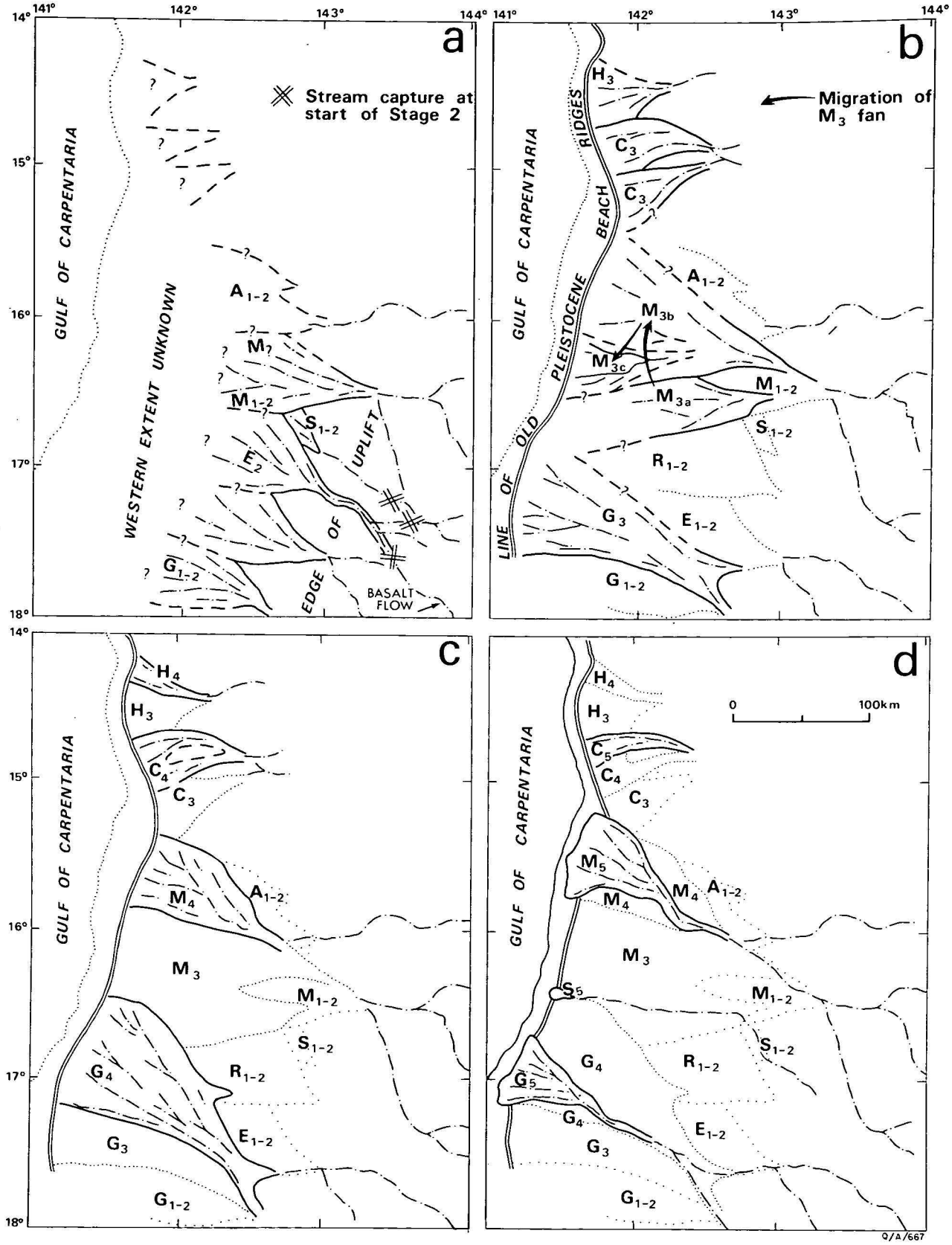

Figure 4. The development of the fans with time. a. Pliocene to Pleistocene; b. late Pleistocene (ca. 120 000 yr BP); e. late Pleistocene to Holocene; d. Holocene.

5B). The sequence of clayey sand, sandy clay and sand in the central and western part of the valley is the result of mixing material from both source areas. To the west the deposits were confined by the Savannah Downs Ridge and only in the northern part of the valley, where it joins the Wondoola Valley, did the sandy material migrate further to the west (Fig. 5).

The Millungera and Wondoola Valleys together contain the Wondoola Beds. The Millungera Valley lies between the Savannah Downs Ridge and the Mount Brown Ridge (Fig. 5A). This valley is filled mainly with clay derived from the predominantly mudstone lithologies of the Cretaceous Rolling Downs Group in the Julia Plain to the south (Figs. 1 and 5A). A tongue of sand extends along the southern part of this valley (Fig. 5B), and probably is material transported as bed load down the valley from the southernmost part of the Gilberton Plateau. The small area of sand extending across the southern part of the Mount Brown Ridge could be more recent deposits of material from the same source, deposited by the Flinders River after the valley had filled and the ridge ceased to be a barrier.

The southern part of the Wondoola Valley is filled almost entirely by clay derived from the Julia Plain. The western tributaries of the valley contain both clayey and sandy areas, and this reflects the mixed lithologies of the Isa Highland—which include granites, volcanics, metamorphics, and various sedimentary rock types.

In its central part, the Wondoola Valley is joined by the Millungera Valley; here it is filled mainly by muds with a thin belt of sand and clayey sand along the western margin, adjacent to a local source area, the labile sandstone of the Donors Plateau (Fig. 5). In the far north the Wondoola Valley is joined by the Claraville Valley; there is little bore data, but the area apparently contains clayey sands. If so, this would suggest that the influx of sandy material from the Claraville palaeo-Valley was more abundant than the clays moving north along the Wondoola and Millungera Valleys.

As the deposits built up in the valleys, the intervening ridges were eventually buried and no longer acted as barriers to stream migration. The results of this, as seen in the present surface deposits, are that firstly the river, which previously flowed along the length of the Millungera Valley, has now swung west to become the Flinders River and crosses the Mount Brown Ridge at about latitude 20°S to join the present-day Gilliat and Cloncurry Rivers; secondly, since the filling of the Claraville Valley, the Saxby River has breached the partly buried Savannah Downs Ridge and is probably responsible for the sheet of sand which was spread over the older muds of the Wondoola Beds to form the sandy Millungera Plain. Similarly, the Clara and Norman Rivers now cross the buried Savannah Downs Ridge further to the north, and are extending the sandy deposits of the Claraville Plain over the eastern margin of the Wondoola Beds.

These westerly stream migrations are possibly contemporaneous with the Pleistocene upwarping between Croydon and Normanton first postulated by Twidale (1966), and the breakthrough of the Flinders River west of Normanton.

The structural contours of Figure 5A are the main evidence for this upwarping, which involved an uplift of the southwest margin of the Gilbert-Mitchell Trough (Needham, 1971; Simpson, 1973; Doutch, in press). The Pleistocene inner barrier beach ridges formed after this event as they show no distortion by it. Later deposits have been restricted to the neighbourhood of the major streams.

Evolution of the southern plains. A fivefold division can be made in the southern plains, but the divisions are not as clear as in the case of the Gilbert and Mitchell Fans. The stages are indicated by numbers on Figure 1, and in more detail on the 1:1 000 000 geological map (Smart and others, 1977, in prep.).

The oldest deposits of the Claraville Cycle in this southern area appear to be the clay, sand, and gravel beds in the Cloncurry Plain, and also about the margins of the southern half of the Donors Plateau (Fig. 1). These deposits stand topographically above the level of later deposits and their original surfaces have suffered some dissection during later stages of the cycle. They are ferricretes or calcretes in places—the calcrete areas adjoin outcrops of calcareous Corella Formation, and represent lithological rather than climatic control. These early deposits are correlated with Stage 1 of the fan sequence.

Much of the surface of the Wondoola and Claraville Plains seems to be Stage 2, though Stage 1 deposits probably occur at depth. This correlation is based on the ferruginised nature of the Claraville Beds and on relationships with the Stage 3 Millungera Plain which postdates the Wondoola Beds.

The sands of the Millungera Plain are only a few metres thick and sit on the Stage 2 muds of the Wondoola Beds, which are exposed through windows in the sand sheet. The Millungera Plain also contains elongated sandy dune-like bodies; these have a northwest trend, and definite dunes occur in the south. The Plain apparently owes some of its morphology to aeolian processes. It has been slightly modified by later erosion (Stage 4 and 5 streams). Thus the Millungera Plain appears to have a Holroyd Surface component, and it is this, together with the proposition that its sands overlie the deposits of the Wondoola Plain, that suggests a mainly Stage 3 age for it and older ages for the bulk of the Wondoola and Claraville Plains.

Some parts of the Clara Fan (Fig. 1) may be equivalent to the Millungera Plain, i.e. to Stage 3. However, Doutch (1977) maps this feature as Stage 4. Unlike the contemporary deposition of the northern fans, that of the Clara Fan does not reach the coast and it contains a zone of drainage that is being incised downstream from its youngest floodout sediments (Doutch, 1977); the reason for this difference appears to be a smaller supply of detritus and of water for transporting it than is the case for the Gilbert and Mitchell Fans.

Apart from the floodouts of the Clara Fan the Stage 4 and 5 deposits are limited to major stream channels and their immediate vicinity. Present-day deposition is restricted in a similar manner (Simpson & Doutch, 1977).

The form lines on Figure 1 (computer-plotted from elevations of BMR helicopter gravity stations) show that the slope of the Wondoola Plain is less than that of the Claraville Plain and the fans to the north. This probably reflects present and past differences in provenance and rainfall between the Wondoola and other plains. Differences in the elevation of contemporary source areas are probably the most important factor; present source areas for the other areas being closer and higher than those for the Wondoola Plain.

Drainage patterns differ between the Wondoola Plain and the sandy plains; the patterns reflect slope and sediment load. The reticulate pattern, levees, and other

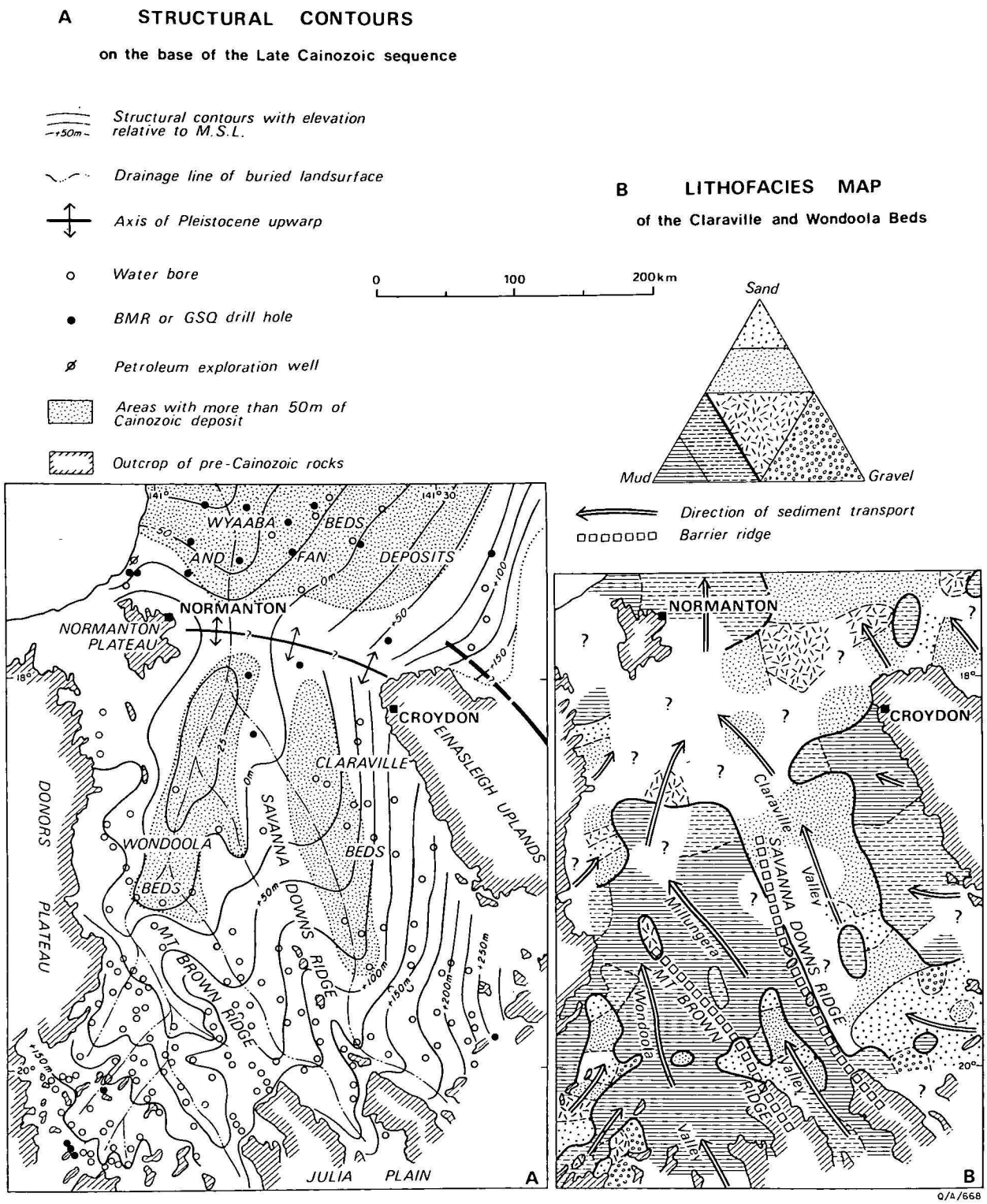

Figure 5. Structure of the basal surface and lithofacies of the Claraville and Wondoola Beds beneath the southern Plains.

characteristics of the Flinders and Cloncurry River drainage of the Wondoola Plain (Whitehouse, 1941), contrast broadly with fan distributaries and floodout deposits elsewhere. The numerous levee deposits along the Flinders and Cloncurry Rivers, and the clayey sediments of the Wondoola Plain suggest that backswamp conditions (Leopold and others, 1964) have occurred over large areas. However, the spread of muddy floodwaters beyond the levees in January 1974 was not very extensive (Simpson & Doutch, 1977); they suggested that contemporary erosion and deposition is operating within constraints set by physiographic features resulting from different conditions in the past.

Discussion

The most important result of this study is the recognition of the five stages of deposition during the Claraville Cycle: dating from late Pliocene time up to the present. This sequence appears to have been controlled by three factors. The first factor was the discontinuous

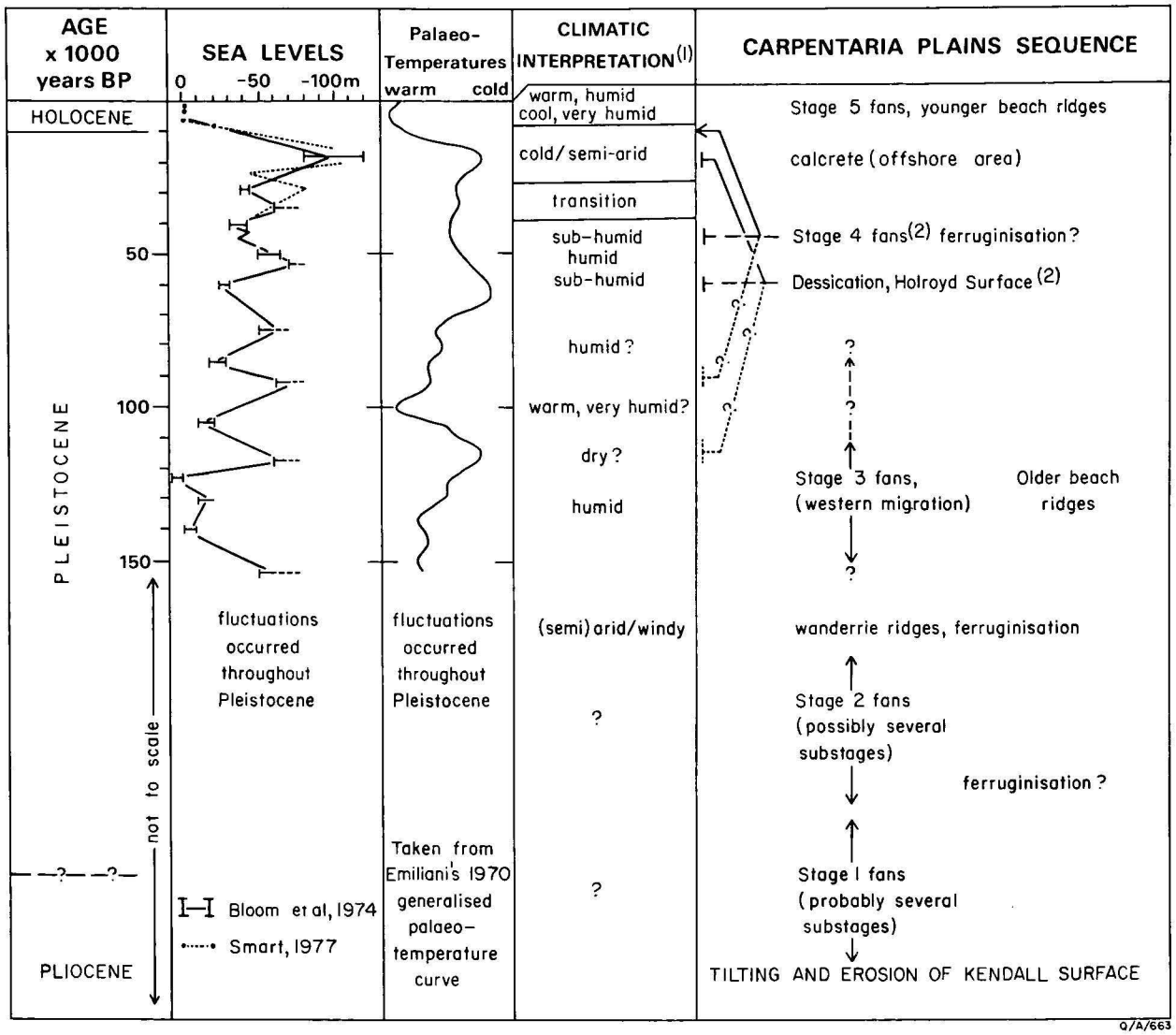

Figure 6. Quaternary development of the Carpentaria Plains.

(1) Based on Kershaw's (1975) interpretation back to about 60 000 BP, and on the theories of Nix & Kalma (1972), and Webster & Streten (1972), for older times. (2) Several correlations with the climatic events are possible.

earth movements in the upland source areas, which may have been a reflection of the Pliocene to Holocene orogeny in New Guinea (Doutch, 1976). A direct correlation between the fans and the dated bouts of basaltic volcanism in the uplands is not easy, however the interval between the first and second stages in the Gulf could correlate with a pause in eruptive activity between 1.7 and 2.1 million years ago, and the interval between Stages 2 and 3 may be related to a pause between 0.5 and 0.9 million years ago.

The second controlling factor was sea level. Sea level has fluctuated throughout the Quaternary in response to glacial advance and retreat. The consequent flooding and draining of the Gulf would have changed the base levels of the streams, and would therefore have been an important factor in stream incision or flood-plain accretion. Unfortunately the fluctuations during the earlier part of the Pleistocene are not well documented and correlations with the first two stages are not possible. Correlations between the three younger stages and the sea-level fluctuations are suggested in Figure 6.

The third influence on deposition would have been the climatic changes of the Quaternary, which are consequent on both the glacial events and the related sea-level changes. Webster & Streten (1972), and Nix & Kalma (1972), have proposed climatic models for the area in which aridity occurred during glacial periods as a result of the cooling of the sea waters, and also the exposure of large areas of the Gulf floor and the continental shelf as the sea level was reduced; while more humid conditions, similar to the present, occurred during the interglacial and interstadial periods when the gulf was flooded. These theories have been substantiated by the vegetation studies of Kershaw (1975) for the last 60 000 years (Fig. 6).

The tectonic movements would not have affected sedimentary sequences outside northern Queensland; however the sea levels and related climatic changes would have influenced much of Queensland, especially the eastern coast. One would therefore expect some correlation between the sequence in the Gulf and that seen elsewhere in the state. In many areas alluvial terraces occur which might be related to the last three stages in the Gulf. Correlates with the first two stages are less easy to find, possibly because they can be related more to the local earth movements than to eustatic and cli-

matic factors. Some examples of correlative sequences from areas which have been studied in more detail are given below.

In the Charters Towers area Wyatt & Webb (1970), and Wyatt and others (1971), have delineated a sequence of events which can be dated by their relationships to the basalt flows. This area provides the best correlation with the sequence in the Carpentaria Plains as it has suffered the same history of upwarping as well as of eustatic and climatic fluctuations. The sequence here consists of (1) the late Pliocene to early Pleistocene Campaspe Beds, which are now ferricretes; (2) the early Pleistocene Selheim Beds, (3) the later Pleistocene 'older alluvium' and (4) the younger Pleistocene to Holocene stream terraces, which are at two levels. If we consider the younger terraces as representing two stages then a fivefold sequence similar to that of the Gulf is obtained.

In the Townsville coastal plain the sequences described by Hopley & Murtha (1975) could be correlated with the Carpentaria Plains sequence, as follows: the Holocene 'active or recently active' deposits would relate to Stage 5, the late Pleistocene to Holocene 'younger inactive' unit would be Stage 4, and the 'older inactive' group might be mainly Stage 3. Some of the deeply weathered piedmont deposits and older outwash fans of this group may date back to the earlier stages of the Carpentaria Plains sequence.

Further south, in the Rubyvale area of central Queensland, recent mapping by Grimes has recognised three stages of late Pleistocene and Holocene alluvial deposits, which may correlate with the last three stages of the Gulf, and the older, high level 'sapphire wash' which might correlate with Stages 1 and 2 of the Carpentaria Plains.

In southeastern Queensland Thompson (1973) has recognised three distinct terraces in the Mary Valley, while in the Brisbane region Cranfield and others (1976) recognise two or three alluvial terraces and in places a higher 'Pleistocene' terrace; in both cases a correlation with the last three stages of the Gulf is possible.

Thus it would seem that, with care, the depositional sequence in the Carpentaria Plains could provide a base for correlating similar sequences throughout much of Queensland.

Acknowledgements

We are indebted to our colleagues in the Carpentaria Basin field party for use of their published and unpublished results, and in particular to J. Smart for assistance throughout the preparation of this report. R. W. Day, P. J. G. Fleming, and G. E. Wilford made constructive criticism of the manuscript at various stages. K. G. Grimes publishes with the permission of the Under-Secretary, Queensland Department of Mines.

References

BLOOM, A. L., BROEKER, W. S., CHAPPELL, J. M. A., MATHEWS, R. K., & MESOLELLA, P. J., 1974—Quaternary sea level fluctuations of a tectonic coast: new 230 Th/234 U dates from the Huon Peninsula, New Guinea. *Quaternary Research* **4**, 185-205.

CRANFIELD, L. C., SCHWARZBOCK, H., & DAY, R. W., 1976—Geology of the Ipswich and Brisbane 1:250 000 Sheet areas. *Geological Survey of Queensland, Report* **95**.

DOUTCH, H. F., 1976—The Karumba Basin, northeastern Australia and southern New Guinea. *BMR Journal of Australian Geology and Geophysics*, **1**, 131-40.

DOUTCH, H. F., 1977—Croydon, Qld—1:250 000 Geological Series. *Bureau of Mineral Resources, Australia—Explanatory Notes* **SE/54-11**.

DOUTCH, H. F., INGRAM, J. A., SMART, J., & GRIMES, K. G., 1970—Progress report on the geology of the southern Carpentaria Basin. *Bureau of Mineral Resources, Australia—Record* **1970/39** (unpublished).

DOUTCH, H. F., SMART, J., GRIMES, K. G., GIBSON, D. L., & POWELL, B. S., 1973—Progress report on the geology of the Carpentaria Basin in Cape York Peninsula, *Bureau of Mineral Resources, Australia—Record* **1973/187** (unpublished).

DOUTCH, H. F., SMART, J., GRIMES, K. G., NEEDHAM, S., & SIMPSON, C. J., 1972—Progress report on the geology of the central Carpentaria Basin. *Bureau of Mineral Resources, Australia—Record* **1972/64** (unpublished).

EMILIANI, C., 1970—Pleistocene paleotemperatures. *Science*, **168**, 822-25.

GALLOWAY, R. W., GUNN, R. H., & STORY, R., 1970—The lands of the Mitchell-Normanby area, Queensland. *CSIRO, Land Research Series*, **26**.

GRANT, K., 1968—Terrain classification for engineering purposes of the Rolling Downs Province, Queensland. *CSIRO, Division of Soil Mechanics—Technical Paper* **3**.

GRIFFIN, T. J., & MCDOUGALL, I., 1975—Geochronology of the Cainozoic McBride Volcanic Province, northern Queensland. *Journal of the Geological Society of Australia*, **22**, 387-96.

GRIMES, K. G., 1973—Millungera, Queensland—1:250 000 Geological Series. *Bureau of Mineral Resources, Australia—Explanatory Notes* **SE/54-15**.

GRIMES, K. G., 1974—Mesozoic and Cainozoic geology of the Lawn Hill, Westmoreland, Mornington and Cape Van Diemen 1:250 000 sheet areas, Queensland. *Bureau of Mineral Resources, Australia—Record* **1974/106** (unpublished).

GRIMES, K. G., 1977—Holroyd, Queensland—1:250 000 Geological Series. *Bureau of Mineral Resources, Australia—Explanatory Notes* **SD/54-11**.

GRIMES, K. G., in prep. a—The nature and development of old landsurfaces of northern Queensland.

GRIMES, K. G., in prep. b—Cainozoic stratigraphy: the Karumba Basin *in* SMART, J., GRIMES, K. G., & DOUTCH, H. F.: The Mesozoic Carpentaria and Cainozoic Karumba Basins, Queensland. *Bureau of Mineral Resources, Australia—Bulletin*.

GRIMES, K. G., & WHITAKER, W. G., 1977—Walsh, Queensland—1:250 000 Geological Series. *Bureau of Mineral Resources, Australia—Explanatory Notes* **SE/54-4**.

HOPLEY, D., & MURTHA, G. G., 1975—The Quaternary deposits of the Townsville coastal plain. *James Cook University, Department of Geography, Monograph Series* **8**.

INGRAM, J. A., 1972—Donors Hill, Queensland—1:250 000 Geological Series. *Bureau of Mineral Resources, Australia—Explanatory Notes* **SE/54-10**.

INGRAM, J. A., 1973—Burketown, Queensland—1:250 000 Geological Series. *Bureau of Mineral Resources, Australia—Explanatory Notes* **SE/54-6**.

ISBELL, R. F., WEBB, A. A., & MURTHA, G. G., 1968—Atlas of Australian Soils, Sheet 7, North Queensland, with explanatory data. *Melbourne, CSIRO and Melbourne University Press.*

KERSHAW, A. P., 1975—Late Quaternary vegetation and climate in northeastern Australia; *in* SUGGATE, R. P., & CRESSWELL, M. M. (Editors)—QUATERNARY STUDIES *Royal Society of New Zealand—Bulletin* **13**, 181-7.

LEOPOLD, L. B., WOLMAN, M. G., & MILLER, J. P., 1964—FLUVIAL PROCESSES IN GEOMORPHOLOGY. *San Francisco, Freeman.*

MABBUTT, J. A., 1963—Wanderrie Banks: micro-relief patterns in semi-arid Western Australia. *Geological Society of America Bulletin* **74**, 529-40.

NEEDHAM, R. S., 1971—Notes on the Mesozoic and Cainozoic stratigraphy of the Georgetown area, Queensland. *Bureau of Mineral Resources, Australia—Record* **1971/100** (unpublished).

NEEDHAM, R. S., & DOUTCH, H. F., 1973a—Galbraith, Queensland—1:250 000 Geological Series. *Bureau of Mineral Resources, Australia—Explanatory Notes* **SE/54-3.**

NEEDHAM, R. S., & DOUTCH, H. F., 1973b—Rutland Plains, Queensland—1:250 000 Geological Series. *Bureau of Mineral Resources, Australia—Explanatory Notes* **SD/54-15.**

NEEDHAM, R. S., SMART, J., GRIMES, K. G., & DOUTCH, H. F., 1971—Stratigraphic drilling in the southern Carpentaria Basin, 1970. *Bureau of Mineral Resources, Australia—Record* **1971/142** (unpublished).

NIX, H. A., & KALMA, J. D., 1972—Climate as a dominant control in the biogeography of northern Australia and New Guinea: *in* WALKER, D. (Editor), BRIDGE AND BARRIER: THE NATURAL AND CULTURAL HISTORY OF TORRES STRAIT. *Australian National University, Department of Biogeography & Geomorphology—Publication* **BG/3**, 61-91.

PERRY, R. A., SLEEMAN, J. R., TWIDALE, C. R., PRITCHARD, C. E., SLATER, R. O., LAZARIDES, M., & COLLINS, F. H., 1964—General report on the lands of the Leichhardt-Gilbert area, Queensland, 1953-54. *CSIRO, Land Research Series* **11.**

POWELL, B. S., GIBSON, D. L., SMART, J., GRIMES, K. G., & DOUTCH, H. F., 1976—New and revised stratigraphic nomenclature, Cape York Peninsula. *Queensland Government Mining Journal* **77**, 178-89.

SIMPSON, C. J., 1973—Normanton, Queensland—1:250 000 Geological Series. *Bureau of Mineral Resources, Australia—Explanatory Notes* **SE/54-7.**

SIMPSON, C. J., & DOUTCH, H. F., 1977—The 1974 wet season flooding of the southern Carpentaria Plains, northwest Queensland. *BMR Journal of Australian Geology and Geophysics,* **2**, 43-51.

SMART, J., 1976—The nature and origin of beach ridges, western Cape York Peninsula, Queensland. *BMR Journal of Australian Geology and Geophysics,* **1**, 211-18.

SMART, J., 1977—Late Pleistocene sea-level changes, Gulf of Carpentaria, *Geology,* **5**, 755-9.

SMART, J., & BAIN, J. H. C., 1977—Red River, Queensland—1:250 000 Geological Series. *Bureau of Mineral Resources, Australia—Explanatory Notes* **SE/54-8.**

SMART, J., GRIMES, K. G., & DOUTCH, H. F., 1972—New and revised stratigraphic names, Carpentaria Basin. *Queensland Government Mining Journal,* **73**, 190-201.

SMART, J., GRIMES, K. G., DOUTCH, H. F., & PINCHIN, J., in prep.—The Mesozoic Carpentaria and Cainozoic Karumba Basins, Queensland. *Bureau of Mineral Resources, Australia—Bulletin.*

SMART, J., GRIMES, K. G., DOUTCH, H. F., SWOBODA, R. A., & RUSSELL, E. A., 1977—Geology of the Carpentaria, Karumba and part Laura Basins, 1:1 000 000 scale, Preliminary edition. *Bureau of Mineral Resources, Australia.*

SMART, J., MORRISSEY, J. A., & HASSAN, S. E., 1975—Index to drillhole data—Carpentaria, Laura, and Karumba Basins, Queensland. *Bureau of Mineral Resources, Australia—Record* **1975/167** (unpublished).

THOMPSON, C. H., 1973—The Mary River terraces. *International Association for Quaternary Research IX Congress,* Guidebook for excursion D3, Queensland section, Southeastern Queensland and Great Barrier Reef, 55-60.

TWIDALE, C. R., 1956—Chronology of denudation in northwest Queensland. *Geological Society of America Bulletin,* **67**, 3-23.

TWIDALE, C. R., 1966—Geomorphology of the Leichhardt—Gilbert area, northwest Queensland. *CSIRO Land Research Series,* **16.**

WARNER, K. R., 1968—Gilbert-Staaten Rivers groundwater investigations. *Geological Survey of Queensland, Report* **24.**

WEBSTER, P. J., & STRETEN, N. A., 1972—Aspects of late Quaternary climate in tropical Australasia, *in* WALKER, D., (Editor), BRIDGE AND BARRIER: THE NATURAL AND CULTURAL HISTORY OF TORRES STRAIT. *Australian National University, Department of Biogeography and Geomorphology—Publication* **BG/3**, 39-60.

WHITEHOUSE, F. W., 1941—The surface of western Queensland. *Proceedings of the Royal Society of Queensland,* **53**, 1-22.

WYATT, D. H., PAINE, A. G. L., CLARKE, D. E., GREGORY, C. M., & HARDING, R. R., 1971—Geology of the Charters Towers 1:250 000 Sheet area, Queensland. *Bureau of Mineral Resources, Australia—Report* **137.**

WYATT, D. H., & WEBB, A. W., 1970—Potassium-argon ages of some north Queensland basalts and an interpretation of late Cainozoic history. *Journal of the Geological Society of Australia,* **17**, 39-51.

The sediments of the Argo Abyssal Plain and adjacent areas, northeast Indian Ocean

P. J. Cook[1], J. J. Veevers[2], J. R. Hiertzler[3], and P. J. Cameron

A series of geophysical traverses by the Atlantis II across the Argo Abyssal Plain, together with coring at a number of selected localities has provided new information on sedimentary and tectonic processes in this region of the northeast Indian Ocean. Isopach maps prepared from the seismic profiles show that sediment thicknesses crudely parallel the bathymetry. The presence of some diapirs in the Argo Abyssal Plain was indicated. It was not possible to say from the present program whether the probable diapirs are salt or mud-cored. A diverse group of cores were obtained from a variety of sites including siliceous clays from below the CCD, calcareous oozes from above the CCD, calcareous clays (showing evidence of abundant sulphate reduction) from a fore-arc basin site, and manganese nodules from an abyssal site. In addition, hyaloclastites from the Joey Rise area (north of the Exmouth Plateau), suggest that the Joey Rise, and possibly also the Roo Rise, are underlain by basaltic material. A sample of basalt was also recovered from the outer part of the Exmouth Plateau.

Introduction

The purpose of this paper is to report on some of the sedimentary results of the cruise by the RV Atlantis II of the Woods Hole Oceanographic Institution in the northeast Indian Ocean. The cruise took place from 29 October to 26 November 1976, commencing at Darwin and finishing at Singapore (Fig. 1). During the course of the cruise bathymetric, seismic (reflection and refraction), gravity, and magnetic surveying was undertaken. In addition, 9 core and 2 dredge sites were attempted. Using this range of techniques it was possible to add significantly to the amount of geophysical and geological information available on this region.

The aims of the cruise were as follows:

(i) To define the magnetic anomaly field in the Argo Abyssal Plain. Results from the Deep Sea Drilling Program had already shown this area to be underlain by upper Jurassic basement.

(ii) To determine whether domal structures underlying the Argo Abyssal Plain are true diapiric structures and, if so, whether they were likely to be salt or mud domes.

(iii) To clarify the early spreading history of the northeastern Indian Ocean.

The area studied included five physiographic regions (Fig. 2):

(i) the Australian Margin; (ii) the Argo Abyssal Plain; (iii) an oceanic rise off the northwest Exmouth Plateau (the name Joey Rise is proposed by Heirtzler and others (in press) for this feature; (iv) the Roo Rise; (v) the western sill of the Argo Abyssal Plain, south of Roo Rise, and a northern sill which is the lip of the Java Trench.

Of these, only the Australian margin had previously been surveyed in detail.

Preliminary results have already been summarised by Heirtzler and others (1977), and detailed discussion of the bathymetric and geophysical results is provided by Heirtzler and others (in press). This publication deals with the sedimentary (seismic and coring) results and some of the implications arising from those results.

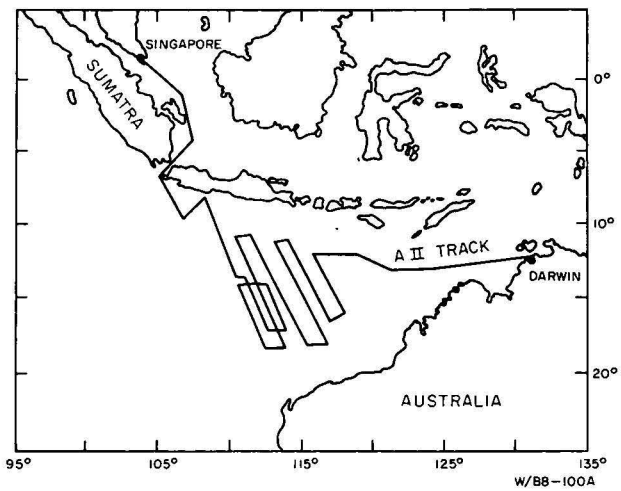

Figure 1. General location.

Methods

Seismic profiling

Continuous seismic reflection measurements were made at an underway speed of approximately 8 kn. An 80 and a 40 cubic-inch airgun were fired simultaneously as an energy source. The outputs of two trailing hydrophone strings were summed for the acoustic signal recorded. Two records were made: one with a 2.5 sec. sweep and the other with 5.0 sec. sweep. The delay before the sweep was separately variable on each of the recorders. Twenty geophysical lines were made, with seismic, magnetic, and gravity measurements on each (Fig. 1).

Sediment sampling

Conventional coring and dredging techniques were used. Coring was by means of a piston corer with a barrel up to 10 m long. For dredging operations, a steel-mesh dredge was used. Difficulties in obtaining samples were experienced at several sites, possibly owing to a lack of soft sediment. No dredge samples were obtained. Smear mounts were prepared for shipboard petrology. It was not possible to split cores longitudinally on

1. Research School of Earth Sciences, The Australian National University, P.O. Box 4, Canberra 2600, Australia.
2. School of Earth Sciences, Macquarie University. North Ryde, New South Wales 2113, Australia.
3. Department of Geology and Geophysics, Woods Hole Oceanographic Institution, Woods Hole, Massachusetts 02543, U.S.A. (Cruise Leader.)

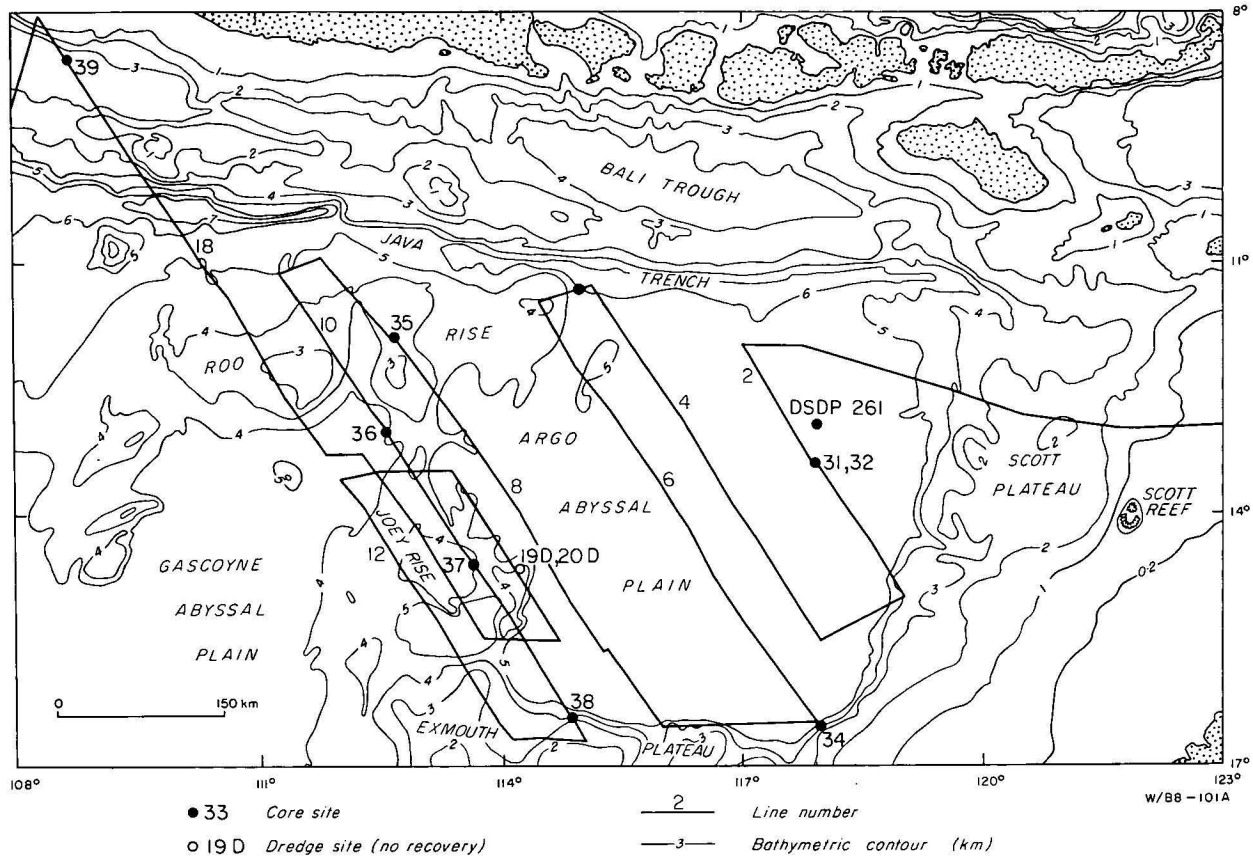

Figure 2. Location of coring sites in the Argo Abyssal Plain and adjacent areas.

board, and consequently only point sampling could be undertaken.

Shipboard geochemistry

The shipboard (geochemical) program was concerned solely with interstitial water geochemistry. Pore waters were extracted from the sediments through a stainless-steel filter press using nitrogen at a pressure of 3500 kPa, and filtered through a millipore filter system. Pore-water salinity was determined by means of a previously-calibrated Goldberg Refractometer. The pH was determined on the water and also in the sediment by means of a Metrohm pH meter. Alkalinity was obtained by the potentiometric titration technique of Gran (1952), modified by Geiskes & Rogers (1973).

Shorebased geochemistry

All shorebased analytical work was undertaken at the Research School of Earth Sciences, Australian National University. Most chemical analyses were by atomic absorption spectrophotometry (using a Varian Techtron AA6), or colorimetry; a Leco analyser was used for C and S (Mr. E. Kiss). Rb, Sr, U, and Th were determined by V-ray fluorescence (Mr P. Beasley). A number of microprobe analyses were also undertaken (Mr. N. Ware). X-ray diffraction analysis of whole-sediment powder and minus-two-micron fractions were carried out on most sediment samples (Mr H. Cutten).

Results

Seismic profiles

Seismic profiles of the area have been described previously by Veevers and other (1974), Veevers (1974), and Veevers & Heirtzler (1974), and have been related to the drilling at DSDP site 261 in the Argo Abyssal Plain (Veevers, Heirtzler, and others, 1974). In the Argo Abyssal Plain, a generally hummocky basement reflector (M), and an intermediate reflector (L), were drilled at site 261, and were found to be basalt (M) and the surface of a layer of late Jurassic and Cretaceous, pelagic clay and claystone (L) respectively. In previous records obtained using lower power seismic sources, the sequence below reflector L was essentially acoustically transparent, but this distinction is much less evident in the Atlantis II records (Heirtzler and others, in press). The entire record above the clay and claystone is overlain by a layer of calcareous ooze which was probably deposited by turbidity currents. Reflector L may be equivalent to a regional reflector found along the western margin of Australia and on the adjacent ocean floor (Reflector R_4 of Veevers & Cotterill (1978)) (Fig. 3).

An additional important feature (discussed later) is the vertical tube or sheet-like structures (? diapirs) which interrupt parts of the sedimentary sequence of the Argo Abyssal Plain, sometimes showing as clear areas on the seismic records (Fig. 4). These structures are particularly well developed along seismic line 2. They range in width from about 200 m to 1 km or more, and in vertical extent from about 200 m to 700 m. They occur in water depths of 4400-5800 m over a wide region of the Argo Abyssal Plain and adjacent areas. There are three main types of structures (Fig. 4).

(1) Those showing a decreased seismic reflectivity of the record, associated localised arching of overlying and flanking sediments, and a sea bottom topographic expression. This type is found only in the eastern part of the abyssal plain and is rare. It includes the largest of the structures.

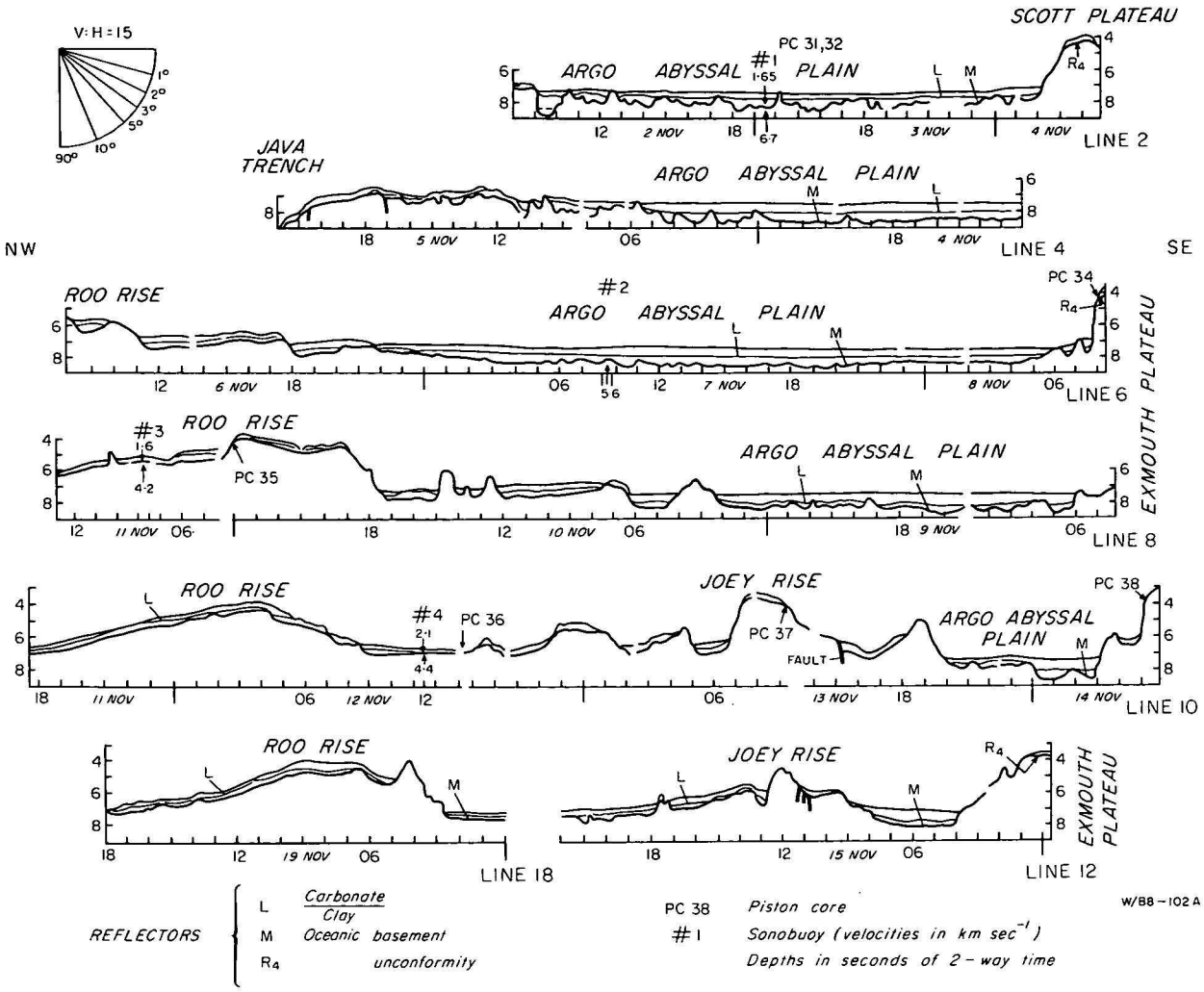

Figure 3. Generalised seismic profiles for the Argo Abyssal Plain and adjacent areas. Ship's speed was about 8 knots. Coring sites are indicated.

(2) Those showing decreased seismic reflectivity and localised arching, but no topographic expression. This type is more common than (1). It is restricted to the central part of the abyssal plain, where it forms an approximately ENE oval-shaped trend.

(3) Those which show only the columns of decreased seismic reflectivity. These are the most widespread, but the smallest, of the three types.

The isopachs of total sediment thickness (Fig. 5A) crudely parallel the bathymetry with the thickest sediments (>1.0s equivalent to 900 m) in the centre of the Argo Abyssal Plain, slightly offset from the area of deepest basement (i.e., deepest with respect to sea level). Figures 5B, C, D show that this correspondence between thickness and structure is due to: (i) the thick accumulation (0.4s or 400 m) of Late Jurassic and Cretaceous claystone in the central depressed part of the Argo Abyssal Plain, and the thin accumulation (<0.2 s) in the southwest part (Fig. 5B). As a consequence, the structure contours on L (Fig. 5C) are almost flat over the Argo Abyssal Plain, except for a slight depression in the southwest corner; and (ii) a compensating extension of the thickest calcareous ooze (Fig. 5D) southwestward from the central area into the L-reflector depression, to produce the flat surface of the present-day plain.

The southeast ends of lines 2, 6, 8, 10 and 12 cross the lower continental slope to reach the edge of the marginal plateaus of the Australian margin. On each of these lines, the breakup unconformity (reflector F of Willcox & Exon, 1976, reflector R_4 of Veevers & Cotterill, 1978) was found (Fig. 3).

Coring

Lithology

Sites at which sampling was successfully carried out are shown in Figures 2 and 3. Results are summarised in Table 1. Sites are referred to by the core number rather than the station number. Dredging was unsuccessfully attempted at two sites on the Joey Rise (Table 1). Aspects of sediment chemistry are given in Tables 2 and 3. Basalt chemistry is given in Table 4.

Sites 31 and 32. These adjacent sites in the Argo Abyssal Plain were cored in an attempt to determine the characteristics of sediments overlying possible diapiric structures (Fig. 3, Profile 2). At both sites the sediments are typical abyssal siliceous clays with abundant whole or fragmentary siliceous organisms including radiolarians, diatoms, and (?) silicoflagellates. Possible fish fragments are present. No calcareous fragments are evident, yet the acid (HCL) soluble fraction ranges from about 17 to 27 percent, suggesting that very fine $CaCO_3$ may be present in greater than normal amounts

Stn no.	*Core no.*	*Dredge no.*	*Begin depth (m)*	*End depth (m)*	*Begin latitude*	*Begin longitude*	*End latitude*	*End longitude*	*Physiographic province*	*Piston core sample (cm)*	*Pilot core sample (cm)*	*Dredge sample*
49	31 PC	—	5698	5698	13°23.12′S	117°54.50′E	13°22.44′S	117°54.12′E	Abyssal plain Wharton Basin	575	141	—
50	32 PC	—	5698	5694	13°22.35′S	117°53.08′E	13°22.18′S	117°53.24′E	Abyssal plain Wharton Basin	896	135	—
51	33 PC	—	6121	6014	11°19.20′S	114°57.27′E	11°19.08′S	114°57.30′E	Axis, Java Trench	710	37	—
54	34 PC	—	3235	3218	16°33.06′S	117°59.33′E	16°31.47′S	117°59.21′E	N edge of Exmouth Plateau	160	16	—
55	35 PC	—	3436	3501	11°54.01′S	112°40.32′E	11°54.10′S	112°40.14′E	Roo Rise	659	88	—
58	36 PC	—	5217	5225	13°01.13′S	112°34.15′E	13°00.34′S	112°34.21′E	Base of Roo Rise (South flank)	312	16	—
59	37 PC	—	3067	3052	14°36.14′S	113°38.47′E	14°36.09′S	113°38.35′E	Joey Rise (SW side)	229	0	—
60	38 PC	—	2636	2824	16°25.44′S	114°51.31′E	16°25.22′S	114°51.51′E	Exmouth Plateau (N flank)	fragments		—
61		19 D	3494	3892	14°39.09′S	114°11.33′E	14°38.44′S	114°10.10′E	Joey Rise	—	—	0 kg
62		20 D	3276	3182	14°40.55′S	114°12.28′E	14°39.26′S	114°13.15′E	Joey Rise	—	—	0 kg
63	39 PC	—	3563	3563	08°31.59′S	108°39.58′E	08°31.37′S	108°40.02′E	Western extension of the Bali Trough	820	111	—

Table 1. Coring and dredging sites in the Eastern Indian Ocean.

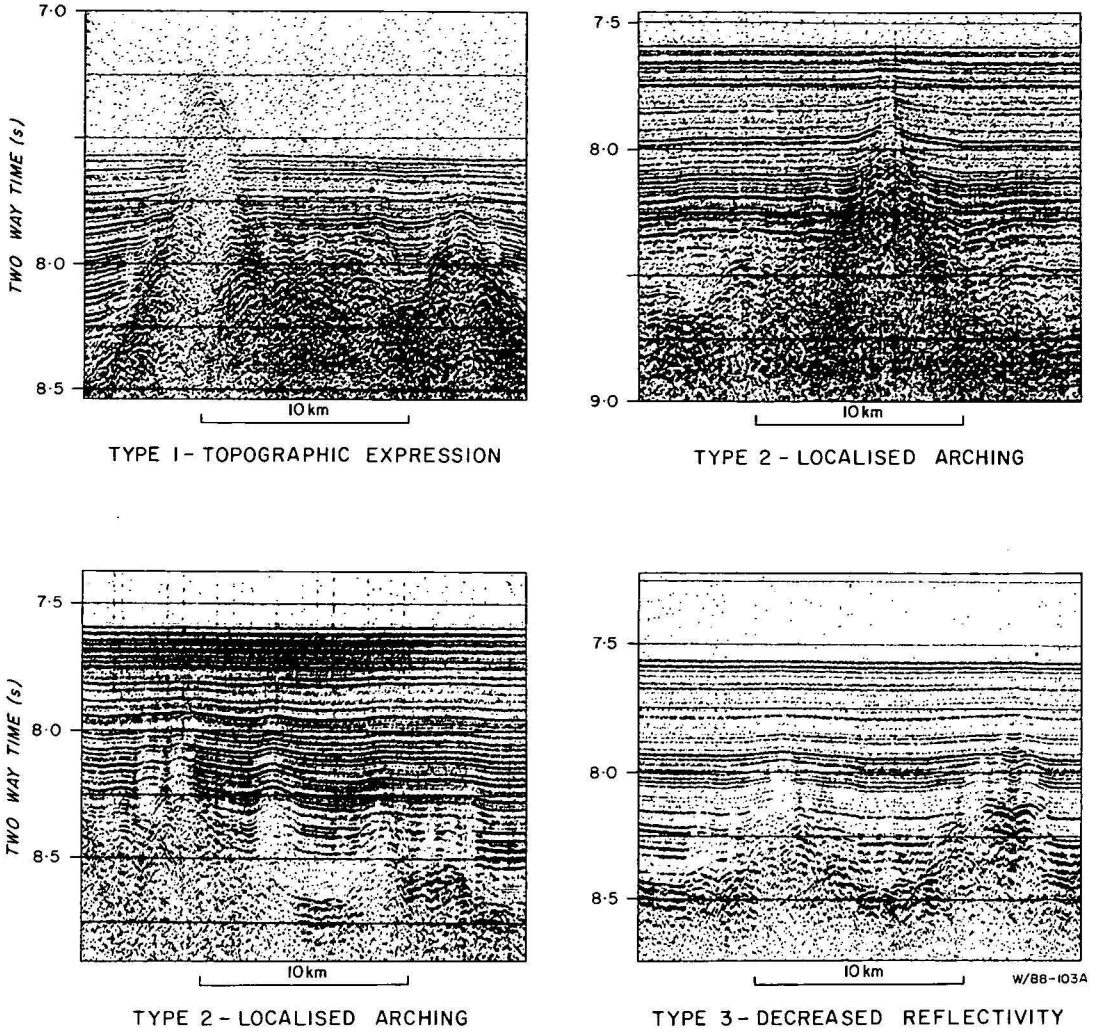

Figure 4. Photographs of seismic records showing possible diapiric structures in the Argo Abyssal Plain area.

for abyssal clays from below the CCD, indicating some input from turbidity currents. The clay component of these sediments is dominantly kaolinite and montmorillorite, with minor illite and traces of chlorite.

Site 33. This site, which was located below the CCD near the axis of the Java Trench, also yielded a siliceous clay with abundant siliceous organisms. The terrigenous sediment is composed mainly of clays, with abundant montmorillonite and kaolinite, intermediate quantities of illite, and minor amounts of chlorite. Unlike the sediment from Sites 31 and 32, there is a minor amount of sub-angular silt-size detrital material (quartz, plagioclase, feldspar, heavy minerals, and probably rock fragments). Pyrite, some of it framboidal, infilling and partly replacing organisms, is fairly common. This is probably a reflection of the higher level of sulphate reduction at this Trench location than is to be found at the abyssal plain sites.

Site 34. Unlike the previous three sites, this site, on the flanks of the Exmouth Plateau (Fig. 3, Profile 6), is well above the CCD. The sediment is a white calcareous ooze composed predominantly of nannofossil remains, with minor foraminifera (5%), small amounts of terrigenous clay (2%), and trace quantities of very fine silt-size quartz grains, possibly of aeolian origin, and rare crystals of heulandite. Coring at this site was attempted in order to obtain a sample from near the break-up unconformity (reflector F of Wilcox & Exon, 1976, and reflector R_4 of Veevers & Cotterill, 1978). The core has been found to contain Early or Mid Oligocene, and Late Paleocene faunas (P. G. Quilty and B. V. Haq, pers. comm.), and is assumed to be from above the breakup unconformity.

Site 35. This site is on the south flank of the Roo Rise (Fig. 3, Profile 8). It is also above the CCD; however, it is darker in colour, richer in organic carbon, and slightly less calcareous than the sediment from Site 34. Nannofossils are dominant (80%), but foraminifera are common (15%), and miscellaneous siliceous organisms are present in trace amounts. The upper part of the core contains abundant faecal pellets, suggesting extensive bioturbation. The foraminifera indicate an Early Pleistocene age at a depth of 439-643 cm within the core. The non-biogenic component forms no more than 5 percent of the total sediment, with quartz and feldspar predominant. Volcanic glass shards form a variable, but significant, proportion of the sediment.

Sites 36, 37, 38. Coring at these sites was to sample prominent seismic reflectors. At all three sites volcanoclastic or volcanic material was obtained.

Site 36, located at the foot of the Roo Rise at a depth of 5200 m (Fig. 3, Profile 10) was originally sampled on the assumption that the flat, acoustically strongly reflective surface probably indicated a manganese

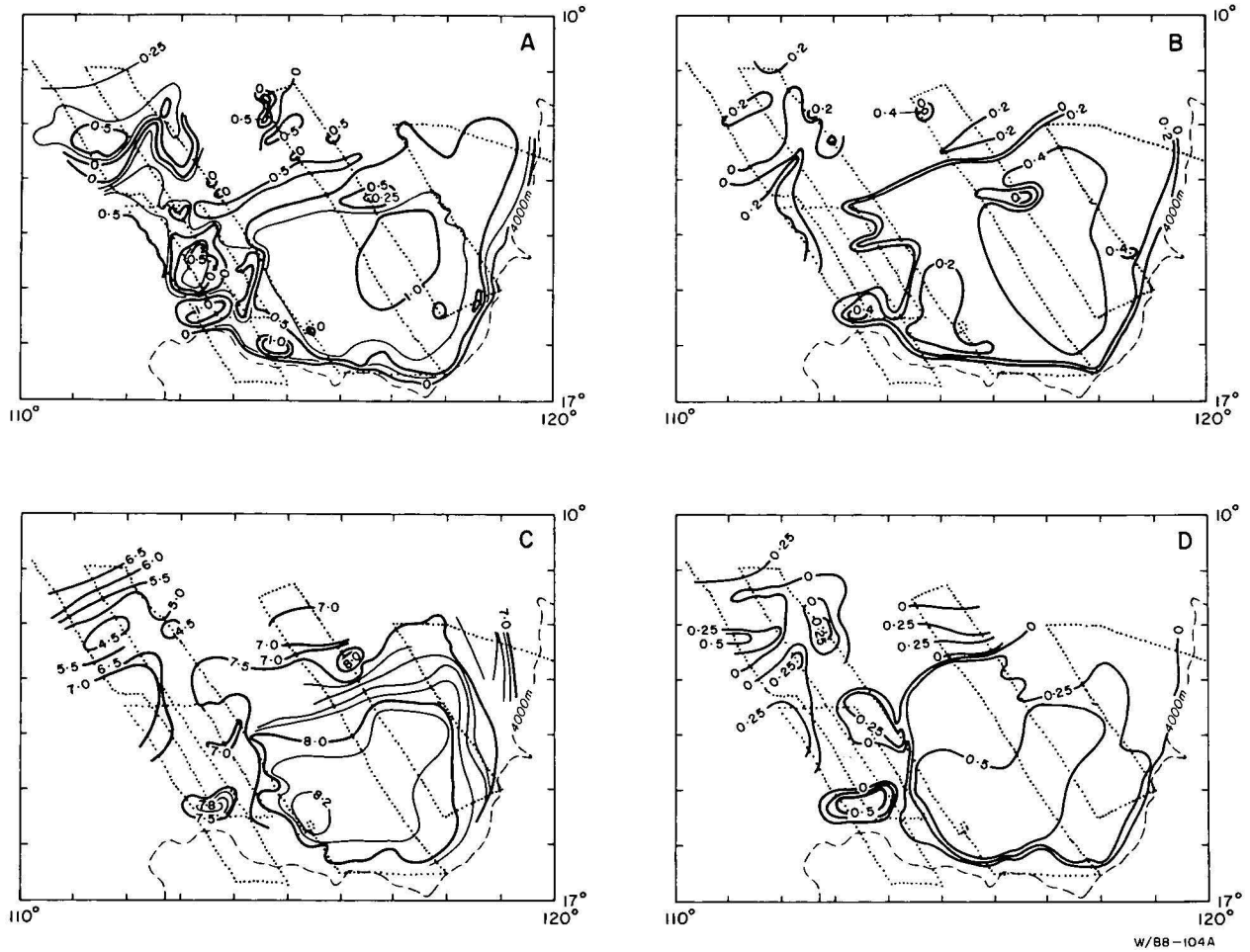

Figure 5. **A—Isopach (in seconds of 2-way time) of oceanic sediments. Contour interval 0.5 seconds 2-way time (heavier line), intermediate contours at 0.25 second intervals (lighter line).**
B—Isopachs (in seconds of 2-way time) of the sediments between basement (reflector M) and reflector L. Contour interval 0.2 second in the Argo Abyssal Plain region.
C—Structure contours (in seconds of 2-way time) on reflector L. Contour interval 0.5 second, with intermediate contours at 0.2 second interval.
D—Isopach (in seconds of 2-way time) of sediments between reflector L and the seafloor. Contour interval 0.25 second.

nodule pavement. The core does contain a 12 cm layer at the top with abundant small nodules (up to 5 cm in diameter) and manganese-coated material. This is underlain by 10-20 cm of manganiferous sediment. However, most of the core is composed of angular to subrounded glassy particles and rock fragments, ranging in size from fine sand to fine gravel (?hyaloclastite), commonly with a manganiferous rind. The matrix, comprising no more than 5-10 percent of the sample, is typical abyssal brown clay containing abundant whole or fragmentary siliceous organisms. The sand and grit-size clasts are of mixed volcanic origin, comprising vesicular (palagonitised sideromelane) (Fig. 6). Phenocrysts and microphenocrysts of plagioclase feldspar are common. Zeolite crystals are present in minor amounts throughout the sediment. Material showing textures and compositions of this type may be present as the variolitic material marginal to basaltic pillows (Furnes, 1973); however, the thickness of this unit (more than 3m were penetrated) suggests that the material is a basaltic hyaloclastite, similar to that described from the St Paul's Rocks region of the Atlantic Ocean (Melson & Thompson, 1973).

Site 37 was located on the flanks of the Joey Rise at a water depth of about 3000 m. Coring was to sample a prominent reflector (Fig. 3, Profile 10). Despite the bathymetric differences between this site and the previous site, the sediments are very similar (Fig. 7), and those at Site 37 are also interpreted as hyaloclastites. The only major difference in the sediment from these two sites is in the matrix, which at Site 37 (located well above the CCD) is predominantly calcareous with abundant foraminifera and minor clay (dominantly montmorillonite). Quilty (pers. comm.) determined the foraminifera as dominantly Early Pleistocene, and suggests that evidence of dissolution may possibly indicate a history below the CCD at some stage.

Site 38, on the northern margin of the Exmouth Plateau in about 2600 m of water (Fig. 3, Profile 10), yielded fragments of bedrock of basaltic composition and a few grams of calcareous ooze. The texture of the basalt, particularly the abundant phenocrysts and microphenocrysts of plagioclase (Fig. 8), is identical to that of many of the sand and grit-size clasts of Sites 36 and 37. However the sample was an angular fragment which clearly had been broken off a larger mass of material. Consequently it seems unlikely that it is a clast from within a hyaloclastite sequence, though it may possibly be parent material of some of the hyaloclastitic material. The calcareous ooze from Site 38 is composed

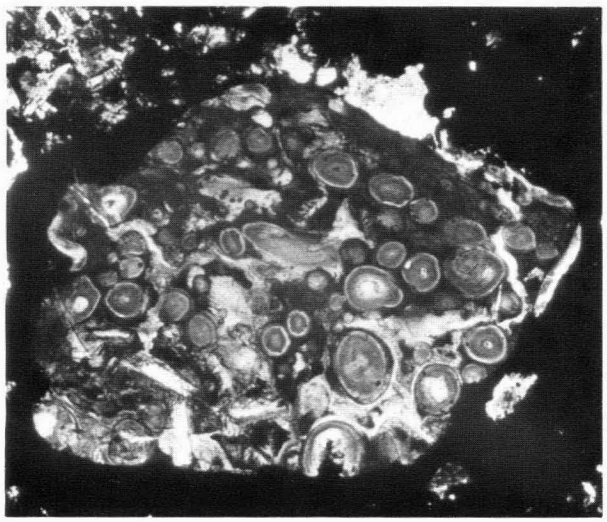

Figure 6. Hyaloclastite from core 36, with a sub-angular fragment of vesicular basalt.

Figure 7. Hyaloclastite from core 37, with a sub-rounded clast of basalt containing microphenocrysts of plagioclase feldspar.

predominantly of nannofossil remains with a few foraminiferans. A small fragment of botryoidal manganese, probably part of a manganiferous encrustation, was also recovered from this site. The ooze from this site is dated by Quilty (pers. comm.) at Late Miocene or younger. It would appear that material from below (basalt) and above (the calcareous ooze) the unconformity were obtained from this site.

Site 39. This site, located on the axis of the northwesterly extension of the Bali Trough (a fore-arc basin) at a water depth of about 3600 m, was sampled primarily to obtain a core of trough sediments from above the CCD for ongoing geochemical studies. The sediments are olive-grey nannofossil, foraminiferal, diatomaceous, radiolarian-bearing clays and silty clays, in which montmorillonite is the dominant clay mineral, with illite and kaolinite somewhat less abundant. Pollen and wood fragments are fairly common. Quilty (pers. comm.) reports Holocene faunas in the core

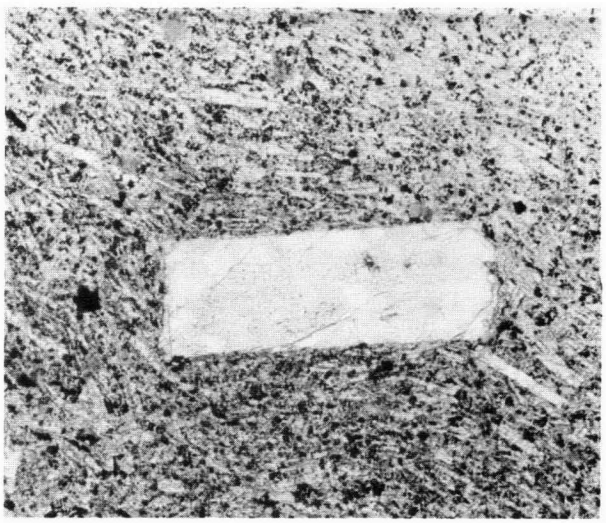

Figure 8. Basalt from core 38 with a large plagioclase feldspar phenocryst.

down to at least 520 cm, which indicates a very rapid rate of sedimentation; however, the next fossiliferous sample, at 820 cm, has a very mixed fauna, with elements of Paleocene, Eocene, and perhaps Early Oligocene age, suggesting extensive reworking of sediments. Pyrite, replacing and infilling wood fragments and siliceous and calcareous organisms, is particularly common. The high alkalinity recorded (up to 24 meq/L) together with the abundance of methane in the core, suggest very active sulphate reduction within these sediments.

Geochemistry

Sediments

Shore-based chemical work is incomplete at the time of writing; consequently, this is a preliminary account of the geochemistry of the sediments and associated volcanic material. Results to date are summarised in Table 2, which gives minor and trace element analyses for the total sediment, and Table 3, which gives minor and trace element contents of the acid (1N HCL) soluble fraction only. Table 2 shows that the sediments are a diverse group, with wide variations shown by almost all components. However, four main groupings are apparent. The siliceous oozes (analyses 31 and 32) are characterised by generally high metal contents (except for Sr and U), possibly concentrated by siliceous organisms as part of their metabolism. Whether these metals are in the siliceous tests or in the associated organic matter as organo-metallic complexes is unknown. Other features of the siliceous sediments include high organic carbon, moderately high sulphur, yet relatively low P_2O_5. The trench and trough clays (analyses 33 and 39) are generally characterised by moderately high metal contents, except for Sr which is fairly low. P_2O_5 remains low, whereas S and C are particularly high. By contrast, the calcareous oozes (analyses 34 and 35), are low in all metals with the exception of Sr and U, which probably substitute for Ca in the $CaCO_3$ lattice. Both the C and S contents are low, suggesting that there is little or no sulphate reduction within these calcareous sediments. The fourth group of sediments (analyses 36 and 37) is characterised by the highest metal contents. Some, perhaps most, of the

Cores	31	32	33	34	35	36	37	39
No of analyses	9 ppm	7 ppm	7 ppm	2 ppm	6 ppm	4 ppm	2 ppm	7 ppm
Cu	173	190	134	38	58	496	50	34
Pb	26	24	18	1	9	72		8
Zn	168	168	145	48	145	223	221	101
Mn	2181	2293	801	150	615	13341	459	633
Fe	44184	42213	41847	11335	25450	71470	86151	48727
Co	26	26	16	3	11	93	19	16
Ni	139	137	67	16	37	560	53	29
Cr	71	65	43	28	20	58	11	46
V	100	126	121	29	62	86	126	117
Rb	79	84	62	18	27	53	60	44
Sr	133	124	188	1026	750	232	223	262
U	0.5	0.5	1.1	1.4	1.0	0.6	1.1	0.5
Th	13	19	13	5	4	28	9	16
P_2O_5	335	319	262	660	377	1848	2145	312
S	839	1066	3160	260	910	330	150	7789
C	10876	6629	5310	449	4137	690	231	12402

Table 2. Average metal, P, S, and organic carbon contents of miscellaneous sediments from the Atlantis II cruise, Eastern Indian Ocean.

Cores	31	32	33	34	35	36	37	39
No. of analyses	9 ppm	7 ppm	7 ppm	2 ppm	6 ppm	4 ppm	2 ppm	7 ppm
Cu	118	139	88	14	31	276	29	15
Pb	27	24	22	4	12	57	5	11
Zn	106	105	91	25	108	124	78	62
Mn	2010	2233	560	140	403	1963	222	538
Fe	17042	13697	11067	2209	8922	10991	11629	15341
Ba	523	342	605	622	736	425	406	321
Sr	74	62	87	1225	784	84	174	199
P_2O_5	234	239	139	507	250	492	457	225
ASF*	22.2%	23.8%	23.2%	78.1%	54.3%	21.1%	30.2%	23.5%

Concentrations in parts per million except where indicated.

* Acid-soluble fraction.

Table 3. Average metal (and P_2O_5) contents of the acid (1N HCl) soluble fraction of miscellaneous sediments from the Atlantis II cruise, Eastern Indian Ocean.

high metal contents may result from the presence of manganese nodules and encrustations in these sediments. It is apparent that the hyaloclastite containing the higher Mn content and the greater abundance of siliceous organisms (analysis 36) also has the higher metal contents of the two. The C and S contents are particularly low in these sediments but, in contrast, the P_2O_5 content is high. This may reflect slow deposition (this is unlikely for hyaloclastites) or a volcanic source rich in phosphorus. Another possibility is that the present sediment-water interface may represent a major hiatus, thus providing ample opportunity for post-depositional phosphatisation. This third possibility is supported by the presence of manganese nodules, which are also generally more abundant in areas with either a slow rate of terrigenous or biogenic sedimentation, or a prolonged hiatus.

It had been assumed that the composition of the acid-soluble fraction (Table 3) would be more uniform than the acid-insoluble fraction (Table 2), reflecting primarily the minor and trace element geochemistry of the carbonate fraction. In fact, the acid-soluble compositions are almost as heterogeneous as the composition of the total sediment. With the exception of the P_2O_5 values, which are much more homogeneous than the values in Table 2, the four main groups are again apparent from the elemental compositions of their acid-soluble fractions. This may be a consequence of the carbonate fraction reflecting the elemental composition of the total sediment fairly closely, and even elements known for their high geochemical affinity for Ca (such as Sr) not being as clearly partitioned in the carbonate and non-carbonate fractions as is generally assumed. Parekh and others (1977) found this situation in Jurassic limestones.

Bedrock

Major element analyses on some of the small chips of basaltic bedrock from Site 38 were obtained by electron microprobe, after first preparing glass beads by the method of Nicholls (1974). These results (Table 4) show that the Site 38 basalt is more alkalic than most of the oceanic basalts from the northeast Indian Ocean. This difference between Site 38 basalt and other Indian Ocean basalts is also illustrated in the $(Na_2O + K_2O)/SiO_2$ plot (Fig. 9), with the core Site 38 basalts apparently falling into the alkalic basalt field of Macdonald & Katsura (1964) (although they do not in fact extend the field beyond 5 percent $N_2O + K_2O$). However the low K/Na ratio, and the low CaO and high Al_2O_3 values, suggest that there has been some alteration of the original basaltic composition; the apparently alkalic nature of the basalt must be regarded as questionable.

Interstitial waters

Interstitial waters were extracted from a number of the cores for shipboard and subsequent geochemistry. Results of the shipboard work are summarised in Table 5. In general, values fall into the range normally encountered in deep-sea sediments. A particular object of the pore-water program was to establish whether

	A	B	C	D	E	F	G
SiO_2	53.0	51.1	50.3	49.9	50.0	52.1	51.2
TiO_2	2.2	1.4	2.2	2.3	1.4	0.8	1.1
Al_2O_3	19.4	14.9	16.0	14.8	16.1	16.1	16.5
FeO (Total Fe)	11.5	10.8	10.3	11.2	9.4	9.6	8.5
MgO	5.8	7.4	7.4	7.7	8.7	6.8	9.1
CaO	1.5	11.9	9.8	10.7	11.3	11.8	9.6
Na_2O	5.7	2.2	3.1	2.4	2.8	2.4	2.9
K_2O	0.9	0.3	0.8	1.0	0.3	0.4	1.1
	100	100	100	100	100	100	100
	ppm	ppm	ppm	ppm	ppm	ppm	ppm
Rb	29	—	—	30	1	5	10
Sr	206	—	—	465	123	200	330

A Dredge sample from site 38, this cruise (mean value based on six electron microprobe analyses by N. Ware, RSES). Volatiles not determined.
B Sill at DSDP site 261 (after Robinson & Whitford, 1974).
C Ocean basalt from DSDP site 261 (after Robinson and Whitford, 1974).
D Average basalt (after Turekian & Wedepohl, 1961).
E Average oceanic tholeiite (after Melson & Thompson, 1971).
F Average island-arc tholeiite (after Jakes & White, 1971).
G Average calc-alkaline basalt (after Jakes & White, 1971).

Table 4. Recalculated basalt compositions (%) from the Indian Ocean compared with average basalts.

there was an increase in interstitial salinities in the vicinity of diapiric structures, which would indicate a salt core. It is evident from the results for Sites 31 and 32 that overall there is no such increase when compared with other core sites. However, if the vertical salinity profiles are examined (Fig. 10), there does appear to be downward increase in salinity at core Site 32, but the increase is fairly small and cannot readily be taken as strong evidence of nearby salt.

The alkalinity values provide a good indication of the level of sulphate reduction occurring within the sediments. From this it is clear that a very high level of sulphate reduction is occurring in the sediments of core 39 from the extension of the Bali Trough. This is supported by ongoing work which shows a depletion of sulphate in these pore waters.

Discussion

The Atlantis II cruise was primarily to obtain geophysical data. Coring and dredging was undertaken for the most part on an opportunity basis; consequently, it is not possible to reach major conclusions from the sedimentological part of the program. There are, nevertheless, a number of discoveries which are of significance to an overall understanding of the processes of sedimentation and tectonic activity in the northeast Indian Ocean.

The origin of the Joey Rise

Many of the rises and marginal plateaus of the northeast Indian Ocean are of uncertain origin. Some, such as the inner part of the Exmouth Plateau, are clearly underlain by continental crust, but for others the evidence is equivocal. Geophysical results in the vicinity of the Joey Rise are discussed by Heirtzler and others (in press); however, some of the samples obtained by coring also provide information which is relevant to our understanding of its origin. The well-defined reflector between the Roo and Joey Rise cored at Site 36, and also the prominent seismic reflector cored at Site 37 on the flanks of the Joey Rise, are both hyaloclastites with a basaltic composition. The reflector

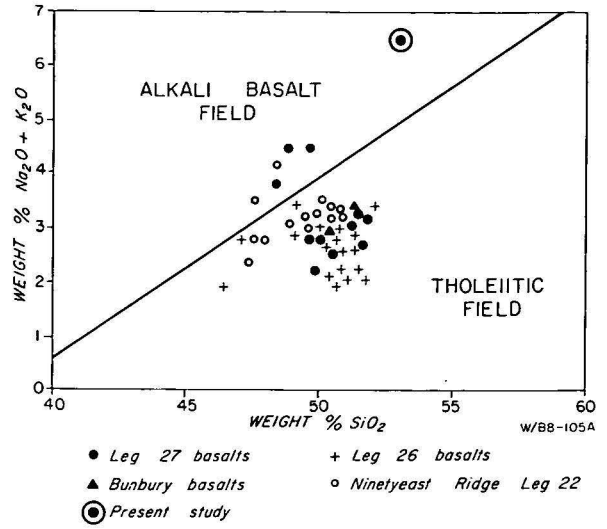

Figure 9. $(Na_2O + K_2O)/SiO_2$ plot of the composition of Indian Ocean basalts, after Robinson & Whitford (1974), and core site 38, this study. The alkali basalt/tholeiite fields are after MacDonald & Katsura (1964), with an extrapolated boundary about 5% $Na_2O + K_2O$.

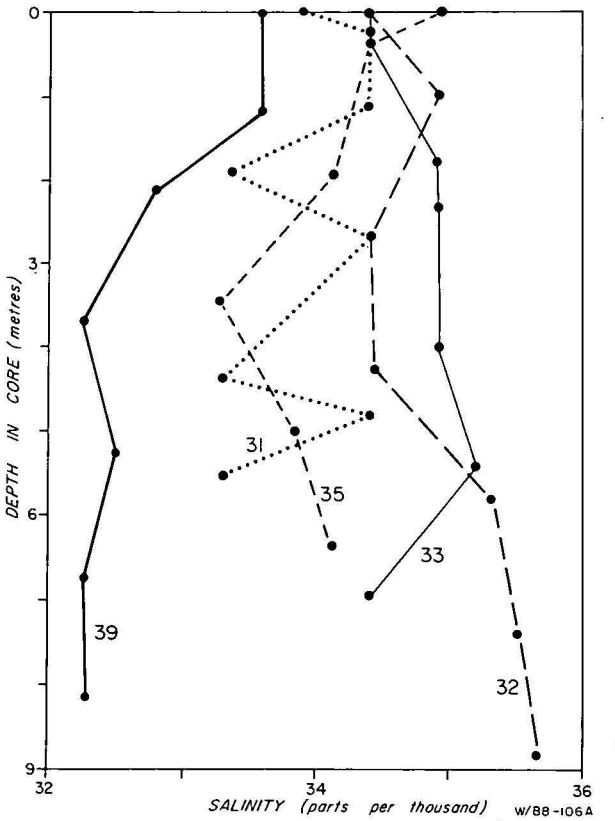

Figure 10. Vertical salinity profiles for interstitial waters from various cores.

cored at Site 38 on the flanks of the Exmouth Plateau (at what is generally taken to be the break-up unconformity) is similarly a basalt. If these basalts are alkalic then such basalts are commonly associated with intraplate volcanism of the type which may result in the formation of seamounts like those of the East Pacific (Batiza, 1977), or the New England Seamounts (Heirtzler and others, 1977). Many such seamounts form along linear structural features, possibly in

Core site	31 (8)	32 (7)	33 (6)	34 (2)	35 (6)	36 (3)	39 (7)	SSW	DSDP 262 (24)
Salinity (ppt)	33.9	34.9	34.7	34.1	34.1	34.7	32.8	35.0	36.3
pH	7.6	7.6	7.6	7.9	7.6	7.5	7.8	7.7	7.7
Alkalinity (meq/L)	3.2	3.5	3.3	i.s.*	3.0	2.5	22.0	1.8	58.3

Numbers in brackets indicate the number of analyses.
* Insufficient sample available for the analysis.

Table 5. Average shipboard geochemical results for salinity, pH, and alkalinity compared with results for standard seawater (SSW) and pore waters from the upper half of DSDP Site 262.

response to the migration of crust over a hotspot, or volcanism along an ancient fracture zone. In this case, linearity is not clear, though a poorly defined north-northwest trend may be present. This trend is approximately at right angles to the anomaly pattern, i.e. consistent with the hot-spot or fracture hypothesis. However, as pointed out earlier, the alkalic composition is questionable, and all that can be said at this time from the coring results is that the Joey Rise and probably also the Roo Rise are underlain by basaltic material and therefore are unlikely to be continental fragments. The fact that the sea-floor spreading magnetic anomalies of the Argo Abyssal Plain extend westward without change into the Joey and Roo Rises (Heirtzler and others in press), suggest that these features are underlain by oceanic basalt. On the basis of earlier seismic and magnetic evidence Veevers & Cotterill (1978) also suggest that the outer part of the Exmouth Plateau may be underlain by oceanic crust; in opposition to the views of Willcox and Exon (1976).

The age of the volcanic activity which resulted in the formation of the Joey Rise is uncertain. The presence of a manganese pavement 12 cm thick, overlying the hyaloclastite at Site 36, suggests the volcanism is at least several million years old. Associated overlying sediments at Site 37 have an Early Pleistocene age; however, this only provides a minimum age for the volcanic activity. The acoustically layered sediment (probably calcareous ooze) which overlies the presumed volcanic material on the crest of the Joey Rise is up to half a second thick. At pelagic rates of sedimentation above the CCD this thickness of sediment could take anywhere from 10 to 50 million years to accumulate, suggesting that the volcanism could be Early Cenozoic or older. The anomaly pattern indicates a Mesozoic age. However, as it is unlikely that normal oceanic basalts would underlie positive topographic features (except at an active spreading ridge), there must have been subsequent uplift associated with for instance a hot spot, or with faulting, to maintain it as a large positive topographic feature.

Sedimentary processes

The types of sediments obtained are those normally found on abyssal plains (siliceous clays), or on topographic highs above the CCD (calcareous ooze). The volcanic glass in the oozes of the Roo Rise was more abundant than in many other calcareous oozes. Whether this reflects volcanic activity on the Roo Rise or on the nearby Indonesian archipelago is not certain, though the latter explanation is more likely. The hyaloclastites were unexpected; this type of volcanogenic sediment had not previously been documented from this part of the Indian Ocean.

An understanding of sulphate reduction is important to our understanding of pyrite in ancient sediments. The current coring program provided evidence of sulphate reduction in the trough site and, to a lesser extent, in the deeper trench site. Minor sulphate reduction may also be taking place in the moderately organic-rich sediments of the sub-equatorial abyssal zone. At the other core sites there is little or no evidence of it. The site in the extension of the Bali Trough is a particularly interesting site because of its very high alkalinity (and presumably a very high rate of sulphate reduction). In this respect it shows similarities to the Timor Trough sediments at DSDP Site 262 (Cook, 1974; Veevers, Heirtzler, and others, 1974). However, the interstitial waters in the Bali Trough sediments show salinities below those of the overlying water column, whereas those in the Timor Trough are much higher. This suggests that there may be some reflux of fresher continental waters under the Bali Trough, producing a decrease in interstitial salinities.

Manganiferous sediment was found at both rise and abyssal locations. The occurrences on rises were probably encrustations. The nodules obtained from Site 36 were smaller than those reported from the Pacific, but this is likely to be a function of the smaller diameter of the corer. Only total sediment analyses are available at present. The most manganiferous sediment (3% Mn) contains 0.06% Cu, and 0.1% Ni. It is reasonable to expect the individual nodules to have metal contents significantly above these concentrations in the total sediment (including matrix). The extent of the manganese nodule pavement is unknown, as it was only traversed on one line. Such a location, at the foot of the Roo and Joey Rises, might be expected to be a site of major calcareous input by turbidity flows, but there is no evidence of this; Site 36 is situated on the sill between the two rises, and is likely to be one of the few places through which bottom waters can enter or leave the Argo Abyssal Plain. Consequently, the location is probably swept by strong bottom currents which will remove any allochthonous calcareous sediment, giving an overall low rate of terrigenous deposition and an enhanced relative development of manganese nodules. This area should be sampled by a comprehensive dredging program to provide a better evaluation of its economic potential.

Diapiric structures

It is uncertain whether all the columnar seismic structures are really true diapirs and the gravity and magnetic data appear at this stage to be of little assistance in resolving this question. The ill-defined type (iii) structures in particular are at times less-than-convincing as diapirs. In some cases, the 'diapirs' may in fact be acoustic artifacts resulting, for instance, from the type of wave diffraction effects (perhaps off a point reflector at the top of a basement high) discussed by Ball (1969), or following differential compaction (Collette & Rutten, 1970), or of side reflection from a nearby basement high. However, from the seismic profiles some

of the structures do have the appearance of piercement (diapiric) structures.

Deep-sea diapirs are known from many parts of the world (Schneider & Johnson, 1970). In areas such as the Mississippi delta, or the Magdalena delta off Colombia, the diapirs are giant mudlumps or mud volcanoes (Shepard and others, 1968). Mud diapirism is a possible explanation for the Indian Ocean structures. Drilling at DSDP Site 261 (Veevers, Heirtzler, and others, 1974) showed that the acoustically transparent layer (which appears to be the diapiric unit) is a Late Jurassic-Cretaceous nannofossil and radiolarian-bearing clay. Shear strengths of these clays at DSDP Site 261 indicate that they would flow relatively easily. The shear strengths also suggest that the overlying calcareous unit is weak, and would be susceptible to piercement by the underlying Mesozoic clays. Montmorillonite is the dominant clay mineral in the lower clays. Kerr and others (1970), who found that montmorillonite is characteristically the preponderant clay in many mud volcanoes, suggest that the mobile, thixotrophic nature of these clays is responsible for their ability to form diapiric structures. As the 'diapiric unit' at Site 261 has an average bulk density of about 1.69 (using the values of Rocher, 1974), compared with a density of about 1.56 for the overlying layered unit, the underlying unit will not rise in response to buoyancy. A more probable cause is tectonism, perhaps associated with the northward movement of the Australian plate and subduction along the Java Trench. Such a cause is supported by an approximately east-west elongation of the diapiric zone roughly parallel to the Java Trench. Alternatively, some diapirism may have been triggered by differential loading of the sediment column. Such a mechanism is possible because most of the upper layered unit was probably deposited as turbidites (Robinson and others, 1974).

So far, it has been assumed that the diapirs have mud cores, but, in fact, many deep-sea diapirs are thought to have salt cores. Pautot and others (1970), Schneider and Johnson (1970), and Kinsman (1975), have pointed out that young rift oceans are commonly the site of large-scale evaporite deposition at low altitudes. Using the polar-wander paths of Schmidt (1976), and the method of Haile (1975) for determining palaeolatitudes, the mid-point of the Argo Abyssal Plain at 155 m.y.—the date of initial rifting in the northeast Indian Ocean (Heirtzler and others, 1973) was at latitude 13°S. A restricted ocean at such a latitude would potentially be a site for salt deposition. The Argo Abyssal Plain area is the only part of the Eastern Indian Ocean where there may be diapiric structures. The Jurassic palaeolatitude for this area and its possible location near a spillway from the open Tethys to the north (analogous to the Atlantic spillways used by Burke (1975) to explain the distribution of Atlantic salt), would have potentially made this area a favoured site for the formation of evaporites.

Palaeozoic salt is known on the West Australian margin (Johnstone and others, 1968); Pliocene (or possibly Miocene) salt is inferred to be present in the Timor Trough area (Veevers, Heirtzler, and others, 1974). However, there is no clear indication of Jurassic-Cretaceous salt in this area. Drilling in the Wharton Basin did not reveal any salt. Generally, the pore-water salinities decrease with depth—except at Site 261, where there is a slight increase in salinity in the seismically transparent Jurassic-Cretaceous sediments.

If the columnar seismic structures are salt domes, then it is possible that this would be reflected in an envelope of elevated salinities in the pore waters. Attempts were made to test this by determining salinity profiles in gravity cores at Sites 31 and 32. Neither core was sufficiently long to be expected to provide a large increase in salinity. At core Site 32 an increase in pore water salinity was noted (from 34.4 p.p.t. at the top of the core to 35.6 p.p.t. at the bottom). No such increase was detected at Site 31 or at any of the gravity cores obtained at Sites 33-38 (Fig. 10). However, this evidence is too tenuous to conclude that the diapiric structures have salt cores.

Conclusions

The seismic profiling generally confirmed the conclusions reached from earlier cruises regarding the distribution and form of the main seismic reflectors. Incorporation of the Atlantis II data with earlier data makes it possible to draw up accurate sediment isopach maps for the Argo Abyssal Plain and adjacent areas. These show that the maximum sediment thicknesses for all seismic units are found in the central or southern part of the Abyssal Plain.

The presence of hyaloclastites at two core sites on or adjacent to the Joey Rise, suggest that these features and possibly also the Roo Rise are not continental fragments but volcanic excrescences. Basalt was recovered from the outer margin of the Exmouth Plateau, but the implications of this occurrence are presently equivocable.

A manganese nodule pavement of unknown extent occurs between the Joey and Roo Rises.

There is abundant evidence of a high level of sulphate reduction in the sediments of the northwestern extension of the Bali Trough.

The cruise confirmed the wide distribution of diapir-like piercement structures underlying the Argo Abyssal Plain, but it is not possible to say whether they are salt or mud-cored.

Acknowledgements

The authors wish to express their thanks to the many colleagues who contributed to this paper through their advice and assistance. The shipboard technical staff were unfailingly efficient and helpful throughout the cruise. The shore-based technical staff at our various institutions similarly provided most valuable assistance with many aspects of the post-cruise work. Dr P. G. Quilty and Dr B. V. Haq undertook palaeontological analysis of the cores. Dr H. A. Jones, Dr W. Johnstone, Dr N. F. Exon and Dr J. F. Truswell, all of BMR, provided editorial comments. The shipboard work was undertaken with Grant Number OCE75-20674 from the National Science Foundation. The figures were drawn by R. and G. Bates.

References

BALL, M. M., 1969—Diapirs of the Magdalena delta. *American Association of Petroleum Geologists, Bulletin* **53**, 2195-6.

BATIZA, R., 1977—Age, volume, compositional and spatial relationships of small isolated oceanic central volcanoes. *Marine Geology*, **24**, 169-83.

BRANSON, J. C., 1974—Structures of the western margin of the Australian continent. *Oil and Gas Journal (Sydney)*, **20**, 24-35.

BURKE, K., 1975—Atlantic evaporites formed by evaporation of water spilled from Pacific, Tethyan and Southern Oceans. *Geology*, **3**, 613-16.

COLLETTE, B. J., & RUTTEN, K. W., 1970—Differentiation compaction versus diapirism in abyssal plains. *Marine Geophysical Researches*, **1**, 104-7.

COOK, P. J., 1974—Geochemistry and diagenesis of interstitial fluids and associated calcareous oozes, Deep Sea Drilling Project, Leg 27, Site 262, Timor Trough. *In* VEEVERS, J. J., HIERTZLER, J. A., AND OTHERS, Initial reports of the Deep Sea Drilling Project, **27**, *US Government Printing Office, Washington*, 463-80.

FALVEY, D. A., & VEEVERS, J. J., 1974—Physiography of the Exmouth and Scott Plateaux, Western Australia, and adjacent northeast Wharton Basin. *Marine Geology*, **17**, 21-59.

FURNES, H., 1973—Variolitic structure in Ordovician pillow lava and its possible significance as an environmental indicator. *Geology* **1**, 27-30.

GEISKES, J. M., & ROGERS, W. C., 1973—Alkalinity determination in interstitial waters of marine sediments. *Journal of Sedimentary Petrology*, **43**, 27-30.

GRAN, G., 1952—Determination of the equivalence point in potentiometric titrations, Part II. *Analyst.*, **77**, 661-71.

HAILE, N. S., 1975—Calculation of paleolatitudes from palaeomagnetic poles. *Geology*, **3**, 174.

HEEZEN, B. C., & THARP, M., 1966—Physiography of the Indian Ocean. *Philosophical Transactions of the Royal Society of London, Series A*, **259**, 137-49.

HIERTZLER, J. R., TAYLOR, P. T., BALLARD, R. D., & HOUGHTON, R. L., 1977—A visit to the New England Seamounts. *American Scientist*, **65**, 466-72.

HIERTZLER, J. R., CAMERON, P., COOK, P. J., POWELL, T., ROESER, H. A., SUKARDI, S., & VEEVERS, J. J., 1977—The Argo Abyssal Plain—Oldest seafloor in the Indian Ocean. *American Geophysical Union* (Abstract).

HEIRTZLER, J. R., CAMERON, P., COOK, P. J., POWELL, T., ROESER, H. A., SUKARDI, S., & VEEVERS, J. J., 1978—The Argo Abyssal Plain (submitted to Earth and Planetary Science Letters).

JAKES, P. J., & WHITE, A. J. R., 1971—Composition of island arcs and continental growth. *Earth and Planetary Science Letters*, **12**, 224-30.

JOHNSTONE, M. J., JONES, P. J., KOOP, W. J., ROBERTS, J., GILBERT-TOMLINSON, J., VEEVERS, J. J., & WELLS, A. T., 1968—The Devonian of Western and Central Australia. *Australian Petroleum Exploration Association Journal*, **8**, 42-50.

KERR, P. F., DREW, I. M., & RICHARDSON, D. S., 1970—Mud volcano clay, Trinidad, West Indies. *American Association of Petroleum Geologists, Bulletin*, **54**, 2101-10.

KINSMAN, D. J. J., 1975—Salt floors to geosynclines. *Nature*, **255**, 375-78.

MACDONALD, G. A., & KATSURA, T., 1964—Chemical composition of Hawaiian lavas. *Journal of Petrology*, **5**, 82-133.

MELSON, W. G., & THOMPSON, G., 1973—Glassby abyssal basalts, Atlantic sea floor near St Paul's Rocks: Petrography and composition of secondary clay minerals. *Geological Society of America Bulletin*, **84**, 703-16.

NICHOLLS, I. A., 1974—A direct fusion method for preparing silicate rock glasses for energy dispersive electron microprobe analyses. *Chemical Geology*, **14**, 151-7.

PAREKH, P. P., MOLLER, P., DULSKI, P., & BAUSCH, W. M., 1977—Distribution of trace elements between carbonate and non-carbonate phases of limestone. *Earth and Planetary Science Letters*, **34**, 39-50.

PAUTOT, G., AUZENDE, J. M., & LE PICHON, X., 1970—Continuous deep sea salt layer along North Atlantic margins related to early phase of rifting. *Nature*, **227**, 351-4.

ROBINSON, P. T., & WHITFORD, D. J., 1974—Basalts from the Eastern Indian Ocean, DSDP Leg 27. *In* VEEVERS, J. J., HIERTZLER, J. R., AND OTHERS—Initial reports of the Deep Sea Drilling Project, **27**, *US Government Printing Office, Washington*, 551-60.

ROBINSON, P. T., THAYER, P. A., COOK, P. J., & MCKNIGHT, B. K., 1974—Lithology of Mesozoic and Cenozoic sediments of the Eastern Indian Ocean, Leg 27, Deep Sea Drilling Project. *In* VEEVERS, J. J., HIERTZLER, J. R., AND OTHERS. Initial reports for the Deep Sea Drilling Project, **27**. *US Government Printing Office, Washington*, 1001-47.

ROCKER, K., 1974—Vane shear strength measurements on Leg 27 sediment. *In* VEEVERS, J. J., HIERTZLER, J. R., AND OTHERS—Initial reports of the Deep Sea Drilling Project, **27**, *US Government Printing Office, Washington*, 425-43.

SCHMIDT, P. W., 1976—The non-uniqueness of the Australian mesozoic palaeomagnetic pole position. *Geophysical Journal of the Royal Astronomical Society*, **47**, 285-300.

SCHNEIDER, E. D., & JOHNSON, G. L., 1970—Deep ocean diapir occurrences. *American Association of Petroleum Geologists, Bulletin*, **54**, 2151-69.

SHEPARD, F. P., DILL, R. F., & HEEZEN, B. C., 1968—Diapiric intrusions in foreset slope sediments off Magdalena Delta, Columbia. *American Association of Petroleum Geologists, Bulletin*, **52**, 2197-207.

TUREKIAN, K. K., & WEDEPOHL, K. H., 1961—Distribution of the elements in some units of the earth crust. *Geological Society of America Bulletin*, **72**, 175-91.

VEEVERS, J. J., 1974—Seismic profiles made underway on Leg 22. *In* VON DER BORCH, C. C., SCLATER, J. G., AND OTHERS—Initial reports of the Deep Sea Drilling Project, **22**, *US Government Printing Office, Washington*, 351-67.

VEEVERS, J. J., & COTTERILL, D,. 1978—Western margin of Australia: evolution of rifted arch system. *Geological Society of America Bulletin*, **89**.

VEEVERS, J. J., FALVEY, D. A., HAWKINS, L. V. & LUDWIG, W. J., 1974—Seismic reflection measurements of northwest Australian margin and adjacent deeps. *American Association of Petroleum Geologists, Bulletin* **58**, 1731-50.

VEEVERS, J. J., & HIERTZLER, J. R., 1974—Bathymetry, seismic profiles and magnetic anomaly profiles. *In* VEEVERS, J. J., HEIRTZLER, J. R., AND OTHERS—Initial reports of the Deep Sea Drilling Project, **27**, *US Government Printing Office, Washington*, 339-81.

VEEVERS, J. J., HEIRTZLER, J. R., AND OTHERS, 1974—Initial reports of the Deep Sea Drilling Project, **27**, *US Government Printing Office, Washington*.

WILLCOX, J. B., & EXON, N. F., 1976—The regional geology of the Exmouth Plateau. *Australian Petroleum Exploration Association Journal*, **16**, 1-11.

The Oenpelli Dolerite — a Precambrian continental tholeiitic suite from the Northern Territory, Australia

P. G. Stuart-Smith and John Ferguson

The Oenpelli Dolerite comprises at least four major sheet-like intrusions up to 250 m thick of continental tholeiitic composition, which have a lateral extent of about 20 000 km². The intrusions were emplaced at about 1720 m.y. into Lower Proterozoic metasediments of the Pine Creek Geosyncline, and postdate an 1880 m.y. regional metamorphic event. The intrusions consist of symmetrically differentiated layers of olivine dolerite, minor felsic differentiates, and rare crosscutting gabbroic pegmatites. Within the thicker sheets minor rhythmic layering is found in olivine dolerite.

The Oenpelli Dolerite contains normative orthopyroxene and the major and trace element chemistry closely parallels the trends of major continental mafic tholeiitic suites.

Projection of the chemical data into the anhydrous CMAS system shows that the rocks crystallised in the pressure range 1 atmosphere to 5 kb. The close match between the observed equilibrium and the 1 atmosphere phase diagrams for dry tholeiitic magmas suggests that the last equilibration of these magmas was at very low pressure. It is concluded that the tholeiitic Oenpelli Dolerite rocks have evolved by polybaric olivine fractionation during slow, or intermittent, uprise from higher magnesia magma generated by partial melting within the upper mantle; plagioclase is an additional liquidus phase at shallow-crustal levels.

Introduction

Dolerite was first mapped in the Alligator Rivers area by Dunn (1962), who differentiated 'altered doleritic rocks and granophyric differentiates' intruding Lower Proterozoic sediments west of the East Alligator River, from 'porphyritic gabbroic rocks' intruding 'Myra Falls Metamorphics' (thought at the time to be Archaean) east of the river. Dunn (1962) described both suites as discordant intrusions emplaced after folding of the Lower Proterozoic metasediments. Walpole (1962), and Dunn (1962), mapped the altered dolerite as Zamu Complex, which was the term applied by Stewart (1959) to the basic intrusives of the South Alligator River valley. Bryan (1962) described phases within the porphyritic gabbro as augite gabbro, porphyritic microgabbro, and dolerite, and the rocks were termed 'basic intrusive rocks of the Oenpelli area'.

Since 1971, BMR has been engaged in reappraising the geology of the Pine Creek Geosyncline. During this work the mafic intrusive rocks of the Oenpelli area have been systematically mapped and named 'Oenpelli Dolerite' (Needham & others, 1974). The unit is more extensive than envisaged by previous workers, and several areas mapped by Dunn (1962), largely by photo-interpretation, as the Nungbalgarri Volcanic Member of the Kombolgie Formation, or as gneiss and schist, are Oenpelli Dolerite (Fig. 1). Contact relationships indicate a younger post-regional metamorphic age for the Oenpelli Dolerite in contrast to the pre-regional metamorphic age for the Zamu Complex. Smart & others (1976) described the unit in some detail and formalised its nomenclature.

After extensive field research, and petrographic examination of more than 200 thin sections, a suite of twelve rock samples was chosen for chemical analysis as being representative of the range of rock types in the Oenpelli Dolerite. This paper expands the description of the unit, and examines its chemical characteristics and magmatic history.

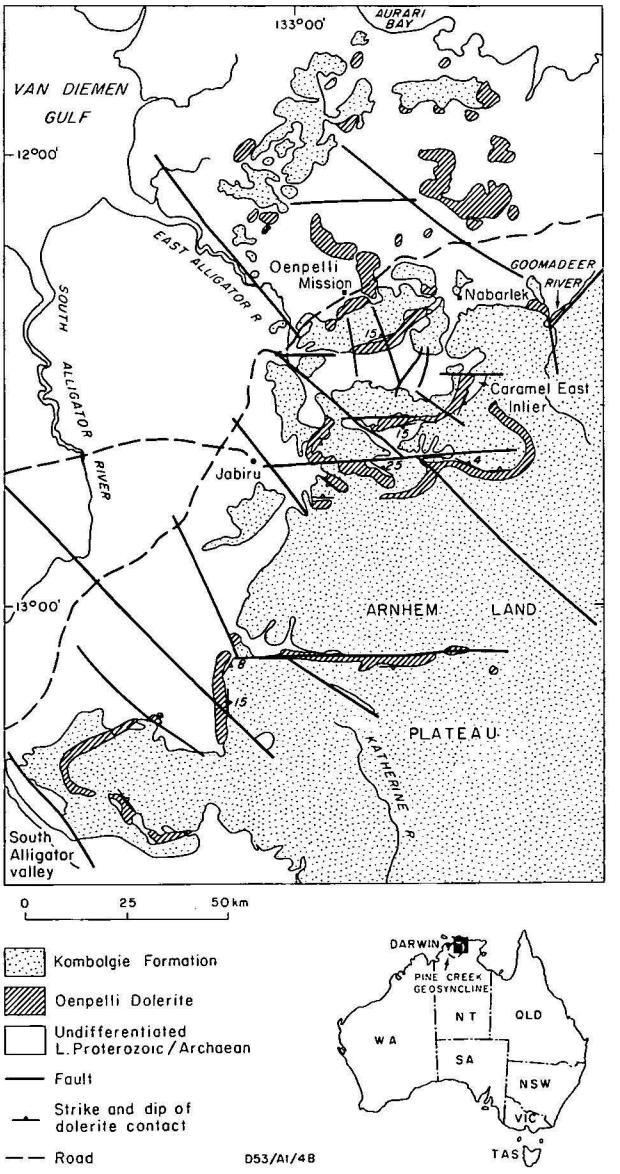

Field relations and age

The Oenpelli Dolerite extends from the western side of the Arnhem Land escarpment to the Goomadeer River in the east, north to the coast at Aurari Bay, and

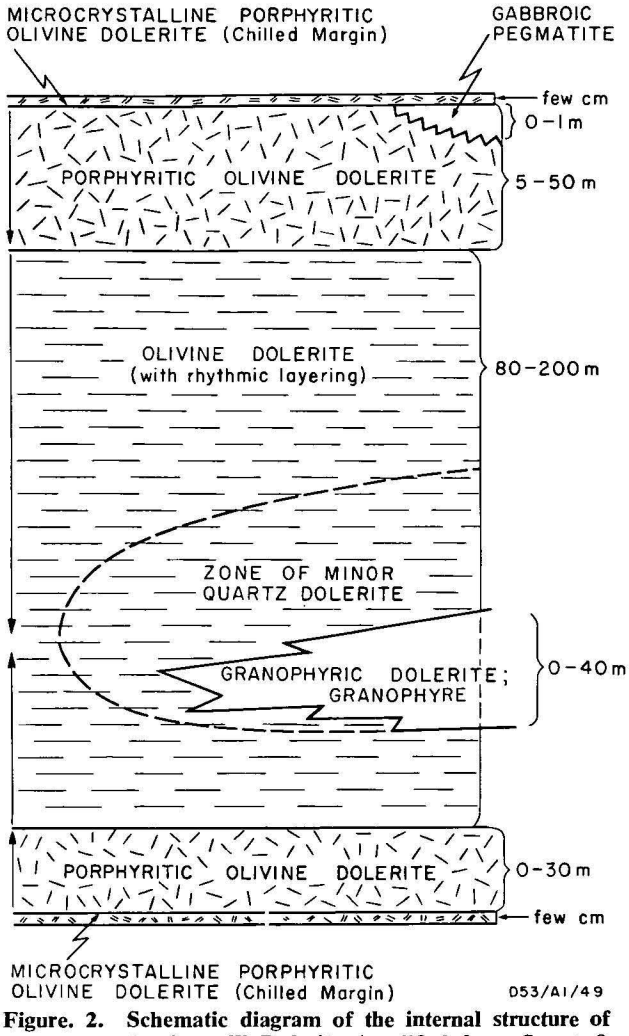

Figure. 2. Schematic diagram of the internal structure of the Oenpelli Dolerite (modified from Smart & others, 1976). Arrows show direction of increase in grainsize of groundmass.

southwards to the headwaters of the Katherine River. It covers an area, mostly subsurface, of 20 000 km^2, which is greater than that occupied by the Tasmanian Jurassic dolerite sheets (McDougall, 1962) and comparable to the Peneplain sill of the mid-Jurassic Ferrar dolerite swarm in Antarctica (Gunn, 1962).

Generally the dolerite is poorly exposed, and its subsurface presence is indicated by aeromagnetic patterns, a distinctive red brown soil, characteristic mixed open forest with a dark photo pattern, or black humic soil flats. Most of the dolerite is capped by sandstone of the Carpentarian Kombolgie Formation which forms the Arnhem Land Plateau, but it is exposed as prominent ridges or low hills within deep gorges in the Plateau or as ridges up to 150 m high near the escarpment, as well as in the adjacent scree slope. East and north of Oenpelli Mission, the Dolerite forms low hills, some of which are capped by Lower Proterozoic metasediments, boulders, and crops out as weathered rock in incised creeks.

The Oenpelli Dolerite intrudes Lower Proterozoic metasediments that were metamorphosed to amphibolite facies 1800 m.y. ago (Page, 1974). The Dolerite yields a concordant Rb-Sr total-rock and mineral age of 1718 ± 65 m.y. (Page, 1974), a date compatible with observed field relations. An unconformity separates the Oenpelli Dolerite from the overlying Carpentarian Kombolgie Formation; dolerite dykes cutting this Formation produce a preliminary age of about 1200 m.y. (Page, 1974).

The Oenpelli Dolerite consists of at least four major and one minor discordant basin-like ellipsoidal lopoliths, some of which are interconnected, and rare, narrow (<1 m) vertical dykes. Two of the basins have major axes of 30-35 km, and minor axes of 10-15 km. The exposed thickness is mostly between 100 and 200 m, although drilling at Nabarlek has revealed a true thickness of 250 m. Dips of Oenpelli Dolerite are comparable to those of the overlying Kombolgie Formation, rarely exceeding 20° and normally ranging from 5° to 15°. However, dips are locally steeper than those of the Kombolgie Formation, indicating that the basinal structures are probably primary features unrelated to later folding.

The intrusions are roughly symmetrically differentiated layered sheets similar to the Jurassic dolerite sills of Tasmania (Fig. 2). The margins of the intrusions are composed of porphyritic olivine dolerite, the groundmass grainsize of which increases inwards. Where present, chilled margins of microcrystalline porphyritic olivine dolerite commonly contain partly assimilated xenoliths of pelitic schist and have sharp or transitional contacts with the coarser porphyritic olivine dolerite. Pods and veins of gabbroic pegmatite occur, rarely, near the upper chilled margin. The porphyritic olivine dolerite grades into ophitic olivine dolerite, which forms the bulk of the intrusion. The olivine dolerite is generally jointed parallel to the margins of the intrusions, giving the rock a layered appearance. Weak rhythmic layering is present in places in the thicker intrusions owing to slight cumulate concentrations of olivine and plagioclase. The central parts of the olivine dolerite zone contain narrow discontinuous lenses of granophyric dolerite in places, as well as minor quartz dolerite differentiates.

Where the Oenpelli Dolerite intrudes the Lower Proterozoic metasediments and granitoids, sharp contacts are present. The metamorphic aureole, in which the pyroxene hornfels facies has been reached, is rarely preserved owing to retrograde metamorphism. Cordierite hornfels is well exposed in the Caramal East inlier, and sillimanite hornfels crops out near the Arnhem Land escarpment 12 km east of Jabiru. The effects of retrograde metamorphism in the contact aureole are best seen near a prominent hill, known locally as Hill 335, 14 km north of Oenpelli Mission. The true width of the aureole is probably less than 50 m, but as the dolerite is relatively flat-lying, and underlies much of the area at shallow depth, hornfelsic schist and gneiss crop out in places over relatively large areas. In the retrograded aureoles, mafic minerals are altered to chlorite, and feldspars to sericite ± chlorite ± epidote. Biotite-feldspar gneiss is altered to quartz-sericite-chlorite rock. Recrystallisation in these rocks is rarely complete, and they are therefore recognisable as hornfelsic gneiss by their relict texture. Retrograde metamorphism has also affected the Dolerite, which is commonly altered to sericite, albite, prehnite and chlorite. In places the upper margin of the Dolerite is serpentinised. The serpentinite, which is markedly slickensided, is readily weathered to yellow-green clay; it crops out only in erosion gullies, which are rarely more than 2 m deep.

A 50-m wide contact aureole is consistent with experimental work by Winkler (1967), who suggests that a gabbro 200 metres thick intruded at a shallow

Rock type	OLIVINE DOLERITE										QUARTZ DOLERITE				GRANOPHYRIC DOLERITE		GRANOPHYRE	
Analysis number	*1*	*2*	*3*	*4*	*5*	*6*	*7*	*8*	*9*	*10*	*11*	*12*	*13*	*14*	*15*	*16*	*17*	*18*
BMR registered number	7212-1134	7508-0287	7212-1174	7212-1020	7212-1177	7312-1075	7312-1164	7212-1047	7312-1171	7312-1170	7312-1108	7508-0305	7312-1047	7212-1207	7212-1211	7212-1221	7312-1066	7212-1064
Quartz						} 2		tr	} tr	} 3	} 13	} 9	} 5	} 7	12	18	} 54	46
Alkali Feldspar				2	tr										10	16		22
Plagioclase	59	64	61	61	55	51	48	56	59	54	45	52	44	58	42	41	30	20
Orthopyroxene			tr	tr	tr				1									
Clinopyroxene	16	20	20	19	28	30	24	33	24	30	22	8	29	14	5	2		
Olivine	22	13	11	12	11		3	4	4									
Amphibole								2		8	14	26	17	17	28	20		
Biotite	1	1	2	1	1			1	2				2	2	tr			
Opaque	2	2	4	2	3	5	8	4	3	5	5	4	3	2	3	3	3	
Apatite		tr	tr	tr	tr	tr	tr	tr	tr	tr	1	1	tr	tr	tr	tr	tr	
Chlorite		tr	2	3	2	12	17		7								13	
Chloritoid																		11
Carbonate		tr													tr			
Epidote															tr	tr		
Prehnite													tr					
Sphene																tr	tr	1

tr = <0.5 percent.

Table 1. Modal analyses of the major phases within the Oenpelli Dolerite.

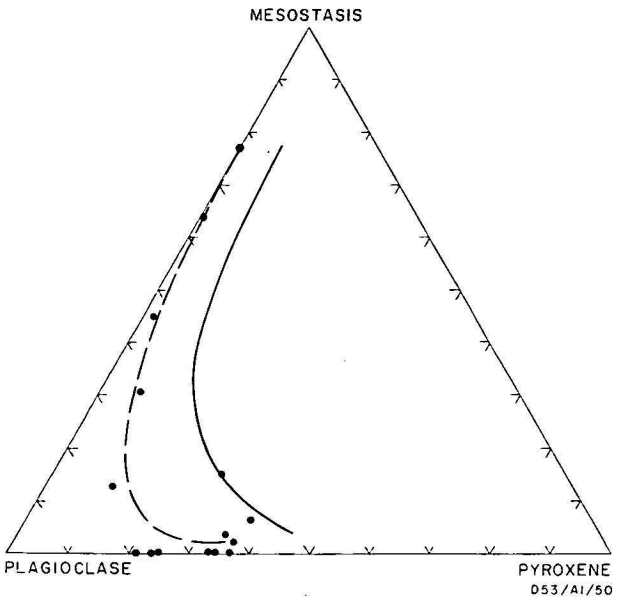

Figure 3. Main modal variations in the Oenpelli Dolerite. Solid line is trend of Tasmanian dolerites and granophyres from McDougall (1962).

depth (1-2 km) would produce a pyroxene hornfels zone at least 40 m wide, and an outer hornblende hornfels zone for a further 40 m.

Petrography

Results of modal analyses of eighteen specimens representative of the major phases of the Oenpelli Dolerite are presented in Table 1. Modal variations of the major mineral groups are illustrated in Figure 3.

Trends observed are typical for differentiated tholeiitic intrusions, in which plagioclase, pyroxene, and olivine decrease with increasing fractionation. An exception to this trend, in one sample of olivine dolerite (Analysis 1, Table 1), is caused by olivine accumulation. The appearance of amphibole in quartz dolerite corresponds to an increase in the proportion of mesostasis, and the disappearance of olivine.

The trend observed in Figure 3 shows pyroxene depletion and plagioclase enrichment relative to the Tasmanian dolerite (McDougall, 1962). This is because of the progressive replacement of pyroxene by amphibole with increasing fractionation.

Petrographic descriptions

Porphyritic olivine dolerite. This phase grades inwards from a strongly porphyritic type with a fine microcrystalline groundmass at the chilled margin to a type with fewer phenocrysts and a coarse groundmass where it becomes transitional into olivine dolerite. The rock is typically fine grained with large (up to 5 cm) discrete or aggregated zoned phenocrysts of plagioclase, whose core to margin composition is $An_{73.1}$ to $An_{70.6}$. Euhedral phenocrysts of greenish yellow olivine ($Fo_{79.1}$) are present in places. The groundmass consists of interlocking plagioclase laths (An_{65}), subhedral granules of pale brown augite, minor olivine, orthopyroxene (En_{80}), magnetite with ilmenite lamellae, and accessory pyrite. Commonly, olivine and augite are altered to chlorite and iron oxides. In some olivine-poor varieties up to 2 percent of mesostasis consisting of mainly alkali feldspar and minor quartz, apatite and opaque minerals is present.

Olivine dolerite. Olivine dolerite (ophitic dolerite of Smart & others, 1976) forms the bulk of the intrusions and is quite uniform in appearance, showing differences only in grainsize and degree of alteration. It is fine to coarse-grained, composed essentially of plagioclase, augite, and olivine.

Characteristically, olivine dolerite has an ophitic or subophitic fabric. Large (<1 cm) subidiomorphic crystals of pale brown, twinned augite, $Ca_{40.6}Mg_{37.5}Fe_{21.9}$ to $Ca_{36.9}Mg_{45.7}Fe_{17.4}$, are moulded around fine-grained (1 to 2 mm) idiomorphic plagioclase crystals ($An_{74.4\text{-}81.2}$). Pigeonite ($Ca_{6.5}Mg_{64.5}Fe_{29.0}$) with exsolved augite along (001) planes forms poikilitic anhedra, up to 1.5 mm in diameter. Pigeonite, augite, and rare colourless orthopyroxene also form small interstitial grains in places. Olivine (Fo_{63}) occurs as rounded colourless fractured crystals or in polygonal aggregates, and is commonly partly or completely pseudomorphed by dark green chlorite and opaques. Rarely, olivine forms euhedral inclusions in coarse-grained zoned plagioclase phenocrysts. Accessory minerals are interstitial pale greenish brown biotite, magnetite with exsolved ilmenite lamellae, chalcopyrite, pyrrhotite, pentlandite, acicular apatite, minor alkali feldspar and, rarely, quartz.

As with other phases of the Oenpelli Dolerite, chlorite, prehnite, epidote, and calcite are common alteration products. In markedly altered rocks, plagioclase is sericitised, albitised or completely replaced by prehnite; clinopyroxene is altered to a dark green fibrous amphibole.

Quartz-dolerite and gabbro. Towards the centres of intrusions, particularly in the thicker intrusions, olivine dolerite increases in grainsize and grades into medium to coarse-grained quartz dolerite or gabbro (ophitic gabbro of Smart & others, 1976). In places small

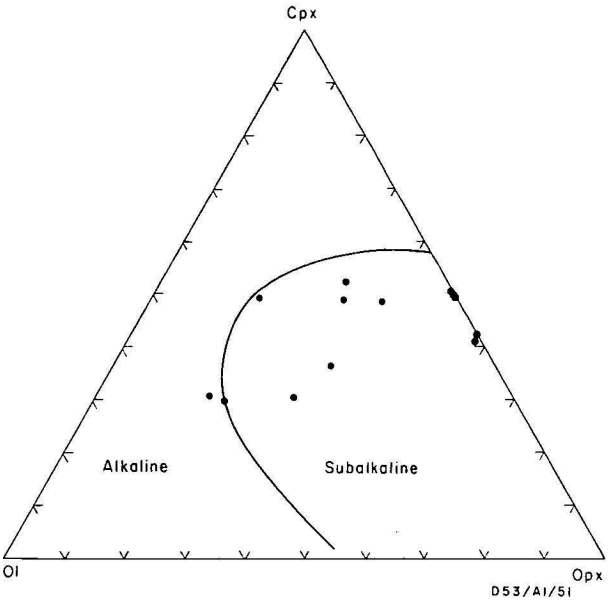

Figure 4. Cpx-Ol-Opx diagram of Oenpelli Dolerite norms. Boundary shown from Chayes (1966).

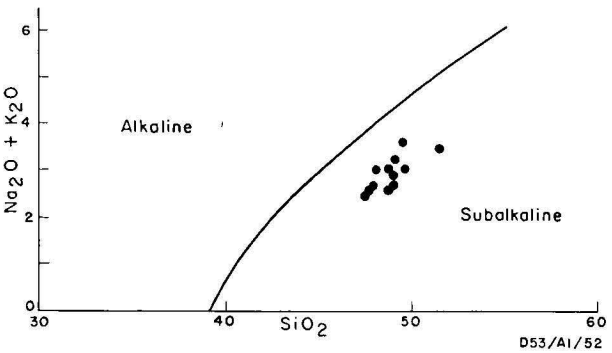

Figure 5. Alkalies-silica plot of the Oenpelli Dolerite. Boundary taken from Irvine & Baragar (1971).

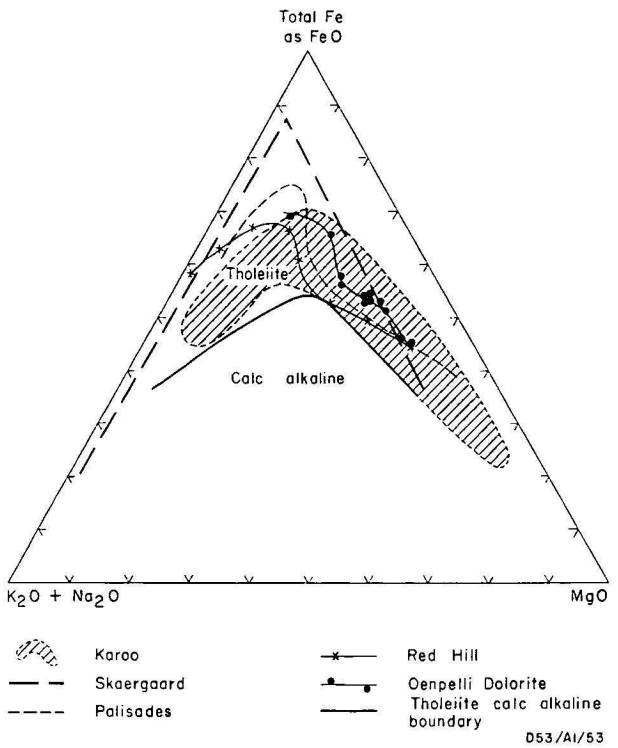

Figure 6. MgO—(total Fe as FeO)—(Na_2O + K_2O) diagrams showing the differentiation trends of the Oenpelli Dolerite and other provinces.
Differentiation trends: Karoo (Walker & Poldervaart, 1949); Skaergaard (Wager, 1960); Palisades (Walker, 1969); Red Hill (McDougall, 1962). Tholeiite-calc-alkaline boundary from Irvine & Baragar (1971).

gabbroic bodies have been found near the upper chilled margin. Typically the rocks have a subophitic texture and prominent mesostasis. Medium to coarse-grained (usually <4 mm) ragged prisms of twinned pale brown augite ($Ca_{29.6}Mg_{43.6}Fe_{26.8}$) surround medium-grained (<2 mm) euhedral plagioclase laths (An_{59}) that are commonly saussuritised, sericitised, and altered to prehnite. The augite is partly or completely replaced by strongly pleochroic greenish brown hornblende, and minor fibrous actinolite and biotite. Alteration is particularly prevalent along grain boundaries, cleavages traces, and factures. Where augite has been completely replaced, relict cleavages and crystal outlines are preserved. The mesostasis consists of graphically intergrown quartz and alkali feldspar, minor anhedral quartz, fibrous aggregates and clots of pleochroic pale greenish brown amphibole and chlorite, and magnetite with exsolved ilmenite lamallae, and accessory acicular apatite. Magnetite with exsolved ilmenite lamellae also forms large (<2 mm) skeletal grains associated with amphibole and biotite, or rims around augite. The skeletal grains in amphibole follow amphibole cleavage.

Granophyric dolerite and granophyre. Granophyric dolerite and granophyre, which forms discontinuous lenses in quartz dolerite, are the most felsic and least abundant differentiates of the Oenpelli Dolerite. Contacts of granophyric dolerite and granophyre are not well exposed, but are probably gradational. They are characterised by the extensive development of a mesostasis consisting of graphically intergrown quartz and alkali feldspar, which amounts to more than 20 percent in granophyric dolerite and 50 percent in granophyre. The rocks contain medium to coarse-grained euhedral laths or rhombs of plagioclase, which are invariably sericitised, chloritised, saussuritised and rarely calcitised; rims of chlorite or alkali feldspar are also present in places. The intensity of alteration appears to be proportional to the amount of mesostasis. Pale brown augite is present in granophyric dolerite, but is extensively altered to dark greenish brown hornblende which forms ragged subprismatic crystals. Hornblende is also present as smaller interstitial grains as well as anhedral sphene, epidote, biotite, acicular apatite, and skeletal iron oxides. In the granophyres, clinopyroxene, and amphibole are absent, but clots of chlorite and chloritoid showing well developed hourglass structures are present.

Chemistry

Major and trace element data and CIPW norms for the mafic and intermediate differentiates of the Oenpelli Dolerite are presented in Table 2. The more felsic differentiates—granophyric dolerite. and granophyre—are considered too altered for useful chemical results, and have not been analysed.

The analytical results and the CIPW norms show that the composition of the Oenpelli Dolerite is close to that of the typical olivine tholeiite of Irvine & Baragar (1971). All the samples are orthopyroxene-

Analysis number	*1*	*2*	*3*	*4*	*5*	*6*	*7*	*8*	*9*	*10*	*11*	*12*
BMR registered number	72121134	75080287	72121174	72121020	72121177	73121075	73121164	72121047	73121171	73121170	73121108	75080305
Chemical analyses												
SiO_2	47.41	47.75	48.08	47.91	48.83	49.05	48.93	49.57	48.79	49.16	49.64	51.51
TiO_2	0.96	0.95	1.39	1.28	1.27	1.51	1.54	1.74	1.50	1.80	2.66	2.26
Al_2O_3	17.04	17.00	16.71	16.32	14.16	15.49	15.26	14.34	15.19	15.36	13.13	15.02
Fe_2O_3	0.89	—	1.16	1.25	1.13	1.87	1.53	0.99	1.78	1.95	3.67	2.50
FeO	9.69	€10.45	11.21	10.12	10.65	9.54	9.88	11.60	9.59	10.13	11.17	10.75
MnO	0.15	0.15	0.18	0.17	0.18	0.19	0.18	0.19	0.17	0.18	0.21	0.12
MgO	10.30	9.55	7.70	8.14	7.83	6.85	6.96	6.16	7.02	5.61	4.66	2.32
CaO	10.31	10.49	9.63	10.37	11.55	10.27	10.62	9.90	10.65	10.02	9.05	8.51
Na_2O	2.01	2.22	2.31	2.15	2.06	2.09	1.98	2.76	2.36	2.37	2.22	2.45
K_2O	0.47	0.38	0.75	0.50	0.56	0.82	0.67	0.87	0.70	0.88	0.84	1.06
P_2O_5	0.08	0.10	0.14	0.11	0.11	0.15	0.15	0.18	0.14	0.18	0.22	0.37
CO_2	n.a.	0.15	n.a.	n.a.	n.a.	n.a.	n.a.	n.a.	n.a.	n.a.	n.a.	0.05
loss	1.04	0.19	1.11	1.16	1.08	1.92	2.15	1.16	1.81	2.16	1.83	1.79
	100.35	99.38	100.37	99.48	99.41	99.75	99.85	99.46	99.70	99.80	99.30	98.71
As	<2	<2	<2	<2	<2	<2	<2	<2	<2	<2	<2	<2
Ba	158	149	237	202	207	263	215	305	223	171	302	213
Bi	<2	n.a.	<2	<2	<2	<2	<2	<2	<2	<2	<2	n.a.
Ce	29	34	35	30	32	33	37	44	31	34	49	65
Ga	22	17	21	22	25	22	18	22	19	21	25	24
La	11	7	17	14	14	15	15	22	15	19	28	28
Mo	7	4	5	7	7	6	5	9	6	7	7	4
Nb	2	4	5	4	4	7	4	7	6	7	9	12
Pb	<2	2	4	2	3	8	3	5	2	3	4	<2
Rb	11	9	19	14	14	18	25	24	18	25	28	32
Sn	<2	<2	<2	<2	<2	<2	<2	<2	<2	2	<2	2
Sr	258	310	304	338	271	295	294	280	309	216	219	270
Th	<2	<2	3	3	<2	2	2	3	<2	2	4	3
U	<2	<2	<2	<2	<2	<2	<2	<2	<2	<2	<2	2
V	161	282	225	216	268	278	283	338	302	361	506	176
Y	16	10	19	13	16	17	18	24	19	24	35	37
Zr	54	46	86	62	67	88	84	111	79	115	155	170
Ratios												
Ce/Y	1.81	3.40	1.84	2.31	2.00	1.94	2.06	1.83	1.63	1.42	1.40	1.76
Nb/Zr	0.037	0.087	0.058	0.065	0.060	0.080	0.048	0.063	0.076	0.061	0.058	0.071
K/Ba	24.7	21.5	26.2	20.8	22.2	25.9	26.0	23.6	26.0	42.7	22.8	41.8
K/Rb	355	356	326	300	329	378	224	300	322	292	246	278
Norms												
Q	—	—	—	—	—	—	0.01	—	—	0.47	6.17	9.27
Or	2.80	2.26	4.46	3.00	3.36	4.95	4.05	5.23	4.22	5.32	5.09	6.46
Ab	17.11	18.92	19.68	18.49	17.71	18.06	17.13	23.74	20.38	20.52	19.26	21.37
An	36.33	35.59	33.26	33.97	28.21	31.14	31.50	24.59	29.41	29.37	23.99	27.71
Hyp *Wo*	6.10	6.36	5.82	7.35	12.24	8.32	8.94	10.09	9.86	8.48	8.59	5.43
Hyp *En*	3.60	3.50	2.96	3.99	6.38	4.45	4.70	4.61	5.30	4.12	3.94	1.64
Hyp *Fs*	2.21	2.63	2.72	3.10	5.52	3.61	3.98	5.40	4.24	4.23	4.58	4.02
Di En	5.47	4.42	6.51	8.16	7.64	12.77	13.04	6.10	8.63	10.19	7.96	4.32
Di *Fs*	3.36	3.32	6.00	6.34	6.61	10.36	11.03	7.14	6.90	10.47	9.24	10.59
Ol *Fo*	11.74	11.25	6.90	5.93	4.06	0.15	—	3.43	2.75	—	—	—
Ol *Fa*	7.95	9.33	7.00	5.08	3.87	0.13	—	4.43	2.43	—	—	—
Mt	1.30	—	1.69	1.84	1.67	2.77	2.27	1.46	2.64	2.90	5.46	3.74
Il	1.84	1.82	2.66	2.47	2.45	2.93	2.99	3.36	2.91	3.50	5.18	4.43
Ap	0.19	0.24	0.33	0.26	0.26	0.36	0.36	0.43	0.34	0.44	0.53	0.90
cc	—	0.34	—	—	—	—	—	—	—	—	—	0.12
Normative Plagioclase	$An_{68.0}$	$An_{65.3}$	$An_{62.8}$	$An_{64.8}$	$An_{61.4}$	$An_{63.3}$	$An_{64.8}$	$An_{50.9}$	$An_{59.1}$	$An_{58.9}$	$An_{55.5}$	$An_{56.5}$

€ = total Fe as FeO n.a. = not analysed < = less than 2,6,7 porphyritic olivine dolerite, 1,3,4,5,8,9 olivine dolerite, 10,11,12 quartz dolerite

Table 2. Chemical analyses and norms from the Oenpelli Dolerite.

	Sr (*ppm*)	*Rb* (*ppm*)	*K/Rb*	Sr^{87}/Sr^{86}
Ferrar Dolerite[1] *(olivine tholeiite)*	100	12	267	0.7111
Karoo dolerite[1]	180-400	11-12	395-425	0.7057
Oenpelli Dolerite[2] *(olivine dolerite)**	295	17	320	0.704
Skaergaard[3] *(chilled marginal gabbro)*	267	5.8	360	0.7065
Tasmanian dolerite[1]	130	33	200	0.7111

* average of 9 analyses

1. Compston & others, 1968; 2. this paper; 3. Hamilton, 1963; Wager & Brown, 1968.

Table 3. Comparison of Sr, Rb values, K/Rb and Sr^{87}/Sr^{86} ratios of the Oenpelli Dolerite and other major tholeiitic provinces.

normative, and plot within the subalkaline field on the Cpx-Ol-Opx ternary projection (Fig. 4) of the Cpx-Ol-Ne-Q tetrahedron (Chayes, 1966), and on the alkalies-silica diagram (Fig. 5) The FMA plot (Fig. 6) shows that the Oenpelli Dolerite falls within the tholeiitic field, and closely follows the differentiation trends characteristic of other major tholeiitic provinces.

Trace-element concentrations conform with the accepted pattern for tholeiitic differentiation series: Ba, La, Nb, V, Y, Zr, Ce, and Rb increase, and Mo and Ga remain fairly constant throughout differentiation of the olivine and quartz dolerites. Sr, Th, and Pb appear to be irregularly distributed, and do not conform to any trend. As, Bi, Sn, and U are present in very low concentrations and are usually undetectable. Ce/Y, Nb/Zr, K/Ba and K/Rb ratios are fairly constant throughout fractionation. The Oenpelli Dolerite has an average Sr concentration of about 295 ppm and an initial Sr^{87}/Sr^{86} ratio of 0.704. The Sr^{87}/Sr^{86} ratio, and K/Rb ratios of about 320 in olivine dolerite, are comparable to those of the Karoo dolerites of South Africa and the Skaergaard intrusions (Table 3), and are characteristic of an uncontaminated tholeiitic magma derived from the upper mantle (Compston & others, 1968). The K/Rb ratio is noticeably higher than those of Antarctic (Ferrar Dolerite) and Tasmanian dolerites, which are considered to be contaminated tholeiitic magmas.

Projections and mixing models

Stereo-pair plotting of the Oenpelli Dolerite rock compositions into the anhydrous system of CMAS space (O'Hara, 1968) demonstrates the close clustering of all the points. On the basis of this stereoscopic viewing a clinopyroxene projection was selected as offering the least distortion for the planar projection of the Oenpelli Dolerite rock compositions within the CMAS tetrahedron (Fig. 7). Figure 7 indicates that the Oenpelli Dolerite rocks plot near the 1 atmosphere and 5 kb pseudo-invariant points. Relative to the 5 kb pseudo-invariant point, a number of the Oenpelli Dolerite rock compositions fall within the primary phase field of orthopyroxene, a feature unsupported by petrographic evidence. On the other hand, consideration of the atmospheric pseudo-invariant point places the Oenpelli Dolerite rock compositions within the primary phase volume of olivine, with most values close to the olivine-plagioclase phase boundary—a feature supported by the petrographic evidence. Taken in conjunction with the petrography, other planar projections

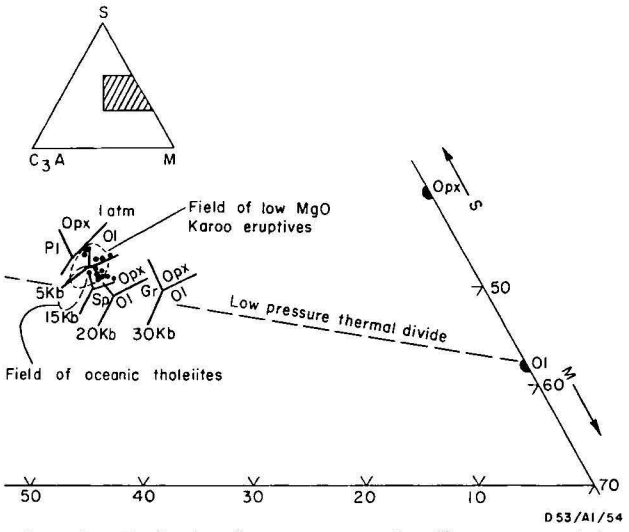

Figure 7. Projection from, or towards, clinopyroxene into the plane C_3A-M-S showing pseudo-invariant points at varying pressures.

Field of low-Mgo Karoo eruptives taken from McIver (1975), of oceanic tholeiites after McIver & Lenthall (1974). Phase boundaries are after O'Hara (1968), and Jamieson (1970). Abbreviations used: ol = olivine; opx = orthopyroxene; cpx = clinopyroxene; sp = spinel; pl = plagioclase; gr = garnet; kb = kilobars.

within the CMAS tetrahedron also confirm that the rock compositions lie in the low-pressure range.

In the CMAS projections the field of the Oenpelli Dolerite rocks roughly coincides with the field of oceanic tholeiites (McIver & Lenthall, 1974) and low-MgO Karoo rocks (McIver, 1975). The Oenpelli Dolerite rock compositions fall on the hypersthene-normative side of the low-pressure thermal divide, thus confirming their tholeiitic character (Fig. 7).

In view of the suggested low pressure of equilibration of the Oenpelli Dolerite compositions the analyses were recast into the simple phase diagrams for dry tholeiitic magmas at 1 atmosphere (Fig. 8). The corners of the tetrahedron represented by this 'natural' basalt system are Ol-Cpx-Pl-Qz. With the exception of specimens 11 and 12 these rocks are poor in the Qz component; it follows that the projection from Qz into the Ol-Cpx-Pl side of the tetrahedron would produce the least distortion, and show the primary phase fields directly where they intersect this plane (Fig. 8d). The Qz projection shows that, with the exception of the two quartz-rich dolerites (specimens 11 and 12) and specimen 10, all the rocks lie in the Ol + Liquid field near the Pl + Liquid boundary. The remaining three specimens plot within the Pl + Liquid field. Four of the specimens approach the pseudo-quaternary point of the 'natural' systems, falling in the near-cotectic fields of 'natural' basalts. The positions of the Oenpelli Dolerite rock compositions in the Qz projection support the petrographic evidence, which suggests that the predicted order of crystallisation is olivine followed by plagioclase. The trend displayed by the rock compositions in the Qz projection suggests that both olivine and plagioclase are the fractionating phases in the development of the more evolved rocks lying in the near-cotectic field of 'natural' basalts (Fig. 8d). That olivine and plagioclase are early crystallising phases is supported by the Pl and Ol-projections (Fig. 8a, c), where the rock compositions fall into the Ol+Pl+Liquid phase

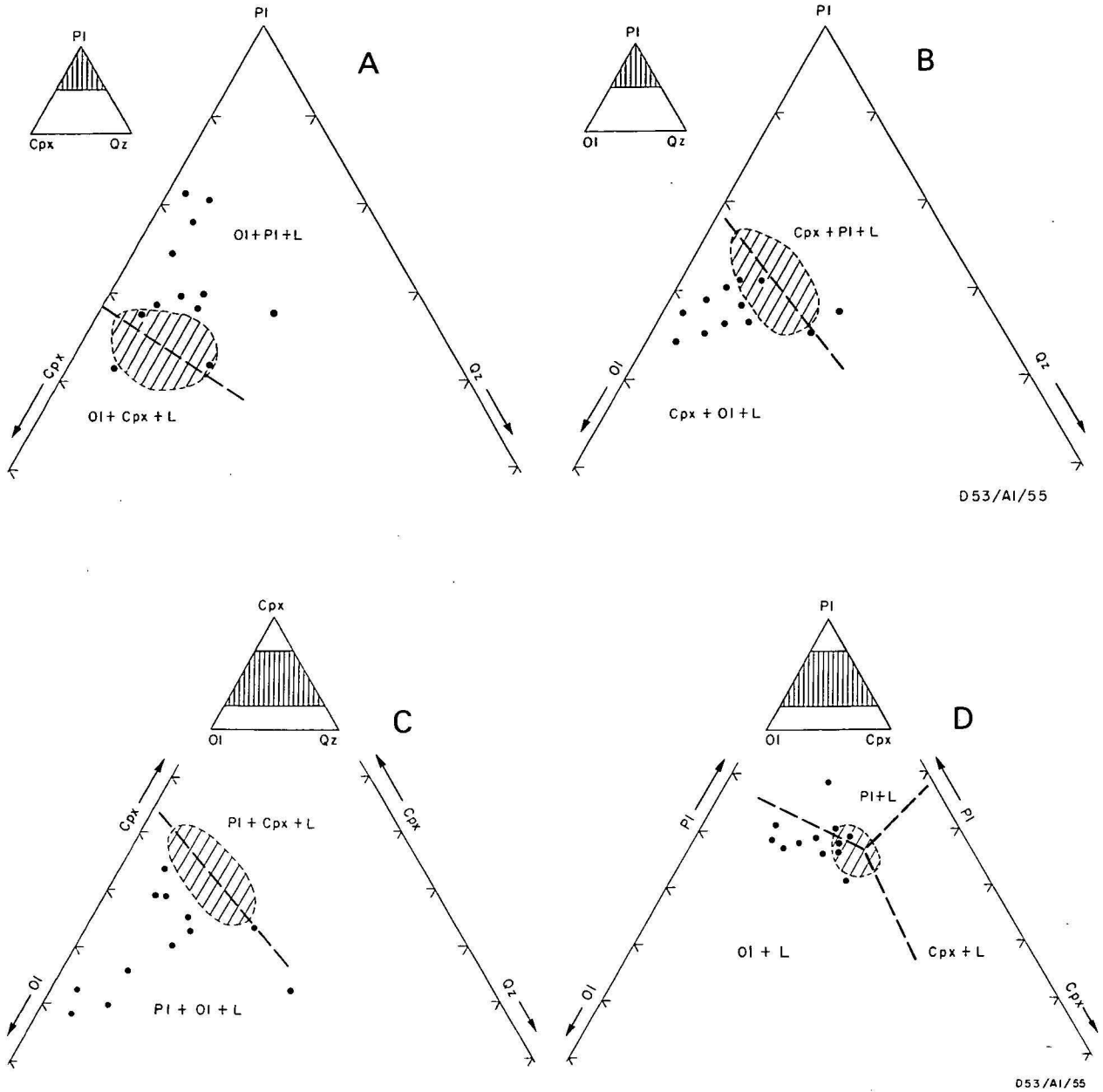

Figure 8. a-d. Projection of data into the pseudo-quaternary system Ol-Cpx-Pl-Qz. (a) projection from Ol, (b) projection from Cpx, (c) projection from Pl, (d) projection from Qz. Numbers for analyses correspond to those in Table 1.

Shaded area represents the field of those rocks melted by Tilley & others, (1963, 1964, 1965, 1967) and show the entry of all three phases (Ol, Pl, Cpx) within a temperature interval of 30°C or the second and third phases with that interval, in which case the data point is projected only from the first phase. Broken lines indicate approximate trends of loci of liquids in equilibrium with all three phases in (a), (b) and (c). The method of data projection after O'Hara (1965), Cox & Hornung (1966), and Clarke (1970). The phase boundaries used are those given by Cox & Bell (1972) which are in turn based on the quenching data of Tilley & others (1963, 1964, 1965, and 1967) for natural basalts.

fields. Specimen 6 provides the only exception to this, as in the Ol-projection this point lies in the Ol+Cpx+Liquid phase field and also in the near-cotectic field. Cox & Bell (1972, p. 5) point out that uncertainties about the positions of phase boundaries in these simplified systems mean that safe predictions can be made only for compositions that do not lie too close to the near-cotectic fields in these projections. In the Cpx-projection (Fig. 8) the plot once again demonstrates the importance of olivine fractionation in these rocks. As in the Qz and Ol-projections, the trend away from the Ol-Pl join shows the importance of these two phases in the fractionation history of the more evolved rocks.

In order to assess a model relating the more magnesian members of the olivine dolerite suite to the less magnesian members by a process of olivine and plagioclase fractionation a series of least-square linear-mixing calculations was made. In these calculations a fine-grained, even-textured olivine dolerite composition was chosen as representing the least evolved liquid (1, Table 1), and olivine ($Fo_{62.9}$) and plagioclase ($An_{81.2}$), being phases within this rock, were subtracted from it in various proportions in an attempt to match the compositions of the more evolved rocks. Considering the porphyritic, and minor cumulative nature of some of the rocks, a moderately good correlation was obtained between the observed and calculated com-

positions. The results of these mixing calculations thus appear to be consistent with the generation of the more evolved olivine dolerites from the more primitive members of this suite, by olivine and plagioclase fractionation (a tabulation of these mixing calculations is available on request).

Summary and discussion

The Oenpelli Dolerite constitutes a major tholeiitic province. It extends, mostly subsurface, over an area of 20 000 km^2, and comprises at least four major 100 to 200 m thick sheet-like intrusions which consist of symmetrically differentiated layers of olivine dolerite and minor felsic differentiates.

The intrusions crystallised from the upper and lower margins towards the centre where the more felsic differentiates were concentrated. Rare rhythmic layering in olivine dolerite indicates that gravity settling processes were also involved in fractional crystallisation of the magma.

The subalkaline nature of the Oenpelli Dolerite rocks is indicated by normative orthopyroxene and low ratios of total alkalies to silica. Major and trace element chemistry—in particular for the ratios K/Rb, K/Ba, Nb/Zr and Ce/Y—confirms their tholeiitic character. Trace-element concentrations also conform to the established pattern of tholeiitic differentiates: Ba, La, Nb, V, Y, Zr, Ce, and Rb increase with differentiation.

The anhydrous polybaric CMAS projections and contact effects indicate that the intrusions equilibrated at depths less than 15 km, and intruded at depths as shallow as 1 to 2 km. The site of generation of these magmas would require depths in excess of 15 km, as an improbably high geothermal gradient would be required for melting at this depth. Additionally the area is underlain by a thick cratonic sequence of Archaean and Lower Proterozoic granitoids, probably to a depth well in excess of 15 km; rocks of this composition could not produce the compositions encountered in the Oenpelli Dolerite suite. In keeping with general concepts of basalt genesis (see, for example, Ringwood, 1975) the origin of the Oenpelli Dolerite suite is more readily accounted for by postulating partial melting of upper mantle material. The moderately evolved nature of the Oenpelli Dolerite magma compositions suggests that their development could conform to the following model: partial melting of upper mantle material, followed by slow or intermittent rise of magma undergoing polybaric olivine fractionation, with plagioclase being an additional fractionating phase at shallow-crustal levels.

From a consideration of the Karoo rocks which display a wide range of chemical composition, McIver (1975) was able to demonstrate that low-magnesia eruptives, similar to the Oenpelli Dolerite, can be accounted for by polybaric olivine fractionation. The 1-atmosphere phase diagrams for dry tholeiitic magmas match the observed equilibrium well, and so it is suggested that the last equilibration of the Oenpelli Dolerite magmas was at very low pressures.

Acknowledgements

This paper is partly based on observed field relations, and samples collected, by P. G. Smart, R. S. Needham, and A. L. Watchman during 1:100 000 mapping of the Alligator Rivers Region during 1972 and 1973. The authors wish to extend their appreciation to the following: R. S. Needham and P. G. Smart for support and encouragement; W. B. Dallwitz, R. W. Johnson, D. E. Mackenzie, J. R. McIver, R. S. Needham, and C. E. Prichard for criticism of the draft; Queensland Mines Ltd for providing drill core; and B. W. Chappell for making his mixing program available; R. Fabbo and G. Butterworth for drafting the figures.

References

BRYAN, R., 1962—Lower Proterozoic basic intrusive rocks of the Katherine-Darwin area. *Bureau of Mineral Resources, Australia, Record* **1962/7** (unpublished).

CARMICHAEL, I. S. E., TURNER, F. J., & VERHOOGEN, J., 1974—IGNEOUS PETROLOGY. *McGraw-Hill, New York,*

CHAYES, F., 1966—Alkaline and subalkaline basalts. *American Journal of Science,* **264**, 128-45.

CLARKE, D. B., 1970—Tertiary basalts of Baffin Bay: possible primary magma from the mantle. *Contributions to Mineralogy and Petrology,* **25**, 203-24.

COMPSTON, W., MCDOUGALL, I., & HEIER, K. S., 1968—Geochemical comparison of the Mesozoic basaltic rocks of Antarctica, South Africa, South America and Tasmania. *Geochimica et Cosmochimica Acta,* **32**, 129-49.

COX, K. G., & BELL, J. D., 1972—A crystal fractionation model for the basaltic rocks of the New Georgia Group, British Solomon Islands. *Contributions to Mineralogy and Petrology,* **37**, 1-13.

COX, K. G., & HORNUNG, G., 1966—The petrology of the Karoo basalts of Basutoland. *American Mineralogist,* **51**, 1414-32.

DUNN, P. R., 1962—Alligator River, N.T., 1:250 000 geological series. *Bureau of Mineral Resources, Australia, Explanatory Notes* **SD/53-1**.

GUNN, B. M., 1962—Differentiation in Ferrar Dolerites of Antarctica. *New Zealand Journal of Geology and Geophysics,* **5**, 820-63.

HAMILTON, E. I., 1963—The isotopic composition of strontium in the Skaergaard intrusion, East Greenland. *Journal of Petrology,* **4**, 383-91.

HEIER, K. S., & MCDOUGALL, I., 1965—Thorium and uranium concentrations, and the isotopic composition of strontium in the differentiated Tasmanian dolerites. *Geochimica et Cosmochimica Acta,* **29**, 643-59.

IRVINE, T. N., & BARAGAR, W. R. A., 1971—A guide to the chemical classification of the common volcanic rocks. *Canadian Journal of Earth Sciences,* **8**, 523-48.

JAMIESON, B. G., 1970—Phase relations in some tholeiitic lavas illustrated by the system R_2O_3-XO-YO-ZO_2. *Mineralogical Magazine,* **37**, 537-54.

MCDOUGALL, I., 1962—Differentiation of the Tasmanian dolerites: Red Hill dolerite-granophyre association. *Geological Society of America, Bulletin* **73**, 279-316.

MCIVER, J. R., 1975—Aspects of some high magnesia eruptives in Southern Africa. *Contributions to Mineralogy and Petrology,* **51**, 99-118.

MCIVER, J. R., & LENTHALL, D. H., 1974—Mafic ultramafic extrusives of the Barberton Mountain Land in terms of the CMAS system. *Precambrian Research,* **1**, 327-43.

NEEDHAM, R. S., SMART, P. G., & WATCHMAN, A. L., 1974—A reinterpretation of the geology of the Alligator Rivers Uranium Field, Northern Territory. *Search,* **5**, 397-9.

O'HARA, M. J., 1965—Primary magmas and the origin of basalts. *Scottish Journal of Geology,* **1**, 19-40.

O'HARA, M. J., 1968—The bearing of phase equilibria studies in synthetic and natural systems on the origin and evolution of basic and ultrabasic rocks. *Earth Science Reviews,* **4**, 69-133.

PAGE, R. W., 1974—Implications of new geochronological data in the Alligator Rivers area, Northern Territory, *in* BMR symposium abstracts, Canberra 1974. *Bureau of Mineral Resources, Australia, Record* **1974/35** (unpublished).

RINGWOOD, A. E., 1975—COMPOSITION AND PETROLOGY OF THE EARTH'S MANTLE. *McGraw-Hill, New York.*

SMART, P. G., WILKES, P. G., NEEDHAM, R. S., & WATCHMAN, A. L., 1976—Geology and geophysics of the Alligator Rivers Region, 285-301. *In* KNIGHT, C. L. (Editor), ECONOMIC GEOLOGY OF AUSTRALIA AND PAPUA NEW GUINEA, **1**, Metals. *Australasian Institute of Mining and Metallurgy, Melbourne.*

STEWART, J. R., 1959—Proterozoic igneous rocks in the Katherine-Darwin region, Northern Territory. *M.Sc. thesis, University of New England* (unpublished).

TILLEY, C. E., YODER, H. S., & SCHRAIRER, J. F., 1963—Melting relations of basalts. *Carnegie Institution, Washington, Yearbook* **62**, 77-84.

TILLEY, C. E., YODER, H. S., & SCHRAIRER, J. F., 1964—New relations on melting of basalts. *Carnegie Institution, Washington, Yearbook* **63**, 92-7.

TILLEY, C. E., YODER, H. S., & SCHRAIRER, J. F., 1965—Melting relations of volcanic tholeiitic and alkali rock series. *Carnegie Institution, Washington, Yearbook* **64**, 69-82.

TILLEY, C. E., YODER, H. S., & SHRAIRER, J. F., 1967—Melting relations of volcanic rock series. *Carnegie Institution, Washington, Yearbook* **65**, 260-269.

WAGER, L. R., 1960—The major element variation of the layered series of the Skaergaard intrusion, *Journal of Petrology*, **1**, 364-98.

WAGER, L. R., & BROWN, G. M., 1968—LAYERED IGNEOUS ROCKS. *Oliver & Boyd, Edinburgh.*

WALKER, F., & POLDERVAART, A., 1949—Karroo Dolerites of the Union of South Africa. *Geological Society of America, Bulletin* **60**, 591-706.

WALKER, K. R., 1969—The Palisades Sill, New Jersey: A reinvestigation. *Geological Society of America, Special Paper*, **111**.

WALPOLE, B. P., 1962—Mount Evelyn, N.T., 1:250 000 Geological Series. *Bureau of Mineral Resources, Australia, Explanatory Notes*, **SD/53-5**.

WINKLER, H. G. F., 1967—PETROGENESIS OF METAMORPHIC ROCKS. *Springer-Verlag, Berlin.*

Nannofossil and planktic foraminiferal biostratigraphy around the Oligocene-Miocene boundary in parts of the Indo-Pacific region

Samir Shafik and George C. H. Chaproniere

Nannofossil evidence suggests that the up-sequence appearance of *Globigerinoides quadrilobatus primordius* is depth-related, and first occurs at a lower stratigraphic level in shallow marginal-marine than in deep oceanic sediments. The species is recorded associated with several late Oligocene nannofossil species, such as *Sphenolithus ciperoensis*, in three marginal-marine sections within the Indo-Pacific region; a study of the literature has revealed similar coeval occurrences elsewhere. However, evidence in deep oceanic sediments indicates that the lowest occurrence of *G. quadrilobatus primordius* is early Miocene in age.

***Globorotalia opima opima* occurs with *G. quadrilobatus primordius* in one section; published data indicate that this overlap is repeated elsewhere. This suggests that the planktic foraminiferal Zones N.3 and N.4 should be combined into Zone N3/4, the base of which is defined by the lowest occurrence of *Globigerinoides quadrilobatus primordius*.**

To account for the difference in the timing of the lowest occurrence of *G. quadrilobatus primordius* in hemipelagic and oceanic sediments, changes in the thickness of the zone between the lysocline and carbonate compensation depth during the latest Oligocene, and bathymetric shifts of this zone during the earliest Miocene, are invoked.

Evidence for precisely delineating the Oligocene-Miocene boundary is tenuous; the *Globigerinoides* datum is late Oligocene in age, contrary to the unratified recommendation of the Neogene Committee at Bologna in 1967, and at present no general agreement has been reached on nannofossil evidence to mark the boundary. For these reasons, a buffer zone representing the Oligocene-Miocene transition is suggested for the interval between the definite late Oligocene *Sphenolithus ciperoensis* (extinction) datum and the definite early Miocene *Sphenolithus belemnos* (base of range) datum. In hemipelagic sediments, this buffer zone may include several biostratigraphic events, such as the disappearance of the solution-prone *Zygrhablithus bijugatus*.

Introduction

This paper results from two independent investigations of nannofossils and planktic foraminiferids from Ashmore Reef No. 1 Well (Fig. 1) in the Bonaparte Gulf Basin of Western Australia. Because of the conflicting biostratigraphical results between the two investigations and published results from other areas, it became necessary to study some other sections which contain the same biostratigraphic evidence encountered in Ashmore Reef No. 1 Well, and which contain well preserved nannofossils and planktic foraminiferids. Two other sections were studied: the Meleri Beds from the Nassau Range, Irian Jaya (see Belford, 1974 for locality details) and core 5 from Capricorn No. 1A Well, Capricorn Basin, Queensland (Fig. 1).

Negatives of all figured nannofossil specimens, their permanent mounts and all figured planktic foraminiferids are deposited in the Commonwealth Palaeontological Collection in the Bureau of Mineral Resources and the numbers are prefixed by CPC.

G. C. H. Chaproniere is responsible for the section dealing with the planktic foraminiferids of the 'Cartier Beds' in this paper, S. Shafik for the balance.

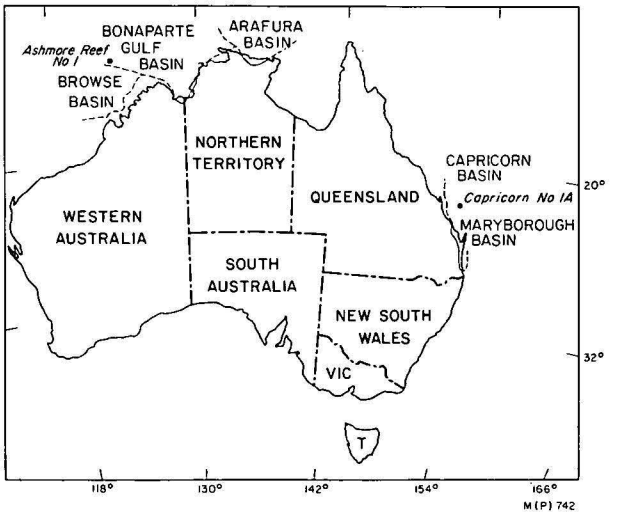

Figure 1. Locality map.

Material studied

Ashmore Reef No. 1 Well

All samples are from the 'Cartier Beds'. This is a sequence of calcareous shales, clays, and marls which disconformably overlies the Eocene 'Hibernia Beds' and passes gradationally into the conformably overlying unnamed calcarenites (Craig, 1968). Excellent nannofossil and planktic foraminiferal assemblages are restricted to most of the 'Cartier Beds', but the preservation of these assemblages deteriorates gradully up-section and in the overlying unnamed calcarenite.

Nine sidewall cores and one conventional core were studied, in addition to ditch-cuttings covering the non-cored parts of the sequence. The distribution of these cores against the main lithologies is shown in Figure 6.

Irian Jaya

The locality details for the three samples studied are given by Dow (1968), and Belford (1974). They are from the Meleri Beds, a sequence of marls and calcareous siltstones, which includes a limestone member and lenses of calcarenite and minor glauconitic sandstone. These beds are rich in nannofossils and planktic foraminiferids (Fig. 2).

NANNOFOSSIL SPECIES (Shafik, this paper)	SAMPLE No C17a		C17b		C18b		PLANKTIC FORAMINIFERIDA (after Belford, 1974)
Sphenolithus ciperoensis	*	•		•	*	•	*Globigerinoides quadrilobatus primordius*
Cyclicargolithus abisectus	*		*	•	*		*Globorotalia (Turborotalia) kugleri*
Helicopontosphaera euphratis	*	•	*			•	*Globorotalia (Turborotalia) obesa*
Helicopontosphaera recta	?	•		•	*		*Globorotalia (Turborotalia) siakensis*
Coccolithus cribellum	*	•	*	•		•	*Globorotalia (Turborotalia) opima nana*
Coccolithus eopelagicus	*	•	*	•	*		*Globigerina praebulloides occlusa*
Reticulofenestra scissura	*	•		•	*		*Globigerina venezuelana*
Reticulofenestra scrippsae	?	•		•	*	•	*Globigerina tripartita*
Discoaster deflandrei	*	•	*	•	*	•	*Globigerina sellii*
Sphenolithus conicus	*		*	•		•	*Globigerina sastrii*
Sphenolithus moriformis	*	•		•	*		*Globigerina gortanii gortanii*
Sphenolithus dissimilis		•	*			•	*Globigerina angustiumbilicata*
Coccolithus sp. cf. *C. pelagicus*	*	•			*		*Globigerina ouachitaensis ciperoensis*
Pontosphaera plana		•	*	•	*	•	*Globigerinita dissimilis*
Cyclicargolithus floridanus		•		•	*		*Globorotaloides suteri*
Braarudosphaera bigelowi		•	*	•		•	*Globigerinita unicava unicava*
Micrantholithus flos	*						
Triquetrorhabdulus carinatus	?		*				

M(P)744

* *Nannofossil occurrence* • *Planktic foraminiferid occurrence*

Figure 2. Distribution of late Oligocene nannofossils and planktic foraminiferids in the Meleri Beds, Irian Jaya.

Capricorn No. 1A Well

One sample from core 5 (877.3 m) was studied from this well. According to Palmieri (1971) the lithology at this level is sandy limestone.

Previous work

Ashmore Reef No. 1 Well

Previous faunal studies of the 'Cartier Beds' have been made by Belford (1968), Coleman (1968), and Chaproniere (1975). All three authors investigated the planktic and larger foraminiferal faunas. Belford (1968) assigned the middle parts of the 'Cartier Beds' a late Oligocene age based on a fauna from core 7 (1104-1109 m) which he placed in the *Globorotalia kugleri* Zone of Bolli (1957, 1966). Species recorded by Belford included: *Globigerinoides quadrilobatus primordius, Globigerina augustiumbilicata, G. ouachitaensis, Globigerinita unicava, Globorotalia mayeri, G. obesa, Globoquadrina* sp. cf. *G. dehiscens,* and the group of *Globigerina praebulloides* which includes *G. praebulloides praebulloides* and *G. praebulloides occlusa.* Coleman (1968) assigned an Oligocene age to the 'Cartier Beds' below the level of large foraminiferids which he considered early Miocene in age. Chaproniere (1975) recognised two of his eight larger foraminiferal associations in the upper part of the 'Cartier Beds'; the *Operculina complanata*-smaller benthonic foraminiferal association, which was overlain by the *Cycloclypeus* (*Cycloclypeus*) *eidae-Operculina complanata* association; he referred the beds to planktic Zones N.3 to N.5 without giving their faunal content. No previous studies of nannofossils from this well have been made.

Irian Jaya

The planktic foraminiferids have been studied previously by Belford (1974), and their results are summarised in Figure 2. The nannofossils from these samples have not been previously studied.

Capricorn No. 1A Well

Palmieri (1971, 1974, 1975) has discussed the planktic foraminiferids and their biostratigraphy for this well. Hekel (1973) recognised the *Sphenolithus ciperoensis-Dictyococcites abisectus* zonal interval from ditch-cuttings between 914.4 m to 883.9 m, and in a sample from core 5 at 876.9 m; he assigned this zonal interval to the late Oligocene-early Miocene.

Nannofossils

Assemblages

'Cartier Beds'. Five integrated nannofossil assemblages have been recognised from the 'Cartier Beds' in Ashmore Reef No. 1 Well. Representatives of most of the species recognised are shown in Figures 3-5, 8-9. The basal 46 m of the 'Cartier Beds' contain abundant, moderately preserved nannofossil elements. In this segment, cored material is represented by a single side-wall core at 1187.5 m (i.e. 34.8 m above the base of the 'Cartier Beds'). The following species have been recorded from this level: *Braarudosphaera bigelowi, Coccolithus cribellum, C. eopelagicus, Cyclicargolithus abisectus, C. floridanus, Discoaster deflandrei* (overcalcified), *Helicopontosphaera euphratis, H. recta* (common), *Micrantholithus fornicatus, Pontosphaera multipora, Reticulofenestra scissura* (frequent), *Sphenolithus ciperoensis* (abundant) and *Triquetrorhabdulus carina-*

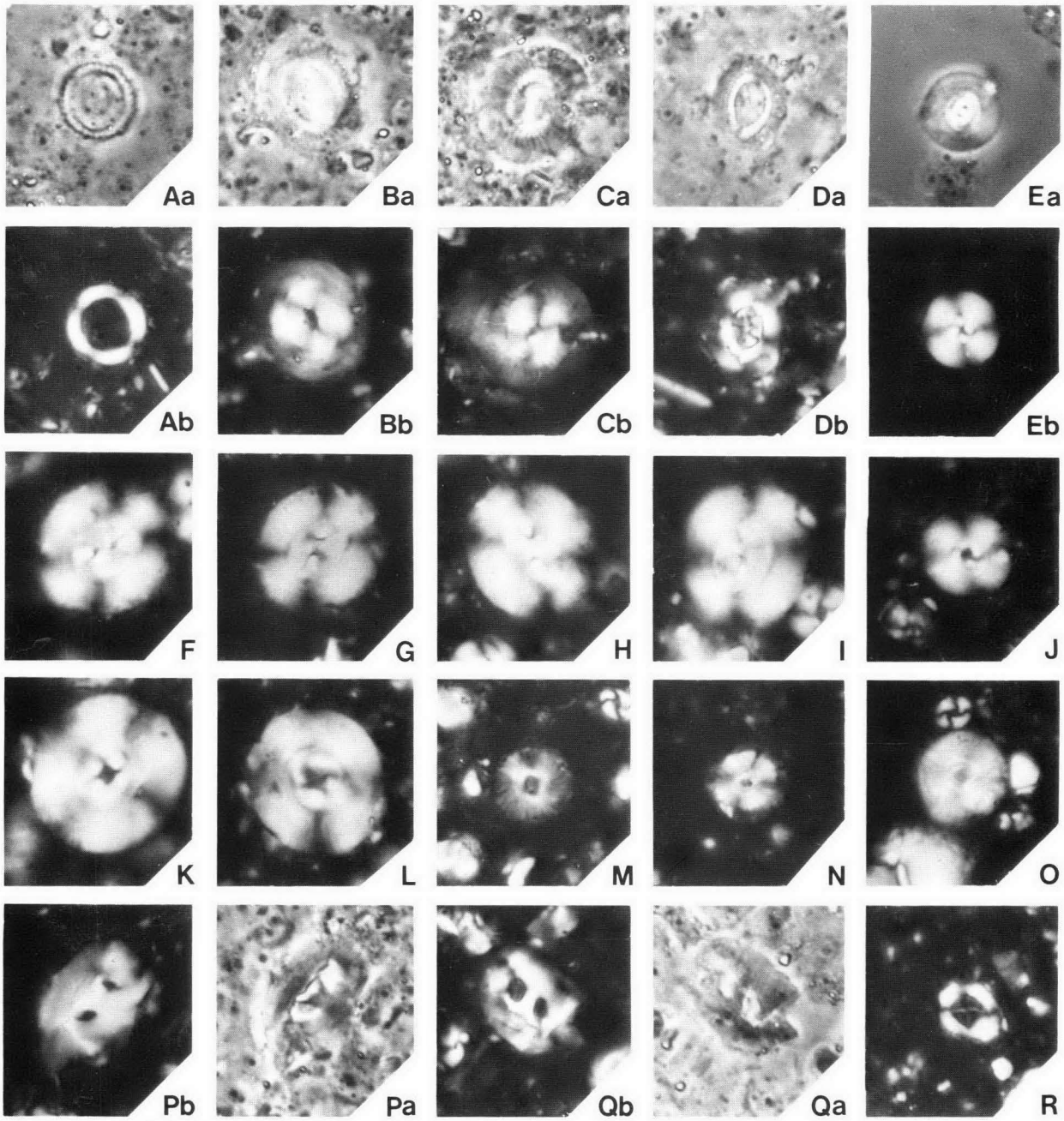

Figure 3. (All photographs are x2000)

Aa-b *Coronocyclus nitescens* (Kamptner), CPC 18143; Ba-b, Ca-b *Coccoliths eopelagicus* (Bramlette & Riedel): B = CPC 18144, C = CPC 18145; Da-b *Coccolithus cribellum* (Bramlette & Sullivan) CPC 18146; Ea-b, J *Cyclicargolithus floridanus* (Roth & Hay) E = CPC 18147, J = 18148; F-I *Reticulofenestra scissura* Hay, Mohler & Wade: F = CPC 18149, G = CPC 18150, H = CPC 18151, I = CPC 18152; K-L *Cyclicargolithus abisectus* (Müller): K = CPC 18153, L = CPC 18154; M-O *Cycloccolithina leptopora* (Murray & Blackman): M = CPC 18155, N = CPC 18156, O = CPC 18157; Pa-b, Qa-b *Helicopontosphaera recta* (Haq): P = CPC 18158, Q = CPC 18159; R ?*Chiasmolithus altus* Bukry & Percival, CPC 18160.

tus (rare). Samples of cuttings from the basal 46 m confirmed the presence of species such as *H. recta, R. scissura, S. ciperoensis,* and *T. carinatus* and revealed the occurrence of *Pontosphaera plana, Reticulofenestra aragonensis, R. scrippsae, Sphenolithus conicus, S. moriformis* and *Zygrhablithus bijugatus.* A few specimens of *Sphenolithus predistentus* have been observed in cuttings from near the base of the sequence.

The overlying 72 m of the 'Cartier Beds' are characterised by slightly different assemblages. *Reticulofenestra scissura* and *R. scrippsae* disappear, but most of the other species persist, with the addition of a few new elements. Core 7 occupies the upper part of this section. A representative sample from core 7 (at 1104.3 m; i.e. 118 m above the base of the 'Cartier Beds') contains *Braarudosphaera bigelowi, Coccolithus cribellum, C.eopelagicus, C.* sp. cf. *C. pelagicus, Corannulus germanicus, Coronocyclus serratus, Cyclicagrolithus abisectus, C. floridanus, Dakylethra* sp., *Discoaster deflandrei* (group), *Helicopontosphaera euphratis, H. intermedia, H. obliqua, H. recta, Holodiscolithus macroporus, Micrantholithus fornicatus, Pontosphaera multipora, P.*

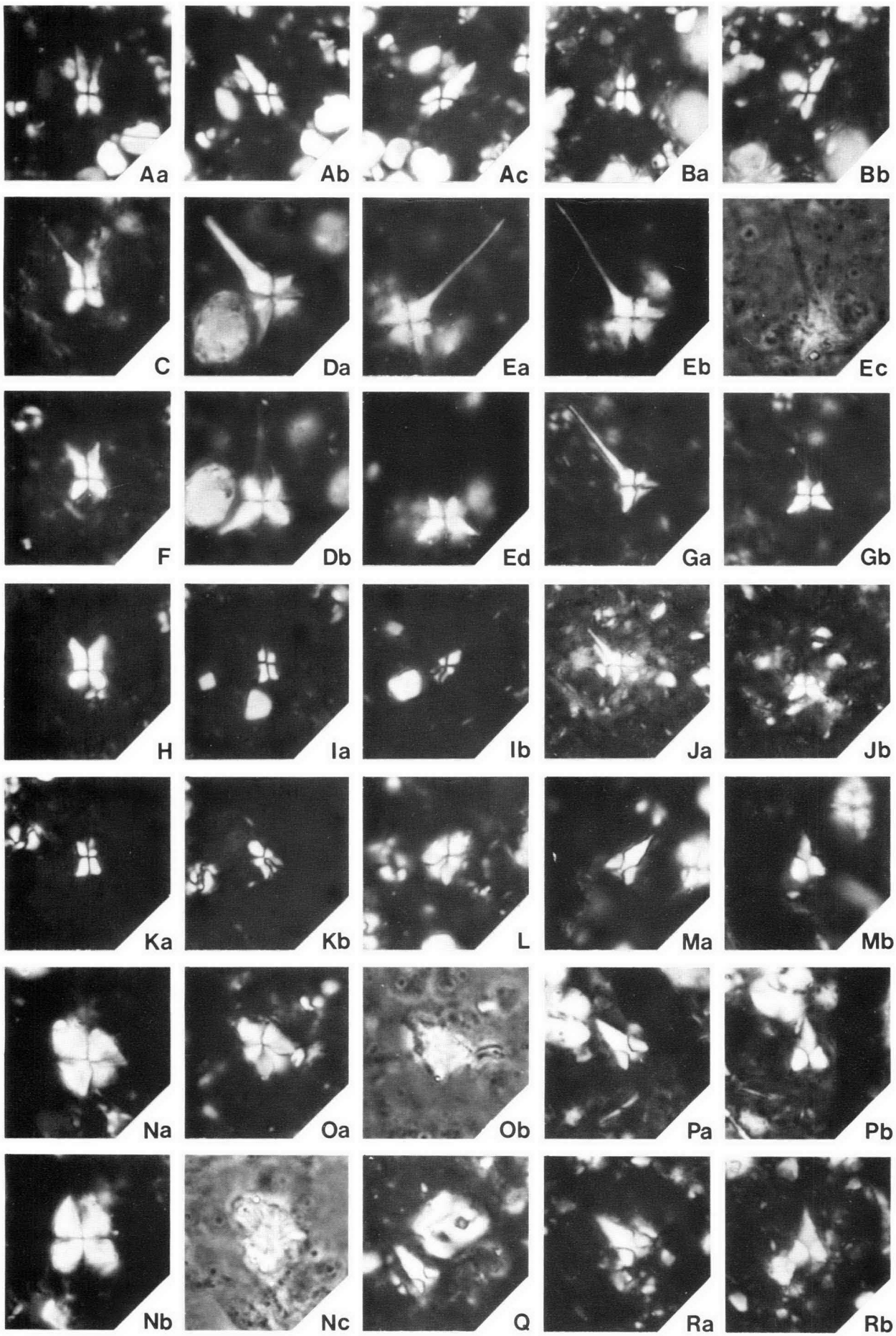
Aa
Ab
Ac
Ba
Bb
C
Da
Ea
Eb
Ec
F
Db
Ed
Ga
Gb
H
Ia
Ib
Ja
Jb
Ka
Kb
L
Ma
Mb
Na
Oa
Ob
Pa
Pb
Nb
Nc
Q
Ra
Rb

plana, Rhabdosphaera sp., *Sphenolithus ciperoensis* (frequent), *Triquetrorhabdulus carinatus* (frequent), and *Zygrhablithus bijugatus.*

S. ciperoensis persists throughout core 7; it is abundant to common in the lower levels but becomes rare in the higher parts. This species has its highest appearance in the 'Cartier Beds' at about 1104 m level.

The next segment (about 50 m thick from about 120 m to 170 m above base) of the 'Cartier Beds' contains assemblages that are only slightly different from those in the immediately underlying beds, but are distinct from those in the bottom segment. In addition to the appearance of *Sphenolithus delphix,* the change in the nannofossil elements is highlighted by the absence of *S. ciperoensis.* Typical species of this segment are those found in the side-wall core at 1052.7 m (i.e., 169.6 m above the base of the 'Cartier Beds'). These are *Braarudosphaera bigelowi, Coccolithus cribellum, C. eopelagicus, C.* sp. cf. *C. pelagicus, Corannulus germanicus, Coronocyclus serratus, Cyclicargolithus abisectus, C. floridanus, Dakylethra* sp. *Discoaster deflandrei* (group), *Helicopontosphaera euphratis, H. intermedia, H. obliqua, H. recta, H.* sp. aff. *H. kamptneri, Holodiscolithus macroporus, Micrantholithus fornicatus, M.* sp. cf. *M. vesper, Pontosphaera multipora, P. plana, Rhabdosphaera* sp., *Sphenolithus capricornutus, S. conicus, S. delphix, S. moriformis* (elongated variety), *Triquetrorhabdulus carinatus,* and *Zygrhablithus bijugatus. Sphenolithus delphix* disappears above 1048.5 m level.

The overlying 105 m of the 'Cartier Beds' are characterised by less diversified nannofossil assemblages. The assemblages are mostly poorly preserved (partly due to recrystallisation, which is probably a result of percolating water); some mixing might have occurred. *Helicopontosphaera recta* and *Zygrhablithus bijugatus* persist in the cuttings up to between 993.9 m and 997 m, and are also present in the sidewall core at 997.6 m (i.e., 224.7 m above the base of the 'Cartier Beds') in association with a few newly appearing species: small *Cyclococcolithina leptopora, Hayaster perplexus,* and *Sphenolithus* sp. aff. *S. belemnos.* Side-wall core 993.9 m (228.4 m above base of the 'Cartier Beds') contains severely battered fossils with a high percentage of fragments but whole specimens show a fairly good state of preservation. The assemblage recovered from this side-wall core includes: *Braarudosphaera bigelowi, Coccolithus eopelagicus, Cyclicargolithus abisectus, C. floridanus, Coronocyclus nitescens, Discoaster deflandrei* (group—including *D.* sp. cf. *D. druggii*), *Helicopontosphaera euphratis, H. intermedia, H. obliqua, Sphenolithus dissimilis* and *Triquetrorhabdulus carinatus.* In addition to these species, small *Cyclococcolithina leptopora,* narrow *Helicopontosphaera* sp. aff. *H. kamptneri, Hayaster perplexus, Discoaster* sp. cf. *D. exilis, D.* sp. cf. *D. variabilis, Pontosphaera multipora, Micrantholithus* sp. cf. *M. vesper,* and *M.* sp. cf. *M. pinguis* have been found in side-wall core 992.7 m (i.e., 229.6 m above the base of the 'Cartier Beds').

Side-wall cores 992.1 m and 991.5 m contain similar assemblages to those recorded from side-wall core 992.7 m, except that odd specimens of a form similar to *Chiasmolithus altus* are found in side-wall core 992.1 m and a few specimens of *Zygrhablithus bijugatus* are noted in side-wall core 991.5 m. These occurrences of *?Chiasmolithus altus* and *Zygrhablithus bijugatus* probably are due either to contamination or mixing.

Triquetrorhabdulus carinatus occurs consistently up to side-wall core 991.5 m, and sporadically up to between 972 m and 975 m in samples of cuttings; it has not been recorded from the overlying beds.

Assemblages recovered from samples of cuttings between 991.2 m and 943.3 m levels (a thickness of about 52 m) are generally similar to those recorded from side-wall core 992.7 m except that they are very poorly preserved. *Sphenolithus belemnos* first appears (up-sequence) between 945 m and 948 m, but this is probably an unreliable appearance and may represent downhole contamination.

The top segment (about 10 m) of the 'Cartier Beds' immediately below the unnamed calcarenite contains residual assemblages; recrystallisation has obliterated most of the nannofossils, but *Cyclicargolithus abisectus, C. floridanus, Cyclococcolithina leptopora, Sphenolithus belemnos, S. capricornutus, S. conicus, S. dissimilis, S. moriformis, Coccolithus* sp. cf. *C. pelagicus, C. cribellum, Coronocyclus nitescens, Helicopontosphaera euphratis, H. kamptneri* and *Pontosphaera plana,* could be identified in side-wall core 943.6 m. Large numbers of small unidentifiable placoliths dominate this segment. *Sphenolithus belemnos* has been noted in the basal parts of the unnamed calcarenite.

Meleri Beds. The composition of the nannofossil assemblages of the three studied samples (Fig. 2) closely resembles that from the basal segment of the 'Cartier Beds' in Ashmore Reef No. 1 Well. *Triquetrorhabdulus carinatus* is recorded with certainty in only one sample (C17b), but its absence in the other two samples may be attributed to the high susceptibility of this species to overcalcification and hence difficulties of recognition. *Helicopontosphaera recta, Reticulofenestra scissura* and *Sphenolithus ciperoensis* are common to samples C17a and C18b.

Capricorn No. 1A Well. The nannofossils recovered from core 5 (877.3 m) include: *Cyclicargolithus abisectus, C. floridanus, Discoaster deflandrei, Helicopontosphaera euphratis, H. recta, Pontosphaera plana, Reticulofenestra scissura, Sphenolithus ciperoensis, S. moriformis* and *Zygrhablithus bijugatus.*

Biostratigraphy

The biostratigraphic approach adopted here is not one of zonal assignment, but rather a recognition of sequential order of biostratigraphic events; for correlation purposes such an approach is thought best because it is not hampered by differing concepts of zones described by various authors.

Ashmore Reef No. 1 Well. Immediately above the disconformity with the Eocene 'Hiberina Beds', the 'Cartier Beds' are rich in *Sphenolithus ciperoensis,* but

---

Figure 4. (All photographs are x2000)

Aa-c Sphenolithus sp. aff. *S. belemnos* Bramlette & Wilcoxon CPC 18171; Ba-b *Sphenolithus belemnos* CPC 18173; C, F, H *Sphenolithus capricornutus* Bukry & Percival: C = CPC 18174, F = CPC 18175, H = CPC 18176; Da-b, Ea-d, Ga-b, Ja-b *Sjhenolithus delphix* Bukry: D = CPC 18177, E = CPC 18178, G = CPC 18179, J = CPC 18180; Ia-b, Ka-b *Sphenolithus dissimilis* Bukry & Percival: I = CPC 18181, K = CPC 18182; L, Oa-b *Sphenolithus conicus* Bukry: L = CPC 18183, O = CPC 18184; Na-c *Sphenolithus moriformis* (Bronnimann & Stradner) CPC 18185; Ma-b, Pa-b, Ra-b *Sphenolithus ciperoensis* Bramlette & Wilcoxon: M = CPC 18186, P = CPC 18187, R = CPC 18188; Q *Helicopontosphaera recta* CPC 18189, and *Sphenolithus ciperoensis* CPC 18190.

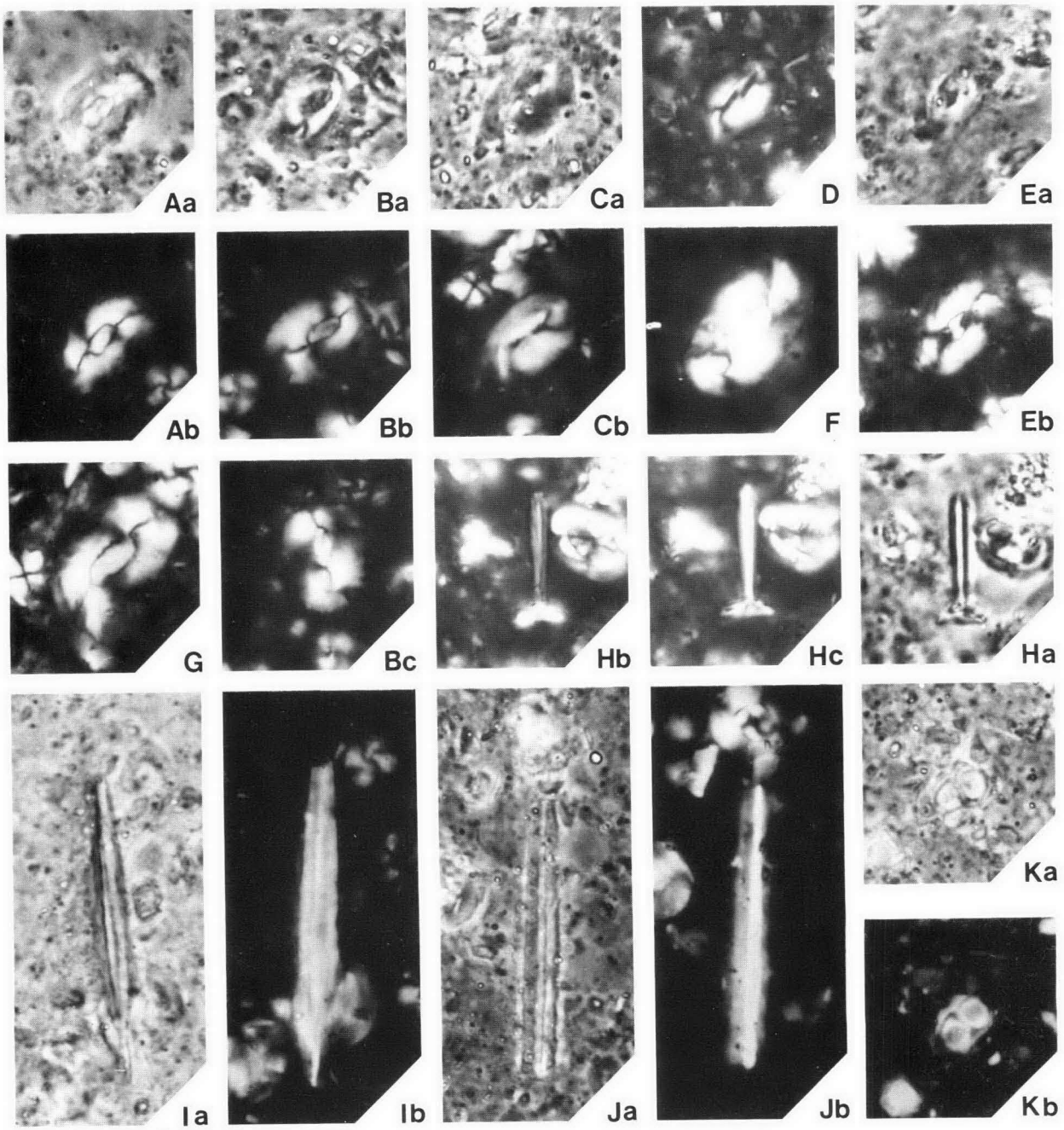

Figure 5. (All photographs are x2000)

Aa-b, Ba-c, G *Helicopontosphaera euphratis* (Haq): A = CPC 18161, B = CPC 18162, G = 18163; Ca-b, D *Helicopontosphaera obliqua* (Bramlette & Wilcoxon): C = CPC 18164, D = CPC 18165; Ea-b *Helicopontosphaera intermedia* (Martini), CPC 18166; F *Helicopontosphaera kamptneri* Hay & Mohler, CPC 18167; Ha-c *Rhabdosphaera* sp., CPC 18168; Ia-b, Ja-b *Triquetrorhabdulus carinatus* Martini: I = CPC 18169, J = CPC 18170; Ka-b *Zygrhablithus bijugatus* (Deflandre), CPC 18171.

lack *S. distentus*. The ranges of these species (*S. distentus* is the progenitor of *S. ciperoensis*) overlap in complete sections, and the absence of *S. distentus* from the 'Cartier Beds' is taken to indicate that the base of the unit is well above the *S. ciperoensis* (evolution) datum.

Figure 6 shows the biostratigraphic events that occur within the 'Cartier Beds'. These are: (a) highest appearance of *Reticulofenestra scissura* (the oldest); (b) highest appearance of *Sphenolithus ciperoensis;* (c) highest appearance of *S. delphix;* (d) highest appearance of both *Helicopontosphaera recta,* and *Zygrhablithus bijugatus;* (e) highest appearance of *Triquetrorhabdulus carinatus;* and (f) the lowest appearance of *Sphenolithus belemnos* (the youngest).

The horizons of highest appearance of *R. scissura* and *S. ciperoensis* are usually closely spaced (Bukry, 1973), but appear well separated in sequences with high sedimentation rates such as that of DSDP Site 289 on the Ontong Java Plateau (Shafik, 1975). That these horizons are well separated in the 'Cartier Beds' suggests a high sedimentation rate for that part of the sequence. Conversely, in the overlying part of the 'Cartier Beds' which is bracketed by the highest appearance of *Sphenolithus delphix* and the lowest appearance of *Sphenolithus belemnos,* the close disappearance of both *Helicoponto-*

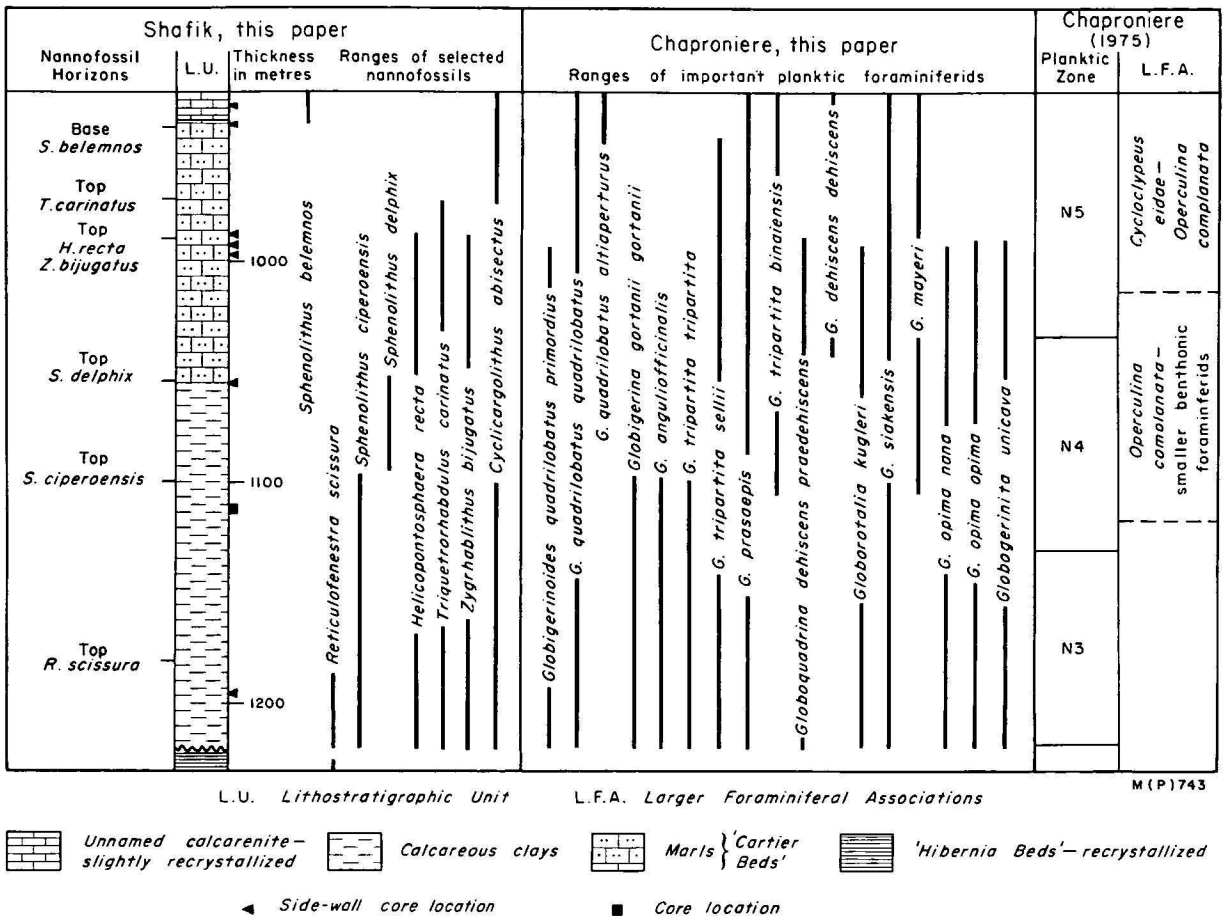

Figure 6. Dominant lithologies, biostratigraphies and biostratigraphic ranges of selected fossils in the 'Cartier Beds' of Ashmore Reef No. 1 Well, Bonaparte Gulf Basin.

sphaera recta and *Zygrhablithus bijugatus* may suggest condensed sedimentation and/or hiatus. Foraminiferal evidence in the same part of the sequence supports this conclusion; several foraminiferids became extinct at about the same level of disappearance of *H. recta* and *Z. bijugatus* (Fig. 6).

Meleri Beds. The joint occurrence of *Reticulofenestra scissura* and *Sphenolithus ciperoensis* in samples C17a and C18b suggests a correlation with the basal segment of the 'Cartier Beds'; sample C17b is possibly younger, and probably correlative with, that segment of the 'Cartier Beds' between the *S. ciperoensis* (extinction) datum and the last appearance of *Triquetrorhabdulus carinatus.* On the basis of the ranges of several planktic foraminiferal species (Fig. 2), Belford (1974) assigned these samples to the lower part of Zone N.3 (late Oligocene).

Capricorn No. 1A Well. The concurrence of *Reticulofenestra scissura* and *Sphenolithus ciperoensis* in the studied samples indicates a correlation with the basal part of the 'Cartier Beds'. Immediately above this sample, Palmieri (1975) recorded the planktic foraminiferids *Globigerinoides primordius* and *Globorotalia kugleri.*

Planktic foraminiferids of the 'Cartier Beds'

Assemblages

Forms referable to the *Globigerinoides quadrilobatus* group are ubiquitous throughout the 'Cartier Beds'. The lowest sample, (side-wall core 1187.5 m) contains both *G. quadrilobatus primordius* and *G. quadrilobatus quadrilobatus.* Other important planktic foraminiferids in this sample are: *Globigerina gortanii gortanii, G. officinalis angulofficinalis, G. officinalis angulisuturalis, G. ouachitaensis ciperoensis, G. tripartita sellii, G. tripartita tripartita, G. venezuelana, Globigerinita unicava, Globoquadrina dehiscens praedehiscens, Globorotalia (Turborotalia) kugleri kugleri, G. (T.) kugleri mendacis, G. kugleri pseudokugleri* and *G. (T.) opima nana;* in addition, populations of *G. (T.) siakensis* contain *G. (T.) opima opima* morphotypes. The same assemblage occurs in core 7 (1104.3-1108.5 m); *Globigerinoides quadrilobatus immaturus,* forms intermediate between *Globigerina tripartita sellii* and *G. tripartita binaiensis, Globoquadrina baroemoenensis* and *Globorotaloides suteri* first appear at this level. Morphotypes of *Globorotalia (T.) mayeri* and *G. (T.) opima opima* occur in populations of *G. (T.) siakensis* in core 7. *Globigerina gortanii gortanii, G. officinalis angulofficinalis, G. officinalis angulisuturalis* and *G. tripartita* do not occur above 1108.5 m. Typical *Globigerina tripartita binaiensis* and *Globoquadrina dehiscens dehiscens* first appear at 1052.7 m, overlapping with the highest *Globoquadrina dehiscens praedehiscens.* The assemblage from the side-wall core at 1052.7 m is typical of that at 993.9 and 991.5 m; these last two levels are marked by the last appearance of *Globigerina tripartita sellii, Globigerinita unicava, Globigerinoides quadrilobatus primordius, Globorotalia (T.) kugleri kugleri, G. (T.) kugleri mendacis, G. (T.) kugleri pseudokugleri* and *Globorotaloides suteri; Globorotalia (T.) siakensis* becomes rare and the morphotypes of *G. (T.) mayeri* and *G. (T.) opima opima*

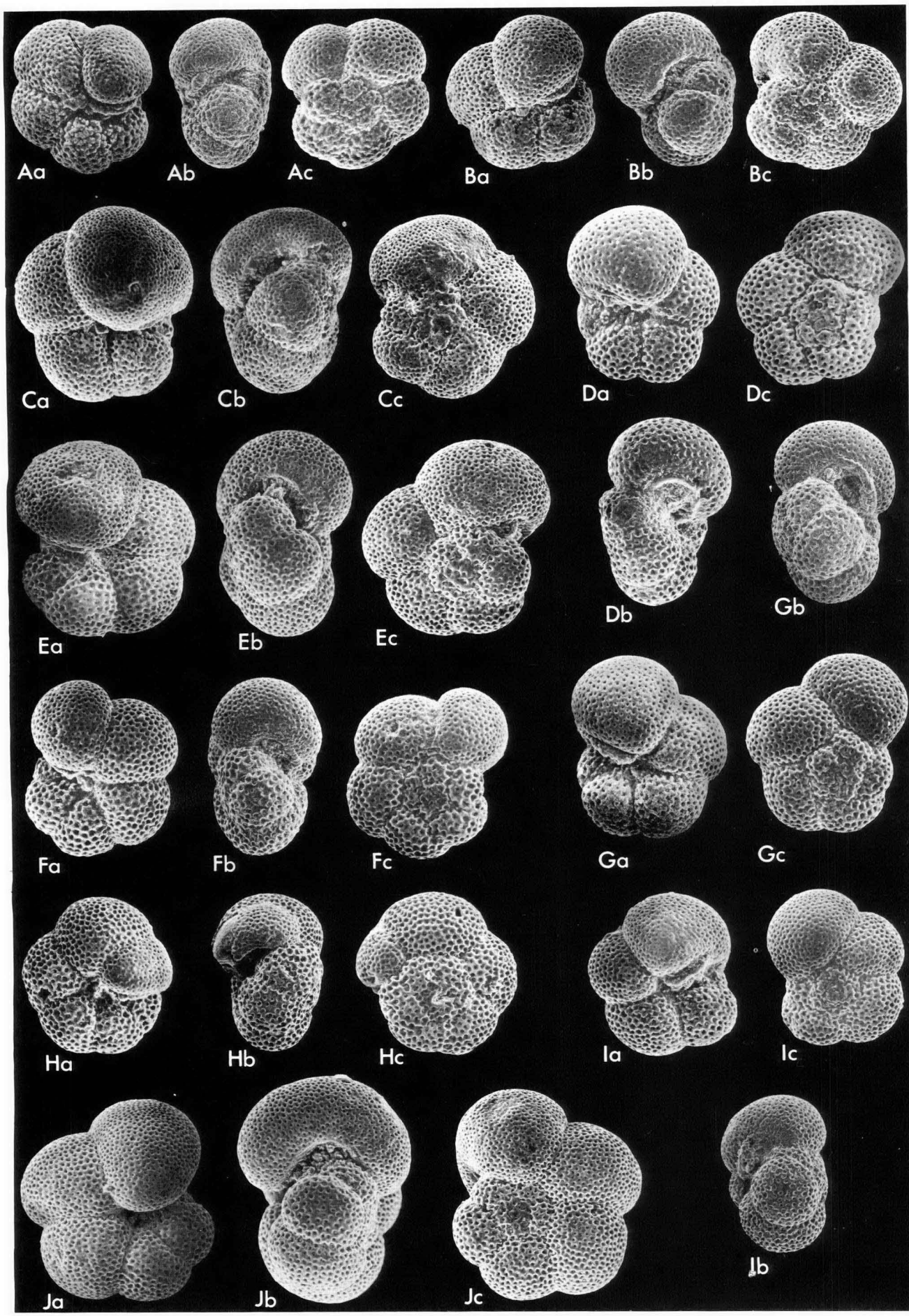
Aa
Ab
Ac
Ba
Bb
Bc
Ca
Cb
Cc
Da
Dc
Ea
Eb
Ec
Db
Gb
Fa
Fb
Fc
Ga
Gc
Ha
Hb
Hc
Ia
Ic
Ja
Jb
Jc
Ib

disappear; *Globigerina ouachitaensis ciperoensis* has a similar distribution to *Globorotalia siakensis*. Planktic foraminiferal faunas are poor in the uppermost parts of the 'Cartier Beds' and the lowermost parts of the unnamed calcarenite. However, *Globigerinoides quadrilobatus altiaperturus* first appears at 943.6 m, near the top of the 'Cartier Beds'.

Biostratigraphy

The presence of *Globigerinoides quadrilobatus primordius* and *G. quadrilobatus quadrilobatus* together with *Globorotalia (Turborotalia) kugleri kugleri* indicates Zone N.4 of Blow (1969) for the lower parts of the 'Cartier Beds' below core 7 (1108.5 m). *Globigerinoides quadrilobatus immaturus*, a form which makes its initial appearance in the middle parts of Zone N.4 (Blow, 1969) is first found at 1108.5 m; this suggests that the 'Cartier Beds' below this level were deposited early in Zone N.4. *Globorotalia (T.) kugleri kugleri* has not been recorded above 992.1 m in Ashmore Reef No. 1 Well: the extinction of this form defines the base of Zone N.5 (Blow, 1969, p. 325). Furthermore, *Globigerinoides quadrilobatus altiaperturus* has not been found below 943.6 m; this taxon first appears 'near the base of Zone N.5' (Blow, 1969, p. 325). For these reasons the N.4/N.5 zonal boundary must lie in the interval between 992.1 m and 943.6 m, near the top of the 'Cartier Beds'.

As noted earlier, the *Globorotalia (T.) siakensis* populations in the lower and middle parts of the 'Cartier Beds' contain forms referable to *Globorotalia (T.) opima opima, G. (T.) opima nana* and *G. (T.) mayeri*, as well as typical *G. (T.) siakensis* (see Fig. 7); all morphotypes are linked by intermediates (e.g. Fig. 7C, H, I). The *opima, nana* and *siakensis* morphotypes occur together below 1108.5 m; between 1108.5 m and 922.1 m these three are joined by the *mayeri* morphotype; above 992.1 m only *siakensis* is found. In all populations the *siakensis* type is dominant. This evidence indicates a close relationship between the *opima, siakensis* and *mayeri* forms, suggesting an evolutionary bioseries commencing with *Globorotalia (T.) opima opima* and culminating in *G. (T.) mayeri* (which is longer ranging elsewhere); the overlapping biostratigraphic ranges of the various morphotypes is to be expected in such a series. Blow (1969), in agreement with Jenkins (1960, 1971), suggested that *G. (T.) mayeri* was derived from *G. (T.) peripheroronda*, and that many forms previously identified as *G. mayeri* were best referred to *siakensis*. Palmieri (1975) disagreed with both Blow (1969) and Jenkins (1960, 1971), and considered that *G. mayeri* descended from *G. siakensis; G. peripheroronda* was thought to be a descendant of *G. mayeri*. The specimens here identified as *mayeri* (Fig. 7D, G) are very similar to those figured by Cushman & Ellisor (1939, pl. 2, figs 4a-c) differing in having fewer chambers (five instead of six), and radial (instead of slightly recurved) umbilical sutures; these features suggest that they are probably phylogenetically primitive forms, best referred to that taxon.

A number of taxa which Blow (1969) recorded as becoming extinct below the base of Zone N.4 and which are present in faunas typical of Zone N.4, are listed in Table 1, together with the ranges recorded by Blow (1969). He regarded the extinction of *Globorotalia (T.) opima opima* as marking the top of Zone N.2; the concurrence of *G. (T.) opima opima* and *Globigerina angulisuturalis* typifies Zone N.2. Blow suggested that the evolution of *G. angulisuturalis* from *G. angulisofficinalis* occurs at the top of Zone N.1. Both *G. officinalis angulisuturalis* and *G. officinalis angulisofficinalis* occur in the lower parts of the 'Cartier Beds'.

Taxon	*Range according to Blow (1969)*
Glibogerina gortanii gortanii	Base N.2 to earliest N.3
G. officinalis angulisofficinalis	P.17 to within N.2
G. prasaepis	Within P.17 to near N.2/3 boundary
G. tripartita sellii	Base P.19 to within N.3
G. tripartita tripartita	Within P.14 to within N.3
Globorotalia (T) opima nana	Within P.15 to early N.3
G. (T.) opima opima	Within P.19 to top N.2

Table 1. Planktic foraminiferids previously recorded by Blow (1969) as occurring below the initial appearance of *Globigerinoides quadrilobatus primordius*.

Elsewhere *Globorotalia (T.) opima opima* has been recorded on at least six occasions with *Globigerinoides quadrilobatus primordius*. Caralp and others (1965) recorded *Globigerinoides trilobus* as appearing below the initial appearance of *Globorotalia kugleri*, and occurring with *G. opima opima* and *Globigerina ciperoensis angulisuturalis* in samples from the southern Aquitaine region of France. Bolli· (1970, figs 2, 6) shows both species occurring with *Catapsydrax dissimilis, Globigerina venezuelana, Globorotalia kugleri* and *G. opima nana*, together with taxa known only below the middle Eocene; the Eocene forms were considered to have been reworked, but no explanation concerning the presence of *G. opima opima* in the assemblages was given. Poag (1972a) found a typical specimen of *Globigerinoides primordius*? (sic) with a fauna typical of either Zone N.2 or N.3. Poag (1972b) tentatively identified specimens of *G. opima opima* with *Globigerinoides quadrilobatus primordius, Globigerina angulisuturalis, G. sellii* and *G. tripartita*. Vincent and others (1974, table 6) identified *Turborotalia opima opima, T. opima nana, T. kugleri, T. siakensis, Globoquadrina tripartita* with *Globigerinoides quadrilobatus immaturus*. Heiman and others (1974, table 3) recorded *Turborotalia opima opima* with *Catapsydrax dissimilis, Globigerinoides quadrilobatus immaturus, Globoquadrina sellii, G. tripartita, Turborotalia kugleri, T. opima nana* and *T. siakensis;* the occurrence of *Globigerinoides* in this assemblage was explained by mixing. Gelati (1975) recorded *G. opima opima* with typical Zone N.4 and N.5 faunas from Turkey. Furthermore, Baumann (1972), Belford (1974), and Poag (1972b) have recorded *Globigerina gortanii, G. sellii* and *G. tripartita* with *Globigerinoides quadrilobatus primordius*. Palmieri (1974) found *Globigerina gortanii* and *G.* aff. *tripartita* with *Globorotalia kugleri* and *Globigerinoides primordius*. *Globigerina sellii* and *G. tripartita* occur with *Globigerinoides primordius* and *Globorotalia kugleri* in Cores 9 and 10 from Site 159 in the eastern equa-

Figure 7. The range of variation of morphotypes in the *Globorotalia (Turborotalia)* siakensis populations from the middle and lower parts of the 'Cartier Beds'. a, umbilical view; b, side view; c, spiral view.
Aa-Bc *opima* morphotype; A = CPC 16910 x 110; B = CPC 16911 x 100. Ca-c Specimen ex interc. *opima*—siakensis morphotypes CPC 16912 x 100. Da-e, Ga-c, Ia-c *mayeri* morphotype, D = CPC 16913 x 130, G = CPC 16916 x 110; I = CPC 16918 x 110. Ea-c, Fa-c, Ja-c *siakesis* morphotype; E = CPC 16914 x 100; F = CPC 16915 x 110, J = CPC 16919 x 100. Ha-c Specimen ex interc. *siakensis-mayeri* morphotypes CPC 16917 x 110.

torial Pacific Ocean (Kaneps, 1973). Seiglie (1973) found *Globigerinoides trilobus primordius* with *Globigerina ciperoensis ciperoensis, G. angulisuturalis, G.* cf. *binaiensis, G. sellii sellii* without *Globorotalia kugleri.*

In conclusion, there are several records of taxa previously thought to have become extinct below Zone N.4 now known to occur with *Globigerinoides quardilobatus primordius,* the zonal taxon used to define Zone N.4 by Blow (1969). The concurrence of these species indicates that the biostratigraphic interval previously recognised as Zone N.3 cannot be identified either in Ashmore Reef No. 1 Well or in three other localities (those of Bolli, 1970, Poag, 1972b, and Heiman and others, 1974; see also Wright, 1977 for the Northwest Australian shelf); in Ashmore Reef No. 1 Well the extinction of *Globorotalia (T.) opima opima* occurs well above the first appearance of both *Globigerinoides quadrilobatus primordius* and *Globorotalia kugleri kugleri.* For these reasons either the usage of Zone N.3 should be discontinued, or the interval previously recognised as Zone N.4 be now referred to as Zone N.3/4, similar to the combination of Zones P.19/20 suggested by Blow (1970a); the term N.3/4 is probably preferable. The boundary between Zones N.2 and N.3/4 is then defined by the first appearance of *Globigerinoides quadrilobatus primordius.* These results also nullify the *Globigerina ciperoensis ciperoensis* Zone of Bolli (1966) which also equates with Zone N.3 of Blow (1969).

Conditions of deposition

Nannofossil evidence suggests that deposition of most of the studied material was in shallow-water environments, probably in nearshore basins. Species such as *Braarudosphaera bigelowi, Helicoptosphaera recta, Holodiscolithus macroporus, Micrantholithus fornicatus, M.* sp. cf. *vesper, Pontosphaera multipora, P. plana,* and *Zygrhabilithus bijugatus* occur in variable numbers in most of the material examined. These species seldom occur in deep oceanic sediments but are usually common in coeval hemipelagic sediments (see e.g., Bukry, 1973). Lithologic evidence does not negate such an interpretation. Previously, Coleman (1968) advocated a shallow-water environment on the basis of patchy occurrences of ostracods in the 'Cartier Beds' in Ashmore Reef No. 1 Well, and Chaproniere (1975) suggested that the upper part of the 'Cartier Beds' was deposited under progressively shallower depths, within the euphotic zone.

Surface waters were probably warm, hence the abundance of species of *Sphenolithus* and *Discoaster;* representatives of these two genera are either absent or occur sparsely in coeval high-latitude sediments (Perch-Nielsen, 1972), but are usually abundant in low-latitude sediments (see e.g., Bukry, 1973). The occurrence of larger foraminiferids supports this conclusion. In addition, the planktic foraminiferal fauna has a distinctly warm-water aspect, with large numbers of the *Globigerinoides quadrilobatus* group and *Globorotalia obesa,* forms which are typical of modern warm seas (Bé, 1960; Jones, 1968).

Integration of biostratigraphic results and age assignments

Correlation is best achieved by using datums (biostratigraphic horizons) rather than zones. This applies equally to the biostratigraphic use of nannofossils and planktic foraminiferids. Biostratigraphy is primarily based on recognition of events in a sequential order, and it is when these do not appear in the same sequential order that correlation becomes exceedingly difficult. Some of the biostratigraphic events (i.e. datums) are more important and/or reliable than others.

A comparison of the foraminiferal results of the present study with the works of Bolli (1957, 1966), and of Blow (1969) as well as with other works (e.g., Wright, 1977) indicates that the level of the *Globorotalia opima opima* (extinction) datum is inconsistent in relation to the levels of other important datums such as *Globorotalia kugleri kugleri* (base of range), *Globigerinoides quadrilobatus primordius* (evolution), and *Globorotalia kugleri kugleri* (extinction). The present study proposes the Zone N.3/4 based on the lowest occurrence of *Globigerinoides quadrilobatus primordius.* Although several authors (e.g., Lamb & Stainforth, 1976) showed some concern about the reliability of the lowest occurrence of *G. quadrilobatus primordius,* the alternatives are probably worse.

The sequential order of nannofossil events recognised in the present study (Fig. 6) is consistent with other results obtained elsewhere (e.g., Bramlette & Wilcoxon, 1967; Martini, 1971; Bukry, 1973; Gartner, 1974 and others) if provision is made for dealing with different types of sediments (pelagic and hemipelagic). In comparison with most of the other diagnostic nannofossil species present in the 'Cartier Beds', *Sphenolithus ciperoensis* and *S. belemnos* are known to occur in both hemipelagic and deep-oceanic sediments, and their vertical ranges are better known; these species are therefore best suited for correlations and age assignments. The *Sphenolithus ciperoensis* (extinction) and *S. belemnos* (base of range) datums are chosen to integrate the nannofossil biostratigraphic results of the present study with those of the planktic foraminiferids.

Sphenolithus ciperoensis (extinction) datum and the Globigerinoides quadrilobatus primordius (evolution) datum

The geographic distribution of *Sphenolithus ciperoensis* and *Globigerinoides quadrilobatus primordius* indicates that both are of low-latitude origin, and thus provides some grounds for analysing their biostratigraphic relationship, and also their dissolution patterns.

The ranges of both species overlap in the 'Cartier Beds' (Fig. 6), and they both occur in the Meleri Beds of Irian Jaya (Fig. 2). Furthermore, examination of the works of Hekel (1973) and Palmeri (1975) indicates that the top part of the range of *Sphenolithus*

Figure 8. **(All photographs are x2000)**
Aa-b, Ia-b *Braarudosphaera bigelowi* (Gran & Braarud): A = CPC 18191, I = CPC 18192; Ba-b, Fa-b, Ha-b *Micrantholithus* sp. cf. *M. vesper* Deflandre: B = CPC 18193, F = CPC 18194, H = CPC 18195; Ca-b, Da-b, Ga-b, Ja-b *Micrantholithus fornicatus* Martini: C = CPC 18196, D = CPC 18197, G = CPC 18198, J = CPC 18199; Ea-b *Micrantholithus* sp. cf. *M. pinguis* Bramlette & Sullivan CPC 18200; Ka-b—N, P, Q *Dakylethra* sp.: K = CPC 18201, L = CPC 18202, M = CPC 18203, N = CPC 18204, P = CPC 18205, Q = CPC 18206; O *Zygrhablithus bijugatus* CPC 18207; R, S, U, V *Pontosphaera multipora* (Kamptner): R = CPC 18208, S = CPC 18209, U = CPC 18210, V = CPC 18211; T *Pontosphaera plana,* Bramlette & Sullivan CPC 18212.

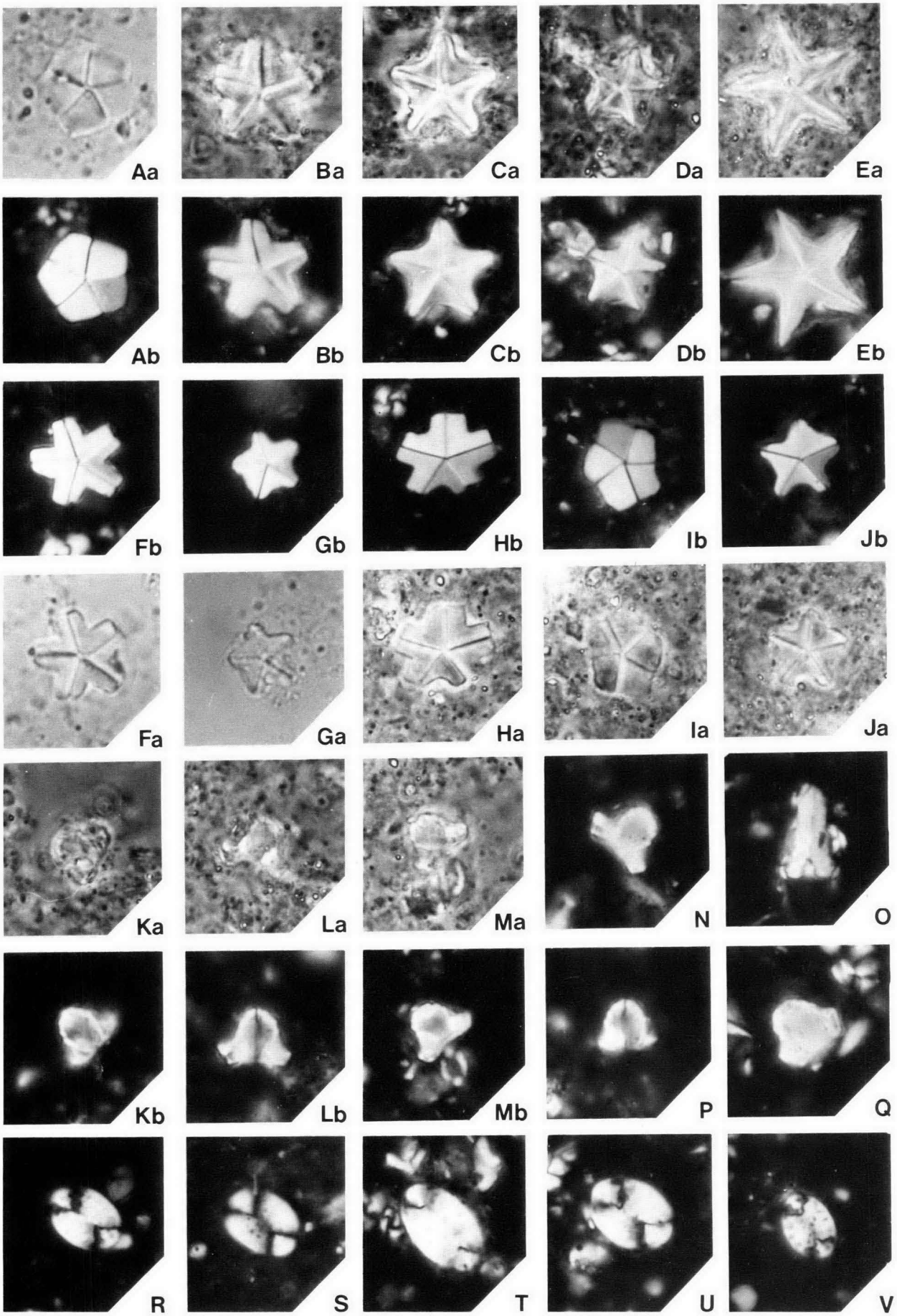
Aa
Ba
Ca
Da
Ea
Ab
Bb
Cb
Db
Eb
Fb
Gb
Hb
Ib
Jb
Fa
Ga
Ha
Ia
Ja
Ka
La
Ma
N
O
Kb
Lb
Mb
P
Q
R
S
T
U
V

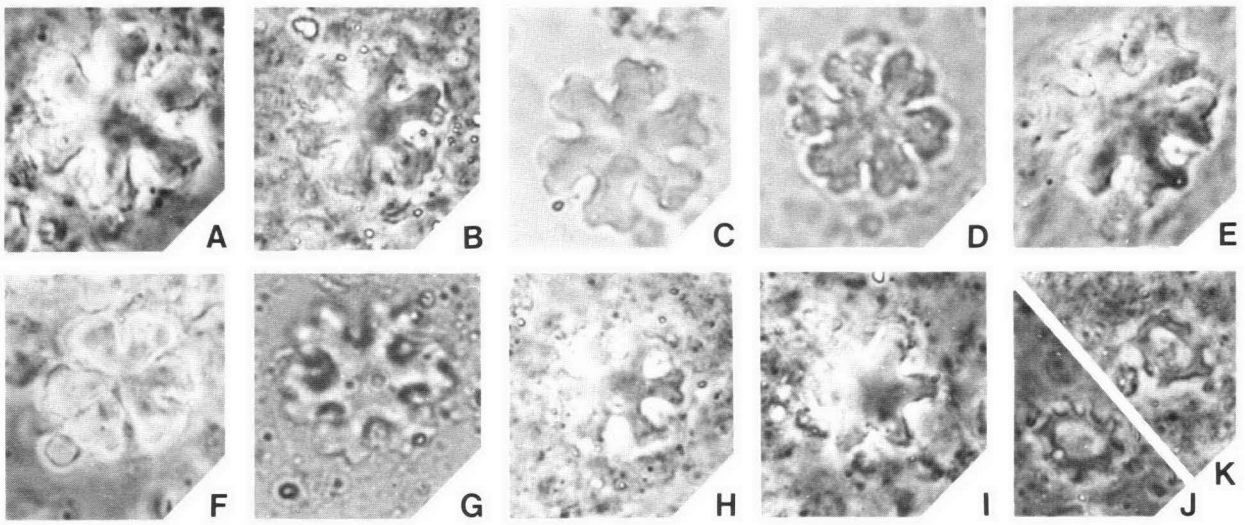

Figure 9. **(All photographs are x2000)**
A-H *Discoaster deflandrei* Bramlette & Riedel 'group': A = CPC 18213, B = CPC 18214, C =CPC 18215, D = CPC 18216, E = CPC 18217, F = CPC 18218, G = CPC 18219, H = CPC 18220; I *Discoaster* sp. cf. *D. druggi* Bramlette & Wilcoxon CPC 18221; J-K *Corannulus germanicus* Stradner: J = CPC 18222, K = CPC 18223.

ciperoensis overlaps with the basal part of the range of *Globigerinoides primordius* in the Capricorn Basin. The present study records *S. ciperoensis* in a sample from Capricorn No. 1A Well (Core 5 at 977.3 m) which yielded a planktic foraminiferal assemblage dominated by a small specimen of either juvenile *Globigerinoides quadrilobatus primordius* or its direct ancestor *Globigerina praebulloides occlusa;* these may represent the evolutionary change of *G. praebulloides occlusa* to *Globigerinoides quadrilobatus primordius.*

A common characteristic among these Australian and Irian Jayan records of the concurrence of *Sphenolithus ciperoensis* and *Globigerinoides quadrilobatus primordius* is that the containing sediments are hemipelagic (marginal-marine) deposited in shallow environments. Published data indicate that the overlap in the ranges of these species is repeated elsewhere, and also reveals that this overlap is tied to the depth of deposition of the containing sediments.

Hemipelagic and slightly deeper sediments. The strata at Escornebeou and St d'Orthe in southwest France (Chattian of Drooger, 1960) were deposited under shallow-water, nearshore conditions with good access to open sea (Butt, 1966). *Sphenolithus ciperoensis* has been recorded in these strata (Bramlette & Wilcoxon, 1967) as well as *Globigerinoides primordius* (Butt, 1966; Berggren, 1971). Upper Oligocene sediments on the Bahama Banks (DSDP Site 98) were deposited in a fairly shallow-marine environment as shown by the presence of *Braarudosphaera rosa, Helicopontosphaera recta,* and *Micrantholithus* sp. (Bukry, 1972). Within these sediments (Core 98-5), *S. ciperoensis* overlaps with the lower part of the range of *G. quadrilobatus primordius* (compare Wilcoxon, 1972, and Poag, 1972a). The upper Oligocene sequence at the DSDP Site 238, close to the southern end of the Chagos-Laccadive Plateau (Indian Ocean), was probably deposited in a less shallow environment as braarudesphaerids seem to be restricted to the lower part of the sequence (Core 238-53 to 234-48). Roth (1974) recorded *S. ciperoensis* consistently up to Core 238-49-2 and sporadically at higher levels (Cores 238-47-4 and 234-43-1), and Vincent and others (1974) identified *G. quadrilobatus immaturus* as ranging from Core 238-47-1 to the upper part Core 238-42 (though Roth considered the highest occurrence of *S. ciperoensis* at Site 238 as due to reworking, no supporting evidence was given). At Site 57 (northern flank of the Caroline Ridge), *S. ciperoensis* was found in hole 57.0 sediments—Core 1 with rare *G. primordius,* and in hole 57.1 sediments, *S. ciperoensis* occurs through Core 4-5 to Core 2-1 but *G. primordius* (rare) occurs only at the top of Core 4 (Fischer, Heezen, and others, 1971). That *G. primordius* is missing from Cores 3 and 2 of hole 57.1 seems to correlate with the lack of nannofossil species indicative of shallow-water deposition.

Deep oceanic sediments. At the Ontong Java Plateau Site 289, *S. ciperoensis* and *G. quadrilobatus primordius* are present, but the *S. ciperoensis* (extinction) datum occurs well below the lowest occurrence of *G. quadrilobatus primordius* (and also below the *Globorotalia opima opima* extinction datum; Andrews, Packham and others, 1975). The total lack of nannofossil species characteristic of shallow-water deposition from the relevant parts of the sequence at Site 289 is an indication of deep deposition; the vertical gap between the ranges of *S. ciperoensis* and *G. quadrilobatus primordius* is evident. At Site 287 (Coral Sea), *S. ciperoensis* first appears in Core 287-10-4 (30-31 cm) and has its highest occurrence in Core 287-10-2 (4-5 cm), within the base of a brown clay unit largely devoid of calcareous planktic remains (Shafik, 1975). *Globorotalia (Turborotalia) kugleri* (without *Globigerinoides quadrilobatus primordius*) was found only at one level (287-10-2, 100-102 cm) within the range of *S. ciperoensis* at this site; other levels within the range of *S. ciperoensis* are either devoid of planktic foraminiferids or contain these in a poor state of preservation (Andrews, Packham, and others, 1975); deposition of the relevant parts was interpreted as near the carbonate compensation depth. Similarly, at Site 286 near New Hebrides, *S. ciperoensis* ranges from Core 286-6-cc up to Core 286-5-cc, immediately below zeolite-rich brown clays (Shafik, 1975); only one level within this range contains age-diagnostic planktic foraminiferids (Andrews, Packham, and others, 1975), i.e. *Globigerina sellii* and *Globorotalia siakensis* were identified in core 286-6-3 (23-25 cm). In shallow-water deposits *G. sellii* and *G. siakensis* have been recorded in association with *Globigerinoides quadrilobatus primordius* (Cicha and

others, 1971; Poag, 1972b; Baumann, 1972; Belford, 1974; present study, 'Cartier Beds'), but rarely in relatively deeper DSDP sites (e.g. Douglas, 1973, Tab. 5; Gartner and others, 1974); this evidence seems to suggest that the absence of *G. quadrilobatus primordius* from Site 286 sediments is consistent with deposition near the carbonate compensation depth as previously indicated by Andrews, Packham, and others (1975).

Thus whereas in hemipelagic sediments (marginal-marine deposition) the ranges of *Sphenolithus ciperoensis* (latest part) and *Globigerinoides quadrilobatus primordius* (earliest part) overlap, in deep-oceanic sediments these ranges are separated by a gap; in sediments deposited under intermediate depths the two species may occasionally occur together. This is best explained as due to differences in the dissolution characteristics of these species with depth.

Discussion. There is a general tendency for foraminiferids inhabiting the surface to have lesser resistance to solution than those from deeper waters (Savin & Douglas, 1973); modern *Globigerinoides* spp. are most abundant at the surface (Bé & Tolderlund, 1971; Boltovsky, 1971), and these are among the most readily dissolved of modern planktic foraminiferids (Berger, 1970). The absence or extreme paucity of *Globigerinoides quadrilobatus primordius* from many DSDP sections has already been explained as due to the species dissolution (e.g., Jenkins & Orr, 1972); ample evidence indicating that the species is susceptible to dissolution can be identified from its distribution and quality of preservation in oceanic sediments (e.g. Blow, 1970b, Site 31; Edgar & Saunders, 1971, Site 149). On the other hand, *Sphenolithus ciperoensis* is considered as a highly solution-resistant nannofossil species, because it has been found in sediments either lacking calcareous planktic remains or containing residuals of these remains (e.g., sediments of Sites 286 and 287 referred to above).

Roth & Berger (1975) concluded that the dissolution patterns of coccoliths and planktic foraminiferids are dissimilar. The majority of coccoliths in both the plankton and in pristine sediments are solution-resistant. Planktic foraminiferids in similar sediments include a high percentage of delicate forms, but these decrease in number in etched sediments. Earlier, Hay (1970) indicated that the total dissolution of nannofossils in the oceanic realm occurred at greater depths than those of the planktic foraminiferids throughout the Cretaceous and Cainozoic. Considering these data and the conclusion (above) that *Sphenolithus ciperoensis* is solution resistant and *Globigerinoides quadrilobatus primordius* is solution-prone, it is suggested that these species represent extremes in the dissolution 'scale' of calcareous microfossils. As a biostratigraphic index, *G. quadrilobatus primordius* is incompatible with *S. ciperoensis* in slightly etched oceanic sediments, whereas in well-preserved hemipelagic sediments the two species are equally important.

Age assignment and further discussion. No attempt has been made to relate the biostratigraphic results presented in this study to the chronological time scale, because of the many problems and controversies surrounding the European stratotypes. However, correlations by many authors indicate that *Sphenolithus ciperoensis* is a late Oligocene species, and accordingly by association, the *Globigerinoides quadrilobatus primordius* (evolution) datum is late Oligocene in age. This conclusion is at odds with the recommendation of the Neogene Committee (at Bologna, 1967), which stated that this datum defines the Oligocene-Miocene boundary; views against this recommendation have been expressed repeatedly. Steininger, Rögel, & Martini (1976, p. 179) stated that 'the first occurrence of *Globigerinoides primordius* was found to be worthless as an index to define the Oligocene-Miocene boundary' (see also Seiglie, 1973; Lamb & Stainforth, 1976; Wright, 1977).

Evidence indicating that the part of the 'Cartier Beds' containing *Sphenolithus ciperoensis* is late Oligocene in age is overwhelming: the highest occurrence of *Helicopontosphaera recta* has been used to delineate the Oligocene-Miocene boundary (e.g., Martini, 1971), and *Zygrhablithus bijugatus* which has been identified in the Chattian stratotypes (Anderson and others, 1971; Haq, 1971; Martini & Müller, 1975) is not known *in situ* in sediment younger than the Oligocene; both species have their highest occurrence well above that of *S. ciperoensis* in the 'Cartier Beds'. Therefore, the lowest occurrence of *Globigerinoides quadrilobatus primordius* in hemipelagic sediments (thus including its evolution datum), where the species overlaps with the range of *S. ciperoensis,* is late Oligocene in age; associated foraminiferids (e.g. *Globigerina gortanii gortanii, G. angulisofficinalis, G. tripartita tripartita, G. tripartita sellii, Globorotalia opima opima,* and *Globogerinita unicava* in the 'Cartier Beds') support this conclusion.

Although the evolutionary appearance of *Globigerinoides quadrilobatus primordius* occurred during the late Oligocene (e.g., Capricorn No. 1A Well), the species first occurs in most of the oceanic records at higher stratigraphic levels (mostly early Miocene in age); the lowest occurrence of *G. quadrilobatus primordius* in deep oceanic sediments where it is separated from the *Sphenolithus ciperoensis* (extinction) datum by a gap (e.g., the Ontong Java site) is early Miocene in age, as shown by the associated nannofossils and planktic foraminiferids (see Andrews, Packham, and others, 1975).

To account for younger lowest occurrences of *G. quadrilobatus primordius* in the oceanic record relative to its evolutionary appearance during the late Oligocene (as it is documented in hemipelagic sections), two possibilities are proposed. The first is that the species might have developed a more solution-resistant variant during the early Miocene; the second is that some changes in the oceanic realm related to the dissolution of the calcareous microplankton remains might have occurred during the early Miocene. The first possibility is beyond the scope of the present study; and the answer probably lies in studying the wall structure of the species through time. The second possibility is discussed below.

The dissolution and ultimate disappearance of calcareous microplankton remains have been linked with two conceptual parameters: the lysocline, and the carbonate compensation depth (e.g., Heath, 1969; Berger, 1970; Parker & Berger, 1971; Berger, 1973; Berger & Winterer, 1974; Ramsay, 1974; Van Andel and others, 1975); the implication is that the intervening zone is the main domain for selective dissolution. Lohman (1974) suggested that changes in the thickness of this zone produce an increase in calcite dissolution in deep-water sediments corresponding to a decrease in that dissolution in shallow-water sediments, whereas bathymetric shifts of the entire zone result in similar patterns of dissolution in both deep and shallow-water sediments. That effects of changes in the thickness of the lysocline-compensation depth zone are noted in upper Eocene sediments, whereas effects of bathymetric shifts of the

zone are recorded in middle Eocene sediments (Lohman, 1974) suggest that changes in the zone are climatically controlled; the late Eocene is known to have been cooler than the middle Eocene (Shackleton & Kennett, 1975; Savin, Douglas, & Stehli, 1975). During the Oligocene-Miocene transition, a drop in the temperature of the oceans to a minimum of 4°C in high latitudes occurred late in the Oligocene, and was followed by a warming through the early Miocene (Savin and others, 1975). This may have resulted in changes in the thickness of the zone between the lysocline and compensation depth during the latest Oligocene, and a downward shift of this zone during the earliest Miocene. The latest Oligocene changes in the thickness of the zone caused depth-related fractionation with the result that shallow-water carbonate sediments (hemipelagic) are better preserved than deep-oceanic carbonate; the presence of *Globigerinoides quadrilobatus primordius* in upper Oligocene hemipelagic sediments, and its absence in coeval deep-oceanic sediments are taken to indicate that this was the case. The downward shift of the zone (lysocline-compensation depth) during the early Miocene produced equally good preservation of hemipelagic and most of the deep-oceanic carbonates; the presence of *G. quardilobatus primordius* in lower Miocene deep-oceanic and hemipelagic sediments is considered as a sound indication of this zonal shift.

Sphenolithus belemnos datum and associated foraminiferal evidence in the 'Cartier Beds'

Correlations by several authors (e.g., Martini, 1971; Berggren & Couvering, 1974) suggest that the *Sphenolithus belemnos* (base of range) datum approximates the N.5/N.6 boundary or slightly older, even though earlier records (Bramlette & Wilcoxon, 1967; Roth, 1970) suggested correlation with Zone N.3. The base of Zone N.6 is defined by the incoming of *Globigerinatella insueta* (Blow, 1969), but this species has not been found in the studied material. Instead, *Globigerinoides quadrilobatus altiaperturus* is recorded within the topmost part of the 'Cartier Beds'; this species extends from near the base of Zone N.5 to within the lower part of Zone N.7 (Blow, 1969).

The extinction of *Sphenolithus belemnos* occurs within the top part of Zone N.6 (Bramlette & Wilcoxon, 1967; Martini, 1971). Thus, based on the presence of *S. belemnos* in the uppermost part of the 'Cartier Beds' (Fig. 6), a correlation with the interval from top part of Zone N.5 to within Zone N.6 can be made; the occurrence of *Globigerinoides quadrilobatus altiaperturus* supports this correlation, and the absence of *Globigerinatella insueta* may be due to its provincial distribution.

Oligocene-Miocene boundary

The recommendation of the Neogene Committee (at Bologna, 1967) regarding the *Globigerinoides* datum as defining the Oligocene-Miocene boundary has not been ratified, and there are indications that this recommendation is unsatisfactory (see also Drooger and others, 1976; Benda and others, 1977). Belford (1974) reviewed several papers dealing with the Oligocene-Miocene boundary, particularly those in connection with the *G. quadrilobatus primordius datum*. On the basis of the available knowledge of the stratigraphical distribution of planktic foraminiferids, he concluded that the *G. quadrilobatus primordius* datum may be near the N.2/N.3 zonal boundary. Furthermore, Fleisher (1975) noted that the boundary N.4/P.22 of Blow (1969) cannot be consistently delineated because of the paucity of *G. primordius* (where present) near the base of its range, or its appearance in horizons older than the initial appearance of *'Turborotalia' kugleri*.

Various nannofossil criteria have been used to locate the Oligocene-Miocene boundary, but none are satisfactory. Roth (1970) suggested that the boundary is at or slightly above the first appearance of *Sphenolithus belemnos*. Martini (1971) used the last appearance of *Helicopontosphaera recta* to delineate the top of the Oligocene; *H. recta* occurs consistently in widely distributed hemipelagic sediments, but it is either absent or occurs sporadically in oceanic sediments. Bukry (1973) used the end-acme of *Cyclicargolithus abisectus* to locate the boundary, but cases where this could not be applied have been reported by Bukry (1974, DSDP Site 214). Roth (1973) employed the last appearance of *C. abisectus* to delineate the boundary; however, there is evidence suggesting that *C. abisectus* straddles the Oligocene-Miocene boundary (e.g. Bukry, 1973; Shafik, 1975). Moreover, Thierstein (1974) and Shafik's own observations indicate that distinction between *Cyclicargolithus floridanus* and *C. abisectus* by light microscopy is sometimes difficult, because the criteria for their differentiation are greatly affected by preservation; *C. floridanus* definitely extends into the Miocene (e.g. Shafik, 1975). Edwards (1973) suggested that the extinction level of *R. scissura* best approximates the Oligocene-Miocene boundary (see also Haq & Lipps, 1971); *R. scissura* disappears before the sequential disappearances of several other upper Oligocene species. Gartner (1974) used the first appearance of *Triquetrorhabdulus carinatus* to delineate the boundary.

It is apparent that nannofossil criteria proposed by many authors to delineate the Oligocene-Miocene boundary are often problematical for use with oceanic sediments. Therefore, it is reasonable to recognise a buffer zone representing the Oligocene-Miocene transition, between sediments that are definitely at, or below, the late Oligocene *S. ciperoensis* (extinction) datum, and those that are definitely above the early Miocene *S. belemnos* (base of range) datum. In hemipelagic sediments, the buffer zone may include several biostratigraphic events such as the disappearance of the solution-prone *Helicopontrosphaera recta* and *Zygrahablithus bijugatus*.

Acknowledgements

Dr M. R. Walter read an earlier draft, and Drs D. J. Belford, K. Perch-Nielsen read the manuscript submitted. We thank both for their constructive criticism. The figures were drawn by R. Fabbo.

References

ADELSECK, C. F., & BERGER, W. H., 1975—On the dissolution of planktonic foraminifera and associated microfossils during settling and on the sea floor. *In* SILTER, W. V., BE, A. W. H., & BERGER, W. H. (Editors), DISSOLUTION OF DEEP-SEA CARBONATES. *Cushman Foundation for Foraminiferal Research, Special Publication* **13**, 70-81.

ANDERSON, A. J., HINSCH, W., MARTINI, E., MULLER, C., & RITZHOKWSKI, S., 1971—*Chattian. Giornale di Geologia*, **37**, 69-79.

ANDREWS, J. E., PACKHAM, G. H., and others, 1975—Leg 30. *Initial Reports of the Deep Sea Drilling Project*, **30**, 1-705, Washington, US Government Printing Office.

BAUMANN, P., 1972—Les Faunas de Foraminifères de l'Éocène Supérieur a la base du Miocène dans le Bassin de Pasir, sud de Kalimantan (Bornéo). *Revue de l'Institut Française du Pétrole*, **27**, 817-29.

BÉ, A. W. H., 1960—Ecology of Recent planktonic foraminifera II. *Micropaleontology*, **6**, 373-92.

BÉ, A. W. H., & TOLDERLUND, D. S., 1971—Distribution and ecology of living planktonic foraminifera in surface waters of the Atlantic and Indian Ocveans. *In* FUNNEL, B. M., & RIEDEL, W. R. (Editors)—THE MICROPALAEONTOLOGY OF OCEANS, 105-149, Cambridge University Press.

BECKMANN, J. P., 1971—The foraminifera of Sites 68 to 75. *In* TRACEY, J. I., SUTTON, G. H., and others, *Initial Reports of the Deep Sea Drilling Project*, **8**, 713-726, Washington, US Government Printing Office.

BELFORD, D. J., 1968—Palaeontological report, Ashmore Reef No. 1 Well. *Burmah Oil Company of Australia Ltd Report* (unpublished).

BELFORD, D. J., 1974—Foraminifera from the Ilaga Valley, Nassau Range, Irian Jaya. *Bureau of Mineral Resources, Australia, Bulletin* **150**, 1-26.

BENDA, L., MEULENKAMP, J. E., SCHMIDT, R. R., STEFFENS, P., & ZACHARIASSE, J., 1977—Biostratigraphic correlations in the Eastern Mediterranean Neogene. *Newsletters on Stratigraphy*, **6**, 1-22.

BERGER, W. H., 1970—Planktonic foraminifera: selective solution and the lysocline. *Marine Geology*, **8**, 111-38.

BERGER, W. H., 1971—Sedimentation of planktonic foraminifera. *Marine Geology*, **11**, 325-58.

BERGER, W. H., 1973—Deep-sea carbonates: evidence for a coccolith lysocline. *Deep-sea Research*, **20**, 917-21.

BERGER, W. H., & WINTERER, E. L., 1974—Plate stratigraphy and the fluctuating carbonate line. *In* HSU, K. J., & JENKYNS, H. (Editors), PELAGIC SEDIMENTS ON LAND AND UNDER THE SEA. *International Association of Sedimentologists, Special Publication* **1**, 11-48.

BERGGREN, W. A., 1971—Tertiary boundaries and correlations. *In* FUNNEL, B. M., & RIEDEL, W. R. (Editors)—THE MICROPALAEONTOLOGY OF THE OCEANS, 693-809, *Cambridge University Press.*

BERGGREN, W. A., & VAN COUVERING, J. A., 1974—The late Neogene-biostratigraphy, geochronology and paleoclimatology of the last 15 million years in marine and continental sequences. *Palaeogeography, Palaeoclimatology, Palaeoecology*, **16**, 1-216.

BLOW, W. H., 1969—Late Middle Eocene to Recent planktonic foraminiferal biostratigraphy. *Proceedings of the First International Conference on Planktonic Microfossils, Geneva, 1967*, **1**, 199-421, *Leiden, E. J. Brill.*

BLOW, W. H., 1970a—Validity of biostratigraphic correlations based on the Globigerinacea. *Micropalaeontology*, **16**, 257-68.

BLOW, W. H., 1970b—Deep Sea Drilling Project, Leg 4 foraminifera from selected samples. *In* BADER, R. G., GERAD, R. D., and others. *Initial Reports of the Deep Sea Drilling Project* **4**, 383-400, *Washington, US Government Printing Office.*

BOLLI, H. M., 1957—Planktonic foraminifera from the Oligocene-Miocene Cipero and Lengua Formations of Trinidad, B.W.I. *US National Museum, Bulletin* **215**, 97-124.

BOLLI, H. M., 1966—Zonation of Cretaceous to Pliocene marine sediments based on planktonic foraminifera. *Asociacion Venezolana de Geologia, Mineria y Petroleo, Boletin Informativo* **9**, 3-32.

BOLLI, H. M., 1970—The foraminifera of Sites 23 to 31, Leg 4. *In* BADER, R. G., GERARD, R. D., and others, *Initial Reports of the Deep-Sea Drilling Project*, **4**, 577-623, *Washington, US Government Printing Office.*

BOLTOVSKOY, E., 1971—Planktonic foraminiferal assemblages of the epipelagic zone and their thanatocoenoses. *In* FUNNEL, B. M., & RIEDEL, W. R. (Editors), THE MICROPALAEONTOLOGY OF OCEANS, 277-88, *Cambridge University Press.*

BRAMLETTE, M. N., & WILCOXON, J. A., 1967—Middle Tertiary calcareous nannoplankton of the Cipero section, Trinidad, W.I. *Tulane Studies in Geology and Paleontology*, **5**, 93-131.

BUKRY, D., 1972—Coccolith stratigraphy Leg 11, Deep Sea Drilling Project. *In* HOLLISTER, C. D., EWING, J. L., and others, *Initial Reports Deep Sea Drilling Project*, **11**, 475-82, *Washington, US Government Printing Office.*

BUKRY, D., 1973—Low-latitude coccolith biostratigraphic zonation. *In* EDGAR, N. T., SAUNDERS, J. B., and others, *Initial Reports of the Deep Sea Drilling Project*, **15**, 685-703, *Washington, US Government Printing Office.*

BUKRY, D., 1974—Coccolith and silicoflagellate stratigraphy, Eastern Indian Ocean, Deep Sea Drilling Project, Leg 22. *In* VON DER BORCH, C., SCLATER, J. G., and others. *Initial Reports of the Deep Sea Drilling Project*, **22**, 601-5, *Washington, US Government Printing Office.*

BUTT, A. A., 1966—LATE OLIGOCENE FORAMINIFERA FROM ESCORNEBEOU, SW FRANCE. *Schotanus & Jens, Utrecht.*

CARALP, M., VALETON, S., & VIGNEAUX, M., 1965—Les foraminiferes pelagiques du Tertiaire terminal sud-aquitan. *Academie Science Paris, Comptes Rendues*, **261**, 3431-4.

CHAPRONIERE, G. C. H., 1975—Palaeoceology of Oligo-Miocene larger Foraminiferida, Australia. *Alcheringa*, **1**, 37-58.

CICHA, I., HAGN, H., & MARTINI, E., 1971—Das Oligozan und Miozan der Alpen Karpaten. Ein Vergleich mit Hilfe planktonischer Organismen. *Bayerische Staatssammlung fur Palaontologie und historische Geologie, Mitteilungen* **11**, 279-93.

COLEMAN, P. J., 1968—Palaeontological report, Ashmore Reef No. 1 Well. *Burmah Oil Company of Australia Ltd Report* (unpublished).

CRAIG, R. W., 1968—Ashmore Reef No. 1 Well. *Burmah Oil Company of Australia Ltd Report* (unpublished).

CUSHMAN, A., & ELLISOR, A. C., 1939—New species of Foraminifera from the Oligocene and Miocene. *Cushman Laboratory for Foraminiferal Research, Contributions*, **15**, 1-14.

DOUGLAS, R. G., 1973—Planktonic foraminiferal biostratigraphy in the central North Pacific Ocean. *In* WINTERER, E. L., EWING, J., and others, *Initial Reports of the Deep Sea Drilling Project*, **17**, 673-94, *Washington, US Government Printing Office.*

DOW, D. B., 1968—A geological reconnaissance in the Nassau Range, West New Guinea. *Geologie en mijnbouw*, **47**, 37-46.

DROOGER, C. W., 1960—*Miogypsina* in northwestern Germany. *Koninklijke Nederlandse Akademie von Wetenschappen, Proceedings* **B63**, 38-50.

DROOGER, C. W., MEULENKAMP, J. E., SCHMIDT, R. R., & ZACHARIASSE, W. J., 1976—The Paleogene-Neogene Boundary. *Koninklijke Nederlandse Akademie van Wetenschappen, Proceedings* **B79**, 317-29.

EDGAR, N. T., SAUNDERS, J. B., and others, 1973—Sites 146/149. *Initial Reports of the Deep Sea Drilling Project*, **15**, 17-168, *Washington, US Government Printing Office.*

EDWARDS, N. T., SAUNDERS, J. B., and others, 1973—Sites 146/149. *Initial Reports of the Deep Sea Drilling Project*, **15**, 17-168, *Washington, US Government Printing Office.*

EDWARDS, A. R., 1973—Calcareous nannofossils from the Southwest Pacific, Deep Sea Drilling Project, Leg 21. *In* BURNS, R. E., ANDREWS, J. E., and others, *Initial Reports of the Deep Sea Drilling Project*, **21**, 641-91, *Washington, US Government Printing Office.*

FISCHER, A. G., HEEZEN, B. C., and others, 1971—Leg 6. *Initial Reports of the Deep Sea Drilling Project*, **6**, *Washington, US Government Printing Office.*

FLEISHER, R. L., 1975—Oligocene planktonic foraminiferal biostratigraphy, central North Pacific Ocean, DSDP Leg 32. *In* LARSON, R. L., MOBERLY, R., and others, *Initial Reports of the Deep Sea Drilling Project*, **32**, 753-63, *Washington, US Government Printing Office.*

GARTNER, S., junior, 1974—Nannofossil Biostratigraphy, Leg 22, Deep Sea Drilling Project. *In* VON DER BORCH, C., SCLATER, J. G., and others, *Initial Reports of the Deep Sea Drilling Project*, **22**, 577-99., *Washington, US Government Printing Office.*

GARTNER, S., junior, JOHNSON, D. A., & MCGOWRAN, B., 1974—Paleontology synthesis of Deep Sea Drilling results from Leg 22 in the Northeastern Indian Ocean. *In* VON DER BORCH, C. C., SCLATER, J. G., and others, *Initial Reports of the Deep Sea Drilling Project*, **22**, 805-13, *Washington, US Government Printing Office.*

GELATI, R., 1975—Miocene marine sequence from the Lake Van area, eastern Turkey. *Rivista Italiana di Paleontologia*, **81**, 477-90.

HAQ, B., 1971—Paleogene calcareous nannoflora. Part 2, Oligocene of Western Germany. *Stockholm Contributions in Geology*, **25**, 57-97.

HAQ, B., & LIPPS, J. H., 1971—Calcareous nannofossils. *In* TRACEY, J. I., junior, SUTTON, G. H., and others, *Initial Reports of the Deep Sea Drilling Project*, **8**, 777-89, *Washington, US Government Printing Office.*

HAY, W. W., 1970—Calcium carbonate compensation. *In* BANNER, R. G., and others, *Initial Reports of the Deep Sea Drilling Project*, **4**, 672, *Washington, US Government Printing Office.*

HEATH, G. R., 1969—Carbonate sedimentation in the abyssal equatorial Pacific during the last 50 million years. *Geological Society of America, Bulletin* **80**, 689-94.

HEKEL, H., 1973—Late Oligocene to Recent nannoplankton from the Capricorn Basin (Great Barrier Reef Area). *Geological Survey of Queensland, Publication* **359**, *Palaeontological Paper* **36**, 1-24.

HEIMAN, M. E., FRERICHS, W. E., & VINCENT, E., 1974—Paleogene planktonic foraminifera from the western tropical Indian Ocean, Deep Sea Drilling Project Leg 24. *In* FISHER, R. L., BUNCE, E. T., and others, *Initial Reports of the Deep Sea Drilling Project*, **24**, 851-76, *Washington, US Government Printing Office.*

JENKINS, D. G., 1960—Planktonic foraminifera from the Lakes Entrance oil shaft, Victoria, Australia. *Micropaleontology*, **6**, 345-71.

JENKINS, D. G., 1971—New Zealand Cenozoic planktonic foraminifera. *New Zealand Geological Survey, Paleontological Bulletin* **42**.

JENKINS, D. G., & ORR, W. N., 1971—Cenozoic planktonic foraminiferal zonation and the problem of test solution. *Revista Espanola di Micropaleontologia*, **3**, 301-4.

JENKINS, D. G., & ORR, W. N., 1972—Planktonic foraminiferal biostratigraphy of the eastern equatorial Pacific—DSDP Leg 9. *In* HAYES, J. D., and others, *Initial Reports of the Deep Sea Drilling Project*, **9**, 1060-193, *Washington, US Government Printing Office.*

JONES, J. I., 1968—The relationships of planktonic foraminiferal populations to water masses in the western Caribbean and lower Gulf of Mexico. *Bulletin of Marine Science of the Gulf and Caribean*, **18**, 946-82.

KANEPS, A. C., 1973—Cenozoic planktonic foraminifera from the eastern equatorial Pacific Ocean. *In* VAN ANDEL, T. H., HEATH, G. R., and others, *Initial Reports of the Deep Sea Drilling Project*, **16**, 713-45, *Washington US Government Printing Office.*

LAMB, J. L., & STAINFORTH, R. M., 1976—Unreliability of *Globigerinoides* datum. *American Association of Petroleum Geologists, Bulletin* **60**, 1564-9.

LOHMAN, G. P., 1974—Bathymetric variation of calcite dissolution recorded in Eocene pelagic sediments on Barbados, West Indies. *Third Planktonic Conference, Kiel, Symposium Marine plankton and sediments*, 1974, *Abstracts*, 48.

MARTINI, E., 1917—Standard Tertiary and Quaternary calcareous nannoplankton zonation. *In* FARINACCI, A. (Editor), *Proceedings of the Second Planktonic Conference, Roma, 1970*, 739-785. *Rome, Edizioni Tecnoscienza.*

MARTINI, E. & MULLER, C., 1975—Calcareous nannoplankton from the type Chattian (upper Oligocene). *Proceedings of the Sixth Congress Regional Committee on Mediterranean Neogene Stratigraphy, Bratislava*, 37-41.

MULLER, C., 1974—Calcareous nannoplankton from mid-Tertiary stratotypes. *Bureau de Recherches Geologiques et Miniere, Memoire* **78**, 427-32.

PALMIERI, V., 1971—Tertiary subsurface biostratigraphy of the Capricorn Basin. *Geological Survey of Queensland, Report* **52**, 1-18.

PALMIERI, V., 1974—Correlation and environmental trends of the subsurface Tertiary Capricorn Basin. *Geological Survey of Queensland, Report* **86**, 1-14.

PALMIERI, V., 1975—Planktonic Foraminiferida from the Capricorn Basin, Queensland. *Geological Survey of Queensland, Publication* **362**, *Palaeontological Paper* **36**, 1-47.

PARKER, F., & BERGER, W. H., 1971—Faunal and solution patterns of planktonic foraminifera in surface sediments of the South Pacific. *Deep Sea Research*, **181**, 73-107.

PERCH-NIELSEN, K., 1972—Remarks on late Cretaceous to Pleistocene coccoliths from the North Atlantic. *In* LAUGHTON, A. S., BERGGREN, W. A., and others, *Initial Reports of the Deep Sea Drilling Project*, **12**, 1003-70, *Washington, US Government Printing Office.*

POAG, C. W., 1972a—Neogene planktonic foraminiferal biostratigraphy of the western North Atlantic: DSDP Leg 11. *In* HOLLISTER, C. D., EWING, J. J., and others, *Initial Reports of the Deep Sea Drilling Project*, **11**, 483-520, *Washington, US Government Printing Office.*

POAG, C. W., 1972b—Planktonic foraminifers of the Chickasawhay Formation, United States Gulf Coast. *Micropaleontology*, **18**, 257-77.

RAMSAY, A. T., 1974—The distribution of calcium carbonate in deep-sea sediments. *In* HAY, W. W. (Editor), Studies in Paleoceanography. *Society of Economic Paleontologists and Mineralogists, Special Publication* **20**, 58-76.

ROTH, P. H., 1970—Oligocene calcareous nannoplankton biostratigraphy. *Eclogae Geologicae Helvetiae*, **63**, 799-881.

ROTH, P. H., 1973—Calcareous nannofossils—Leg 17, Deep Sea Drilling Project. *In* WINTERER, E. L., EWING, J. J., and others, *Initial Reports of the Deep Sea Drilling Project*, **17**, 675-796, *Washington, US Government Printing Office.*

ROTH, P. H., 1974—Calcareous nannofossils from the northwestern Indian Ocean, Leg 24, Deep Sea Drilling Project, *In* FISHER, R. L., BUNCE, E. T., and others, *Initial Reports of the Deep Sea Drilling Project*, **24**, 969-94, *Washington, US Government Printing Office.*

ROTH, P. H., & BERGER, W. H., 1971—Distribution and dissolution of coccoliths in the South and Sentral Pacific. *In* SILTER, W. V., BÉ, A. W. H., & BERGER, W. H. (Editors), Dissolution of deep-sea carbonates. *Cushman Foundation for Foraminiferal Research, Special Publication* **13**, 87-113.

ROTH, P. H., MULLIN, M. M., & BERGER, W. H., 1975—Coccolith sedimentation by fecal pellets: Laboratory experiments and field observations. *Geological Society of America, Bulletin* **86**, 1079-84.

SAVIN, S. M., & DOUGLAS, R. G., 1973—Stable isotope and magnesium geochemistry of Recent planktonic foraminifera from the South Pacific. *Geological Society of America, Bulletin* **84**, 2327-42.

SAVIN, S. M., DOUGLAS, R. G., & STEHLI, F. G., 1975—Tertiary marine paleotemperatures. *Geological Society of America, Bulletin* **86**, 1499-510.

SEIGLIE, G. A., 1973—Revision of mid-Tertiary stratigraphy of southwestern Puerto Rico. *American Association of Petroleum Geologists, Bulletin* **57**, 405-6.

SHACKLETON, N. J., & KENNETT, J. P., 1975—Paleotemperature history of the Cenozoic and the initiation of Antarctic glaciations: oxygen and carbon isotope analysis in deep sites. *In* KENNETT, J. P., HOUTZ, R. E., and others, *Initial Reports of the Deep Sea Drilling Project*, **29**, 743-55, *Washington, US Government Printing Office.*

SHAFIK, S., 1975—Nannofossil biostratigraphy of the southwest Pacific, Deep Sea Drilling Project, Leg 30. *In* ANDREWS, J. E., PACKHAM, G. H., and others, *Initial Reports of the Deep Sea Drilling Project,* **30**, 549-97, *Washington, US Government Printing Office.*

THIERSTEIN, H. R., 1974—Calcareous nannoplankton—Leg 26, Deep Sea Drilling Project. *In* DAVIES, T. A., LUYENKYK, B. P., and others, *Initial Reports of the Deep Sea Drilling Project,* **26**, 619-69, *Washington, US Government Printing Office.*

VAN ANDEL, T. H., HEATH, G. R., & MOORE, T. C., junior, 1975—Cenozoic history and paleoceanography of the central equatorial Pacific: A regional synthesis of the DSDP data. *Geological Society of America, Memoir* **143**.

VINCENT, E., FRERICHS, W. E., & HEIMAN, M. E., 1974—Neogene planktonic foraminifera from the Gulf of Aden and the western tropical Indian Ocean, Deep Sea Drilling Project, Leg 24. *In* FISHER, R. L., BUNCE, E. T., and others, *Initial Reports of the Deep Sea Drilling Project,* **24**, 827-45, *Washington, US Government Printing Office.*

WILCOXON, J. A., 1972—Calcareous nannoplankton ranges, Deep Sea Drilling Project. *In* HOLLISTER, C. D., EWING, J. J., and others, *Initial Reports of the Deep Sea Drilling Project,* **11**, 459-73, *Washington, US Government Printing Office.*

WRIGHT, C. A., 1977—Distribution of Cainozoic Foraminiferida in the Scott Reef No. 1 Well, Western Australia. *Geological Society of Australia, Journal* **24**, 269-78.

BMR Journal of Australian Geology & Geophysics, 3, 1978, 153-162

Gravity evidence for abrupt changes in mean crustal density at the junction of Australian crustal blocks

Peter Wellman

The major gravity anomalies in central and western Australia occur as elongate dipoles, either in isolation or in a series. Each dipole is thought to be caused by an abrupt change in mean crustal density at the junction of two crustal blocks and by the associated isostatically compensating masses. Typically one block has along its margin a strip with anomalously high mean crustal density, and the other block has normal density crust covered by several kilometres of low density sediment. The observed anomalies are consistent with the anomalous masses being isostatically compensated by variations in the thickness of the crust, the crustal thickness variations being gradual and extending to about 100 km from the boundaries of the anomalous bodies.

The crustal block boundaries inferred from dipole anomalies correspond in position with the crustal block boundaries inferred from geology, and approximately with the position of block boundaries inferred from changes in the gravity trend pattern. Usually the block with younger basement has high density material along its margin, and the other, older block is covered with sediment; both these features are likely to be caused by the process that created or emplaced the younger block. The presence of relatively dense material high in the crust along the margins of the younger blocks suggests that younger blocks are not superficial features on a uniform old crust. The dipole anomalies on the Australian Precambrian crust are similar in magnitude and tectonic position to those recognised at Precambrian province boundaries in Canada.

Introduction

The largest gravity anomalies on the Australian continent lie in the central and western parts of Australia (BMR, 1976a). These anomalies are generally very elongate, and consist of associated and parallel highs and lows with peak-to-peak amplitudes up to 180 mGal. This paper discusses two independent but related aspects of their interpretation: it develops geometrical models for the observed anomalies showing that they can be explained largely by isostatically compensated strips of relatively dense crust, and in the second part of the paper shows that the relatively dense crust is developed along the junction of crustal blocks with a different geological history.

The large gravity anomalies must be at least partly caused by variations in crustal density, because many of the positive anomalies are over dense, high-grade metamorphic rock, while many of the negative anomalies are over sedimentary basins. The remaining portions of the anomalies are interpreted here as caused by masses that isostatically compensate these variations in crustal density, the compensation being by variations in crustal thickness. Previously the Australian anomalies were interpreted as due solely to density variation within the crust (Anfiloff & Shaw, 1973; Fraser, 1974a, b), or mainly to crustal thickness variation which are out of isostatic equilibrium (Mathur, 1976; Kennewell, Mathur, & Wilkes, 1977). Within the Canadian shield similar gravity anomalies were interpreted by Gibb & Thomas (1976) as due to abrupt changes in mean crustal density, the adjacent pieces of crust being close to, but not exactly in, isostatic equilibrium. Models with the crust in exact isostatic equilibrium are a better fit for these Canadian anomalies.

Wellman (1976a) has shown that in central and western Australia the mean free-air anomalies of 1° x 1° areas have a small negative correlation with the mean altitude of 1° x 1° areas, but there is a large variation in anomaly about the mean correlation line. The small negative correlation suggests that the topographic masses, and presumably other anomalous masses, are isostatically compensated near the base of the crust. The large scatter shows that the isostatic compensation may not be complete within 1° x 1° areas, implying that compensation may be regional rather than local. McNutt & Parker (1978) have applied linear transform function analysis to gravity and topographic data from the whole of the Australian continent. They conclude that the continent, treated as a single unit, is isostatically compensated at the base of the crust, and that the compensation may either be local or complete for small areas, the inferred flexural rigidity of the lithosphere being between 0 and 5.10^{20} Nm. Both of these studies suggest that isostatic compensation is achieved near the base of the crust, and both are consistent with the compensation being local or having a small regional component in central and western Australia. These two studies investigated the compensation of topography. The present topography is much younger than the emplacement time of the crustal masses of anomalous density, and plastic flow is likely to have occurred at the base of the crust over the long periods since emplacement, so that these anomalous crustal masses may have isostatic compensation with a different regional component than that for topography.

Crustal density variation of wavelength longer than about 3°, if gradual and completely compensated by underlying masses, would give little resultant anomaly, because the gravity effect of the mass and its compensation would almost completely cancel one another. Short wavelength crustal density variation would result from either the abrupt termination of wide bodies, or from narrow bodies. Even if completely compensated locally or regionally it will result in positive and negative anomalies, because of the edge effects of a narrow body and its compensation. The sort of anomalies found is shown in Figure 1—they are small if compensation is local, and larger if compensation is

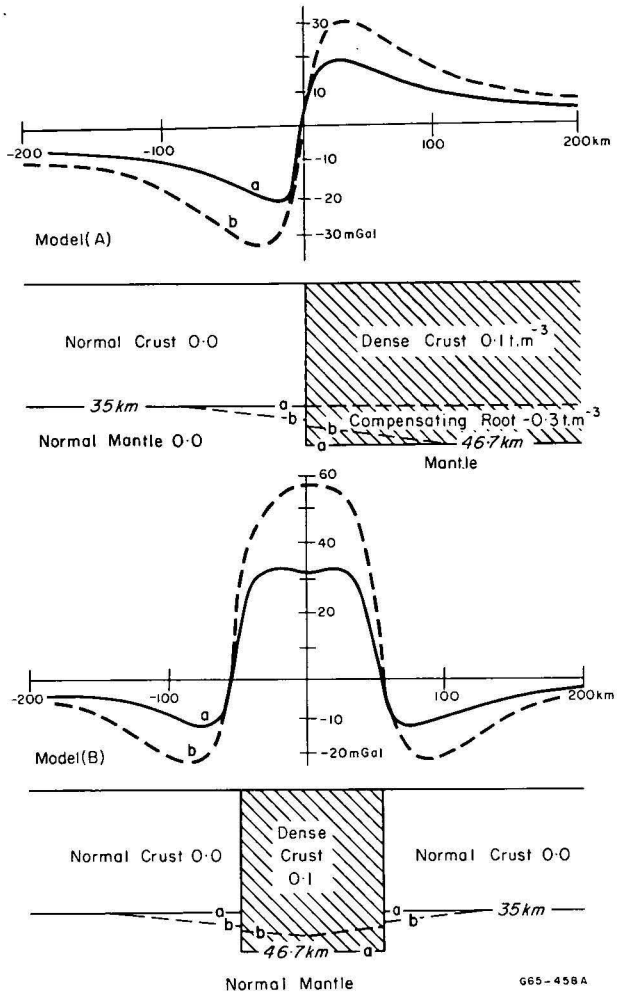

Figure 1. Cross-sections showing gravity anomalies due to isostatically compensated changes in mean crustal density.
A, Abrupt change in mean crustal density; B, strip of dense crust. In each cross-section solid lines (a) show local isostatic equilibrium, and dashed lines (b) show regional isostatic equilibrium. Numbers are distances in kilometres, and density contrasts from a standard crust in t m^{-3} = gm cm^{-3}.

regional. The real earth approximates the flat earth; for the flat earth the positive anomalous masses must exactly equal the negative anomalous masses for isostatic compensation. According to Gauss' theorem, if these masses are equal in magnitude, then in the gravity anomaly profile the positive and negative areas must be equal, i.e. the net anomaly associated with the feature is zero.

The basement rocks of Australia has previously been divided into a set of blocks; within each block the basement rocks have similar geological character and a similar history of igneous, sedimentary and metamorphic events, while between blocks these characteristics show major differences (GSA, 1971). Only some blocks and some junctions have well exposed basement. More commonly parts of the blocks and the junction are covered by much younger sediments; in these areas surface geology does not give differences in the history of the blocks or the exact position of the junction. Some information on the position of the block boundaries and the relative age of the major deformation of the blocks is given by gravity (Wellman, 1976b) and magnetic trend patterns. Similar, but complementary information is given by the large gravity anomalies that lie over many block boundaries; these anomalies are the subject of this paper.

Distribution of interpreted anomalies

The locations of the steep gradients of the large elongate anomalies in central and western Australia are shown in Figure 2, and the major Australian tectonic units named in the text are given in Figure 3. The anomalies each consist of a peak and trough of similar amplitude, separated by a steep gradient. The outer flanks of the anomalies have relatively gentle gradients. The word dipole is used for these anomalies—a pair of horizontally displaced positive and negative anomalies of similar amplitude.

The anomalies can be divided into two types: isolated dipole anomalies, where one positive and one negative occur together and are isolated from other large anomalies (Fig. 2, anomalies A,B,D,I,J,M,N,O,P,Q); and multiple dipole anomalies, where several dipoles overlap (anomalies C,E,F,G,H,K,L,R,S,T). This study is restricted to large anomalies within the Australian continent, anomalies along the continental margin are not considered, except where they influence the specific interpretation of anomaly K and L.

Method of interpretation

Interpretation of gravity anomalies is best carried out by removing a 'regional' long wavelength anomaly from the observed anomaly field, isolating the anomaly to be investigated and defining its marginal 'tails'. The gravity anomalies in this study are assumed to consist mainly of two components: relatively short wavelength anomalies, caused by short wavelength density variation in the crust, and the isostatic compensation of this at the base of the crust; and long wavelength anomalies, unrelated to crustal density changes and their compensating masses. Anomalies of wavelength greater than 20° form a relatively steep gradient over Australia as they vary from near −20 mGal in the southwest to +30 mGal in the northeast. This gradient is part of a worldwide system of major anomalies, and it is thought to be due to density differences supported by fluid motion in the mantle, the motion being essentially decoupled from the lithosphere (Cochran & Talwani, 1977). In this paper long wavelength effects were minimised by subtracting from the free-air anomalies the mean values of 5° x 5° areas using the map of Dooley (1973); regional topographic effects have been minimised by using free-air anomalies.

In the two-dimensional interpretation of a gravity anomaly it is usual to fit a complex model exactly to a single 'typical' cross-section of the anomaly. However, with this method it is never clear which features of the model are typical of other cross-sections of the anomaly, and which features are local. In the present study an alternative approach is adopted; regularly spaced, straight cross-sections are drawn across an anomaly and a simple model is presented that fits the common features of all cross-sections. Observed and calculated anomalies would show better agreement if the models were more complicated; in particular, if the regionality of the isostatic compensation was varied, the horizontal density contrasts were changed from 0.1 t m^{-3}, and bodies of more than four sides were used.

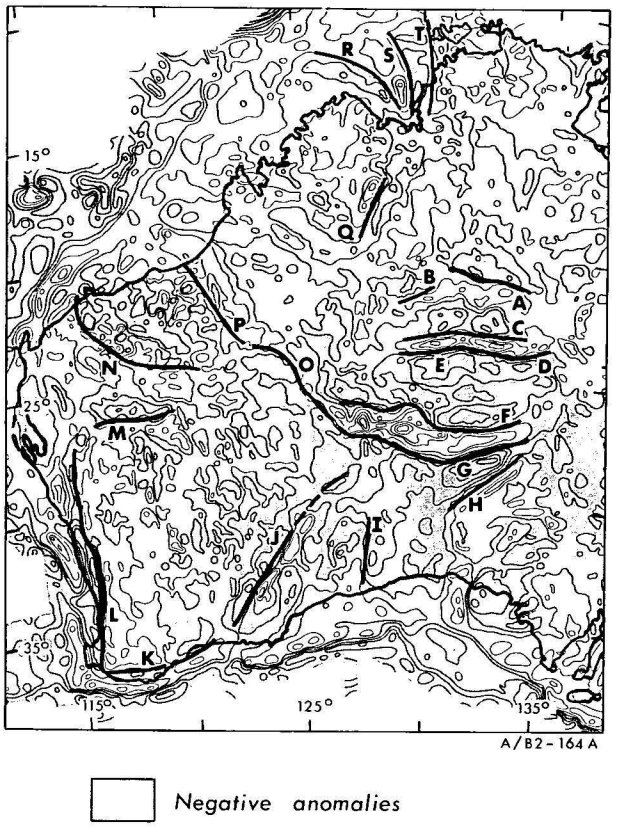

Figure 2. Location of the steep gradients of the major dipole gravity anomalies.
Base shows free-air map of central and Western Australia with contour interval of 20 mGal; areas of negative free-air anomaly are stippled (from BMR, 1976).

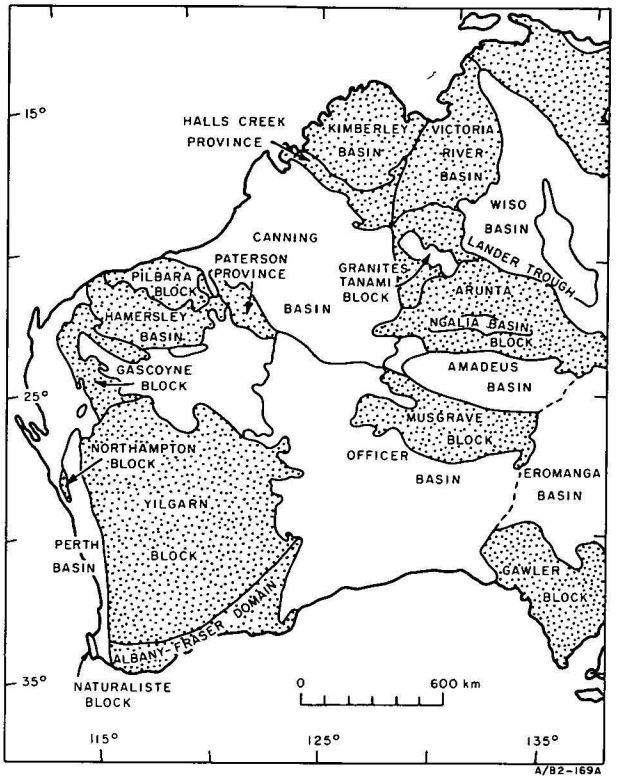

Figure 3. Major tectonic units in central and Western Australia.

Many of the anomalies are large and similar along strike; variation in the anomaly profile is well defined by drawing cross-sections across the anomaly at 50 km intervals. Along these sections anomalies were scaled off a 1:2 500 000 free-air map with 5 mGal contours. However, anomalies N and P (east and south of the Pilbara Block) are smaller than the others in average amplitude and more irregular in shape—partly because of terrain effects. For these anomalies Bouguer anomaly profiles were drawn where the anomaly was well developed, and the profiles were roughly corrected for height by adding the Bouguer plate correction for the mean height at the centre of the profile. Modelling was not attempted for anomalies B, I, and M, because the anomalies varied markedly along strike, nor for R, S, and T, because the role of sediment thickness variation is not adequately defined in this area.

Density within the crust and mantle is poorly determined, but it generally increases with depth owing to more mafic compositions and denser mineral phases. Fortunately gravity anomalies are caused only by horizontal density differences, so the crustal models in this paper are based on large volumes with constant density differences from the standard crust and mantle. These constant density differences are superimposed on the average vertical density gradient.

In modelling the isostatic compensation, the critical assumptions are the depth of compensation and the degree of regionality of the compensation; the compensating mass is fixed as equal in magnitude to the anomalous crustal mass, and changes in the density contrast between the crust and mantle have only a slight effect on the effective depth of compensation. For ease of modelling a fixed density contrast of 0.4 t m^{-3} between crustal roots and mantle has been assumed for Figures 5-11, even though density changes of 0.1 t m^{-3} are modelled in the crust overlying a uniform mantle.

Isolated dipole anomalies

Figure 4 shows cross-sections of dipole anomalies A,D,J,N,P, and Q. The anomalies have peak-to-trough amplitudes generally between 60 and 100 mGal, peak-to-trough distances of 50 to 60 km, and the tails of the anomalies generally extend further than 200 km from the steep gradients.

These anomalies are interpreted by considering the simple models of Figure 5. All the anomalies are interpreted as primarily due to a change in mean crustal density with regional isostatic compensation (Figure 5, model A). The change in mean crustal density is under the maximum anomaly gradient, the change in density being about 0.1 t m^{-3}. Crusts of both densities are isostatically compensated by changes in the thickness of the crust, the full change in crustal thickness being gradual over a distance of the order of 200 km centred over the density change. Well away from the abrupt density change the density contrast between the crustal blocks and the crustal thickness difference must both decrease, so that the two blocks have the same density and thickness, at a distance of the order of 500 km from the boundary. Differences between the observed anomalies and this model anomaly can be explained by minor variations in the model, as discussed below and illustrated in models B-D in Figure 5.

If the crust has anomalous density only in its upper half, then a density contrast of only 0.15 t m^{-3} (com-

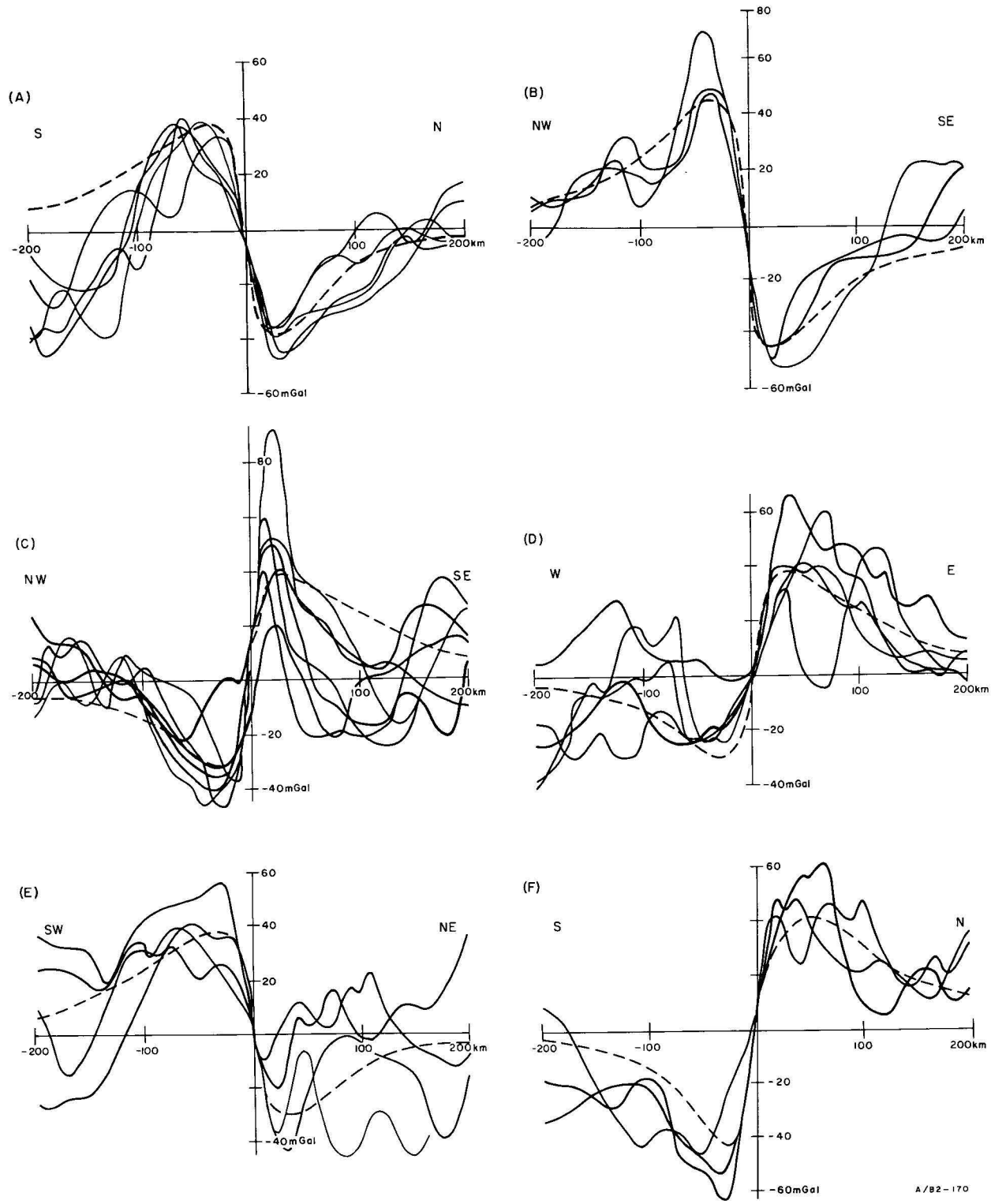

Figure 4. Free-air gravity across dipole anomalies.
Solid lines show stacked profiles at 50 km spacing, dashed lines show model anomaly for the model given in the text. A, anomaly A of Figure 2, from Arunta Block to Lander Trough; B, anomaly Q from Kimberley Basin to the Victoria River Basin; C, anomaly J from the Pilbara Block to the Albany-Fraser Domain at Fraser Range; D, anomaly P from the Paterson Province to the Pilbara Block; E, anomaly N from the Hamersley Basin to the Gascoyne Block; F, anomaly D from the Arunta Block to the Amadeus Basin.

pared with 0.1 t m^{-3} for the whole crust), would give essentially the same magnitude and shape anomaly. Hence the depth extent of the anomalous density material is poorly defined, and is assumed for convenience only to be the full thickness of the crust.

In the assumed model the density of the high density block decreases away from the block boundary, and is the same as the low density block 500 km away from the block boundary. This decrease in density away from the block boundary is supported by the general observation that wide crustal blocks do not differ radically from one to another in type of outcropping rock, and that the surface occurrence of high density rock is either scattered throughout the block, or for high den-

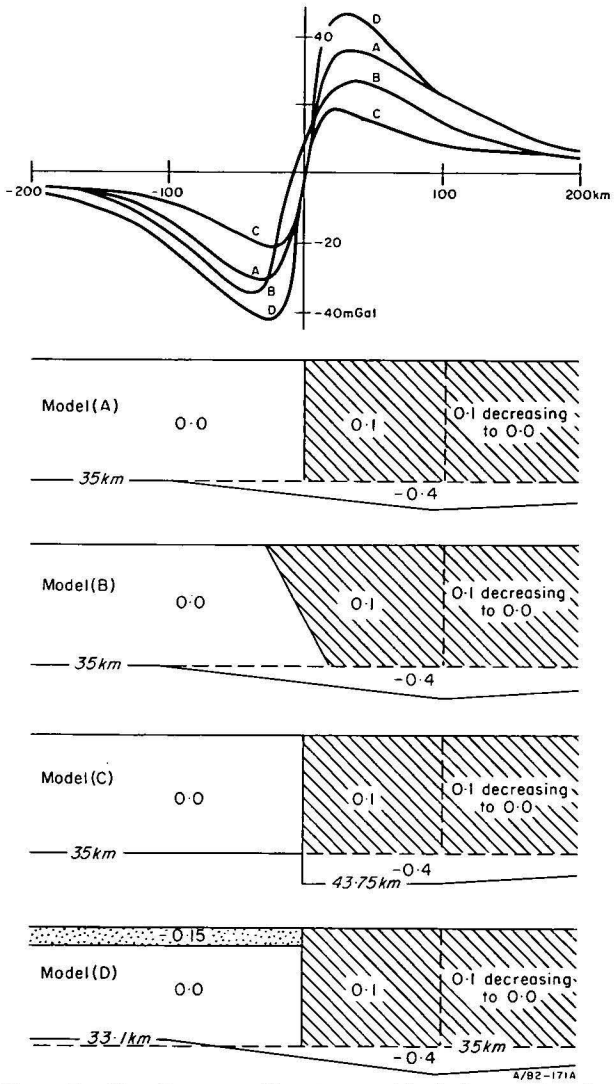

Figure 5. Gravity anomalies due to block boundaries in isostatic compensation.
Model A, vertical contact and regional compensation; model B, sloping contact and regional compensation; model C, vertical contact and local compensation; model D, vertical contact and regional compensation with 5 km of compensated sediments over the less dense block. In this and subsequent figures the densities are given as horizontal density contrasts, and a fixed density contrast of 0.4 t m^{-3} between crustal roots and mantle has been assumed.

sity blocks is concentrated close to the block boundary. The decrease in density away from the block boundary must be more gradual than the abrupt decrease at the block boundary, because if both density decreases were equally abrupt, then the gravity high would be flanked by lows of similar amplitude (Fig. 1, model B)—and this is not observed.

The contact between the crusts of different density is assumed to be vertical in model A of Figure 5; this gives positive and negative anomalies that are very similar in size and shape and with a contact between the two crustal blocks outcropping midway between the peak and trough. If the contact dips 45° towards the highest-density crust (model B), then the peak of the positive anomaly becomes wider, the trough of the negative anomaly narrower, and the contact between the two crustal blocks crops out near the trough. The observed anomalies are too irregular in shape to define the slope of the contact uniquely; however, the observed surface position of the crustal density change can be used to define the slope. The contact is inferred to be vertical for anomalies A,J,N,P, and Q, and dipping about 45° for anomaly D.

Variations in crustal thickness are assumed to be gradual (over a distance of 200 km) in Model A (regional isostatic equilibrium); this gives well-peaked anomalies standing above low tails, with a peak-to-trough distance of about 60 km. If local isostatic equilibrium is assumed (model C), the positive and negative peaks are closer together (40 km apart). If variations in crustal thickness are gradual for distances greater than 200 km, then the anomalies are less peaked, and merge gradually with the tails. These two latter extreme cases are not found.

The effect of sediments and their compensation is to increase the amplitude of both the positive and negative peaks of the dipole anomaly. Compensated sediment 5 km thick, and of density contrast −0.15 t m^{-3} relative to the upper crust, increases the peak-to-trough dipole anomaly by about 22 mGal (Fig. 5, model D).

Model anomalies derived from Figure 5, model A, but modified where necessary to take into account sediments or the dip on the crustal contact, are shown as dashed lines in Figure 4. Differences between the observed and model anomalies can be used to infer possible variation from these simple models.

The anomaly on Figure 4A extends from the northern part of the Arunta Block to the Lander Trough (anomaly A). The Lander Trough is modelled as a wedge of sediment 80 km wide and 2 km thick at the crustal block contact (Kennewell and others, 1977). The model anomaly is close to the observed anomaly, except in the south where anomalies from the multiple dipole C-E interfere.

Figures 4B and C show the anomalies extending across the Halls Creek Mobile Belt from the Kimberley Basin to the Victoria River Basin (anomaly Q), and the anomaly extending from the Pilbara Block across the Fraser Range (anomaly J). The Victoria River Basin is modelled by a 5 km slab of sediments. Both sets of observed and model anomalies agree well, except between the positive peak and positive tail. In both areas it is likely that most of the high density material is in the upper crust close to the block boundary, with only minor amounts under the positive anomaly tail.

Figures 4D,E show the anomalies between the Pilbara Block and the Paterson Province (anomaly P) and the anomaly across the southern margin of the Hamersley Basin (anomaly N). There is considerable variation along these anomalies and the profiles shown represent the dipole anomaly as most fully developed. The observed and mode anomalies match only roughly, in particular the observed negative anomalies are generally narrower than in the model. The lack of a well developed negative trough again suggests that the anomalously high density material is mainly in the upper part of the crust.

Figure 4F shows the anomaly across the eastern part of the boundary between the Arunta Block and the Amadeus Basin (anomaly D). The model anomaly is for a crustal block boundary dipping 45° towards the high density crust, and for 5 km of sediment in the Amadeus Basin. The observed and model anomalies agree well in shape; anomalies would agree better in amplitude if the crustal density contrast was higher, or isostatic equilibrium was more regional.

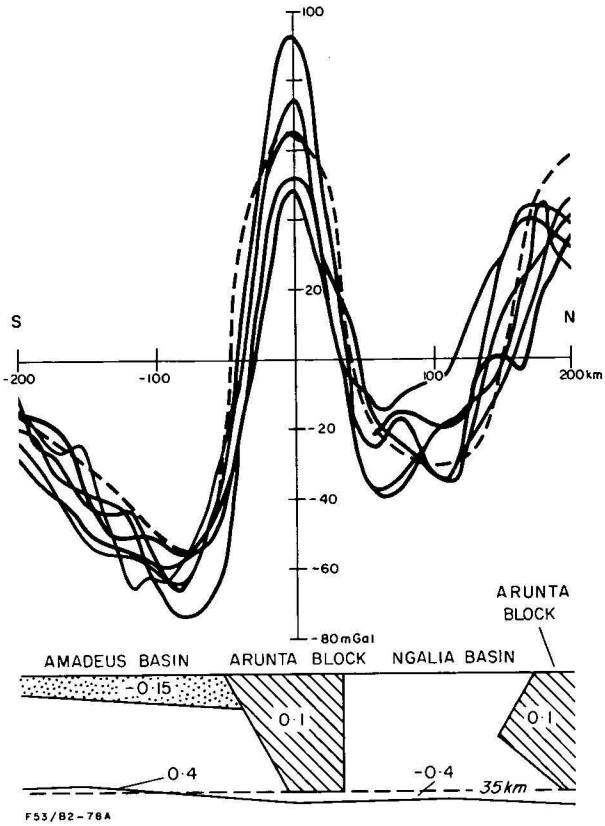

Figure 6. Profile across the southwest part of the Arunta Block. Stacked gravity anomalies and interpretation (anomalies C, E).

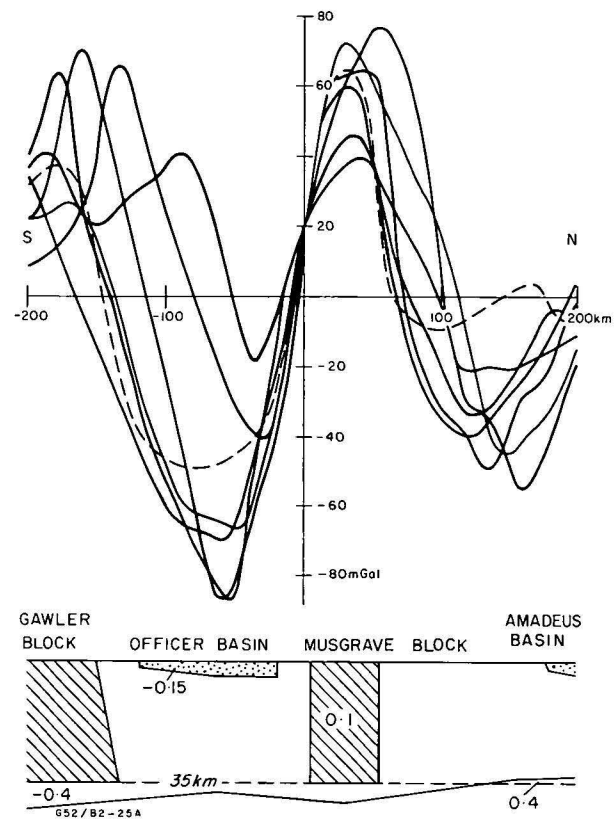

Figure 7. Profile across the eastern part of the Musgrave Block. Stacked gravity anomalies and interpretation (anomalies F, G, and H).

Multiple dipole anomalies

The multiple dipole anomalies of Figure 2 are individually interpreted below. Most anomalies can be attributed to narrow sections of the crust with a density 0.1 t m^{-3} higher than normal, and the effects of low-density sediments.

Central Australia

The isolated and multiple anomalies over the Arunta Block (anomalies A,B,C,D, & E) can be modelled by two bands of high-density crust. A northern dense band is about 100 km wide with abrupt edges towards the Lander Trough (Fig. 4A) and towards the basin south of the Granites-Tanami Block, and with a more gradual irregular southern side about 21.5° south. A southern dense band is about 90 km wide and 400 km long; it has Amadeus Basin sediments to the south (Figs. 4F, 6). The gradational contact is modelled by a wedge of high-density crust within normal crust, although in the real crust a gradational contact is likely to have a different form. The positive peak of the model anomaly is slightly too wide, so a narrower and denser crustal block would give a better fit to the observed anomalies.

The gravity anomalies F,G,H,, over the eastern end of the Musgrave Block and to the south are modelled (Fig. 7) by a belt of high-density crust about 50 km wide situated near the southern part of the Musgrave Block (south of 26.2°S), by Officer and Amadeus Basin sediments, and by high density crust along what may be the northwestern edge of the Gawler Block. The calculated and observed anomalies agree reasonably well, except that the calculated anomaly over the Gawler Block edge is too wide, and the anomaly over the northern Musgraves is too high.

To the west of this over the central Musgrave Block the gravity anomalies F and G form a complex, wide, high flanked by lows (Fig. 8). The high is interpreted as due to a wide area of crust with variable, but high, density forming the Musgrave Block south of 25.5° south, with Officer Basin sediments to the south. The most positive part of the anomaly is known to be underlain by ultramafic rocks; these are represented in the model by a body +0.2 t m^{-3} denser than normal crust. The model shows that a wide area of high anomaly can be modelled by dense, isostatically compensated crust.

For comparison, the two previous models for a central Australian crustal section near 133° east longitude and the one proposed here are shown on the same scale and vertical exaggeration in Figure 9. In the models similar sedimentary effects have been assumed. In model A, Anfiloff & Shaw (1973) have extrapolated surface densities downwards; gravity highs are due to high density upper crust and the gravity lows are to sediments and granites of low density, there being no relative density changes below 20 km. A crustal warping model (B) with a strong negative correlation between gravity anomalies and crustal thickness was given by Mathur (1976), and the section was extended by Kennewell, Mathur, & Wilkes (1977). In model C a crustal block interpretation is given, in which crustal thicknesses differ from those given in Figures 4A, 6, and 7—because they have been adjusted to include the effect of crustal loading by topography. Models A and C are similar, but in model A gravity lows are caused by low crustal density, and in model C they are caused by variation in crustal thickness. Model A and B are complex in that the number of degrees of freedom is large. Model C is relatively

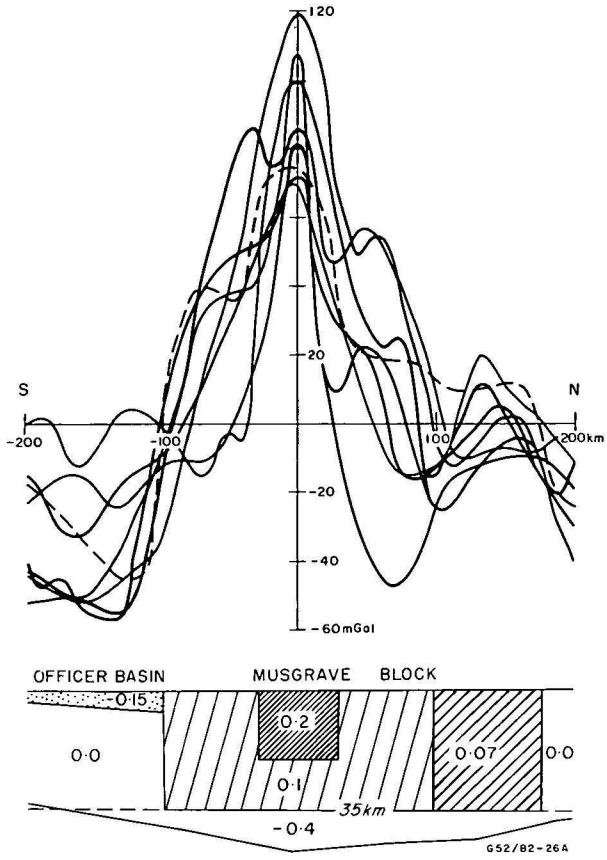

Figure 8. Profile across the central part of the Musgrave Block. Stacked gravity anomalies and interpretation (anomalies F and G).

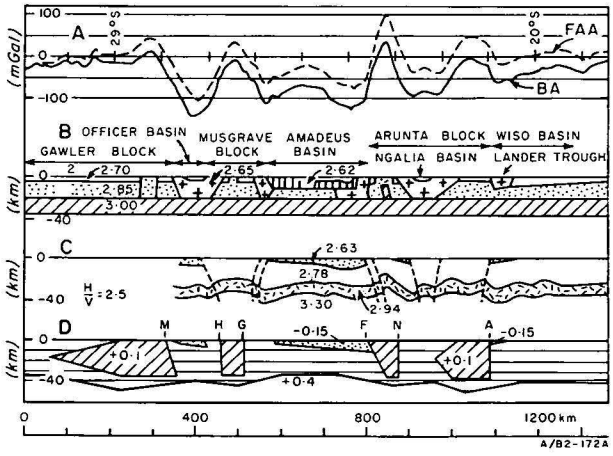

Figure 9. Comparison of crustal profile models for central Australia approximately along 133° east longitude.

At top are profiles of free-air anomalies, and Bouguer anomalies of density 2.2 t m^{-3}. Model A is from Anfiloff & Shaw (1973), model B from Mathur (1976) and Kennewell, Mathur & Wilkes (1977), and model D from Figures 3A, 5 and 6 of this paper modified to include the crustal root due to topographic loading. Densities are given in model A and B, and density differences from a standard column in model C.

simple, in that the main independent variables are the positions and slopes of the six block boundaries.

The relative gravity high along the southern part of the Amadeus Basin is interpreted in this paper as a residual remaining between gravity lows to the north and south that reflect crustal roots, the mean crustal density below the sediments being similar across the Amadeus Basin and the northern part of the Musgrave Block.

Southwest Australia

A series of elongate highs and lows follows along the southern margin of the Yilgarn Block; they are interpreted as due to the continental edge effect and a change in mean crustal density (anomaly K). The rocks of anomalous density are low density granites in the Albany area. The anomaly calculated for the model of Figure 10 agrees well with the observed anomaly—except close to the continental edge.

The gravity anomaly low over the Perth Basin is flanked by highs over the Yilgarn Block (anomaly L), and over the Naturaliste and Northampton Blocks. A model across the southern Perth Basin, using aeromagnetic depths to basement to control the sedimentary basin shape (Fig. 11), shows that the sediments and their compensation explain the main features of the observed anomaly without the need to postulate changes in the mean density of the rest of the crust, though a small density change is possible. In the northern Perth Basin the anomalies are complicated by the continental-edge effect. A narrow gravity high 30 km wide and 10 mGal in amplitude follows along the whole western edge of the Yilgarn Block. Because this anomaly is narrow it is likely to be due to dense crust along the upper part of the block edge.

The two cross-sections extending into the Yilgarn Block (Figs. 10, 11) show that the regional free-air anomaly high in the southwestern corner of the block is likely to be caused mainly by crustal thinning associated with the Perth Basin, granites near Albany, and the continental edge. Previously Everingham (1965),

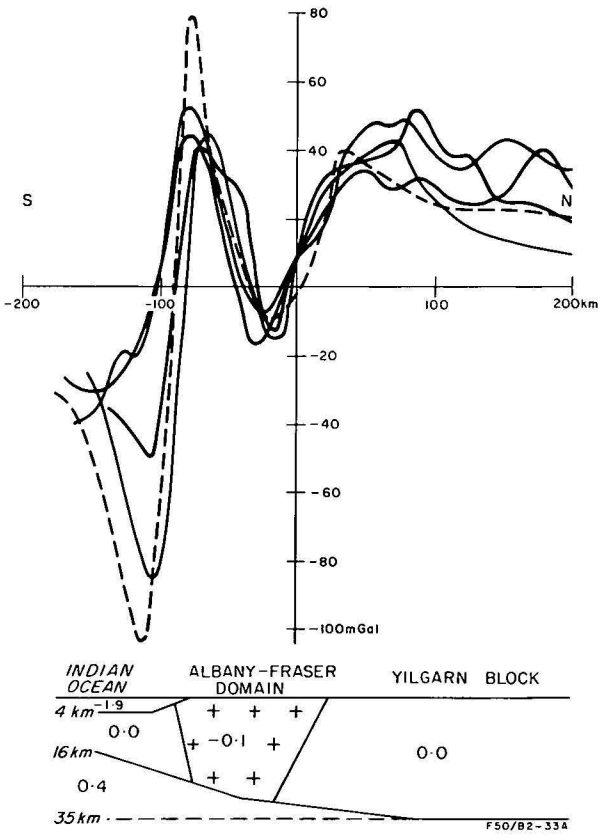

Figure 10. Profile from the Yilgarn Block to the Albany area. Stacked gravity anomalies and interpretation (anomaly K).

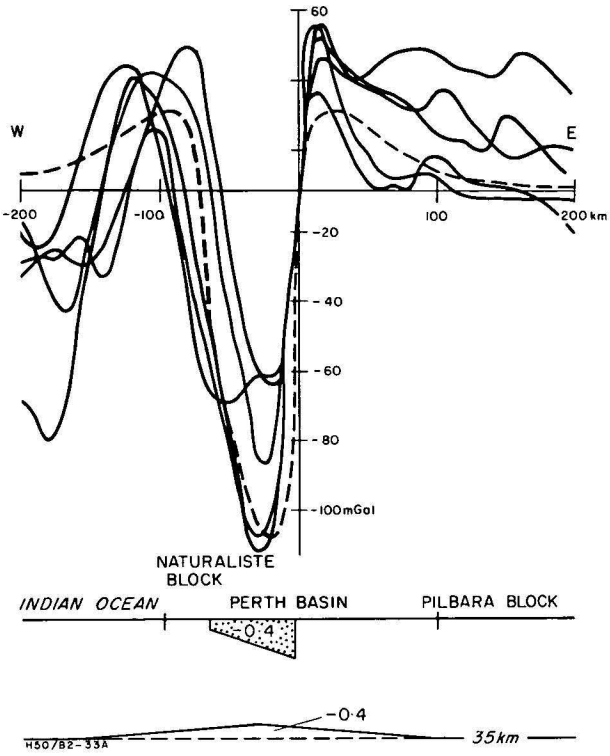

Figure 11. Profile from the Yilgarn Block, over the Perth Basin to the Naturaliste Block. Stacked gravity anomalies and interpretation (anomaly I).

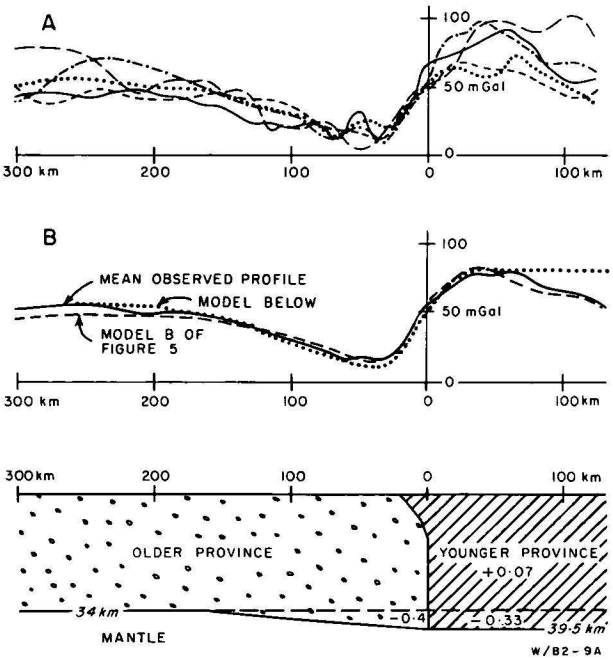

Figure 12. Gravity anomalies at Canadian Shield Precambrian province boundaries.
A, Bouguer gravity profiles across five province boundaries; B, Bouguer profiles—solid line is mean profile of A, dotted line is anomaly of model below, and dashed line is from model B of Figure 5; and C, crustal model of Gibb and Thomas (1976).

Mathur (1974), and Fraser (1974b) interpreted the gravity high as being caused by an area of higher mean crustal density and similar crustal thickness compared with the adjacent part of the Yilgarn Block to the northeast.

Occurrence of dipole anomalies over crustal block boundaries

Gibb & Thomas (1976) show that in Canada five out of seven Precambrian province boundaries are marked by elongate pairs of high and low anomalies. Where most fully developed the anomalies are about 66 mGal peak-to-peak (Fig. 12A), with the peak of the gravity low over the province contact, and the peak of the gravity high over the younger province. They infer from the mean anomalies that the younger province is about 0.07 t m^{-3} denser at the boundary than the older province, and that the boundary dips towards the younger province (Fig. 12C). The model explains the positive peak of 24 mGal by having the younger province crust 1.92 km too thin to be in isostatic equilibrium. The anomaly calculated for their model (Fig. 12B, dotted line) is a poor match for the positive tail of the observed anomaly; this portion was not shown in the published figure, and it has been calculated from their model and inserted. A better overall fit to the observed mean anomaly is obtained using a model for crust in regional isostatic equilibrium similar to that used for the Australian block boundaries (Fig. 12B, dashed line), or later interpretations by Thomas & Gibb (1977a, b).

In Australia most of the major dipole anomalies follow known or suspected block boundaries; anomalies B,J,K,L,M, and P of Figure 2 are above block boundaries of the Tectonic Map of Australia and New Guinea (GSA, 1971) (Fig. 3), and anomalies A,G,H, N,O, and Q are at or close to block boundaries inferred from the gravity trend pattern (Wellman, 1976b). Geological evidence is not sufficiently definitive to determine whether anomalies C, E, and F in the Musgrave and Arunta Blocks reflect crustal block boundaries, or

Figure 13. Inferred block boundaries from dipole gravity anomalies and gravity trend pattern.
The 'V' marks are on the older crust.

are within single blocks and reflect areas of higher metamorphic grade and higher proportion of mafic rocks.

Using the relative ages on the Tectonic Map the younger blocks have gravity highs over them at three boundaries (J,N,P), and gravity lows over them at two boundaries (K,M); and using relative ages from the gravity trend pattern the younger blocks have gravity highs over them at three boundaries (A,B,G). In Canada younger blocks have gravity highs over them at five boundaries. Hence in eleven out of thirteen cases gravity highs and relatively dense crust form the edge of the younger block.

Known and inferred block boundaries often mark the edge of preserved sediments, sediments being over the inferred older block at A,B,G, and K, over possible older blocks at C,E,H, and Q, and over the younger block at L. The sediment distribution is irregular at J,M,N, and P.

The dipole anomalies along block boundaries vary in magnitude (but only in sign in the case of anomaly J-K), so the density contrast across the block boundary varies along the boundary. For sections of some boundaries the density contrast is likely to be very small and result in undetectable anomalies.

The block boundaries inferred from large dipole anomalies are slightly displaced from those inferred from gravity trends (Wellman, 1976b). The boundaries coincide if trend area boundaries are drawn using only the anomalies due to anomalous crustal masses, that is ignoring anomalies due to isostatically compensating masses. A block boundary map inferred using a combination of gravity trends and large dipole anomalies is given in Figure 13. Further study of geology and the gravity and magnetic fields should result in more refined and more complete boundaries for the crustal blocks.

Crustal block boundaries are not just the junction of two blocks with different history. The important contributions from the gravity work are in confirming that one block is younger and it has structural trends parallel to the block boundary, and showing that if pre-Phanerozoic in age this younger block usually has abnormally dense crust along the block boundary zone. The structural trend pattern could be explained if the younger block consisted of sediments over an old block basement, with the sediments and basement in the younger block deformed in the direction parallel to the edge of the block. However, the presence of a band of abnormally dense crust suggests that the difference between pre-Phanerozoic old and young blocks is more fundamental, and involves major crustal or lithospheric processes to raise dense material to high levels in the crust.

The major dipole anomalies generally follow the boundaries of crustal blocks that are known from geology or inferred from the gravity trend pattern. However, it is possible that some Musgrave and Arunta anomalies reflect density variation within a crustal block. Block boundaries generally have anomalously high density crust along the edge of the younger block, and at many boundaries sediment overlies the older block only. These common features are likely to be due directly or indirectly to the process of creation or emplacement of the younger block. The presence of relatively dense material high in the crust suggests that the formation of younger blocks involves major crustal or lithospheric processes, and that the younger blocks are not superficial features on a uniform old crust.

Conclusions

In central and Western Australia the low correlation of free-air anomaly and surface altitude suggests that the topographic masses have some degree of regional isostatic compensation, and the association of major free-air anomalies with similar anomalies of opposite sign suggests that masses of anomalous density in the crust likewise have regional isostatic compensation. The observed anomalies are consistent with isostatic compensation by variations in the depth to the base of the crust, this variation being gradual and extending about 100 km from the anomalous body. This mode of isostatic compensation implies a weak positive correlation between gravity anomaly variations and crustal thickness variations, and implies fairly low long-term crustal and lithospheric strengths.

This isostatic compensation is possible only if the regional free-air anomaly field (5° x 5° area means or greater) does not reflect deviations from isostatic equilibrium. Following Cochran & Talwani (1977) the long wavelength anomalies are interpreted as being caused by fluid motion in the mantle, the motion being largely decoupled from the lithosphere.

Each major dipole anomaly is interpreted as primarily due to a strip of crust with anomalous mean density and associated isostatic compensation of this strip, and secondarily to sediments and their compensation. Each strip has an abrupt edge where the anomaly gradients are steep, and a gradual edge where the anomaly gradients are gentle. The body of anomalous density has an upper surface near ground level, and the depth to the lower surface is the base of the crust or shallower. If the body occupies the whole crust the density contrast to normal crust is about 0.1 t m^{-3}, if it is only the top half of the crust the density contrast is abou 0.15 t m^{-3}.

Acknowledgements

I thank Dr D. A. Falvey for his constructive criticism of the manuscript. The figures were drawn by Mrs A. Jaensch.

References

ANFILOFF, W., & SHAW, R. D., 1973—The gravity effects of three large uplifted granulite blocks in separate Australian shield areas. *Proceedings Symposium on Earth's Gravitational Field & Secular Variation in Position. Sydney*, 273-289.

BMR, 1976a—Gravity map of Australia, 1:5 000 000. *Australian Bureau of Mineral Resources, Canberra.*

BMR, 1976b — Free-air anomaly map of Australia, 1:25 000 000. *BMR Journal of Australian Geology and Geophysics*, 1(4), insert.

COCHRAN, J. R., & TALWANI, M., 1977—Free air gravity anomalies in the world's oceans and their relationship to residual elevation. *Geophysical Journal of the Royal Astronomical Society*, **50**, 495-552.

DOOLEY, J. C., 1973—The gravity anomalies of central Australia and their significance for long term tectonic movements. *Proceedings Symposium on Earth's Gravitational Field & Secular Variation in Position. Sydney*, 248-60.

EVERINGHAM, I. B., 1965—The crustal structure of the southwest of Western Australia. *Bureau of Mineral Resources, Australia, Record* **1965/97** (unpublished).

FRASER, A. R., 1974a—Reconnaissance helicopter gravity survey of the northwest of western Australia, 1969. *Bureau of Mineral Resources, Australia, Record* **1974/27** (unpublished).

FRASER, A. R., 1974b—Reconnaissance helicopter gravity survey of the southwest of Western Australia, 1969. *Bureau of Mineral Resources, Australia, Record* **1974/26** (unpublished).

GSA, 1971—Tectonic Map of Australia and New Guinea 1:5 000 000. *Geological Society of Australia, Sydney.*

GIBB, R. A., & THOMAS, M. D., 1976—Gravity signature of fossil plate boundaries in the Canadian Shield. *Nature,* **262**, 199-200.

KENNEWELL, P. J., MATHUR, S. P., & WILKES, P. G., 1977—The Lander Trough, southern Wiso Basin, Northern Territory. *BMR Journal of Australian Geology and Geophysics,* **2**, 131-6.

MCNUTT, M. K., & PARKER, R. L., 1978—Isostasy in Australia and evolution of the compensation mechanism. *Science,* **199**, 773-5.

MATHUR, S. P., 1974—Crustal structure in southwestern Australia from seismic and gravity data. *Tectonophysics,* **24**, 151-82.

MATHUR, S. P., 1976—Relation of Bouguer anomalies to crustal structure in southwestern and central Australia. *BMR Journal of Australian Geology and Geophysics,* **1**, 277-86.

THOMAS, M. P., & GIBB, R. A., 1977a—Gravity anomalies and deep structure of the Cape Smith fold belt, northern Ungava, Quebec. *Geology,* **5**, 169-72.

THOMAS, M. P., & GIBB, R. A., 1977b—Reply to Comment by A. J. Baer on 'Gravity anomalies and deep structure of the Cape Smith fold belt, northern Ungava, Quebec. *Geology,* **5**, 651-3.

WELLMAN, P., 1976a—Regional variation in gravity, and isostatic equilibrium of the Australian crust. *BMR Journal of Australian Geology and Geophysics,* **1**, 297-302.

WELLMAN, P., 1976b—Gravity trends and the growth of Australia: a tentative correlation. *Journal of the Geological Society of Australia,* **23**, 11-14.

Stratigraphic significance of a discovery of Lower Proterozoic tuff in the Pine Creek Geosyncline

I. H. Crick, P. G. Stuart-Smith, and R. S. Needham

Introduction

Recent investigations in the Pine Creek Geosyncline in the northern part of the Northern Territory have revealed the presence of tuff within the Lower Proterozoic metasediments (Needham and others, 1978). The tuff is confined to one horizon, and crops out in the central and eastern parts of the Geosyncline, enabling stratigraphic correlations to be made between formations previously believed to have been deposited in two separate basins. Previous workers believed different kinds of sediment were laid down in each basin, and that only limited correlation was possible between the basins (Walpole and others, 1968).

The regional stratigraphic concept of earlier workers was dominated by lateral and lesser vertical facies interfingering of units (formations), which were placed into groups, each of which contained a number of 'laterally disposed, lithogenetically related' formations (Walpole and others, 1968). Tuff, by its depositional nature, is a time-stratigraphic indicator, so its regional conformity with metasedimentary units in the Geosyncline suggests that they are also time-stratigraphic in character, and not facies equivalents or time-transgressive as proposed previously.

The tuff unit crops out in the Burnside area 120 km south-southeast of Darwin (Batchelor 1:100 000 Sheet area) within the Golden Dyke Formation of Walpole

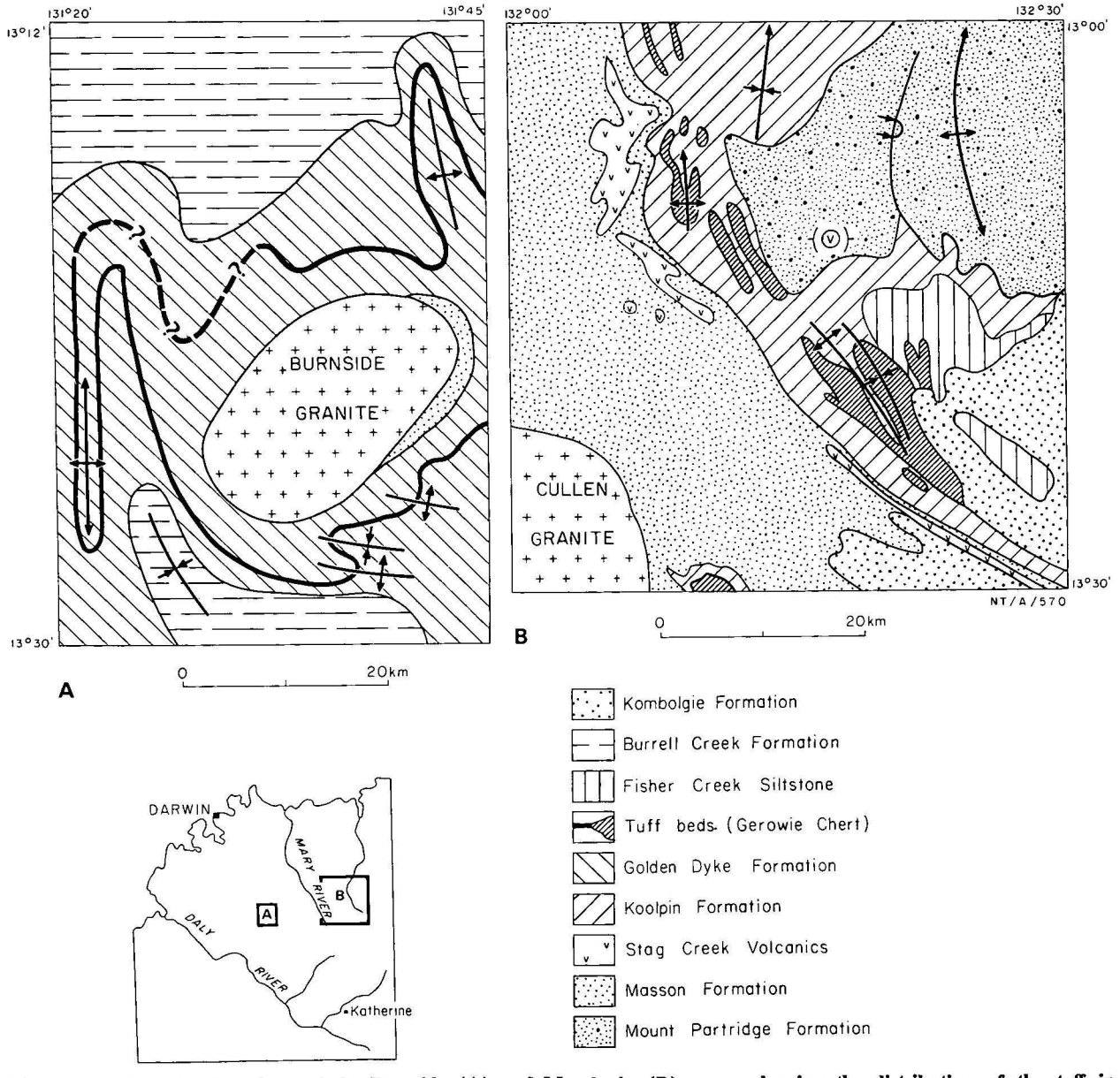

Figure 1. Generalised geology of the Burnside (A) and Mundogie (B) areas, showing the distribution of the tuff in the Golden Dyke Formation and the Gerowie Chert.

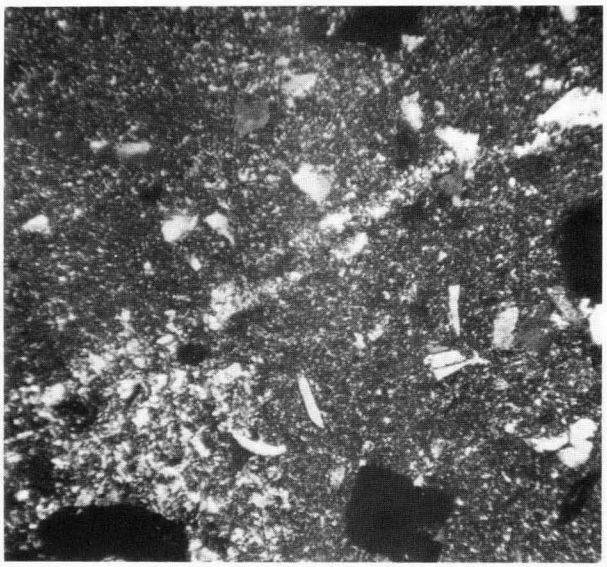

Figure 2. Coarse-grained tuff, Gerowie Chert. Note curved and angular fragments, X30.

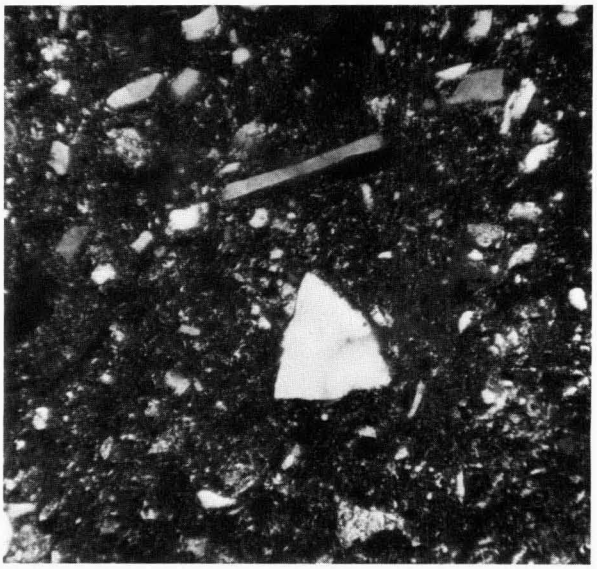

Figure 3. Lithic tuff, Gerowie Chert, X30.

and others (1968), and in the South Alligator Valley area 250 km east-southeast of Darwin (Mundogie 1:100 000 Sheet area) within the Gerowie Chert of Walpole and others (1968) (Fig. 1). We suspect, from the results of regional sampling forays, that the tuff unit extends into other areas between and to the west of these.

The Golden Dyke Formation was described by Walpole and others (1968) as mainly dolomitic and carbonaceous siltstone, quartz siltstone, dolomite, and chert (thought to be diagenetically altered dolomite). The Gerowie Chert was described as mainly siliceous siltstone, impure chert (in places rich in albite), and chert, all of which were regarded as possibly diagenetically altered dolomitic sediments. The 'chert' of the Golden Dyke Formation, and the 'siliceous siltstone, impure chert and chert' of the Gerowie Chert are all in fact volcanogenic sediments, dominantly tuff.

Description of the tuff unit

Tuff of the Golden Dyke Formation in the Burnside area (Fig. 1A) forms a dark grey, commonly massive and cherty bed about 200 m thick, mostly evident only as blocky rubble on level or slightly rising ground. It was mapped in places as a hornfels by Sullivan & Iten (1952). In a specimen collected 2 km north of the Burnside Granite, curved elongate or angular crystal fragments (<0.3 mm) of quartz and potassium feldspar which constitute about 10 percent of the rock, are preserved in a cryptocrystalline matrix containing scattered flakes of biotite and knots of muscovite, and reveal the volcanic origin of the rock. Elsewhere the tuff is very fine-grained with minor flakes of mica; perhaps metamorphism (probably both contact and regional) has largely obliterated the original texture.

The Gerowie Chert (Fig. 1B) crops out as long, low rubble-strewn ridges in the lowlands, rising to 180 m above the plains adjacent to the Arnhem Land Escarpment. Characteristically it has about two to three times background radioactivity for the region (radioactivity of outcrops in the Burnside area has not been tested). The unit is up to 750 m thick, and is composed mainly of tuff of which three types are present: a fine-grained, thin-bedded, blocky, black, chert-like variety with fragments <0.25 mm, and commonly having a white weathered shell; a coarser-grained more feldspathic tuff with fragments <0.5 mm, which has a dull green, white-spotted appearance; and a coarse-grained, greyish green lithic tuff with fragments <1 mm (Figs. 2 & 3).

The black cherty tuff is composed of angular, curved, and elongate fragments of quartz and potassium feldspar set in a very fine-grained granoblastic matrix of quartz and potassium feldspar. The spotted tuff is similar, but also contains fragments of sodic plagioclase; preferential weathering of the feldspar fragments gives the rock a spotted appearance. The lithic tuff

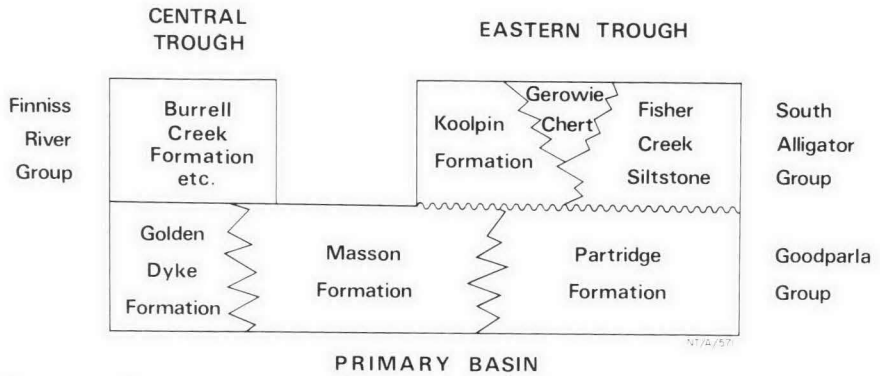

Figure 4. Diagrammatic relationships of the Finniss River, South Alligator and Goodparla Groups, after Walpole and others (1968).

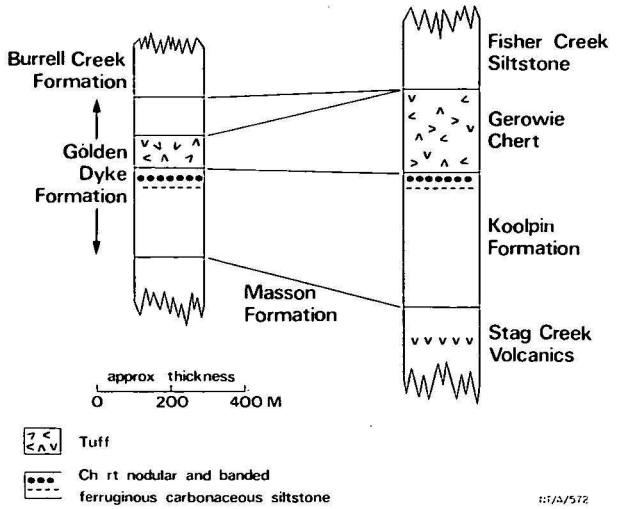

Figure 5. Stratigraphic correlation between the Golden Dyke Formation, and the Koolpin Formation and Gerowie Chert.

consists of curved, elongate, and angular fragments of quartz, potassium feldspar, minor sodic plagioclase, biotite, quartzite, chert, and traces of garnet in a fine-grained matrix of quartz and saussuritised and sericitised feldspar.

Discussion

The Pine Creek Geosyncline was thought by Walpole and others (1968) to have initially been a shallow basin ('Primary Basin') in which sediments of the Goodparla Group (the Golden Dyke Formation, Masson Formation and Mount Partridge Formation) were deposited. The formations were thought to interfinger and represent facies changes from a trough environment in the west (Golden Dyke Formation) through a transitional environment (Masson Formation) to a marginal environment in the east (Mount Partridge Formation) (Fig. 4).

During or soon after the last stages of deposition of the Goodparla Group, the Primary Basin was considered to have become divided into two basins by the upfaulting of Archaean basement (Stag Creek Volcanics) which formed a barrier trending parallel to the South Alligator Valley. The South Alligator Group sediments (the Koolpin Formation, Gerowie Chert, and Fisher Creek Siltstone) were then deposited to the east of this barrier in the 'Eastern Trough' and to the west, the Finniss River Group (the Burrell Creek Formation and others) was deposited in the 'Central Trough' (Fig. 4).

The Gerowie Chert was considered to be a dolomitic facies variant of the Koolpin Formation and the Fisher Creek Siltstone, lying laterally between and interfingering with them. However, this facies relationship model is invalid now that the volcanic origin of the Gerowie Chert is understood.

The Stag Creek Volcanics, interpreted by Walpole and others (1968) as forming an Archaean ridge between the Central and Eastern Troughs, are now known to be Lower Proterozoic, being interbedded with Masson Formation metasediments (Foy & Miezitis, 1977), and so no evidence remains at all for basement ridges separating depositional areas in South Alligator Group/Finniss River Group times. Like Walpole and others (1968), Foy & Miezitis noted the lithological similarities of the Golden Dyke and Koolpin Formations, but recognising that the areas of deposition of the two formations were probably continuous, were able to suggest a correlation between them (between the upper part of the Golden Dyke Formation, which contains the tuff unit, and the Koolpin Formation). However, they still retained Walpole and others' concept of facies equivalence of the Koolpin Formation, Gerowie Chert, and Fisher Creek Siltstone.

The recognition and correlation of tuff units in the Golden Dyke Formation and Koolpin Formation is the first tangible evidence of the stratigraphic equivalence of the two units. Furthermore, the tuff is underlain by chert-banded and nodular ferruginous siltstone and ironstone overlying pyritic carbonaceous shale, siltstone, and carbonate rocks in both the Burnside and South Alligator Valley areas (Fig. 5); this demonstrates that, like the tuff unit, the iron-rich sediments and the carbonaceous pelitic rocks and carbonate rocks beneath it, are time-stratigraphic units. We predict that with further work, a layer-cake stratigraphy, continuous throughout at least the central and western parts of the Geosyncline, will emerge, and that development of marginal facies variants around the Archaean terrains in the west and northeast of the Geosyncline may be the only major exceptions to this model.

Conclusions

1. Most of the chert in the Pine Creek Geosyncline is tuff, not diagenetically altered dolomite.

2. The tuff forms a time-stratigraphic unit, and therefore previous interpretations based on extensive interfingering of units need revision.

3. The Gerowie Chert and underlying sediments of the Koolpin Formation are equivalent to the tuff and underlying sediments of the Golden Dyke Formation, and probably continuous with them.

4. There were no 'Eastern and Central Troughs'; all sedimentation in the Geosyncline probably took place in the same basin.

Acknowledgements

We gratefully acknowledge the helpful criticism of W. B. Dallwitz and G. M. Derrick. The figures were drawn by G. Butterworth and R. Stephens.

References

Foy, M. F., & Miezitis, Y., 1977—Uranium mineralisation at Anomaly 2J, South Alligator Valley, Northern Territory, and its significance concerning regional structure and stratigraphy. *Proceedings of the Australian Institute of Mining and Metallurgy*, **261**, 1-11.

Needham, R. S., Crick, I. H., & Stuart-Smith, P. G., 1978—Pine Creek Geosyncline *in* Geology Branch Summary of Activities. *Bureau of Mineral Resources, Australia, Report* **208**.

Sullivan, C. J., & Iten, K. W. B., 1952—The geology and mineral resources of the Brocks Creek District, Northern Territory. *Bureau of Mineral Resources, Australia, Bulletin* **12**.

Walpole, B. P., Crohn, P. W., Dunn, P. R. & Randall, M. A., 1968—Geology of the Katherine-Darwin region, Northern Territory. *Bureau of Mineral Resources, Australia, Bulletin* **82**.

A system for the simulation of sedimentary environments

Bohdan Bubela[1], Ian A. Johns[1], and James Ferguson

A system is described capable of simulating simultaneously a number of controlling parameters occurring in sedimentary environments. The system is composed of an experimental tank, reservoir tank, hydraulic, heating and illuminating attachments, and an electronic control programmed to regulate cyclic and non-cyclic operations of duration between 1 second and 10^5 seconds. The electronic component is capable of controlling several simulating systems simultaneously, their number being dependent on their complexity.

Introduction

A proper evaluation of geobiological processes occurring in nature is frequently hindered by the complexity and interaction of the various factors involved.

Therefore a number of systems simulating environments of geobiological interest has been constructed in our laboratory (Bubela and others, 1969; Lambert and others, 1970; Bubela and others, 1973; Hallberg and others, in prep.). These systems provide an experimental tool bridging the complexity of the natural environments and the oversimplicity of studying individual parameters experimentally. Furthermore, such systems permit a controlled variation of parameters associated with the environment under study.

The experimental evidence obtained with such systems proved to be useful in the evaluation of a number of biological and abiological processes occurring in environments of geobiological interest (Davies and others, 1973; Ferguson and others, 1974; Davies and others, 1975; Bubela and others, 1975; Davies and others, 1977; Hallberg and others, in prep.; Mooney and others, 1978).

To facilitate the investigation of marine evaporative environments it was necessary to devise a simulating system capable of accommodating associated features occurring in nature. The major requirements were controlled cyclic horizontal and vertical movement of waters of variable composition through the sediments at variety of time cycles, temperature and illumination cycyles, and adjustable water level.

Therefore it became desirable to devise a simple inexpensive electronic control capable of being programmed to operate systems simulating a variety of environments, with the influencing paramenters occurring cyclically or non-cyclically with a variable mutual dependency.

This paper describes such a system (Fig. 6).

Apparatus

Hydraulics

The central (non-electronic) structure of the system is a tank (1) made of high-density polypropylene (1 m x 1 m x 1 m). The bottom of the tank is perforated by 100 holes 5 mm in diameter (2). Four horizontal rows of the same diameter are located around the tank spaced vertically at 10 cm intervals. These may be closed or open as required (3). The bottom of the tank is covered with fibreglass cloth (4). A vertical row of sampling ports (5) is located at the side of the tank. The sampling ports are fitted with polypropylene taps and flanges (Bubela & Ferguson, 1973). The tank is placed in a bath (6) made of fibreglass (1.2 m x 1.2 m x 1.5 m) and rested on supports (7) 10 cm from the bottom of the bath. The bath is connected through waterlines (8) to a reservoir (9) via a magnetic valve (10) and a pump (11). An alternative pathway for the water is provided by a waterline 12) via a magnetic valve (13). The valves and the pumps are regulated by a controller (14). Heating and illuminating cycles are provided by a lamp (15) regulated by a controller (14) and a thermo-detector (17), and monitored by a recorder (16) via thermoprobes (15). The flow through the waterlines is regulated by taps (18 and 19). The water level in the tank and the bath is regulated by adjustable level detectors (20) and a controller (14). For safety reasons all powerlines are connected through core balance earth leakage protection units to supply points.

Electronics

The main electronic control applied to this simulating system, the Synchronous Electronic Master Clock (SEMC), is divided into two sections, A and B. Section A starts and stops events at pre-selected times, whereas Section B advances only when Section A recycles, thus providing facilities for experiments of long duration.

Section A has a considerable degree of flexibility because of the range of cycle durations and time units available. Time intervals of 1 second to 3.5×10^5 seconds can be programmed. The start and stop functions are generated by digital comparison of clock and memory data. Each of the five channels in Section A has 16 input lines from the real-time clock coded as 4 binary coded decimal (BCD) digits. Start and stop times can be determined by a 4-digit resolution. Real time is continuously displayed on a 4-digit read-out. Section B is electronically similar to Section A, but has 3 channels—each with 12 input lines, coded and displayed as 3 BCD digits.

All channels contained in the SEMC are mutually independent, allowing time overlap and non-sequential operation. Light-emitting diodes provide continuous-state monitoring of all channels.

Block diagrams of the SEMC and the control interface are presented in Figure 2. The logic diagrams relevant to the simulated system described in this paper are presented in Figures 3 and 4.

If Section A is programmed to perform function F_1 during a cycle time T_A, then Section B may be programmed to perform functions F_A and n_BF, where n_B is the selected B recycle time between limits T_A and

1. Baas Becking Geobiological Laboratory, CSIRO, P.O. Box 378, Canberra, ACT, Australia.

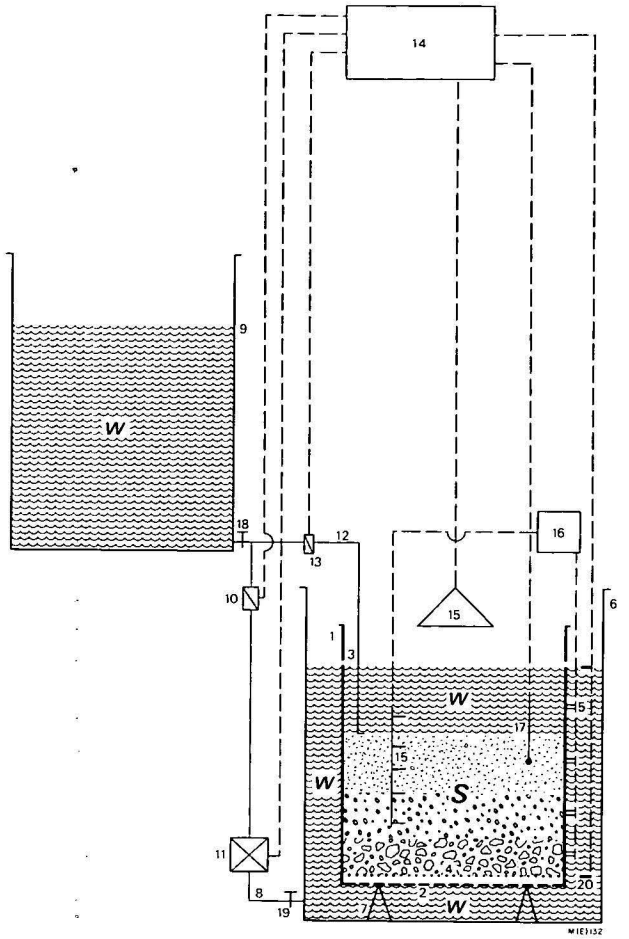

Figure 1. Schematic diagram of the simulating system. Not to scale. Description of the system is presented in the text.

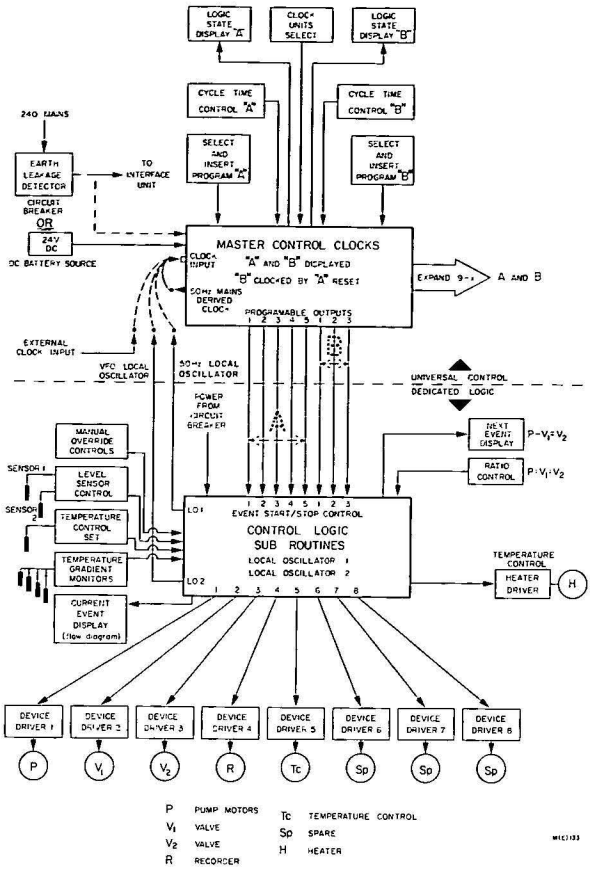

Figure 2. Block diagrams of the Synchronous Electronic Master Clock (SEMC) and the Control Interface (CI).

10^3T_A. Application of the 'cycling' capacity of the electronic component is illustrated by the following example:

Normal tides occur in 8-hour cycles, spring tides twice every lunar month. Therefore Section A will control function F_1 (normal tides), and Section B will control function F_2 (spring tide) with $n_B = 24/8 \times 14 = 42$.

An electric bell alarm is incorporated into the system to indicate that a power supply has been disconnected. Detailed information on individual circuits may be obtained on request from the authors.

Operation

Sediments

The tank is filled with sedimentary material depending on the nature of the area being simulated. It may consist of one or more layers of carbonates, sands, clays, and organic materials. They are introduced into the tank in the form of a slurry to prevent airpockets and chanelling. The composition of the aqueous phase differs with each experiment, and may be altered during the experiments. The monitoring probes are inserted into the sediments through the sampling ports, or inserted through the sediment surface. They may be left in the sediment permanently, or removed after individual measurements.

Hydraulics

The inflow of water into the tank may follow two different pathways (Fig. 1):

(a) The water is introduced to the bottom of the bath from waterline (8), and enters the sediment through the tank's perforated bottom. The water level is regulated by the level detectors. If the water is introduced into the bath at a rate faster than it can penetrate the sediment, and is brought to a position above the peripheral holes (3), it will flood the surface of the sediment—possibly without being depleted of some of its components by passing through the sediment. After the desired idential time the water is removed by reversal of the above process. The water movement is activated by pump (11).

(b) If downward penetration of the water through the sediment is required, it is introduced through waterline (12). It is then removed as in (a).

The illumination and heating sequences are produced by a lamp (15). The quality of the radiation is determined by the design of the lamp.

Electronics

The master control (Fig. 5) is set by the following procedure:

Previous memory of the system is erased with the A and B clearance button. Desired recycle time is inserted by A and B reset buttons, and corresponding time units are introduced by the toggle switch above the display window. Indication of real time on the display

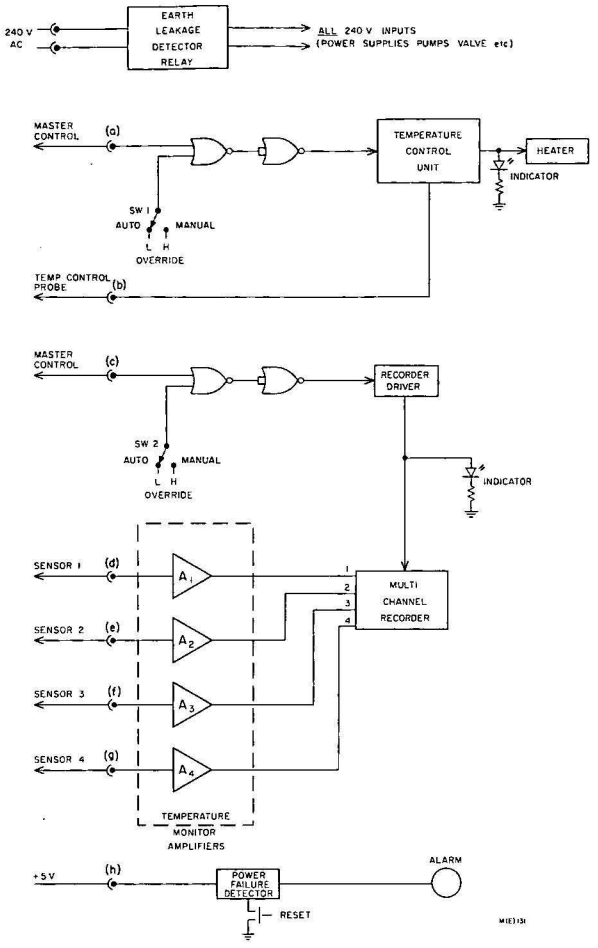

Figure 3. Block diagram showing the Control Logic for Earth Leakage Temperature Control, Recorder Driver, Multichannel Recorder, and Power Failure Detector.

window is obtained by operating the rapid-advance drive at the back of the unit.

Individual cycle programmes are inserted into the selected channel by placing the address switch into 'S' position, by selecting the desired start-time by the thumbwheel switch, and pressing the insert button. The stop-time is obtained similarly but with the address switch in 'F' position. The procedure is repeated for each individual channel. Both sections, A and B, are operated in a similar way.

The interface and logic section is operated as follows:

The desired temperature is selected by the 10-turn potentiometer. The water-flow pathway pattern is obtained by placing the main valve switch and the pump switch into 'Auto' position and by selecting the pathway cycles by the V_1/V_2 ratio switch.

If simulation of the evaporative stage of the environment is required, the hydraulic system is programmed to remove the water wholly or partly from the sediment surface, and the heating lamp is activated for a required time or until a present temperature of the sediment or overlying water is obtained. The temperature limits, duration, and repetition of the evaporative cycle is regulated by the controller (14). Sampling of the sediments and/or the overlying water is done through the sampling ports using a microsampler and/or coring rig equipped with self-closing bit. The sampling methods, probes, specifications and detailed methodology have been described previously (Bubela & Ferguson, 1973; Bubela and others, 1975).

Conclusions

The system described in this paper is capable of simulating a variety of environments. Its electronic components can independently control a number of systems, each of them performing a variety of func-

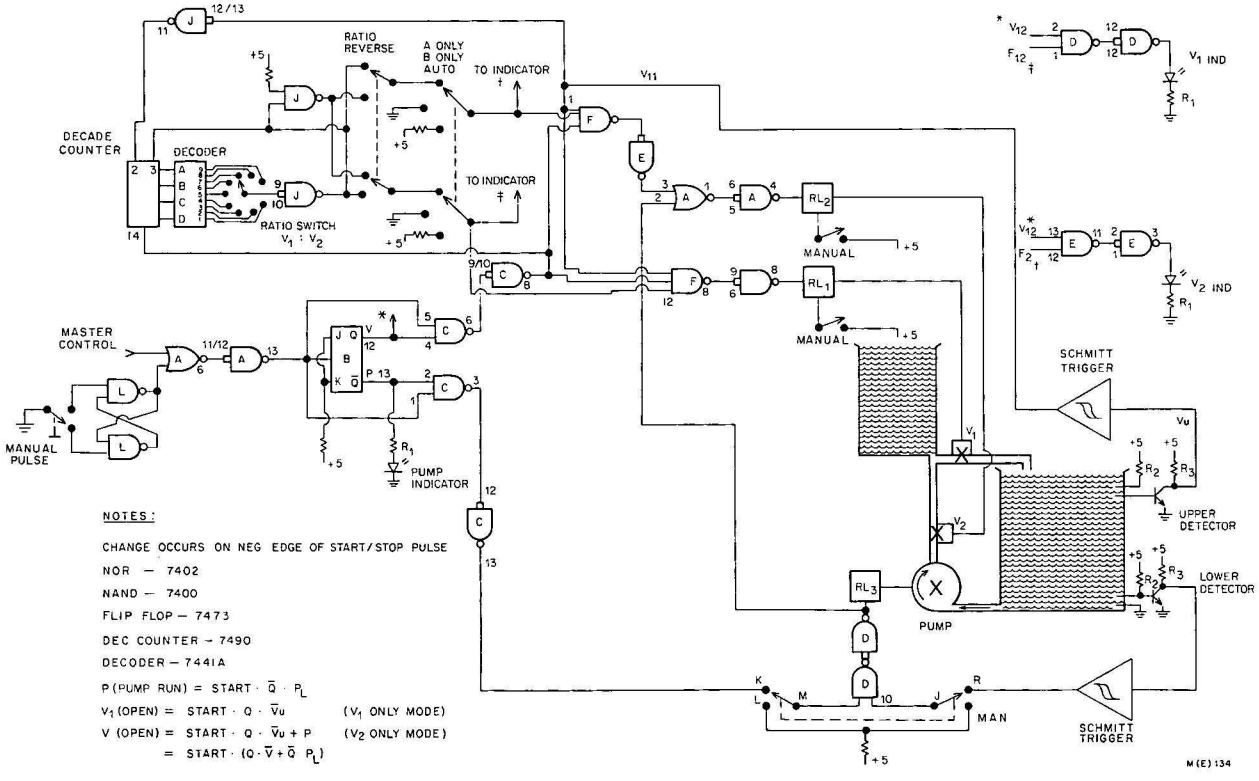

Figure 4. Block diagram showing the Control Logic for the Hydraulic System.

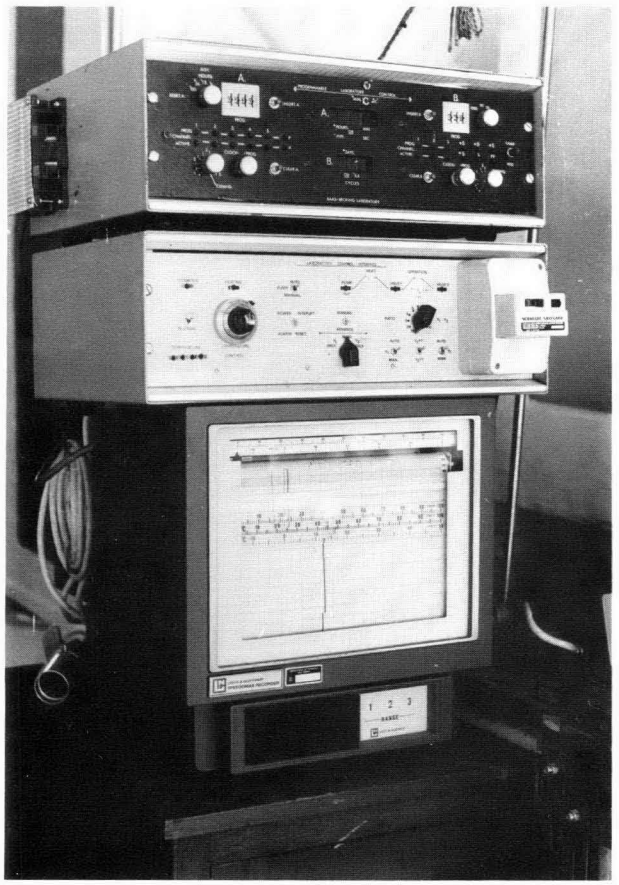

Figure 5. The synchronous electronic master clock and the interface-logic unit.

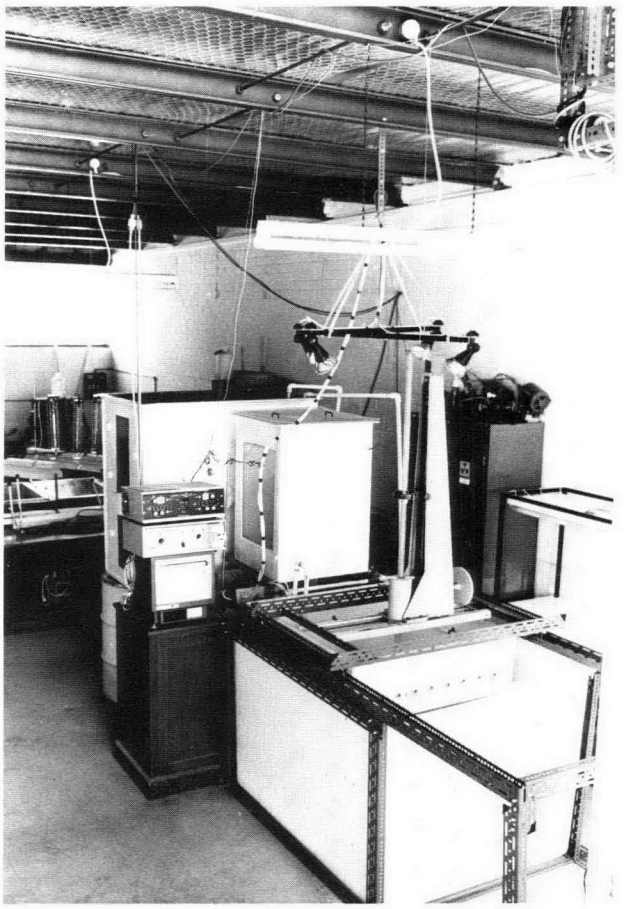

Figure 6. Photographic view of the simulating system.

tions. The cycling capacity of the system covers the range up to 10 years. At the present time the SEMC is controlling a sabkha (Fairbridge, 1968) simulating system, as well as a system (to be described later) designed to simulate an environment where polluting airborne metal particles travel through a water column before they are incorporated in sediment.

Acknowledgements

We wish to thank C. R. Robison for his enthusiastic and skilful help with the project. The Baas Becking Laboratory is supported by the Bureau of Mineral Resources, the Commonwealth Scientific and Industrial Research Organization, and the Australian Mineral Research Association Limited.

References

BUBELA, B., & FERGUSON, JAMES, 1973—Apparatus for studies of artificial sediments. *Journal of Sedimentary Petrology,* **43**, 1167-70.

BUBELA, B., FERGUSON, JAMES, & DAVIES, P. J., 1975—Biological and abiological processes in a simulated sedimentary system. *Journal of the Geological Society of Australia,* **22**, 135-44.

BUBELA, B., & MCDONALD, J. A., 1969—Formation of banded sulphides: Metal ion separation and precipitation by inorganic and microbial sulphide sources. *Nature,* **221**, 465-6.

DAVIES, P. J., & BUBELA, B., 1973—The transformation of nesquehonite into hydromagnesite. *Chemical Geology,* **12**, 239-300.

DAVIES, P. J., BUBELA, *B.*, & FERGUSON, JAMES, 1975—Dolomite and organic matter. *Nature,* **255**, 472.

DAVIES, P. J., BUBELA, B., & FERGUSON, JAMES, 1977—Simulation of carbonate diagenetic processes: Formation of dolomite, huntite and monohydrocalcite by the reaction between nesquehonite and brine. *Chemical Geology,* **19**, 181-214.

FAIRBRIDGE, R. W., 1968—THE ENCYCLOPEDIA OF GEOMORPHOLOGY. *Reinhold, New York.*

FERGUSON, JAMES, BUBELA, B., & DAVIES, P. J., 1974—Simulation of ore-forming processes: concentration of Pb on Zn from brines into organic and Fe-bearing carbonate sediments. *Geologische Rundschau,* **64**, 767-82.

HALLBERG, R. O., BUBELA, B., & FERGUSON, JAMES, in prep.—Simulation of metal chelating in two reducing sedimentary systems.

LAMBERT, I. B., & BUBELA, B., 1970—Banded sulphide ores. The experimental production of monomineralic sulphide bands. *Mineralium Deposita,* **5**, 92-102.

MOONEY, J., BUBELA, B., FERGUSON, JAMES, & HALLBERG, R. O., 1978—Mathematical modelling of experimental systems simulating metal chelating in reducing sedimentary environments. *BMR Journal of Australian Geology & Geophysics,* **3**, 93-100.

BMR Journal of Australian Geology & Geophysics, 3, 1978, 170-172

New microform publications

BMR has decided that future issues in its Report series will be on microfiche. A hard-copy contents listing, and abstract, will accompany each Report.
Summaries of the first microfiche Reports to be released are given below.

Report 180
Microform MF14

Preliminary catalogue of tsunamis for the New Guinea/ Solomon Islands region, 1768-1972.

by *I. B. Everingham*

ISBN 0 642 03162 2

78 pp., 7 pls., 1977. **Price $0.50.**

A catalogue of tsunamis for the period 1768-1972 has been compiled for the New Guinea/Solomon Islands region. This catalogue includes the results of Iida, Cox & Pararas-Carayannis, and data from local newspapers, government Administration reports, recently installed seismograph stations, and miscellaneous sources. The data are most complete for the Papua New Guinea region.

Results are that: (a) nine tsunamis were noted before, and 56 since, 1900; (b) tsunamis have occurred along the coastline around the Solomon Sea, particularly in the northern and western regions, and along the northern New Guinea coastline, but only one has been noted on the south coast of mainland Papua New Guinea; (c) only three tsunamis were caused by volcanoes and four by distant earthquakes, whereas the majority, 54, resulted from local earthquakes; (d) of 14 waves that reached a maximum height of 4 m or more and could be considered dangerous, the most disastrous resulted from a volcanic explosion at Ritter Island in 1888, when the wave height reached about 12 m; (e) tsunamis with a maximum height of around 2 m are relatively frequent, and have occurred on an average of once every two years; (f) tsunamis generally occur as steady rises and falls of sea level, and the most damaging waves from earthquake-induced tsunamis usually occur in relatively small areas where a large build-up of sea level is due to topographic irregularities.

A simple precaution against tsunami damage is to construct buildings about 3 m above the highest tide level. Because of the uncertainty where disastrous waves will strike, it is difficult to devise precautions against them.

Report 185
Microform MF8

Digital data acquisition system in geophysical survey aircraft VH-BMG

by *D. N. Downie*

ISBN 0 642 03115 0

57 pp., 2 pls., 1977. **Price $0.50.**

When BMR's new Twin Otter aircraft was being fitted out for geophysical surveying, an integrated system for acquisition of digital data was developed. The system records information from one magnetic channel, four gamma-ray spectrometer channels, and two Doppler navigation channels, in addition to altitude and fiducial numbers. Sampling rate is one second, except for magnetic data, which are sampled every 0.2 seconds.

The integrated system is built around a Hewlett-Packard 2114B general-purpose digital computer, interfaced to a 16-channel digital input multiplexer and magnetic tape recorder. A visible and permanent analogue record of the input data is maintained by chart recorders, to enable the operator to monitor data quality and to assist later in interpretation of the data. The chart drive motors can be run at five fixed speeds or coupled to the Doppler signal so that chart speed is proportional to ground speed. The Doppler signals are also coupled to a display unit which assists the pilot to follow the planned flight path.

The system is extremely reliable, and error-free flights are common.

Report 188
Microform MF12

Distribution and major-element chemistry of late Cainozoic volcanoes at the southern margin of the Bismarck Sea, Papua New Guinea.

by *R. W. Johnson*

ISBN 0 642 03014 6

170 pp., 55 figs., 1977. **Price $3.00.**

Late Cainozoic volcanoes at the southern margin of the Bismarck Sea can be grouped into western and eastern arcs. The volcanoes of the western arc form a narrow zone which is associated with a broad zone of seismicity that marks the boundary between the South Bismarck and Indo-Australian plates. The western arc is considered to overlie a near-vertical downgoing slab which, throughout the late Cainozoic, may have been characterised by generally higher rates of subduction nearer its eastern end. The eastern arc consists of volcanoes arranged on three principal lines: (1) an east-west line formed by the Witu Islands (excluding Unea), (2) a north-south chain of volcanoes forming Willaumez Peninsula, and (3) a broad, northeast-southwest belt along the north central coast of New Britain between the southern end of Willaumez Peninsula and Likuruanga. At the present day, the volcanoes of the eastern arc overlie the northward dipping New Britain Benioff zone, which is thought to represent subduction of the Solomon Sea plate beneath the South Bismarck plate. To account for the distribution of these eastern volcanoes, an imbricate thrust slice (the Vitiaz slice) in the northwestern corner of the Solomon Sea is believed to have exerted an important influence on the geodynamics of the region throughout the late Cainozoic.

The volcanic rocks of both arcs are hyperthene-normative and highly porphyritic, especially in plagioclase. Other phenocrysts are olivine, clinopyroxene, pleochroic orthopyroxene, amphibole, iron-titanium oxides, quartz, and minor apatite and biotite. Basalts (<53 percent SiO_2) and low-silica andesites ($53 \leqslant SiO_2 < 57$percent) are common in the western arc, high-silica andesites ($57 \leqslant SiO_2 < 62$ percent) are less common, dacites ($62 \leqslant SiO_2 < 70$ percent) are rare, and rhyolites ($\geqslant 70$ percent SiO_2) have not been found. The volcanoes of the Schouten Islands,

at the western end of the western arc, are unusual because basalts appear to be absent. The range of rock types in the eastern arc is wider: andesites are common, basalts and dacites are less common, and rhyolites are rare. Basalts in both arcs are either quartz-normative or olivine-normative. Rocks having high $Mg/(Mg + Fe^{2+})$ values are also present in both arcs, and may represent approximations to primary magmas that were in equilibrium with the olivine of upper mantle peridotite.

In comparing the compositions of rocks containing the same amounts of silica, pronounced changes can be demonstrated (1) *along* the western arc—in a direction parallel to the plate boundary, and (2) *across* the eastern arc—in a direction more or less at right-angles to the plate boundary. The compositional changes in the eastern arc appear to be related to depth to the present-day Benioff zone. A favoured model for petrogenesis in both arcs is the partial melting of upper mantle peridotite (not necessarily of uniform composition) under hydrous conditions to generate mafic primary magmas which rise and fractionate to form magmas of lower magnesia and higher silica contents.

In parts of the eastern arc, and where the downgoing slab is at a shallow depth (less than about 100 km), water may have been released from hydrated oceanic crust in the upper part of the Solomon Sea slab by subsolidus dehydration of amphibole, and may have risen into the overlying mantle and generated primary magmas by partial melting of peridotite. It is suggested that these primary magmas gave rise to the volcanic rocks between the southern end of Willaumez Peninsula and Likuruanga. At depths slightly greater than about 100 km, a hydrous eclogite part of the slab may have melted; derived water-rich siliceous melts may have risen into and partially melted the mantle to generate the primary magmas. Conditions of magma genesis over the deepest parts of the New Britain Benioff zone are as yet uncertain, although as the depth increases the magma compositions are thought to be governed increasingly by inhomogeneities in the source peridotite rather than by the influence of slab-derived melts.

Beneath Willaumez Peninsula, the descending Solomon Sea plate may move past the descending Vitiaz slice; reductions in total pressure, and possible heating by shear strain, in the drag zone between them may have enhanced dehydration or melting of subducted oceanic crust (hydrous eclogite). Water-rich fluids rose into the overlying mantle (which was not necessarily homogeneous), and generated and mixed with primary magmas that subsequently fractionated and erupted from the volcanoes of the peninsula.

The changes in rock compositions along the western arc are considered to be related to differences in the rates of subduction between different parts of the arc. Comparisons between the compositions of rocks from the eastern and western arcs suggest that primary magmas in the western arc (excluding those beneath Viai and Vokeo) may have been formed by partial melting of mantle peridotite under conditions similar to those that existed over the deeper parts of the New Britain Benioff zone. Owing to a predominance of basalts and andesites in the western arc, the primary magmas may have risen more rapidly there than in the eastern arc, where slower rates of magma ascent may have enhanced fractionation resulting in a greater proportion of acid rocks among the eastern volcanoes. Alternatively, the abundance of basalt in the western arc, and in some of the Witu Islands in the eastern arc, may be due to upwelling of hot mantle peridotite which partially melted at relatively shallow depths (possibly in a dilatational environment), so that little time was available for the magmas to fractionate during their relatively short ascent to the surface. Anatexis of young crustal rocks in the South Bismarck plate cannot yet be ruled out as a possible process for the derivation of at least some acid rocks.

Report 192
Microform MF11

Some earthquake focal mechanisms in the New Guinea/ Solomon Islands region, 1969-1971.

by *I. D. Ripper*

ISBN 0 642 03165 7

93 pp., 35 figs., 3 pls., 1977. **Price $1.00.**

Focal mechanism stereographic projections were plotted for 34 earthquakes that occurred in the New Guinea/ Solomon Islands region between 1969 and 1971. Solutions have been obtained for 31 of the earthquakes, of which 27 are reasonably good; of these, six are strike-slip and 21 are dip-slip (13 overthrust, seven normal, and one having one horizontal and one vertical nodal plane).

The data used were P-wave first arrivals, recorded mainly on the World Wide Standard Seismograph Network.

The complexity of the essentially compressional collision zone between the Pacific Plate and the Australian Plate is indicated by several earthquakes for which dip-slip normal solutions were obtained: in the South Bismarck Volcanic Arc; on the Solomon Sea side of the New Britain Trench; in the D'Entrecasteaux Islands region of southeast Papua; on Santa Ysabel Island; and at depths of 115 and 118 km below the Ramu Markham Valley.

Report 197
Microform MF3

An integrated scheme for the laboratory analysis of oil, natural gas, and petroleum source rocks.

by *D. M. McKirdy and Z. Horvath*

ISBN 0 642 02902 4

27 pp., 16 figs., 1977. **Price $0.50.**

In recent years the geochemical study of crude oils, natural gases, and organic matter dispersed in sedimentary rocks has emerged as an important tool in petroleum exploration. The BMR Petroleum Technology Laboratory has developed an integrated scheme for the geochemical evaluation of reservoir hydrocarbons (oil and gas), and potential source-rocks encountered during exploratory drilling in Australia.

The analytical procedures involved are relatively simple in order to permit rapid processing of the samples:

Oil

measurement of API gravity;
determination of sulphur content;
fractional distillation and calculation of USBM correlation index for each fraction;
precipitation of asphaltenes from >250°C fractions;
liquid chromatography of asphaltene-free material on alumina to obtain saturated hydrocarbons (alkanes), aromatic hydrocarbons, and compounds containing O, N, and S;
capillary gas chromatography of C_{15+} alkanes.

Gas

gas chromatography to determine identity and concentration of individual components.

Source-rock

determination or organic carbon content;
Soxhlet extraction of soluble organic matter with benzene/methanol;
liquid chromatography of extract on alumina (as for oil);

capillary gas chromatography of alkanes;
isolation of insoluble organic matter (kerogen) by digestion of rock in HCl/HF;
X-ray diffraction analysis of kerogen;
elemental (C, H, N, S) and ash micro-analysis of kerogen.

Specific examples of oil, gas, and source-rock analyses are presented to illustrate how such geochemical data can be used to indicate:

1. the gross composition and quality of the oil;
2. any alteration (e.g. thermal maturation, biodegradation, water-washing) of the oil after its accumulation in the reservoir;
3. correlation between oils of the same family;
4. the marine or non-marine nature of the precursor organic matter in the source sediments;
5. distinction between oil-prone and gas-prone source-rocks.

The value of petroleum and source-rock geochemistry lies in its ability to predict at an early stage in the exploration of a basin both the type of hydrocarbons present (whether oil, gas-condensate, or dry gas) and their likely distribution within the basin.

Report 198
Microform MF15

The reconnaissance gravity survey of Australia: a qualitative analysis of results.

by *A. R. Fraser, F. Darby, and K. R. Vale*

ISBN 0 642 03101 0

92 pp., 1 fig., 1977. **Price $1.00.**

As a first step towards analysing and interpreting contoured gravity data, it is a common practice to divide the contour pattern into discrete regions of different gravity characteristics. This helps to clarify the overall contour pattern and emphasise significant but less obvious features of the gravity field. It also simplifies the task of describing gravity features, their interrelationship, and their correlation with geological or tectonic elements.

The method has been used by the several authors who have contributed to the interpretation and reporting of the results of reconnaissance gravity surveys in Australia. In general, two classes of feature have been defined and named—gravity provinces and gravity units. A gravity province is a region where the gravity field is characterised by uniformity of at least one property, such as contour trend, gravity level, or degree of contour disturbance, which distinguishes it from neighbouring provinces. A gravity unit is a subdivision of a province. As for provinces, but on a smaller scale, neighbouring units are distinguished from each other by differences in contour trend, gravity level, or degree of contour disturbance.

Gravity provinces have been defined on a continuing basis by various authors, as parts of the reconnaissance gravity survey of Australia were completed. With the reconnaissance survey now virtually complete, this report is a summary and to some extent a rationalisation of the work of all of these authors. Ninety-six gravity provinces are defined over Australia and its northwest continental shelf, and are discussed in relation to known geology and geophysics.

A broad assessment of the causes of gravity features indicates that, in general, provinces of high Bouguer anomaly correspond to Proterozoic or early Palaeozoic metamorphic belts, provinces of low Bouguer anomaly to granitic batholiths or Phanerozoic sedimentary basins, and provinces of complex contour pattern to Precambrian or Palaeozoic orogenic domains.

Report 199
Microform MF27

Seismicity of the New Guinea/Solomon Islands region, 1969.

by *I. B. Everingham*

ISBN 0 642 03284 X

11 pp., 8 figs., 1 pl., 1977. **Price $0.50.**

Earthquakes which occurred in the New Guinea/Solomon Islands region, and intensity data for Papua New Guinea felt earthquakes are listed for 1969. The level of seismicity was relatively low compared with 1967 and 1968. One earthquake (in the Solomon Islands) had a magnitude greater than M 6.9, and fourteen earthquakes had magnitudes between 6 and 6.9.

The highest level of seismic activity was along the northern region of the Solomon Sea between 151° and 155°E. Four small isolated areas of relatively intense activity were recorded in the Solomon Islands. The Bismarck Sea seismic zone was relatively inactive, no earthquake being recorded from the central part of the Bismarck Sea.

Six earthquakes with depths greater than 300 km were recorded: five from the Benioff zone beneath New Britain and northern Bougainville, and one 533 km beneath the Solomon Islands near Santa Ysabel Island. The last provides further evidence of a contorted, possibly fragmented, near-vertical descending lithospheric slab beneath the Solomon Islands.

Isoseismal maps were drawn for the six strongest earthquakes in Papua New Guinea; maximum intensities for these events were only MM V-VI, and damage was negligible.

The magnitude/frequency relation for 1969 was

$$\log N = 7.67 - 1.08M$$

Report 202
Microform MF24

Geochemistry of the Fairfield Group, Canning Basin, W.A.

by *E. C. Druce and B. M. Radke*

ISBN 0 642 03103 7

101 pp., 11 figs., 1977. **Price $1.00.**

The carbonate geochemistry of the Fairfield Group serves to distinguish the previously recognised formations. The oldest unit, the Gumhole Formation, is characterised by high Mn and Pb, and low Mg values. In contrast the elemental concentrations in the Yellow Drum Sandstone are within previously determined averages for dolomitic and clastic-bearing carbonate rocks, and the concentrations in the Laurel Formation are average for non-dolomitic limestones.

Samples from the Gumhole and Laurel Formations can be separated using agglomerative polythetic programs and Q-mode factor analysis, demonstrating that the differences in geochemistry, although slight, are statistically significant.

The only unit with widespread outcrop is the Gumhole Formation, and within it elemental concentrations vary significantly and show that clastic input into the basin was greatest in the southeast part of the northerly margin.

The minor element geochemistry suggests that there has been enrichment of Pb and Zn in the sequence, particularly in the Gumhole Formation.

THE CRUST AND UPPER MANTLE OF SOUTHEAST AUSTRALIA

A Symposium to be held 13-14 February 1979 in Canberra

This symposium seeks to bring together the results of recent and current work on the structure, composition, and tectonic development of the crust and upper mantle in southeast Australia.

Persons wishing to contribute to the symposium should submit titles and return a completed registration form to the organising committee not later than **28 September 1978.** Abstracts will be called for after the papers have been accepted.

A three-day excursion led by Dr Bruce Chappell will be conducted on 15-17 February 1979. Final details are not yet available, but the approximate itinerary is: 15 Feb. Jugiong Kimberlite, Snowy Mountains Highway, Cooma; 16 Feb. Cooma Complex, Kosciusko Batholith; 17 Feb. Berridale Batholith. The excursion cost will depend on the number of participants.

Registration forms are available, on behalf of the organising committee, from c/- Dr. D. Denham,

Bureau of Mineral Resources,

P.O. Box 378,

CANBERRA, ACT 2601.

The symposium is sponsored by: the Department of Geology, Australian National University; the Bureau of Mineral Resources, Geology and Geophysics; and the Geological Society of Australia.

Contents

Notes

R76/1403 (2) Cat. No. 78 7089 1